Insights into the Role of YgfB in β-Lactam Resistance and Beyond

Dissertation

der Mathematisch-Naturwissenschaftlichen Fakultät

der Eberhard Karls Universität Tübingen

zur Erlangung des Grades eines

Doktors der Naturwissenschaften

(Dr. rer. nat.)

vorgelegt von

Ole Hans Heiner Eggers

aus Hamburg

Tübingen

2024

Gedruckt mit Genehmigung der Mathematisch-Naturwissenschaftlichen Fakultät der Eberhard Karls Universität Tübingen.

Tag der mündlichen Qualifikation:	24.09.2024
Dekan:	Prof. Dr. Thilo Stehle
1. Berichterstatter/-in:	PD Dr. Erwin Bohn
2. Berichterstatter/-in:	Prof. Dr. Harald Groß

Table of contents

Abbreviations

ABE	AlpA binding element
AMR	Antimicrobial resistance
anhMurNAc	1,6-anhydro-*N*-acetylmuramic acid
anhMurNAc-3P	1,6-anhydro-*N*-acetylmuramic acid tripeptide
anhMurNAc-4P	1,6-anhydro-*N*-acetylmuramic acid tetrapeptide
anhMurNAc-5P	1,6-anhydro-*N*-acetylmuramic acid pentapeptide
AUC	Area under the curve
AZT	Aztreonam
bp	Basepairs
CAZ	Ceftazidime
cDNA	complementary DNA
CDS	Coding sequence
CF	Cystic fibrosis
CFU	Colony forming units
CIP	Ciprofloxacin
Cp	Crossing point
CV	Column volume
Da	Dalton
DTT	Dithiothreitol
EDTA	Ethylenediaminetetraacetic acid
EMSA	Electrophoretic mobility shift assay
EUCAST	European Committee on Antimicrobial Susceptibility Testing
FDA	Food and Drug Administration
FDR	False discovery rate
FEP	Cefepime
FIC	Fractional inhibitory coefficient
FLP	Flippase
gDNA	Genomic DNA
GlcNAc	*N*-acetylglucosamine
GOI	Gene of interest
GST	Glutathione-S-transferase
HA	Hemagglutinin

HEPES	(4-(2-hydroxyethyl)-1-piperazineethanesulfonic acid
IPM	Imipenem
IPTG	Isopropyl-β-D-thiogalactopyranosid
KOAc	Potassium acetate
LB	Luria-Bertani medium
LFQ	Label-free quantification
LMM	Low molecular mass
LPS	Lipopolysaccharide
LT	Lytic transglycosylase
MBP	Maltose-binding protein
m-DAP	meso-diaminopimelic acid
MDR	Multi drug resistance
MIC	Minimum inhibitory concentration
MS	Mass spectrometry
MurNAc	*N*-acetylmuramic acid
NER	Nucleotide excision repair
NTA	Nitrilotriacetic acid
OD	Optical density
OM	Outer membrane
PBP	Penicillin binding protein
PBS	Phosphate buffered saline
PCA	Protein fragment complementation assay
PCR	Polymerase chain reaction
PG	Peptidoglycan
pI	Isoelectric point
PIP	Piperacillin
POI	Protein of interest
PQS	Pseudomonas quinolone signal
qPCR	Quantitative polymerase chain reaction
rha	Rhamnose
rpm	Revolutions per minute
ROS	Reactive oxygen species
RT-qPCR	Reverse transcription quantitative polymerase chain reaction
SD	Standard deviation

SDS-PAGE	Sodium dodecyl sulfate polyacrylamide gel electrophoresis
SEC	Size exclusion chromatography
STR	Streptomycin
TAZ	Piperacillin/tazobactam
TBE	Tris/Borate/EDTA
TBS	Tris buffered saline
TBS-T	Tris buffered saline with tween
TEV	Tobacco etch virus
Tris	Tris(hydroxymethyl)aminomethan
TSS	Transcription start site
UDP	Uridine diphosphate
UDP-MurNAc	Uridine diphosphate-*N*-acetylmuramic acid
UDP-MurNAc-5P	Uridine diphosphate-*N*-acetylmuramic acid pentapeptide
WT	Wildtype

Summary

Infections with multi drug resistant (MDR) *Pseudomonas aeruginosa* strains are one of the emerging threats in the post-antibiotic age. To better treat such infections and to potentially identify new druggable targets, the mechanisms of how resistance emerges in *P. aeruginosa* need to be better understood and characterized. One of the most important resistance mechanisms for *P. aeruginosa* is overexpression of the inducible β-lactamase AmpC. The previously uncharacterized protein YgfB was recently identified to be a novel player in the complex network leading to AmpC-mediated resistance in the AmpC overexpressing, MDR *P. aeruginosa* strain ID40. YgfB was described to repress production of the amidase AmpDh3, which is known to degrade certain *ampC*-inducing cell wall recycling products. Reduced AmpDh3 levels results in accumulation of these cell wall products and in induction of the *ampC* encoded β-lactamase.

In this work, the mechanism of the YgfB-mediated repression of *ampDh3* was elucidated. YgfB interacts directly with AlpA, a transcriptional regulator of *ampDh3*, and prevents AlpA from binding to its binding site on the *ampDh3* promoter. The effect of YgfB repressing *ampDh3* and thereby mediating resistance is not limited to the isolate ID40 but could also be observed in other MDR *P. aeruginosa* isolates. Furthermore, the expression of *alpA* can be induced by DNA damage, mediated by the fluoroquinolone ciprofloxacin. Increased levels of AlpA lead to upregulation of *ampDh3* expression. In this work it was shown that YgfB, by interacting with AlpA, attenuates an excessive effect of ciprofloxacin-mediated DNA damage on the AmpDh3 production and therefore also on additive effects of a ciprofloxacin/β-lactam antibiotic combination.

YgfB is not only found in *P. aeruginosa*, but also other γ-proteobacteria, including many pathogenic species. AmpDh3 and AlpA are, however, limited mostly to *P. aeruginosa*. To identify a general function of YgfB in γ-proteobacteria, transcriptomic and interactomic analyses in *P. aeruginosa* and *Escherichia coli* were done. So far, various interaction partners of YgfB were found in both *P. aeruginosa* and *E. coli*. Protein-fragment complementation assays led to first validations of several interaction partners involved in diverse cellular functions. Consequently, it can be postulated that the primary function of YgfB may be its interaction with other proteins and the subsequent influence on cellular processes, the consequences of which are currently unknown. An interaction with proteins leading to transcriptional regulation was not found in *E. coli* and seems therefore to be an exception to *P. aeruginosa* rather than the rule.

In summary, this work provides insights into a novel player in the complex regulation of AmpC-mediated β-lactam resistance in *P. aeruginosa*. Evidence is provided that YgfB functions at the intersection of cell wall recycling and the DNA damage response. Additionally, YgfB likely interacts with a set of other proteins with diverse functions and these functions might generalize to other γ-proteobacteria.

Zusammenfassung

Infektionen mit multiresistenten *Pseudomonas aeruginosa*-Stämmen stellen eine wachsende Bedrohung im post-antibiotischen Zeitalter dar. Um eine effektive Behandlung solcher Infektionen zu ermöglichen und möglicherweise neue Angriffspunkte für Medikamente zu identifizieren, ist ein besseres Verständnis und eine Charakterisierung der Mechanismen der Resistenzbildung bei *P. aeruginosa* erforderlich. Einer der wichtigsten Resistenzmechanismen bei *P. aeruginosa* ist die Überexpression der induzierbaren β-Laktamase AmpC. Das bisher nicht charakterisierte Protein YgfB wurde kürzlich als neuer Akteur im komplexen Netzwerk identifiziert, das zur AmpC-vermittelten Resistenz im AmpC-überexprimierenden, multiresistenten *P. aeruginosa* Stamm ID40 führt. Es wurde beschrieben, dass YgfB die Produktion der Amidase AmpDh3 unterdrückt, von der bekannt ist, bestimmte *ampC*-induzierende Produkte des Zellwandrecyclings abzubauen. Ein verminderter AmpDh3-Spiegel führt zu einer Anhäufung dieser Produkte und zur Induktion der *ampC*-kodierten β-Laktamase. In dieser Arbeit wurde der Mechanismus der YgfB-vermittelten Repression von *ampDh3* aufgeklärt. YgfB interagiert direkt mit AlpA, einem Transkriptionsregulator von *ampDh3*, und verhindert, dass AlpA an seine Bindungsstelle am *ampDh3*-Promotor bindet. Dieser Effekt von YgfB ist nicht auf das Isolat ID40 beschränkt, sondern konnte auch bei anderen multiresistenten *P. aeruginosa*-Isolaten beobachtet werden.

Des Weiteren kann die Expression des Gens *alpA* durch DNA-Schäden, welche durch das Fluorchinolon Ciprofloxacin verursacht werden, induziert werden. Erhöhte Level von AlpA führen zu einer Hochregulierung der *ampDh3*-Expression. In dieser Arbeit wurde gezeigt, dass YgfB durch Interaktion mit AlpA eine übermäßige Wirkung Ciprofloxacin-vermittelter DNA-Schädigung auf die AmpDh3-Produktion und damit auch auf additive Effekte einer Ciprofloxacin/β-Laktam-Kombination abschwächt.

YgfB kommt nicht nur in *P. aeruginosa*, sondern auch in anderen γ-Proteobakterien, einschließlich vieler pathogener Arten vor. Das Vorkommen von AmpDh3 und AlpA ist dagegen auf *P. aeruginosa* und einige wenige andere Arten beschränkt. Um eine allgemeine Funktion von YgfB in γ-Proteobakterien zu identifizieren, wurden Transkriptom- und

Interaktomanalysen in *P. aeruginosa* und *Escherichia coli* durchgeführt. Bislang wurden verschiedene Interaktionspartner von YgfB sowohl in *P. aeruginosa* als auch in *E. coli* gefunden. Protein-fragment complementation assays führten zu ersten Bestätigungen mehrerer Interaktionspartner, die an verschiedenen zellulären Funktionen beteiligt sind. Folglich kann postuliert werden, dass die primäre Funktion von YgfB in der Interaktion mit anderen Proteinen und der anschließenden Beeinflussung von zellulären Prozessen besteht, deren Folgen derzeit noch unbekannt sind. Eine Interaktion mit Proteinen, die zu einer Regulation der Transkription führt, wurde in *E. coli* nicht gefunden und scheint daher bei *P. aeruginosa* eher eine Ausnahme als die Regel zu sein.

Zusammenfassend lässt sich sagen, dass diese Arbeit Einblicke in einen neuen Akteur in der komplexen Regulation der AmpC-vermittelten β-Laktam-Resistenz von *P. aeruginosa* gibt. Es wird gezeigt, dass YgfB an der Schnittstelle zwischen Zellwand-Recycling und DNA-Schadensreaktion agiert. Des Weiteren interagiert YgfB wahrscheinlich mit einer Reihe anderer Proteine mit unterschiedlichen Funktionen. Dies könnte Rückschlüsse auf die Rolle von YgfB in anderen γ-Proteobakterien zulassen.

1. Introduction

1.1. *Pseudomonas aeruginosa*

The Gram-negative, rod-shaped bacterium *Pseudomonas aeruginosa* is ubiquitous in nature. It thrives in wet environments and can be found in sinks, showers, toilets, in clinics, as well as in the environment. It is a facultative pathogen and associated with nosocomial infections of the immunocompromised host. *P. aeruginosa* is notorious for its high level of resistance and development of multi drug resistance (MDR). Carbapenem-resistant *P. aeruginosa* has therefore been classified by the World Health Organization as a priority pathogen for which development of new therapeutics is urgently needed (Tacconelli et al., 2018; World Health Organization, 2024). *P. aeruginosa* is part of the ESKAPE group, a group comprising six highly virulent and often drug resistant bacterial pathogens, namely *Enterococcus faecium, Staphylococcus aureus, Klebsiella pneumoniae, Acinetobacter baumannii, Pseudomonas aeruginosa* and *Enterobacter* species (Rice, 2008).

1.1.1. Epidemiology and *P. aeruginosa*-associated disease

P. aeruginosa is one of the leading causes of nosocomial infections and is associated with pneumonia, especially ventilator associated pneumonia, urinary tract infection, wound infections, blood stream infections, and infections in burn patients (Reynolds & Kollef, 2021). A recent study described that in 2019, 559,000 deaths worldwide were caused by *P. aeruginosa* infections with an all-cause age standardized mortality rate of 7.4 deaths per 100,000 individuals (GBD 2019 Antimicrobial Resistance Collaborators, 2022). The syndrome associated with the highest mortality of *P. aeruginosa* infections were infections of the lower respiratory tract and thorax with an age-standardized mortality rate of 3.2 deaths per 100,000 individuals. Blood stream infections were the syndrome with the second highest mortality rate (2.1 deaths per 100,000 individuals). The Robert Koch Institute has published that in 2022, 4.4% of all bacterial isolates from stationary patients identified in participating laboratories in Germany were *P. aeruginosa* isolates (Robert Koch Institut, ARS, https://ars.rki.de, Retrieved: 18.04.2024).

P. aeruginosa is known for its association with antibiotic resistance. Recent publications analyzing the global burden of disease of antimicrobial resistance (AMR) have highlighted the threat of antimicrobial resistance in *P. aeruginosa* and in general. A recent systematic review (Antimicrobial Resistance Collaborators, 2022) has shown that in 2019, 4.95 million deaths worldwide were associated with antimicrobial resistance and of those 1.27 million deaths could be directly attributed to antimicrobial resistance. Of those, approximately 340,000 deaths were

associated with AMR in *P. aeruginosa* and 90,000 directly attributed to AMR in *P. aeruginosa*. In the WHO European region, 43,800 deaths were associated and 10,900 could be directly attributed to antibiotic resistant *P. aeruginosa* infections in 2019 (European Antimicrobial Resistance Collaborators, 2022).

In addition, *P. aeruginosa* is known to colonize the lungs of persons with cystic fibrosis (CF), a genetic disorder caused by mutations in the gene encoding for the cystic fibrosis transmembrane conductance regulator CFTR (Kerem et al., 1989). CF leads to reduced mucociliary clearance, buildup of mucus, structural changes in the lung and finally to death (Davis, 2006). Chronic infections with *P. aeruginosa* are a major complication in CF patients and treatment to eradicate *P. aeruginosa* colonization is highly recommended (Peter J. Mogayzel et al., 2014).

1.1.2. Pathogenicity

P. aeruginosa has a large array of virulence factors at its disposal. Flagella and type IV pili are needed for attachment to respiratory epithelial cells and are therefore especially important in infections of the lungs (Bucior et al., 2012).

Among the main virulence factors are the exotoxins secreted by *P. aeruginosa*. The *Pseudomonas* Exotoxin A is secreted by the type II secretion system (Gérard-Vincent et al., 2002; Voulhoux et al., 2000) and was described to ribosylate elongation factor-2, which leads to cessation of protein biosynthesis (Iglewski et al., 1977; Yates & Merrill, 2004). Other exotoxins such as ExoS, ExoT, ExoU and ExoY are secreted by the type III secretion system (T3SS) (Hauser, 2009), with ExoS and ExoU being the most important effectors. *P. aeruginosa* strains seem to carry either ExoS or ExoU (Feltman et al., 2001), leading to a classification of the phenotypes of *P. aeruginosa* isolates as either invasive ($ExoS^+$) or cytotoxic ($ExoU^+$) (Horna & Ruiz, 2021). ExoS has bifunctional toxicity, disrupting cell-to-cell adhesion and inducing apoptosis in the host (Horna & Ruiz, 2021; Jia et al., 2006; Kaminski et al., 2018; Pederson et al., 1999). ExoU is cytotoxic due to its phospholipase activity, causing host-cell lysis (Deruelle et al., 2021; Sato et al., 2003), and is considered to be one of the most potent toxins (Horna & Ruiz, 2021; Reynolds & Kollef, 2021).

P. aeruginosa also produces several proteases that degrade host-factors such as immunoglobulins and fibrin. In lung infections, they are also described to contribute to damage to the lung. These include LasA, LasB, alkaline protease, and protease IV (Gellatly & Hancock, 2013). Additionally, *P. aeruginosa* is known for its formation of biofilms. Biofilms consist mainly of

extracellular DNA, polysaccharides, lipids, and proteins that form an extracellular matrix, allowing the bacteria to adhere to surfaces. Biofilms protect the cells from stresses by the environment and phagocytosis, promoting colonization of the cystic fibrosis lung (Thi et al., 2020). The formation of biofilm is linked to quorum sensing, a mechanism by which the cells can coordinate adaptation to their environment as a function of their density (Bjarnsholt et al., 2010). Quorum sensing is mediated by autoinducers, small molecules that are constitutively produced and correlate in concentration to the density of the bacteria present. Autoinducers act as cofactors of transcriptional regulators and lead to a coordinated response of all bacteria in the population when present in high enough concentrations (Gellatly & Hancock, 2013).

The *Pseudomonas* pigments pyocyanin and pyoverdine are responsible for the typical coloration of *P. aeruginosa* colonies on cetrimide-agar. These also act as virulence factors, whereby pyocyanine has been described to play a role in induction of oxidative stress in the host, (Lau et al., 2004), while pyoverdine is a siderophore that is able to remove iron from host-tissue and acts as a signaling molecule for other virulence factors (Kang et al., 2018).

Lastly, lipopolysaccharide (LPS) is a complex glycolipid tethered to the outer membrane, facing the extracellular space. LPS is described to play roles in induction of an inflammatory response, facilitating interaction with host-receptors, protection from host-factors and antibiotics, and acts as an endotoxin upon lysis of the bacterial cell. LPS generally consists of three domains. The innermost domain, Lipid A, consists of a disaccharide backbone attached to a several fatty acids that anchor LPS to the outer membrane. To Lipid A, the core antigen is attached, which consists of a branched oligosaccharide. The outermost domain is the O-antigen that is made up of a carbohydrate polymer. Further details on the biosynthesis, role of LPS in pathogenicity, and structure of LPS were reviewed extensively by King et al. (2009), Pier (2007) and Lam et al. (2011).

1.2. Treatment of *P. aeruginosa* infections

As high resistance to antibiotics is common in *P. aeruginosa,* susceptibility testing is of great importance for the treatment (Bassetti et al., 2018; Kalil et al., 2016; Tamma et al., 2021). The most common therapeutics used for treatment of *P. aeruginosa* infections are β-lactam antibiotics, fluoroquinolones, and aminoglycosides (Bassetti et al., 2018; Reynolds & Kollef, 2021), which will be introduced in the following.

1.2.1. β-lactam antibiotics and β-lactamase inhibitors

The peptidoglycan of Gram-negative bacteria is a polymeric structure that allows the bacteria to resist osmotic pressure and gives shape to the cell (Höltje, 1998). The peptidoglycan is made

up of two alternating building blocks, *N*-acetylglucosamine (GlcNAc) and *N*-acetylmuramic acid (MurNAc) that are connected by a β-(1,4)-glyosidic bond. Each MurNAc monomer in addition carries an oligopeptide sidechain containing five amino acids. In Gram-negative bacteria, these amino acids are L-alanine, D-glutamate, meso-diaminopimelic acid (m-DAP), D-alanine, and D-alanine in this order starting from the L-alanine anchor attached to MurNAc. (Glauner et al., 1988; Heilmann, 1972; reviewed in Vollmer et al., 2008)
The peptide sidechains are crosslinked by penicillin-binding proteins (PBPs) that have DD-transpeptidase activity, linking the terminal α-amino group of m-DAP of the acceptor peptide with the carboxy group of the penultimate D-Ala of the donor peptide, with the terminal D-Ala of the donor peptide being removed during the reaction (Lupoli et al., 2011). The crosslinking of the peptidoglycan polymer creates a mesh that increases the strength of the sacculus and allows to withstand osmotic pressure (Vollmer et al., 2008). The synthesis of peptidoglycan will be described in detail in 1.3.5.1.

β-lactam antibiotics are compounds that target the transpeptidation by PBPs. They are bactericidal by pseudo-irreversibly binding to penicillin-binding proteins (PBPs), inhibiting the crosslinking of peptidoglycan (PG) during cell division (Lima et al., 2020; Tipper, 1979; Waxman & Strominger, 1983). In particular, β-lactam antibiotics mimic the D-Ala-D-Ala dipeptide of the peptidoglycan prior to crosslinking by PBPs with transpeptidase activity, which leads to structural and morphological changes that are toxic to the cells as reviewed extensively by Cushnie et al. (2016). β-lactam antibiotics show a time-dependent killing effect, i.e. the time the concentration of β-lactams exceeds the minimum inhibitory concentration (MIC) is predictive of therapeutic success (Turnidge, 1998).

β-lactam antibiotics derive their name from their structure, as the core structure of these antibiotics is 2-azetidinone, the simplest β-lactam ring, and are among the first line therapeutics used in treatment of *P. aeruginosa* infections (Reynolds & Kollef, 2021). The β-lactam antibiotics can be categorized into different classes based on their structure and activity.
Penicillin was the first antibiotic substance to be discovered and also the first β-lactam antibiotic (Fleming, 1922). Of the penicillins, only piperacillin and piperacillin in combination with the β-lactamase inhibitor tazobactam are used in the therapy of *P. aeruginosa* infections (The European Committee on Antimicrobial Susceptibility Testing, 2024). In 2022, 18.5% of *P. aeruginosa* isolates from stationary patients in Germany were resistant to piperacillin and 13.6%

to piperacillin/tazobactam (Robert Koch Institut, ARS, https://ars.rki.de, Retrieved: 18.04.2024).

Cephalosporins differ from penicillins by their 6-membered dihydrothiazine ring instead of the 5-membered thiazolidine ring. The broad spectrum cephalosporins cefepime, ceftolozan and ceftazidime are used to treat *P. aeruginosa* infections (The European Committee on Antimicrobial Susceptibility Testing, 2024). In 2022, 8.9% of *P. aeruginosa* isolates of stationary patients in Germany were resistant to cefepime and 10.0% to ceftazidime (Robert Koch Institut, ARS, https://ars.rki.de, Retrieved: 18.04.2024). A recent development is the cephalosporin cefiderocol (Fetcroja), for which marketing authorization was approved in Europe in 2020 for *"treatment of infections with aerobic Gram-negative bacteria in adults with limited treatment options"* (European Medicines Agency (EMA), https://www.ema.europa.eu/en/medicines/human/EPAR/fetcroja). Cefiderocol makes use of a so called "trojan-horse" strategy as it carries a siderophore conjugated sidechain that forms complexes with free iron (Ito et al., 2016). The siderophore-iron complex is taken up by iron transporters, in particular PiuA in *P. aeruginosa* and CirA and Fiu in *E. coli*, allowing cefiderocol to cross the outer membrane (Ito et al., 2018). Cefiderocol shows a high affinity to PBP3, suggesting the killing effect is mainly due to inhibition of this penicillin-binding protein (Ito et al., 2018).

Of the carbapenem class of β-lactam antibiotics, imipenem and meropenem are used for the treatment of *P. aeruginosa* (The European Committee on Antimicrobial Susceptibility Testing, 2024). Carbapenems are characterized by a C2-C3 double bond, a C1 carbon replacing the sulfur in the 5-membered ring, and their increased stability to β-lactamases (El-Gamal et al., 2017). Imipenem is hydrolyzed by the renal dehydropeptidase I (DHP-I) and is therefore combined with the DHP-I inhibitor cilastatin (Kahan et al., 1983). In 2022, 14.5% of *P. aeruginosa* isolates of stationary patients in Germany were resistant to imipenem and 5.3% resistant to meropenem (Robert Koch Institut, ARS, https://ars.rki.de, Retrieved: 18.04.2024).

Lastly, among the monobactam class of β-lactams, only aztreonam is used for the treatment of *P. aeruginosa* (The European Committee on Antimicrobial Susceptibility Testing, 2024). 11.6% of *P. aeruginosa* isolates from stationary patients in Germany were resistant to aztreonam in 2022 (Robert Koch Institut, ARS, https://ars.rki.de, Retrieved: 18.04.2024).

Due to the high levels of resistance development by β-lactamases, enzymes cleaving the β-lactam ring of the β-lactam antibiotics, antibiotic adjuvants called β-lactamase inhibitors have been developed. These drugs inhibit β-lactamases and prevent degradation of β-lactam antibiotics.

Commonly used β-lactamase inhibitors in *P. aeruginosa* infections are tazobactam, avibactam, relebactam and vaborbactam (The European Committee on Antimicrobial Susceptibility Testing, 2024). Tazobactam is commonly combined with piperacillin and ceftolozan is always administered in combination with tazobactam. Avibactam is combined with ceftazidime and relebactam is combined with imipenem. Lastly, vaborbactam is combined with meropenem (The European Committee on Antimicrobial Susceptibility Testing, 2024).

1.2.2. Fluoroquinolones

Bacterial type II topoisomerases are essential enzymes that are important for maintaining the topology of the bacterial DNA (Goodall et al., 2018). In most bacterial species, two type II topoisomerases exist: gyrase and topoisomerase IV (Gellert et al., 1976; Kato et al., 1990). As reviewed by Collins and Osheroff (2024) gyrase relaxes positively supercoiled DNA and introduces negative supercoils, while topoisomerase IV relaxes positively and negatively supercoiled DNA. In addition, topoisomerase IV is able to remove tangles and knots from the bacterial DNA.

Gyrase and topoisomerase IV form heterotetramers that are constituted of two subunits each. For gyrase, these are GyrA and GyrB, and ParC and ParE for topoisomerase IV. GyrA and ParE form the A-subunit, while GyrB and ParE form the B-subunit of these heterotetramers (Forterre et al., 2007; Kato et al., 1990; Mizuuchi et al., 1978).

Both gyrase and topoisomerase IV have similar ATP-dependent enzymatic mechanisms. In short, both enzymes generate double strand breaks in a part of the DNA, thread a second part of the DNA through the created gap and finally religate the double strand breaks, thereby facilitating unwinding or negative supercoiling. Further details on the exact mechanism of the type II topoisomerases are reviewed in Collins and Osheroff (2024)

Fluoroquinolones are bactericidal antibiotics that act on gyrase and topoisomerase IV. They coordinate a central divalent metal cation (usually Mg^{2+}) to form a metal ion bridge between the C3/C4 keto acid of the fluoroquinolone and the hydroxyl group of a serine and the carboxyl group of an aspartic or glutamic acid of the A subunit of the enzyme (Aldred et al., 2014). The interaction of a fluoroquinolone with gyrase/topoisomerase IV inhibits the religation of the double stand breaks that were introduced by the enzymes by stabilizing the cleaved complexes. The interaction of a fluoroquinolone with gyrase/topoisomerase IV, with gyrase being the main target in Gram-negative bacteria (Khodursky et al., 1995), is finally toxic by two different mechanisms. For one, the stabilization of the cleaved complex inhibits the catalytic function of

the enzymes as a whole, stalling transcription and DNA-replication which finally leads to a slow cell death (reviewed by Bush et al., 2020; reviewed by Collins & Osheroff, 2024). This mechanism usually is observed at lower ratios of drug concentration and minimum inhibitory concentration (MIC) (Bush et al., 2020). The fluoroquinolones act as type II topoisomerase inhibitors in this case. The inhibition of transcription might also be toxic by inhibiting expression of essential genes, resulting in secondary cell death (Collins & Osheroff, 2024).
The second toxic mechanism is observed at higher drug concentration:MIC-ratios where the fluoroquinolones act as topoisomerase poisons (Bush et al., 2020). The cleaved complexes are either resolved by dissociation of the fluoroquinolone or removed by a protein, potentially a nuclease, helicase or exonuclease (Aedo & Tse-Dinh, 2013; Chen et al., 1996; Huang et al., 2021; Malik et al., 2006; Shea & Hiasa, 2003). The removal of the trapped complexes leaves behind a fragmented chromosome that needs to be repaired by DNA repair enzymes. This induces the SOS-response, mutagenesis, and finally leads to cell death (Cirz et al., 2006; López & Blázquez, 2009; López et al., 2007; Tamayo et al., 2009). It was also proposed that part of the killing mechanism of fluoroquinolones is driven by the formation of reactive oxygen species (ROS) (Dwyer et al., 2007; Foti et al., 2012), however, the actual impact of this effect is still under debate and investigation (Dwyer et al., 2015; Hong et al., 2020; Hong et al., 2019; Keren et al., 2013; Liu & Imlay, 2013).

The used fluoroquinolones for *P. aeruginosa* infections are ciprofloxacin and levofloxacin (The European Committee on Antimicrobial Susceptibility Testing, 2024). 10.9% of *P. aeruginosa* isolates from stationary patients in Germany were resistant to ciprofloxacin and 15.9% to levofloxacin (Robert Koch Institut, ARS, https://ars.rki.de, Retrieved: 18.04.2024).
Ciprofloxacin shows a clear AUC/MIC-dependent antibacterial relationship, meaning that the ratio of the area under the concentration time curve of ciprofloxacin in the serum and the MIC of the bacterium to be treated (AUIC) is predictive of successful treatment. Forrest et al. (1993) described a ratio of 125 SIT^{-1} (inverse serum inhibitory titer integrated over time) to be a significant breakpoint of treatment success.
As reviewed by Anwar et al. (2024), the fluoroquinolones have been associated with severe side-effects in the recent years. These include tendinitis and tendon rupture, myopathy, as well as cardiac side effects such as increased risk for aortic aneurism and dissection. Furthermore, neurological side effects such as depression and fatigue were described. This led to the coining of the term Fluoroquinolone-Associated Disability (FQAD) and to issued use limitations by

regulatory bodies such as the german BfArM (Bundesamt für Arzneimittel und Medizinprodukte, 2019).

1.2.3. Aminoglycosides

Another group of agents that is commonly used to treat *P. aeruginosa* infections are aminoglycosides. The commonly used aminoglycosides are amikacin, gentamicin, and tobramycin, with amikacin and tobramycin being used preferably (The European Committee on Antimicrobial Susceptibility Testing, 2024). In 2022, 1.9%, 14.9% and 2.3% of *P. aeruginosa* isolates from stationary patients in Germany were resistant to amikacin, gentamicin and tobramycin respectively (Robert Koch Institut, ARS, https://ars.rki.de, Retrieved: 18.04.2024).

Aminoglycosides bind to the 16S rRNA of the 30S subunit of the ribosome, leading to misreading of the mRNA and binding of the incorrect tRNA. Wrong amino acids are integrated in the nascent peptide, leading to nonsense proteins and cell death. (Becker & Cooper, 2013)

As aminoglycosides are not relevant for this study, they will not be discussed in more detail here.

1.2.4. Combination therapy

For severe infections with difficult to treat pathogens such as *P. aeruginosa,* a combination of two active antibacterial substances, known as double coverage, is often considered and used. The rationale for a combination therapy arises from three different considerations: i) Utilization of a synergistic effect of two antibiotics to increase the odds for a positive outcome of a patient infected with a resistant strain, ii) combination of two antibiotics with different spectra in initial empiric therapy until susceptibility testing is done might increase the odds of successfully targeting a potentially resistant strain, and iii) prevention of the emergence of antibiotics resistance. Combination therapy for *P. aeruginosa* typically consists of a β-lactam antibiotic and an aminoglycoside or a β-lactam and a fluoroquinolone. (Johnson et al., 2011)

The efficacy of such combination therapies in *P. aeruginosa* and other Gram-negative pathogens has been assessed in several *in vitro* studies, clinical studies, and meta-analyses with mixed results and this practice remains controversial (Paul et al., 2004; Paulsson et al., 2017; Tamma et al., 2012; Vardakas et al., 2013). It was also described that using a combination therapy of a β-lactam with ciprofloxacin in *P. aeruginosa* might select for mutant strains that are resistant to a broad-spectrum of antibiotics, mainly due to a mutation in the MexAB-OprM efflux pump repressor *mexR* and (Vestergaard et al., 2016). This could potentially be due to SOS-induced mutagenesis by error prone polymerases following DNA damage resulting from ciprofloxacin treatment (Cirz et al., 2006).

Due to the conflicting clinical evidence for the efficacy of combination therapy, and the potential for increased adverse events and emergence of resistance, the general guidelines for the treatment of MDR *P. aeruginosa* infections suggest using *in vitro*-active novel β-lactams and β-lactamase inhibitors rather than combinations of older antibiotics that might show synergism *in vitro* (Paul et al., 2022; Tamma et al., 2021). Antibiotic combinations should in general only be used to broaden the antibacterial spectrum in early empiric therapy of severe infections until susceptibility testing is done to then deescalate to an *in vitro* active substance in monotherapy. The only exception is the treatment with polymyxins, aminoglycosides or fosfomycin that tested as active *in vitro*. These drugs should generally be combined with a second *in vitro* active drug (Paul et al., 2022; Tamma et al., 2021).

1.3. Antimicrobial resistance in *P. aeruginosa*

P. aeruginosa is known for its high intrinsic resistance to antibiotics and its ability to rapidly develop resistance. Resistance to antibiotics is mediated by intrinsic factors as well as by acquired resistance factors. *P. aeruginosa* has high intrinsic resistance, especially due to its tight outer membrane (OM), inducible expression of efflux pumps, the chromosomally encoded β-lactamase AmpC, and the ability to form biofilm. Additionally, resistance can be acquired by mutation in target genes, regulatory genes, or by plasmid-mediated resistance factors encoding for drug degrading enzymes. I will touch shortly on the outer membrane, efflux pumps, biofilms, and mutation and then focus mainly on AmpC-mediated resistance.

1.3.1. The outer membrane

The permeability of the OM of *P. aeruginosa* for hydrophilic solutes has been estimated to be about 100-fold lower than for *E. coli* (Yoshimura & Nikaido, 1982), reducing influx of antibiotics. Hydrophilic compounds mainly cross the outer membrane by water filled porins, and the main porin of *P. aeruginosa*, OprF, was described to exhibit a much lower permeability than porins in other species (Sugawara et al., 2012). Hydrophobic substances generally cross the outer membrane by passive diffusion, however, LPS forms a tightly packed barrier, reducing passive diffusion (Snyder & McIntosh, 2000). OprD is a porin that is important for the influx of carbapenems, and loss or downregulation of *oprD* was associated with reduced susceptibility to these antibiotics (Köhler, Michea-Hamzehpour, et al., 1999). As reviewed by Lister et al. (2009), reduced levels of OprD can be caused by mutations in the promoter, premature termination, mutations in the CDS, exposure to zinc or copper, or by coregulation with the *mexEF-oprN* efflux pump. It was described that the positive regulator of the *mexEF-oprN* efflux pump MexT negatively regulates *oprD* (Köhler, Epp, et al., 1999; Ochs et al., 1999).

1.3.2. Efflux pumps

While in total 12 efflux pumps that facilitate active export of substances have been described in *P. aeruginosa* (Aeschlimann, 2003; Lister et al., 2009), the main efflux pumps in antibiotic resistance are the MexAB-OprM, MexCD-OprJ, MexEF-OprN, and MexXY efflux pumps. Except for MexXY, each of these efflux pumps consists of a periplasmic membrane fusion protein, a cytoplasmic membrane transporter, and an outer membrane factor (Lister et al., 2009).

The efflux pumps relevant in this study are the MexAB-OprM and MexEF-OprN efflux pumps. MexAB-OprM has the broadest spectrum for the export of β-lactam antibiotics and β-lactamase inhibitors and exports ceftazidime, piperacillin, aztreonam and meropenem. Imipenem and cefepime are not substrates of MexAB-OprM. Furthermore, fluoroquinolones, tetracyclines, chloramphenicol, and macrolides are exported by MexAB-OprM (Aeschlimann, 2003; Lister et al., 2009; Poole & Srikumar, 2001). MexAB-OprM is expressed constitutively in wildtypes and confers intrinsic resistance (Li et al., 1995; Poole et al., 1993). Mutations in the genes *mexR* and *nalD,* encoding for repressors of *mexAB-oprM,* are associated with overexpression of the efflux pump and increased resistance to the substrate antibiotics (Adewoye et al., 2002; Saito et al., 2003; Sobel et al., 2005). Additionally, a mutation in *nalC* leads to overexpression of *armR,* encoding for a protein that interacts with MexR and prevents repression (Cao et al., 2004).

The main substrates of MexEF-OprN are fluoroquinolones, chloramphenicol, and trimethoprim (Köhler et al., 1997). *mexEF-oprN* is expressed at a low level in wildtype strains and the corresponding efflux pump does not play a role in intrinsic resistance (Köhler et al., 1997; Li et al., 2000). *mexEF-oprN* is regulated by a positive regulator, *mexT* (Köhler, Epp, et al., 1999). MexEF-OprN is overexpressed in so called *nfxC*-type mutants, where the wildtype-inactive *mexT* is activated by mutations (Maseda et al., 2000). *nfxC*-type mutants also generally show reduced expression of *oprD* due to the effect of MexT described above and are therefore resistant to carbapenems (Köhler, Epp, et al., 1999; Ochs et al., 1999). Interestingly, MexT was also described to reduce expression of the *mexAB-oprM* efflux pump and to mediate hypersusceptibility to β-lactams in *nfxC* type mutants (Maseda et al., 2004). Overexpression of *mexEF-oprN* was furthermore described to be caused by mutations in *mexS* or *mvaT* (Sobel et al., 2005; Westfall et al., 2006).

Lastly, instead of encoding an outer membrane factor, the MexXY efflux pump is able to associate with the porin OprM (Aires et al., 1999). Substrates are the aminoglycosides, fluoroquinolones, tetracycline, chloramphenicol, erythromycin, and cefepime (Aeschlimann, 2003; Lister et al., 2009). A mutation in the repressor *mexZ* leads to overexpression of the efflux pump (Islam et al., 2004; Vogne et al., 2004).

1.3.3. Biofilms and persister cells

When *P. aeruginosa* cells enter the biofilm state, they become strongly resistant to antibiotics. The underlying mechanisms mediating this resistance are multifaceted and currently under investigation as reviewed by Fernández-Billón et al. (2023). Selected mechanisms are reduced drug penetration, upregulation of efflux pumps, horizontal gene transfer, and induction of AmpC.

Persister cells are frequently observed in biofilms (Wood et al., 2013). They build up a small subfraction of the population that is tolerant to an antibiotic, even if the strain is susceptible to this antibiotic (Wilmaerts et al., 2019). Generally, the effect of antibiotic tolerance of persister cells is attributed to a dormancy of the cells and strongly reduced metabolism, leading to the loss of activity of antibiotics that act on metabolically active cells such as β-lactam antibiotics or fluoroquinolones (Lewis, 2010). Upon cessation of treatment, these persisting subpopulations awake and are able to start reproducing again, leading to treatment failure of chronic infections, for example in patients with cystic fibrosis that are infected with *P. aeruginosa* (Mulcahy et al., 2010). The mechanisms on how bacteria enter persister state and how awakening is mediated is currently under investigation and reviewed by Wilmaerts et al. (2019).

1.3.4. Resistance by mutation

Mutation in target genes as well as in regulatory genes leading to overexpression of resistance factors is another pathway by which *P. aeruginosa* and other bacteria can acquire resistance. Resistance to fluoroquinolones, for example, is often mediated by point mutations in the *gyrA, gyrB* or *parC* genes, leading to reduced affinity of these antibiotics (Feng et al., 2019; Higgins et al., 2003). A study by Cabot et al. (2012) identified AmpC-overproduction, OprD-inactivation, mutations in *gyrA* and *parC,* and a mutation in *mexZ* to be the predominant mutation markers of multidrug resistant *P. aeruginosa*. Henrichfreise et al. (2007) similarly described *gyrA* mutations, MexXY-overexpression, loss of OprD, and AmpC overexpression to be the most frequent mechanisms of resistance by mutation.

The hypermutator phenotype in *P. aeruginosa* is characterized by an increased mutation rate compared to wildtype strains, leading to faster development of resistance due to mutations in

certain resistance genes and higher rates of multi drug resistance in mutator strains (Blázquez, 2003; Maciá et al., 2005). The hypermutable phenotype typically evolves as a response to mutation in genes that play a role in DNA repair such as mismatch repair (*mutS*, *mutL, uvrD*) (Montanari et al., 2007; Oliver et al., 2002; Rees et al., 2019). In addition, mutations in the genes *mutT, mutM* and *mutY,* which are part of the DNA oxidative repair system GO, have also been shown to lead to hypermutable strains (Mandsberg, Ciofu, Kirkby, Christiansen, Poulsen, & Høiby, 2009). The lungs of CF patients in particular seem to be often colonized by hypermutator strains, likely due to the increased pressure to adapt in the CF lung (Ciofu et al., 2005; Maciá et al., 2005; Montanari et al., 2007; Oliver et al., 2000; Rees et al., 2019).
The fluoroquinolone ciprofloxacin induces DNA damage by binding to gyrase and topoisomerase IV as described in 1.2.2. In *P. aeruginosa,* DNA damage caused by ciprofloxacin leads to induction of the error-prone polymerases *imuABC* and *dinB* and *dnaE2*, with *imuABC* and *dnaE2* being controlled by the LexA-mediated SOS-response (Blázquez et al., 2006; Cirz et al., 2006). It was shown that exposure to subinhibitory levels of ciprofloxacin increases the mutation frequency in *P. aeruginosa*, *E. coli* and *Streptococcus pneumoniae* (Henderson-Begg et al., 2006; Thi et al., 2011; Valencia et al., 2017). However, Torres-Barceló et al. (2015) have shown that while exposure to subinhibitory concentrations of ciprofloxacin over longer periods of time leads to increased evolution of resistance, this is not mediated by the SOS-response.

1.3.5. AmpC-mediated β-lactam resistance

1.3.5.1. Synthesis of peptidoglycan

As described in 1.2.1, the murein sacculus of Gram-negative bacteria consists of polymeric peptidoglycan that is made up of β-(1,4)-glycosidically linked alternating amino sugars, namely MurNAc and GlcNAc. MurNAc carries a peptide sidechain that is crosslinked between the third amino acid m-DAP and the fourth amino acid D-Ala to form a mesh that confers stability to withstand osmotic pressure (Lima et al., 2020; Tipper, 1979; Waxman & Strominger, 1983).

Peptidoglycan is synthesized starting with fructose-6-phosphate. The enzymes GlmS, GlmM and GlmU generate the intermediate uridine diphosphate-GlcNAc (UDP-GlcNAc) (Badet et al., 1987; D. Mengin-Lecreulx & J. van Heijenoort, 1996; Dominique Mengin-Lecreulx & Jean van Heijenoort, 1996), which is then turned into UDP-MurNAc by the enzymes MurA and MurB, an enolpyruvyl transferase and a reductase (Barreteau et al., 2008). The Mur ligases MurC, MurD, MurE, and MurF then sequentially add L-alanine (MurC), D-glutamic acid

(MurD), m-DAP in Gram-negatives (MurE), and a D-Ala-D-Ala as a dipeptide to finally form UDP-MurNAc-pentapeptide (UDP-MurNAc-5P) (Barreteau et al., 2008).

MraY then tethers UDP-MurNAc-pentapeptide to undecaprenol pyrophosphate that is bound to the inner leaflet of the inner membrane, removing the UDP moiety, and forming Lipid I in the process (Bouhss et al., 2004). The protein MurG then forms the β-(1,4)-glycosidal link between MurNAc and GlcNAc by adding a GlcNAc moiety to the membrane anchored MurNAc-pentapeptide using UDP-GlcNAc as a substrate (Mengin-Lecreulx et al., 1991). This forms Lipid II that is subsequently flipped to the outer leaflet of the inner membrane by a flippase, whose identity is still under investigation. Two likely candidates are MurJ and FtsW (Egan et al., 2020).

In the periplasmic space, the GlcNAc-MurNac-pentapeptide is integrated into the peptidoglycan. By means of their transglycosylase activity, the high molecular mass penicillin-binding proteins (HMM PBP) PBP1a and PBP1b form a β-(1,4)-glycosidal link between the MurNAc-moiety of the imported GlcNAc-MurNAc-pentapeptide and the GlcNAc-moiety of the peptidoglycan strand (Handfield et al., 1997; Ishino et al., 1980; Suzuki et al., 1980; Terrak et al., 1999). The HMM PBPs PBP1a, PBP1b, PBP2, PBP3 (Chen et al., 2017; Legaree et al., 2007), and, in *P. aeruginosa*, PBP3a (Liao & Hancock, 1997) then form the aforementioned crosslinks between the peptidoglycan chains by attaching the m-DAP moiety of the acceptor peptide to the penultimate D-Ala moiety of the donor peptide, releasing the terminal D-Ala in the process.

1.3.5.2. The peptidoglycan recycling pathway

The peptidoglycan recycling pathway is a mechanism by which bacteria are able to recycle degradation products of the cell wall. During growth, the cell wall is continuously remodeled and degraded to allow for the formation of septa, the integration of new PG-strands and the expansion of the cell (Dik et al., 2018). As reviewed by Park and Uehara (2008), around 60% of the bacterial cell wall is recycled in each generation. In addition, degradation products of the cell wall arise under pressure by β-lactam antibiotics as PBPs are inhibited. Several types of lytic enzymes in the periplasm lead to cell wall degradation products that feed into the peptidoglycan recycling pathway in *P. aeruginosa*.

Lytic transglycosylases (LTs) degrade the murein sacculus by cleaving off GlcNAc-1,6-anhydro-MurNAc (anhMurNAc) and allow for insertion of flagella and secretion systems, remodeling of PG, and aid in division (Heidrich et al., 2002; Höltje et al., 1975; reviewed in Scheurwater et al., 2008). Eleven LTs have been described in *P. aeruginosa* (Dhar et al., 2018) and deletion of the LTs *mltG*, *slt*, *mltF,* and *mltD* was described to reduce resistance to β-lactam antibiotics by reducing *ampC* expression (Sonnabend et al., 2020).

1. Introduction

Cell wall amidases in the periplasm cleave the peptide chain from MurNAc moieties that are anchored in the cell wall as well as from soluble moieties that have already been removed from the cell wall, for example by LTs. There are in total three periplasmic amidases in *P. aeruginosa*: AmiA, AmiB, and AmpDh2. AmiA and AmiB are functional homologs of the *E. coli* amidases AmiA and AmiB that share *N*-acetylmuramyl-L-alanine amidase function, i.e. cleaving the peptide chain from sacculus bound MurNAc (Heidrich et al., 2001; Scheurwater et al., 2007; Tomioka et al., 1983). In *P. aeruginosa,* AmiB is essential for survival and plays an important role in cell separation and in upkeep of the low permeability of the outer membrane. In contrast, AmiA is nonessential, unlike to its homolog in *E. coli* (Yakhnina et al., 2015). The *P. aeruginosa* homolog of AmiD in *E. coli* is AmpDh2. It is located in the periplasm, tethered to the outer membrane and has activity on sacculus bound MurNAc-peptides and on soluble anhMurNac-peptides that are products of LTs (Juan et al., 2006; Zhang et al., 2013). AmpDh2 has two paralogs, AmpD and AmpDh3. AmpDh3 has previously been described to also be located in the periplasmic space (Zhang et al., 2013), however, data of our group (Eggers et al., 2023) and by Colautti et al. (2023) located AmpDh3 in the cytoplasm, together with the paralog AmpD.

The low molecular mass penicillin-binding proteins (LMM PBP) have carboxypeptidase and endopeptidase activity and thereby cleave the terminal D-Ala from a pentapeptide or hydrolyze the crosslink between the peptide sidechains respectively as reviewed by Sauvage et al. (2008). In *P. aeruginosa*, three LMM PBPs have been described and characterized: *dacB* encodes for PBP4, *dacC* for PBP5, and *pbpG* encodes for PBP7 (Dhar et al., 2018). PBP5 has carboxypeptidase activity, PBP7 endopeptidase activity, and PBP4 has both carboxy- and endopeptidase activity (Ropy et al., 2015).

The PG degradation products (muropeptides) of the various enzymes present in the periplasmic space are transported across the inner membrane into the cytoplasm by the permease AmpG and potentially its paralog AmpP. However, the exact role of AmpP could so far not be elucidated (Kong et al., 2010; Perley-Robertson et al., 2016).

In the cytoplasm, the muropeptides are further metabolized to anhMurNAc to finally feed into the anabolic pathway of peptidoglycan as an alternative source of UDP-GlcNAc by the proteins NagZ, LdcA, and AmpD (Dhar et al., 2018).

NagZ has β-*N*-acetylglucosaminidase activity (Stubbs et al., 2008) and therefore cleaves GlcNAc-anhMurNAc-peptides at the GlcNAc-anhMurNAC bond, which results in GlcNAc and anhMurNAc-peptides (Acebrón et al., 2017; Yem & Wu, 1976).

anhMurNAc-peptides and GlcNAc-anhMurNAc-peptides are metabolized by the amidase AmpD. This amidase removes the peptide stem from anhMurNAc-peptides, yielding anhMurNAc, or GlcNAc-AnhMurNAc, depending on the substrate. AmpD has a higher affinity to anhMurNAc-peptides than to GlcNAc-anhMurNAc-peptides, however (Jacobs et al., 1995; Lee et al., 2016; Zhang et al., 2013).

Lastly, LdcA is an LD-carboxypeptidase that mainly modifies anhMurNAc-tetrapeptides (anh-MurNAc-4P), the most abundant muropeptide in the peptidoglycan (Glauner et al., 1988), by cleaving off the terminal D-Ala to form anhMurNAc-tripeptides (anhMurNAc-3P) (Korza & Bochtler, 2005; Templin et al., 1999). The tetrapeptides are products of PBPs with DD-carboxy-peptidase activity such as PBP4 and PBP5 (see above).

The anhMurNAc generated by the three enzymes NagZ, LdcA, and AmpD is then further metabolized in the so-called salvage pathway to generate UDP-MurNAc in *P. aeruginosa* (Borisova et al., 2014; Gisin et al., 2013). Additionally, in *E. coli*, the tri-, tetra- and pentapeptides that were cleaved off by AmpD can be transferred directly to UDP-MurNAc by the murein peptide ligase Mpl (Hervé et al., 2007; Mengin-Lecreulx et al., 1996). While a homolog of Mpl exists in *P. aeruginosa*, the exact role of this ligase has not been studied so far (Dhar et al., 2018).

anhMurNAc is phosphorylated by AnmK to form MurNAc-6-phosphate. MupP then removes the phosphate to form MurNAc. MurNAc is again phosphorylated by AmgK, but at position 1 to form MurNAc-1-phosphate which is then transformed by MurU to form UDP-MurNAc. (Bacik et al., 2011; Borisova et al., 2014, 2017; Fumeaux & Bernhardt, 2017; Gisin et al., 2013) The generated UDP-MurNAc is then reused in the synthesis of peptidoglycan, circumventing *de novo* synthesis.

1.3.5.3. The link between AmpC and peptidoglycan recycling

The cephalosporinase AmpC is an ambler class C β-lactamase or a group 1 β-lactamase according to an updated definition (Ambler, 1980; Bush & Jacoby, 2010; Bush et al., 1995). AmpC is located in the periplasm and is encoded chromosomally in most Enterobacteriaceae as well as in other clinically important Gram-negative species such as *P. aeruginosa* and *A. baumannii*, but can also be plasmid-encoded (reviewed in Jacoby, 2009). The cephalosporins are the preferred substrate of the AmpC β-lactamases, but AmpC can also degrade penicillins, monobactams, and carbapenems, albeit at a lower or much lower rate, depending on the substance (Galleni et al., 1988; Galleni & Frère, 1988; Gates et al., 1986; Murata et al., 1981).

1. Introduction

Resistance mediated by AmpC can generally be classified into four mechanisms: (i) inducible resistance by chromosomal encoded *ampC* in response to β-lactam antibiotics, (ii) stable over-expression of *ampC* by mutation, (iii) noninducible resistance by chromosomally encoded *ampC* genes, and (iv) plasmid encoded *ampC* genes that can be constitutively overexpressed (Jacoby, 2009).

Resistance by induction of *ampC* genes and stable overexpression of *ampC* are the main mechanisms relevant to this study and are linked to the peptidoglycan recycling pathway explained before (1.3.5.1). The degradation of the cell wall by β-lactams leads to the emergence of GlcNAc-anhMurNAc-peptides, which are further catabolized into anhMurNAc-peptides by removal of the GlcNAc-moiety. In the cytoplasm, anhMurNAc-peptides displace UDP-MurNAc-pentapeptides from AmpR, the transcriptional regulator of *ampC*, and induce a conformational shift. Under non-inducing conditions, when primarily bound to UDP-MurNac-pentapeptides, AmpR represses *ampC* to very low levels. The conformational change in AmpR upon binding anhMurNAc-peptides leads to derepression of *ampC* and increased expression (Jacobs et al., 1997; Jacobs et al., 1994).

As anhMurNAc-peptides are degraded by the amidase AmpD, cleaving the stem peptide off the anhMurNAc-peptides and reducing their concentration (Jacobs et al., 1994), mutations in *ampD* are a frequent cause for constitutive overexpression of AmpC (Schmidtke & Hanson, 2006). Mutations in the *ampR* gene are also associated with a stable overexpression of *ampC* (Kaneko et al., 2005; Kuga et al., 2000; Tam et al., 2007).

E. coli, *A. baumannii* and *Shigella* spp. lack AmpR, which results in a β-lactam-uninducible *ampC* β-lactamase, which at least in *E. coli* is regulated as a function of growth rate by a promoter and an attenuator (Bergström et al., 1982; Bou & Martínez-Beltrán, 2000; Honoré et al., 1986; Jaurin et al., 1981).

As alluded to earlier, production of the AmpC β-lactamase can be induced by β-lactam antibiotics. The inducing capacity of β-lactam antibiotics as well as their stability towards hydrolysis by AmpC differs from compound to compound (Livermore & Yang, 1987; Sanders & Sanders, 1986), which can likely be explained by different affinity to the plethora of penicillin-binding proteins, leading to different compositions of *ampC*-inducing catabolites (Sanders et al., 1997). As reviewed by Macdougall (2011) and Meini et al. (2019), ampicillin, and the first generation cephalosporins, cefoxitin and cefotetan are strong inducers as well as good substrates of AmpC, enabling *P. aeruginosa* and enterobacteria with inducible *ampC* to be intrinsically resistant to these antibiotics. Ceftazidime, ceftriaxone, cefotaxime, piperacillin, ticarcillin, and aztreonam

are good substrates but weak inducers of AmpC production. *P. aeruginosa* wildtype is susceptible to ceftazidime, piperacillin, ticarcillin and aztreonam but ceftriaxone and cefotaxime are generally not active against *P. aeruginosa* (The European Committee on Antimicrobial Susceptibility Testing, 2024*)*. Imipenem is a strong inducer but poor substrate, and cefepime and meropenem are both weak inducers and poor substrates. Therefore, *P. aeruginosa* wildtype is susceptible to these β-lactams. The use of *ampC*-inducing β-lactams can select for mutants that stably overexpress *ampC* by mutations in the above mentioned *ampD, ampR,* or *dacB* in *P. aeruginosa* (Bagge et al., 2002; Moya et al., 2009; Schmidtke & Hanson, 2006, 2008; Tam et al., 2007; Tamma et al., 2019). While older β-lactamase inhibitors show no activity against AmpC, the novel β-lactamase inhibitors avibactam, relebactam, and vaborbactam are active against AmpC β-lactamases (de Jonge et al., 2016; Hirsch et al., 2012; Tooke et al., 2019; Wong & van Duin, 2017; Zhanel et al., 2018).

The regulation of AmpC in *P. aeruginosa* differs from that in enterobacteria as it is more complex. For one, next to *ampD* present in enterobacteria, *P. aeruginosa* carries two additional paralogs that also degrade anhMurNAc-peptides, *ampDh2* and *ampDh3*. Additional deletion of these paralogs is associated with a stepwise increased *ampC* expression and resistance to β-lactam antibiotics (Juan et al., 2006). The authors proposed that depending on the deletion of *ampD* paralogs, four different *ampC* phenotypes in *P. aeruginosa* might exist: (i) an *ampC*-inducible phenotype with basal *ampC* expression (all three paralogs intact), (ii) an *ampC*-hyperinducible phenotype with moderate baseline increased *ampC* expression (Δ*ampD*), (iii) an *ampC*-hyperinducible phenotype with high levels baseline *ampC* expression (Δ*ampD*Δ*ampDh3*), and (iv) a completely derepressed phenotype with extremely high level *ampC* expression (Δ*ampD*Δ*ampDh2*Δ*ampDh3*).
Next to the typically described mutations leading to *ampC* overexpression (*ampD*, *ampR)*, in *P. aeruginosa* a mutation in the gene *dacB,* encoding for the low-molecular mass penicillin binding protein PBP4, leads to stable overexpression of *ampC* (Moya et al., 2009). Work by Torrens et al. (2019) has shown that a mutation in the *dacB* gene mostly leads to accumulation of anhMurNAc-pentapeptides (anhMurNAc-5P), while an *ampD* mutation mainly leads to accumulation of anhMurNAc-3P. Deletion of *dacB* has similar effects to exposure to the β-lactam cefoxitin, which also inhibits PBP4. PBP4 is a bifunctional enzyme with DD-carboxypeptidase and 4,3-endopeptidase activity, with the DD-carboxypeptidase trimming the terminal D-Ala off the peptide stem, while the 4,3-endopeptidase cleaves the 4,3-crosslink of muropeptides (Lee et al., 2015). Therefore, loss of the DD-carboxypeptidase activity explains the accumulation of

anhMurNAc-5P, which would otherwise be degraded by PBP4 and the increased *ampC* production observed by Torrens et al. (2019) upon loss of *dacB*.

In *P. aeruginosa,* AmpR does not only regulate AmpC expression, but acts as a global transcriptional regulator. Kong et al. (2005) described that AmpR negatively regulates PoxB β-lactamases, pyocyanin production, production of the staphylolytic protease LasA, and the genes *lasI* and *lasR*. Furthermore, the authors described that AmpR positively regulates the levels of LasB elastase, although indirectly, and the repressor of the quorum sensing genes *rhlR*. Balasubramanian et al. (2012) described 313 differentially expressed genes upon deletion of *ampR* in PAO1 and 207 additional differentially expressed genes if the cells were exposed to a β-lactam, inducing AmpR activity. The authors reported that the efflux pump MexEF-OprN is negatively regulated by AmpR, and that the efflux pump MexAB-OprM and the porin OprD might be positively regulated, all via MexT, although independent of β-lactam-induced activity of AmpR. In addition, Balasubramanian et al. (2012) reported that AmpR positively regulates quorum sensing, pyocin, and pyocyanin production and also regulated biofilm formation negatively. In addition, they described that AmpR also regulates expression of the permeases AmpG and AmpP, which have been introduced previously in this thesis.

1.3.5.4. AmpDh3 in *P. aeruginosa*

AmpDh3 is one of the two paralogs of AmpD in *P. aeruginosa* (Juan et al., 2006). AmpDh3 is a tetrameric enzyme with a central zinc ion, which was described to degrade cell wall-bound peptidoglycan as well as soluble cell wall degradation products by cleaving the peptide moiety from (anh)MurNAc-peptides, either within the larger PG polymer or as soluble degradation products (Lee et al., 2013; Zhang et al., 2013). AmpDh3 was first described to be a periplasmic protein, based on the affinity to synthetic substrates (Zhang et al., 2013). However, data by Colautti et al. (2023) and by our group (Eggers et al., 2023) has provided evidence that AmpDh3 localizes to the cytoplasm.

Furthermore, Wang et al. (2020) described AmpDh3 to be a toxic effector of the type VI secretion system (T6SS), with the gene PA0808 downstream of *ampDh3* encoding the cognate immunity protein. Colautti et al. (2023) and work done by our group, however, could not reproduce these findings. AmpDh3 was previously described by Moya et al. (2008) to play a role in virulence of *P. aeruginosa* in a mouse model of systemic infection, while the paralogs AmpD and AmpDh2 had no marked effect on the virulence of *P. aeruginosa*.

ampDh3 was described to be positively regulated by the antiterminator AlpA that also regulates the *alpBCDE* self-lysis cluster (McFarland et al., 2015; Peña et al., 2021). AlpA and the effect on *ampDh3* will be introduced further in 1.4.3.

1.4. Previous work on the role of YgfB in antibiotic resistance

1.4.1. YgfB as a mediator of resistance to β-lactams

In an attempt to identify contributors to β-lactam resistance using a transposon-directed insertion sequencing approach, Sonnabend et al. (2020) first described *ygfB* to contribute to β-lactam resistance in the multi drug resistant *P. aeruginosa* isolate ID40. ID40 is a clinical blood stream isolate that was described to be susceptible to meropenem at an increased dose and resistant to most other commonly used antipseudomonal β-lactam antibiotics (piperacillin, piperacillin-tazobactam, cefepime, ceftazidime, aztreonam, imipenem) and fluoroquinolones (ciprofloxacin and levofloxacin) with the β-lactam resistance being mediated by a point mutation in the *dacB* gene (Sonnabend et al., 2020; Willmann, Goettig, et al., 2018). A transposon library of ID40 was generated and grown under the selection pressure of either meropenem or cefepime. Determination of the depletion of transposon-inactivated genes in the antibiotic treatment condition vs. a medium control by sequencing allowed to determine genes that became essential under selection pressure exerted by the tested antibiotics (Sonnabend et al., 2020). This led to the identification of *ygfB.* Accordingly, deletion of *ygfB* was associated with reduced resistance to the β-lactam antibiotics meropenem, imipenem, cefepime, ceftazidime, piperacillin, piperacillin/tazobactam, and aztreonam. In addition, expression of the β-lactamase AmpC was reduced upon deletion of *ygfB*. *ygfB* is located in an operon together with the genes *pepP* (PA5224; aminopeptidase), *ubiH* (PA5223; 2-octaprenyl-6-methoxyphenol hydroxylase), TUEID40_03242 (PA5222; hypothetical protein), and *ubiI* (PA5221; 2-octaprenylphenol hydroxylase), with *ubiH* and *ubiI* encoding for essential genes of the ubiquinone biosynthesis (Sonnabend et al., 2020).

1.4.2. YgfB in other γ-proteobacteria

YgfB is found in most γ-proteobacteria, many of which are known as human pathogens. YgfB is found in all the Gram-negative species that belong to the ESKAPE group. Figure 1 (Eggers et al., 2023) shows an alignment of the amino acid sequence of YgfB proteins from several γ-proteobacteria including important pathogens such as *P. aeruginosa*, *E. coli*, *K. pneumoniae,* and *A. baumannii.* To date, two crystal structures have been published, one of YgfB from *Haemophilus influenzae* (PDB ID 1IZM) and one from *Legionella pneumophilia* (PDB ID 4GYT).

1. Introduction

YgfB seems to consist of seven conserved α-helices. Additional research into the structure of a YgfB ortholog in *Haemophilus influenzae* suggested the formation of a homodimer (Galkin et al., 2004).

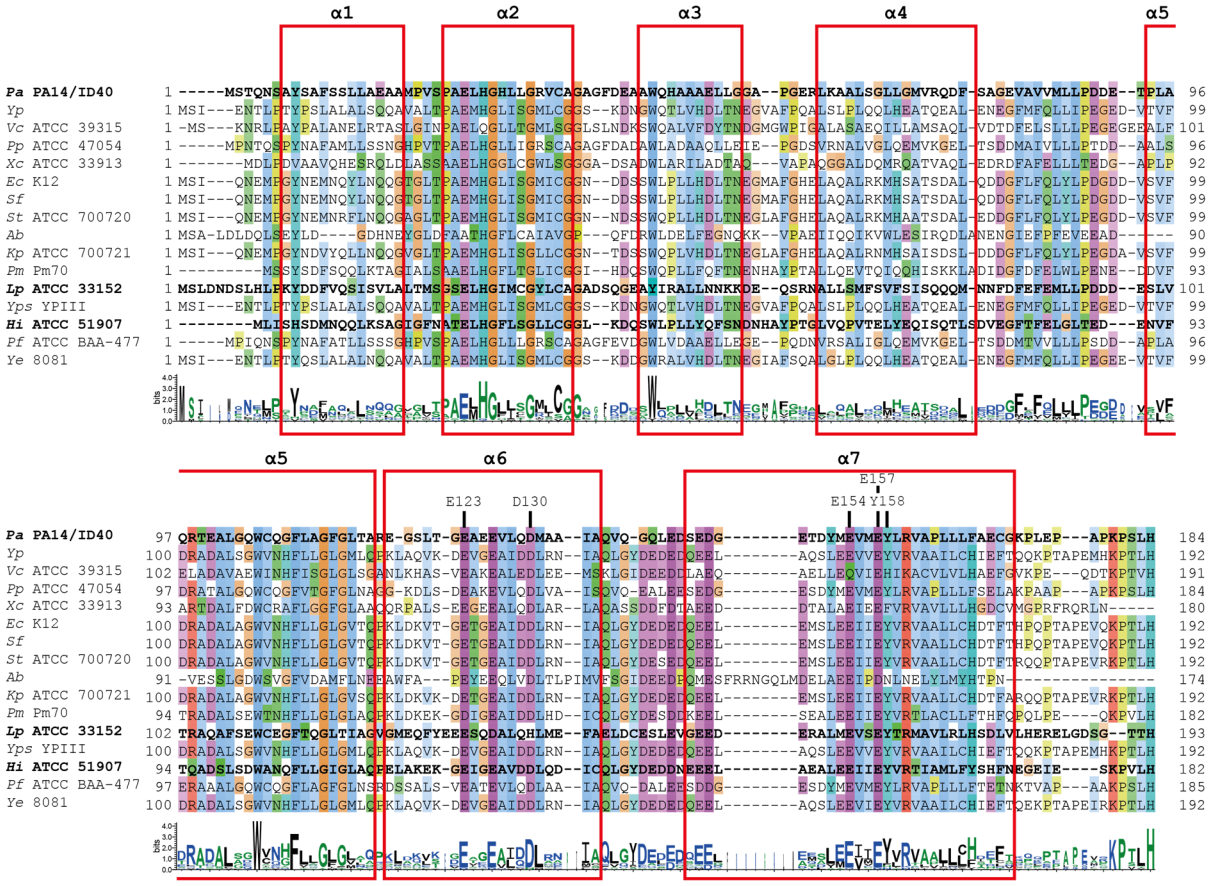

Figure 1: Alignment of YgfB proteins of several γ-proteobacteria. Abbreviation of bacterial strains used in the alignment: **Yp**: *Yersinia pestis;* **Vc ATCC 39915:** *Vibrio cholerae* serotype O1, strain ATCC 39315 / El Tor Inaba N16961*;* **Pp ATCC 47054:** *Pseudomonas putida,* strain ATCC 47054 / DSM 6125 / NCIMB 11950 / KT2440; **Xc ATCC 33913:** *Xanthomonas campestris* pv. *campestris,* strain ATCC 33913 / DSM 3586 / NCPPB 528 / LMG 568 / P 25; **Ec K12:** *Escherichia coli*, strain K12; **Sf:** Shigella flexneri; **St ATCC 700720:** *Salmonella* Typhimurium, strain LT2 / SGSC1412 / ATCC 700720, **Ab:** *Acinetobacter baumanii*; **Kp ATCC 700721:** *Klebsiella pneumoniae* subsp. *pneumoniae,* strain ATCC 700721 / MGH 78578; **Pm Pm70:** *Pasteurella multocida*, strain Pm70; **Lp ATCC 33152:** *Legionella pneumophila* subsp. *pneumophila,* strain Philadelphia 1 / ATCC 33152 / DSM 7513; **Yps YPIII:** *Yersinia pseudotuberculosis* serotype O:3, strain YPIII; **Hi ATCC 51907:** *Haemophilus influenzae*, strain ATCC 51907 / DSM 11121 / KW20 / Rd; **Pf ATCC BAA-447:** *Pseudomonas fluorescens,* strain ATCC BAA-477 / NRRL B-23932 / Pf-5; **Ye 8081:** *Yersinia enterocolitica* serotype O:8 / biotype 1B, strain NCTC 13174 / 8081. The conserved α-helices are labeled by red boxes. The sequence of *P. aeruginosa* and the ones with crystal structures available have been highlighted in boldface. The indicated amino acids are the ones described to be important in the dimerization interface of YgfB. The figure was reproduced unaltered from Eggers et al. (2023) under CC BY 4.0 (https://creativecommons.org/licenses/by/4.0/).

1.4.3. The interconnection between YgfB, AlpA and AmpDh3

In an attempt to identify the role of *ygfB* in *ampC* regulation and β-lactam resistance, differential expression analysis by RNAseq was done by our group prior to this study, revealing a limited effect of *ygfB* deletion on the transcriptome of ID40 (Eggers et al., 2023). In total, next to *ygfB*, only eight genes were differentially expressed upon deletion of *ygfB*, with *ampC* being the only

downregulated gene. The amidase *ampDh3* and the gene TUEID40_01954 (PA0808), that is located in the same operon as *ampDh3,* were upregulated. Additionally, the genes *alpBCDE*, which form a self-lysis cluster in *P. aeruginosa* (McFarland et al., 2015; Peña et al., 2021) and TUEID40_01945, encoding for a Glyoxalase-like protein, were significantly upregulated.
Later work prior to this study, analyzing mRNA expression and β-lactamase activity, has shown that YgfB is causal for the downregulation of *ampDh3,* which leads to increased *ampC* expression (Eggers et al., 2023). Using a *ygfB* deletion mutant as well as a conditional deletion mutant where *ygfB* had been reintroduced under the control of a rhamnose-inducible promoter, it was possible to show that mRNA levels of *ampDh3* and TUEID40_01954 responded inversely to increasing levels of *ygfB* in a dose-dependent fashion. Additionally, mRNA levels of *ampC* were positively correlated with the levels of *ygfB* mRNA. Neither the mRNA levels of *ampD* nor *ampDh2* were affected by deletion of *ygfB* and, while identified in the transcriptome, validation of the genes of the *alpBCDE* cluster was not possible, although tendencies of upregulation could be observed. The relationship between the mRNA levels of *ygfB, ampDh3* and *ampC* was also shown in a time-dependent manner, whereby expression of *ygfB* was induced in a conditional *ygfB* deletion mutant by addition of rhamnose, and mRNA was isolated every 30 minutes after induction, for a total of 3 hours. A clear time-dependent inverse relationship between levels of *ygfB* and *ampDh3* could be observed, while *ampC* levels increased in a delayed fashion. Finally, using single and double deletion of mutants of *ygfB*, *ampDh3* and *ampDh3*/*ygfB* and measuring mRNA levels, β-lactamase activity and resistance to β-lactam antibiotics, they were able to show that the upregulation of *ampDh3* is causal for the reduced levels of *ampC* and consequently the reduced resistance observed upon deletion of *ygfB* (Eggers et al., 2023).

A publication by Peña et al. (2021) has described that in the *P. aeruginosa* strain PAO1, expression of the *alpBCDE* cluster and *ampDh3*-PA0808 (TUEID40_01954) is regulated by the antiterminator AlpA. AlpA was described to bind to an AlpA binding element (ABE) on the promoter of *alpB* and *ampDh3* which then allows AlpA to insert into the exit channel of the RNA polymerase (RNAP). This then prevents the formation of hairpin-loops in the nascent RNA (Peña et al., 2021; Wen et al., 2022). As the mechanism of termination by intrinsic terminators is due to formation of these hairpin loops (reviewed by Ray-Soni et al., 2016) and *ampDh3* carries two and *alpB* one intrinsic terminator upstream of the ORF in the promoter region, it was described by Peña et al. (2021) and Wen et al. (2022) that the interaction of AlpA with the RNAP renders the RNAP resistant to intrinsic terminators. Therefore, AlpA influences

the expression of these genes as a positive regulator by allowing the RNAP to read over intrinsic terminators and expressing the genes downstream.

Additionally, it was described that ciprofloxacin-induced DNA damage leads to increased expression of *alpA* and therefore of *alpBCDE,* and *ampDh3* (McFarland et al., 2015; Peña et al., 2021). The LexA-like repressor of *alpA*, AlpR, undergoes autocleavage upon DNA damage and *alpA* is derepressed. This leads to activation of the programmed cell death pathway by *alpBCDE* in a subset of cells in a population as well as to expression of *ampDh3*-PA0808 (McFarland et al., 2015; Peña et al., 2021). The *alpBCDE*-mediated cell lysis pathway has furthermore been described to contribute to pathogenicity by lysis of a subpopulation of the cells which supported colonization in a murine lung model by a potential release of virulence factors (McFarland et al., 2015). The *alpR-alpA-ampDh3* pathway therefore provides a link between DNA damage, self-lysis, and cell wall recycling. Lastly, it was described that AlpA activity is increased by the alarmone guanosine tetraphosphate (ppGpp), which is part of the stringent response, a response mechanism of bacteria to amino acid starvation and other stress factors (Battesti & Bouveret, 2006; Cashel & Gallant, 1969; Haseltine & Block, 1973; Peña et al., 2021; Vinella et al., 2005). ppGpp was also described to be part of a DNA damage response in *E. coli* (Kamarthapu et al., 2016).

Data generated by our group prior to this work showed that YgfB negatively regulates the promoter activity of *ampDh3* at the same upstream region of the *ampDh3* promoter that was defined by Peña et al. (2021) as containing the ABE and being needed for positive regulation of *ampDh3* by AlpA (Eggers et al., 2023). This region is located between -469 bp and -409 bp upstream of the *ampDh3* coding sequence (CDS) and a transcription start site (TSS) located -413 bp upstream of the start codon of the CDS was defined. Additionally, two intrinsic terminators in the *ampDh3* promoter were predicted by Peña et al. (2021), one at position -387 bp upstream of the *ampDh3* CDS and one between -178 bp and -137 bp upstream of *ampDh3*. In their data, the terminator located at position -387 bp had only minor effects on transcription, while the terminator located between -178 bp and -137 bp was mainly responsible for affecting AlpA-mediated *ampDh3* expression. Figure 2a depicts an overview of the features of the *ampDh3* promoter. The experiments done by our group published in Eggers et al. (2023) (Figure 2b) have shown that for negative regulation of *ampDh3* by YgfB, the promoter fragment needs to contain at least the stretch between -464 bp and -1 bp upstream of *ampDh3*, while a fragment containing the -180 bp to -1 stretch showed no promoter activity confirming the results of Peña et al. (2021). In addition, a -77 bp fragment showed YgfB independent *ampDh3* promoter activity, suggesting a second TSS.

1. Introduction

Furthermore, it was shown that for regulation of the entire *ampDh3* promoter (-532 bp) by *ygfB*, the presence of *alpA* was required (Figure 2c). Regulation of the second TSS (-77 bp), however, was independent of both *ygfB* and *alpA* (Eggers et al., 2023).

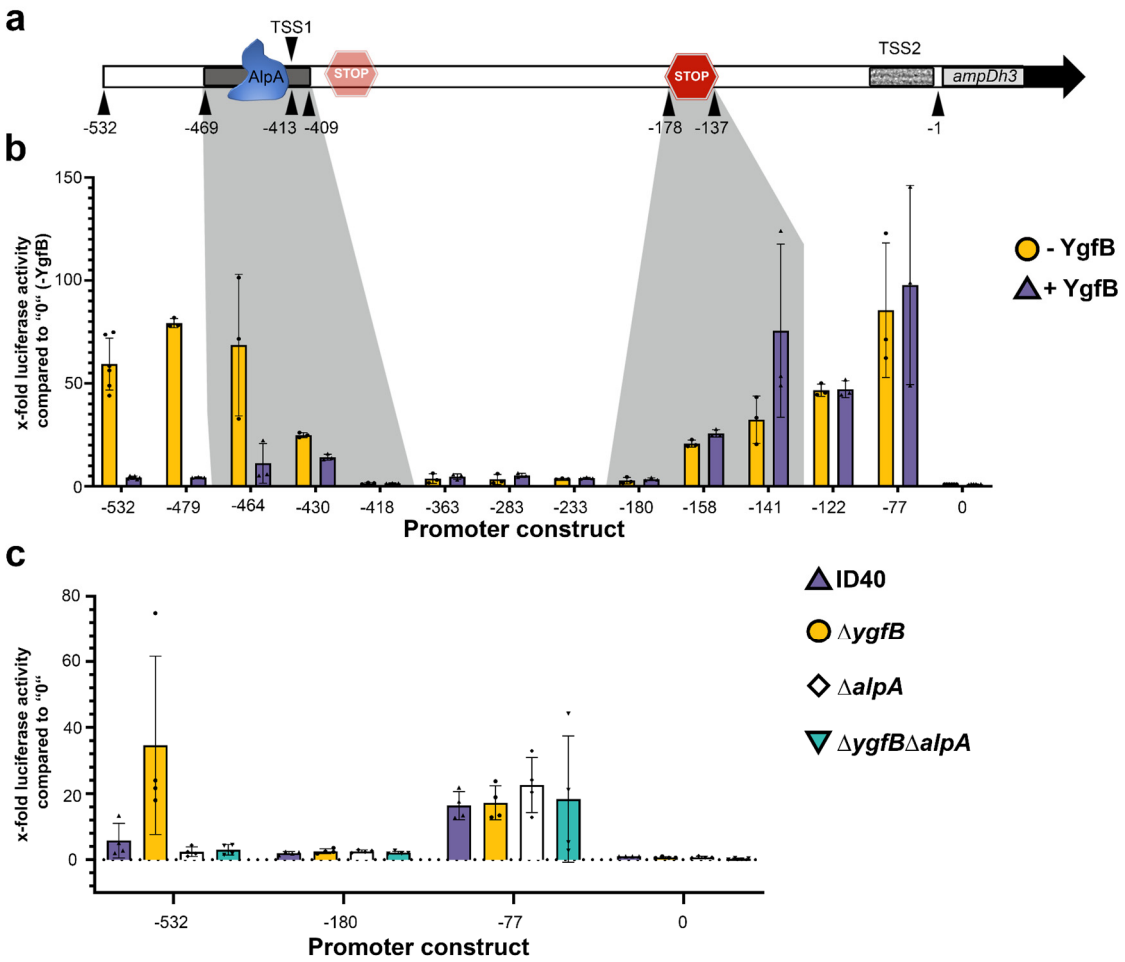

Figure 2: Regulation of the *ampDh3* promoter by YgfB and AlpA. a) A schematic overview of the *ampDh3* promoter, combining data from Peña et al. (2021) with the data generated previously to this work published in Eggers et al. (2023). Numbers blow the promoter stretch depict the basepairs upstream of the *ampDh3* CDS. TSS1 and TSS2 depict putative transcription start sites, while the grey bar with the blue AlpA depicts the ABE. The red STOP signs indicate the intrinsic terminators. **b and c)** Promoter luciferase assays are shown where the indicated promoter fragments (the number indicates the length of the promoter) were fused to the CDS of NanoLuc on the plasmid pBBR1. The respective strains were transformed with this plasmid and luciferase activity was measured (Mean and standard deviation (SD) of x-fold luciferase activity to 0-luc as well as individual data points are shown). **b)** To the strain ID40Δ*ygfB*::rha-*ygfB* carrying the respective plasmids either no rhamnose (-YgfB) or 0.1% rhamnose (+YgfB) was added to induce expression of *ygfB* and luciferase activity was measured. Grey areas indicate how the promoter fragments relate to the promoter depicted in **(a)**. **c)** The strains ID40, ID40Δ*ygfB*, ID40Δ*alpA* and ID40Δ*ygfB*Δ*alpA* were transformed with the respective plasmid and luciferase activity was measured. The figure was reproduced unaltered from Eggers et al. (2023) under CC BY 4.0 (https://creativecommons.org/licenses/by/4.0/).

Taken together, these data have provided evidence that *ygfB* leads to resistance to β-lactam antibiotics by upregulating *ampC*. Upregulation of *ampC* by *ygfB* is caused by repression of *ampDh3*, for which the presence of *alpA* is essential. Additionally, the regulation of *ampDh3* by AlpA and YgfB takes place at the same site of the *ampDh3* promoter.

1.4.4. The effect of YgfB on cell wall derived muropeptides

YgfB represses *ampDh3* in an AlpA-dependent manner and thereby leads to increased expression of *ampC*. As described above, loss of the amidase AmpDh3 is associated with increased *ampC* expression and resistance in PAO1 caused by an altered composition of catabolites of the peptidoglycan recycling pathway (Juan et al., 2006). As previously described, the cell wall recycling products are intimately linked to the expression of *ampC* via the transcriptional regulator AmpR (Jacobs et al., 1997; Jacobs et al., 1994; Torrens et al., 2019). The early recycling products anhMurNAc-3P and anhMurNAc-5P activate *ampC* expression while the late stage recycling product that also arises during *de novo* PG synthesis, UDP-MurNAc-5P, represses *ampC* production. Therefore, the balance between anhMurNAc-3P/-5P and UDP-MurNAc-5P regulates the expression of *ampC* in *P. aeruginosa* (Hanson & Sanders, 1999; Jacobs et al., 1997; Jacobs et al., 1994; Torrens et al., 2019). As described before, AmpDh3 localizes to the cytoplasm (Colautti et al., 2023; Eggers et al., 2023) and was described to degrade soluble 1,6-anhMurNAc-containing-peptides (Lee et al., 2013; Zhang et al., 2013). LC-MS/MS data of our group prior to this study (Figure 3) have shown that the levels of GlcNAc-anhMurNAc-tripeptide (GlcNAc-anhMurNAc-3P), anhMurNAc-3P and anhMurNAc-5P are reduced by deletion of *ygfB* in an *ampDh3*-dependent manner (Figure 3a-c). GlcNAc-anhMurNAc levels were increased upon deletion of *ygfB* in an *ampDh3*-dependent manner (Figure 3d) and GlcNAc-anhMurNAc-3P levels were also increased upon deletion of *ampDh3* or *ampDh3/ygfB* (Figure 3a). Together, this suggests that GlcNAc-anhMurNAc-peptides might be the primary target of AmpDh3, but AmpDh3 also degrades anhMurNAc-3P and anhMurNAc-5P (Eggers et al., 2023). Therefore, AmpDh3 likely functions as a surrogate for AmpD in the cytosol. While the levels of UDP-MurNAc-5P (Figure 3e), UDP-MurNAc (Figure 3f) and anhMurNAc (Figure 3g) were unaffected by deletion of *ygfB*, the balance of the *ampC*-activating and *ampC*-repressing peptides was altered towards the *ampC*-repressing side in an *ampDh3*-dependent manner (Figure 3h), providing a link between the observed levels of *ygfB*, *ampDh3,* and *ampC*.

1. Introduction

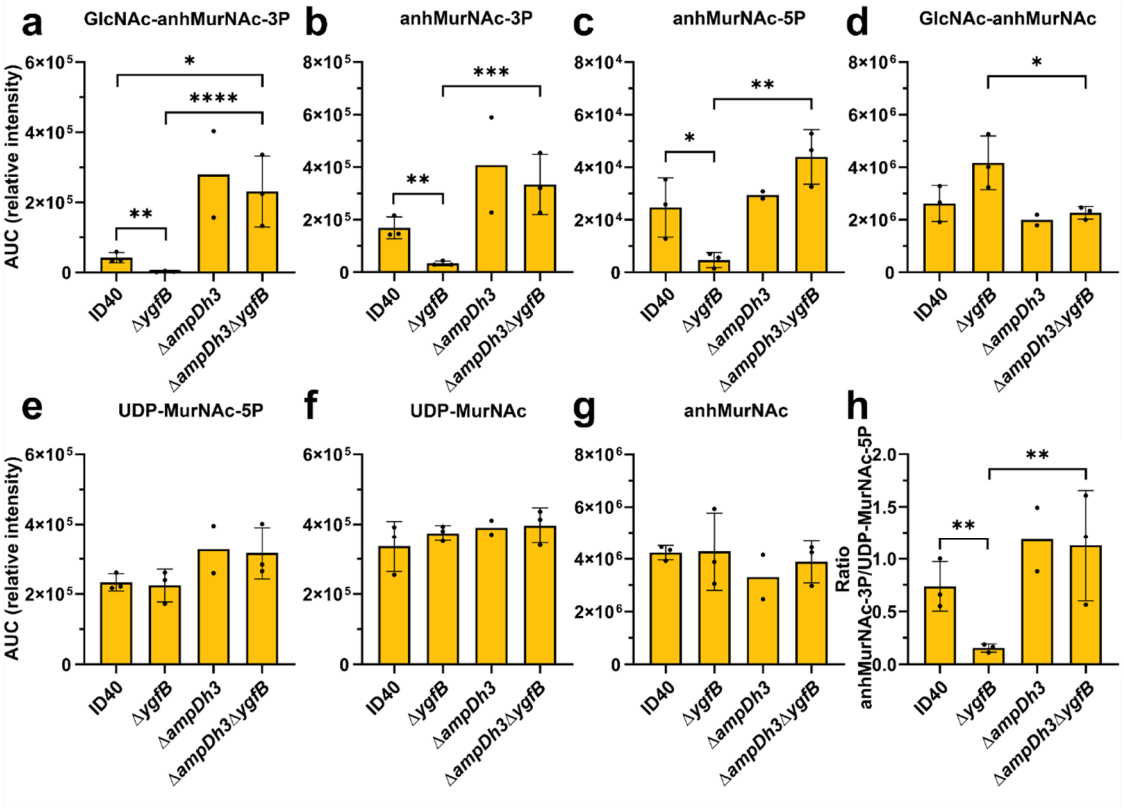

Figure 3: YgfB and AmpDh3 modulate the composition of peptidoglycan recycling products. Cytosolic extracts of the indicated strains were analyzed by LC-MS. In **(a-g)**, the mean and *SD* of the AUC of the peaks obtained for the indicated metabolites are shown. Additionally, in **(h)**, the ratio of the *ampC*-activating anhMurNAc-3P and the *ampC*-inhibiting UDP-MurNAc-5P are shown. Asterisks indicate significant differences of the $\log_{10}$ transformed data using one-way ANOVA with Tukeys test as a post-hoc test (*$p < 0.05$, **$p < 0.01$, ***$p < 0.001$, ****$p < 0.0001$). The figure was reproduced unaltered from Eggers et al. (2023) under CC BY 4.0 (https://creativecommons.org/licenses/by/4.0/).

In summary, YgfB reduces the expression of *ampDh3* in an AlpA-dependent manner. The reduced levels of AmpDh3 lead to an accumulation of anhMurNAc-3P/-5P, which stimulate the expression of *ampC* via AmpR.

1.5. Research question

The goal of this study was to elucidate the molecular mechanism by which YgfB represses *ampDh3*. We hypothesized that YgfB influences the AlpA-mediated regulation of *ampDh3* and changes the muropeptide composition to an *ampC*-activated state. Furthermore, as there seemed to be a connection between AlpA and YgfB, we were interested in whether ciprofloxacin-induced DNA damage had an impact on the *ygfB*-mediated resistance to β-lactam antibiotics, as ciprofloxacin was described to induce expression of *alpA* and therefore *ampDh3*. Lastly, as YgfB is conserved in γ-proteobacteria, while AmpDh3 is found only in some other species, we sought to find out whether there is a function of YgfB that is generalizable and also applies to other γ-proteobacteria.

2. Materials and Methods

Declaration of contributions

Certain materials and methods described in this section are cited literally from Eggers et al. (2023). Literal citations are marked with quotation marks and written in italics. The publication Eggers et al. (2023) was mainly written by PD Dr. Erwin Bohn and me.

The sections 2.3.25 “NanoLC-MS/MS analysis” and 2.3.26 “MS data processing” were written by Dr. Mirita Franz-Wachtel of the Proteome Center Tübingen, who also analyzed the samples that were provided in a Coomassie stained gel by me.

The sections 2.4.19 “Library preparation for RNA sequencing” and 2.4.20 “RNA sequencing” were written using information provided by Christina Engesser and Jennifer Müller of the NGS Competence Center Tübingen, who also performed the sequencing and data analysis.

2.1. Materials

2.1.1. Equipment

Table 1: Equipment used in this study.

Equipment	Official name	Manufacturer
-20°C freezer	G 5216 Index 21B/001	Liebherr, Bulle (CH)
-80°C freezer	Hera Freeze HFU T Series	Thermo Fisher Scientific, Waltham (US)
-80°C freezer	Hera Freeze	Thermo Fisher Scientific, Waltham (US)
Affinity column	GSTrap 4B	Cytivia, Marlborough (US)
Agarose gel elecotro-phoresis chamber	Sub-Cell GT Cell	Bio-Rad, Hercules (US)
Agarose gel imaging system	FastGene FAS-V Imaging System	Nippon Genetics, Düren
Analytical balance	Competence CPA225D-0CE	Sartorius, Göttingen
Balance	Precision balance EG 4200-2NM	Kern, Balingen
Bioanalyzer	Bioanalyzer 2100	Agilent, Santa Clara (US)
Centrifuge	Centrifuge 5417R	Eppendorf, Hamburg
Centrifuge	Centrifuge 5810R	Eppendorf, Hamburg
Centrifuge	Avanti J-26 XP	Beckman Coulter, Brea (US)
Centrifuge	Avanti J-26S XP	Beckman Coulter, Brea (US)
Densitometer	Densicheck Plus	Biomerieux, Marcy-l'Étoile (FR)
Electrophoresis cell	Mini-PROTEAN Tetra Vertical Electropho-resis Cell	Bio-Rad, Hercules (US)
Electroporator	Gene Pulser II	Bio-Rad, Hercules (US)
FPLC system	ÄKTAprime Plus	Cytivia, Marlborough (US)
Gel casting	Mini-PROTEAN Tetra Cell Casting Module	Bio-Rad, Hercules (US)
Gravity columns	Econo Chromatography Columns, 2.5 × 20 cm	Bio-Rad, Hercules (US)
Heating and magnetic stirrer	MR3001 K	Heidolph, Schwabach

2. Materials and Methods

Equipment	Official name	Manufacturer
Heating Block	Thermomixer comfort	Eppendorf, Hamburg
Hybrid quadrupole-Orbitrap mass spectrometer	Q Exactive HF mass spectrometer	Thermo Fisher Scientific, Waltham (US)
Ice machine	AF 156 Xsafe	Scotsman, Vernon Hills (US)
Imaging system for SDS-PAGE gels and Western blots	Fusion Solo S	Vilma Lourbat, Eberhardzell
Incubator	Function Line	Heraeus, Hanau
Laminar flow cabinet	BDK-S 1200, 1300	Weiss, Sonnenbühl
LI-COR	LI-COR Odyssey	LI-COR Biotechnology, Bad Homburg
LightCycler	LightCycler480 II	Roche Diagnostics, Rotkreuz (CH)
Magnetic Stand	MagJET	Thermo Fisher Scientific, Waltham (US)
Multistepper	Multipette Plus	Eppendorf, Hamburg
NanoDrop	NanoDrop One	Thermo Fisher Scientific, Waltham (US)
Nanoflow UHPLC	EASY-nLC 1200	Thermo Fisher Scientific, Waltham (US)
Orbital shaker	SU1000	Sunlab Instruments, Mannheim
Orbital shaker	Unimax 2010	Heidolph, Schwabach
Peristaltic pump	Pump P-1	Pharmacia Biotech, Uppsala (SE)
pH electrode	LE438	Mettler Toledo, Columbus (US)
pH meter	FiveEasy F20	Mettler Toledo, Columbus (US)
Photometer	BioPhotometer	Eppendorf, Hamburg
Pipettes	Research plus	Eppendorf, Hamburg
Pipetting aid	Pipetus	Hirschmann Laborgeräte, Eberstadt
Power supply	PowerPac 300	Bio-Rad, Hercules (US)
Qubit Fluorometer	Qubit 4 Fluorometer	Thermo Fisher Scientific, Waltham (US)
Refrigerator	GKv 6410 Index 23B/001	Liebherr, Bulle (CH)
Refrigerator	KT 1840 Index 24A/001	Liebherr, Bulle (CH)
Rotor for centrifuge	JLA-8.1000	Beckman Coulter, Brea (US)
Rotor for centrifuge	JA-14.50	Beckman Coulter, Brea (US)
SEC column	HiLoad 16/600 Superdex 75 pg	Cytivia, Marlborough (US)
SEC column	HiLoad 16/600 Superdex 200 pg	Cytivia, Marlborough (US)
Sequencer	Illumina NextSeq 500	Illumina, San Diego (US)
Shaking incubator	Ecotron shaking incubator	Infors HT, Bottmingen
Shaking incubator	Multitron shaking incubator	Infors HT, Bottmingen
Shaking incubator	Minitron shaking incubator	Infors HT, Bottmingen
Sonifier	Sonifier 250	Branson Ultrasonics, Brookfield (US)
Tank blotting system	Mini Trans-Blot Cell	Bio-Rad, Hercules (US)
Tecan plate reader	Tecan Infinite 200 Pro	Tecan, Männedorf (CH)
Thermal Printer	DPU-414 Thermal Printer	Seiko Instruments, Chiba (JP)
Thermocycler	C1000 Touch Thermocycler	Bio-Rad, Hercules (US)
Vacuum pump	CVC 2000	Vaccubrand, Wertheim
VIAFLO 12 Channel Pipette	VIAFLO 12 Channel Pipette 5-125 µl	Integra Biosciences, Zizers (CH)

2. Materials and Methods

Equipment	Official name	Manufacturer
VIAFLO 96 Channel Pipetting Head	VIAFLO 96 Channel Pipetting Head 10-300 µl	Integra Biosciences, Zizers (CH)
VIAFLO 96 Channel Pipetting Head	VIAFLO 96 Channel Pipetting Head 5-125 µl	Integra Biosciences, Zizers (CH)
VIAFLO Pipetting aid	VIAFLO 384 Pipetting Assistant	Integra Biosciences, Zizers (CH)
Vortex	Vortex Genie 2	Thermo Fisher Scientific, Waltham (US)
Vortex tube holder	Multi Tube Holder for Vortex Genie 2	Thermo Fisher Scientific, Waltham (US)
Waterbath	WB 10	Memmert, Schwabach
Wheel of fortune	neoLabLine Rotator	neoLab Migge, Heidelberg

2.1.2. Consumables

Table 2: Consumables used in this study.

Consumable	Manufacturer/Source	Application
Acrodisc 25 mm w/0.2 µm Supor STRL	Pall Corporation, New York (US)	Sterile filtration
Adhesive sealing foil for realtime PCR	nerbe plus, Winsen/Luhe	(RT-)qpCR
Amersham Protran 0.45 NC nitrocellulose Western blotting membranes	Cytivia, Marlborough (US)	Western blot
Amicon Ultra 15 ml Centrifugal Filters (10 kDa cutoff, 30 kDa cutoff)	Merck Millipore, Darmstadt	Ultrafiltration of proteins
BD Plastipak, Syringe with Luer-Lok adapter	Becton Dickinson, Franklin Lakes (US)	Syringe
Combitips advanced, multiple volumes	Eppendorf, Hamburg	Pipetting
Screw caps for cryotube	Sarstedt, Nümbrecht	Long term storage of bacteria
Dialysis membrane ZelluTrans, MWCO 3500	Carl Roth, Karlsruhe	Dialysis
Disposable Reservoirs, 10 ml, Sterile, Polystyrene	Integra Biosciences, Zizers (CH)	Pipetting reservoir
Disposable Reservoirs, 25 ml, Sterile, Polystyrene	Integra Biosciences, Zizers (CH)	Pipetting reservoir
Erlenmeyer flask, SIMAX	Kavallierglass, Prague (CZ)	Preparation of solutions, culturing of bacteria
Gene Pulser/MicroPulser Electroporation Cuvettes, 0.2 cm gap	Bio-Rad, Hercules (US)	Electroporation
Glass bottles, Schott Duran	DWK Life Sciences, Wertheim	Storage of liquids
Gloves (Peha-soft nitrile)	Hartmann Heidenheim	Protection
Incolulation loop	Greiner Bio-One, Kremsmünster (AT)	Inoculation of media
Lightcycler 480 multiwell plates, 96 wells	Roche, Rotkreuz (CH)	(RT)-qPCR
Lightcycler 480 sealing foils	Roche, Rotkreuz (CH)	(RT)-qPCR
Injekt, Luer Solo	B. Braun, Melsungen	Syringe
Micro screw tube	Sarstedt, Nümbrecht	Long term storage of bacteria
Micro screw tube caps	Sarstedt, Nümbrecht	Long term storage of bacteria

2. Materials and Methods

Consumable	Manufacturer/Source	Application
Microplate, 96 well, PS, F-bottom (chimney well), white, Lumitrac, med. binding	Greiner Bio-One, Kremsmünster (AT)	Luciferase based assays
Microplate, 96 well, PS, F-bottom, clear	Greiner Bio-One, Kremsmünster (AT)	Checkerboard assay
Mini-PROTEAN TBE Precast Gels, 5%	Bio-Rad, Hercules (US)	EMSA
Mini-PROTEAN TGX Precast Gels (10%, 12%, 4-20%)	Bio-Rad, Hercules (US)	SDS-PAGE
Parafilm	Bemis, Neenah (US)	Sealing
PCR SingleCap Softstrips	Biozym Scientific, Hessisch Oldendorf	PCR
PCR-plate, 96x0.2 ml	nerbe plus, Winsen/Luhe	(RT)-qPCR
Petri dishes	Greiner Bio-One, Kremsmünster (AT)	Preparation of agar plates
Pipette tips (10 µl)	Brand, Wertheim	Refillable pipette tips
Pipette tips with filter (10 µl, 100 µl, 200 µl, 1000 µl)	nerbe plus, Winsen/Luhe	Pipette tips with filter
Pipette tips, 125 µl Griptip (Sterile, Filter)	Integra Biosciences, Zizers (CH)	Pipetting
Pipette tips, 300 µl Griptip (Sterile, Filter)	Integra Biosciences, Zizers (CH)	Pipetting
Qubit Assay Tubes	Thermo Fisher Scientific, Waltham (US)	Fluorometric quantification of nucleic acids
Reaction tube (15 ml, 50 ml)	Greiner Bio-One, Kremsmünster (AT)	Storage of liquids
Reaction tubes (1.5 ml, 2 ml)	Sarstedt, Nümbrecht	Storage of liquids
Reaction tubes, DNA LoBind (1.5 ml)	Eppendorf, Hamburg	(RT-)qpCR, RNAseq
Reaction tubes, Safe-Lock (1.5 ml, 2 ml)	Eppendorf, Hamburg	Storage of liquids
Reagent Reservoirs, 12 Column, Pyramid Bottom, Non-Sterile, Autoclavable, Polypropylene	Integra Biosciences, Zizers (CH)	Checkerboard assay
Reagent Reservoirs, 150 ml Automation Friendly Clear Advantage (Polystyrene)	Integra Biosciences, Zizers (CH)	Checkerboard assay
Reagent Reservoirs, 8 Row, Pyramid Bottom, Non-Sterile, Autoclavable, Polypropylene	Integra Biosciences, Zizers (CH)	Checkerboard assay
Round bottom tubes (5 ml, 14 ml), Falcon	Corning, Corning	Preparation of inocula at McFarland 0.5 (5 ml), Culturing of bacteria in liquid culture (14 ml)
Scalpel	B. Braun, Melsungen	Western blot
Sealing foil, gas-permeable	Thermo Fisher Scientific, Waltham (US)	Susceptibility testing
Sensititre Gram Negative EUX2NF AST Plate	Thermo Fisher Scientific, Waltham (US)	Susceptibility testing
Sensititre Gram Negative GN2F AST Plate	Thermo Fisher Scientific, Waltham (US)	Susceptibility testing
Serological Pipettes (5, 10, 25, 50 ml)	Corning, Corning	Pipetting
Steritop 45 mm Neck Size, Millipore Express PLUS 0.22 µm	Merck Millipore, Darmstadt	Sterile filtration

Consumable	Manufacturer/Source	Application
Volumetric flask, Schott Duran	DWK Life Sciences, Wertheim	Preparation of solutions
Whatman Gel Blotting Paper	GE Healthcare, Chicago (US)	Western blot

2.1.3. Commercial kits, reagents and enzymes

Table 3: Kits, reagents and enzymes used in this study.

Kit/reagents/enzymes	Manufacturer	Application
10x PBS powder	Merck, Darmstadt	Buffer preparation
4x Laemmli buffer	Bio-Rad, Hercules (US)	Preparation of samples for SDS-PAGE
Ambion Nuclease-Free Water	Thermo Fisher Scientific, Waltham (US)	Dilution of RNA, RT-qPCR
BD BBL Mueller Hinton II broth (cation-adjusted), powder	VWR, Radnor (US)	Preparation of MHB II medium
BlueBlock PF (10x)	Serva Electrophoresis, Heidelberg	Western blot
Bradford Reagent, 5x concentrate	Serva Electrophoresis, Heidelberg	Protein purification
Clarity Western ECL Blotting Substrate	Bio-Rad, Hercules (US)	Western blot, detection of HRP-conjuagted secondary antibodies
cOmplete, EDTA-free Protease Inhibitor Cocktail Tablets	Roche Diagnostics, Rotkreuz (CH)	Lysis of bacterial cells, protein purification
DNAse I, powder	Panreac AppliChem, Darmstadt	Lysis of bacterial cells, protein purification
DNase I, recombinant, RNase-free	Roche, Rotkreuz (CH)	DNA digestion for RT-qPCR and RNA seq
DNeasy UltraClean Microbial Kit	Qiagen, Hilden	Isolation of genomic DNA
DpnI	Thermo Fisher Scientific, Waltham (US)	Digestion of methylated DNA
GeneRuler 1 kb Plus DNA Ladder	Thermo Fisher Scientific, Waltham (US)	Size marker for agarose gel-electrophoresis
Gibco DPBS (Dulbecco's Phosphate Buffered Saline)	Thermo Fisher Scientific, Waltham (US)	Buffering solution
Illumina Stranded Total RNA Prep with Ribo-Zero Plus	Illumina, San Diego (US)	Library preperation of RNAseq
KAPA HiFi plus dNTPs	Roche, Rotkreuz (CH)	PCR for generation of fragments for cloning
Lysozyme from chicken egg white	Sigma-Aldrich, St. Louis (US)	Lysis of bacterial cells, protein purification
MagneGST Protein Purification System	Promega, Madison (US)	GST-pulldown
MagneHis Ni Particles 2mL	Promega, Madison (US)	His-pulldown
MangoMix	Meridian Bioscience, Cincinatti (US)	Confirmation of successful cloned plasmids or mutants during mutagenesis
MIDORI Green Xtra	Nippon Genetics, Düren	Staining of nucleic acids
Monarch Plasmid Miniprep Kit	New England Biolabs, Ipswich (US)	Isolation of plasmids
NaCl 0.9%, 10 ml	B. Braun, Melsungen	Antibiotic susceptibility testing
Nano-Glo HiBiT Blotting System	Promega, Madison (US)	Detection of HiBiT-tagged proteins in Western blot
Nano-Glo HiBiT Lytic Detection System	Promega, Madison (US)	Detection of HiBiT-tagged proteins in Western blot

2. Materials and Methods

Kit/reagents/enzymes	Manufacturer	Application
Nano-Glo Luciferase Assay System	Promega, Madison (US)	Promoter luciferase assay
Ni-NTA Agarose	Qiagen, Hilden	Protein purification
Odyssey EMSA Kit	LI-COR, Lincoln (US)	EMSA
PageRuler Prestained Protein Ladder, 10 to 180 kDa	Thermo Fisher Scientific, Waltham (US)	Size marker for SDS-PAGE and Western blot
Phusion High-Fidelity DNA Polymerase	Thermo Fisher Scientific, Waltham (US)	PCR for generation of fragments for cloning, Gibson mix
QuantiFast SYBR Green PCR Kit	Qiagen, Hilden	qPCR
QuantiFast SYBR Green RT-PCR Kit	Qiagen, Hilden	RT-qPCR
Qubit dsDNA BR Assay-Kit	Thermo Fisher Scientific, Waltham (US)	Fluorometric quantification of DNA
Qubit RNA BR Assay-Kit	Thermo Fisher Scientific, Waltham (US)	Fluorometric quantification of RNA
RNA Clean & Concentrator-5	Zymo Research, Irvine (US)	RNA clean up
ROTI-Blue, 5x concentrate	Carl Roth, Karlsruhe	Preperation of colloidal Coomassie solution
Rotiphorese Gel 30 (37.5:1)	Carl Roth, Karlsruhe	Preparation of gels for EMSA
Salmon Sperm DNA Solution	Thermo Fisher Scientific, Waltham (US)	EMSA
T5 Exonuclease 10 U/µl	New England Biolabs, Ipswich (US)	Gibson mix
Taq DNA Ligase 40 U/µl	New England Biolabs, Ipswich (US)	Gibson mix
Wizard SV Gel and PCR Clean-Up System	Promega, Madison (US)	Purification of PCR products
ZymoBIOMICS RNA Miniprep Kit	Zymo Research, Irvine (US)	Isolation of total RNA

2.1.4. Chemicals

Table 4: Chemicals used in this study.

Chemical	Manufacturer/Source
Agar	Carl Roth, Karlsruhe
Acetic acid	Merck, Darmstadt
Ammonium Persulfate (APS)	Bio-Rad, Hercules (US)
Ampicillin Sodium	PanReac AppliChem, Darmstadt
Ampuwa, Solution for Irrigation (Water for injection in bulk), 10 l	Fresenius Kabi, Bad Homburg vor der Höhe
β-mercaptoethanol	PanReac AppliChem, Darmstadt
Aqua ad iniectabilia (Water for injection), 10 ml	B. Braun, Melsungen
Azidothymidine	Thermo Fisher Scientific, Waltham (US)
Aztreonam (European Pharmacopoeia Reference Standard)	Sigma-Aldrich, St. Louis (US)
Boric acid	PanReac AppliChem, Darmstadt
Bovine serum albumin (BSA)	Carl Roth, Karlsruhe
Calcium chloride dihydrate ($CaCl_2$ x $2H_2O$)	Merck, Darmstadt
Carbenicillin Disodium salt	PanReac AppliChem, Darmstadt

2. Materials and Methods

Chemical	Manufacturer/Source
Ceftazidime pentahydrate (European Pharmacopoeia Reference Standard)	Sigma-Aldrich, St. Louis (US)
Ciprofloxacin hydrochloride monohydrate (European Pharmacopoeia Reference Standard)	Sigma-Aldrich, St. Louis (US)
Coomassie Brilliant Blue G-250	Serva Electrophoresis, Heidelberg
Deionized water (DI-water)	In-house water line
Diamino pimelic acid (DAP)	Sigma-Aldrich, St. Louis (US)
Di-sodium hydrogen phosphate heptahydrate (Na2HPO4 x 7 H2O)	Merck, Darmstadt
Dithiothreitol (DTT)	PanReac AppliChem, Darmstadt
Ethanol absolut ≥99,8%, AnalaR NORMAPUR	VWR, Radnor (US)
Ethylenediaminetetraacetic acid (EDTA)	Merck, Darmstadt
Gentamicin sulfate	PanReac AppliChem, Darmstadt
Glucose	Merck, Darmstadt
Glutathione, reduced	PanReac AppliChem, Darmstadt
Glycerol, SOLVAGREEN ≥98 %	Carl Roth, Karlsruhe
Glycin, PUFFERAN ≥99 %, p.a.	Carl Roth, Karlsruhe
HEPES	Carl Roth, Karlsruhe
Hydrochloric acid (HCl)	Merck, Darmstadt
Igepal CA-630	Sigma-Aldrich, St. Louis (US)
Imidazole, ReagentPlus, 99%	Sigma-Aldrich, St. Louis (US)
Imipenem monohydrate (European Pharmacopoeia Reference Standard)	Sigma-Aldrich, St. Louis (US)
Irgasan	Sigma-Aldrich, St. Louis (US)
Isopropyl-β-D-thiogalactopyranosid (IPTG)	VWR, Radnor (US)
Kanamycin sulfate	PanReac AppliChem, Darmstadt
L-Rhamnose Monohydrat, suitable for microbiology, ≥99.0%	Sigma-Aldrich, St. Louis (US)
Methanol ≥99,8%, AnalaR NORMAPUR	VWR, Radnor (US)
Magnesium chloride hexahydrate ($MgCl_2$ x $6H_2O$))	PanReac AppliChem, Darmstadt
Nicotinamide adenine dinucleotide (NAD^+)	Merck, Darmstadt
N,N,N′,N′-Tetramethylethylendiamin (TEMED)	Bio-Rad, Hercules (US)
Orange G	Sigma-Aldrich, St. Louis (US)
PEG-8000	Thermo Fisher Scientific, Waltham (US)
Piperacillin sodium (analytical standard)	Sigma-Aldrich, St. Louis (US)
Potassium acetate (KOAc)	Merck, Darmstadt
Rifampicin ≥90 %, for biochemistry	Carl Roth, Karlsruhe
SeaKem LE Agarose	Lonza, Basel (CH)
Sodium bicarbonate (NaHCO3)	Sigma-Aldrich, St. Louis (US)
Sodium carbonate (Na2CO3)	Merck, Darmstadt
Sodium chloride (NaCl)	VWR, Radnor (US)
Sodium dihydrogen phosphate monohydrate (NaH2PO4 x H2O)	Merck, Darmstadt
Sodium dodecyl sulfate (SDS)	Carl Roth, Karlsruhe
Sodium hydroxide (NaOH)	Merck, Darmstadt
Streptomycin sulfate	PanReac AppliChem, Darmstadt

Chemical	Manufacturer/Source
Sucrose	Merck, Darmstadt
Tetracycline hydrochloride	PanReac AppliChem, Darmstadt
Triethanolamine	Sigma-Aldrich, St. Louis (US)
Triethylenglycol, 99 %	Thermo Fisher Scientific, Waltham (US)
Tris(hydroxymethyl)aminomethan (Tris-base)	Sigma-Aldrich, St. Louis (US)
Triton X-100 for molecular biology	Sigma-Aldrich, St. Louis (US)
Tween 20	Sigma-Aldrich, St. Louis (US)

2.1.5. Buffers and solutions

Table 5: Buffers and solutions used in this study and their preparation.

Buffer/solution	Preparation	Application
5x SDS-PAGE running buffer	Tris-base: 60.55 g Glycine: 288.15 g SDS: 10 g Ampuwa: ad 2000 ml	SDS-PAGE
Coomassie quick stain solution	Coomassie brilliant blue G250: 0.8 g Ethanol: 100 ml Ampuwa: 900 ml HCl 6 M: 5 ml Stir overnight	Coomassie quick stain
10x blotting buffer	Tris-base: 60.0 g Glycine: 288.8 g Ampuwa: ad 2000 ml	Western blot transfer
1x blotting buffer	10x blotting buffer: 100 ml Methanol: 200 ml Ampuwa: ad 1000 ml	Western blot transfer
Ponceau S staining solution	Ponceau S: 1.25 g Glacial acetic acid: 25 g Ampuwa: Ad 500 ml	Reversible, unspecific protein stain during Western blotting
10x TBS	Tris-base: 24 g NaCl: 88 g HCl: to pH 7.6 Ampuwa: ad 1000 ml	Stock solution
TBS	10x TBS: 100 ml Ampuwa: ad 1000 ml	Buffering solution
TBS-T	10x TBS: 100 ml Tween 20: 1 ml Ampuwa: ad 1000 ml	Wash buffer for Western blots
10x PBS	10x PBS powder Ampuwa: Ad 1000 ml	Buffering solution
PBS pH 7.4	10x PBS: 100 ml Ampuwa: 900 ml	Buffering solution
5x TBE	Tris-base: 270 g Boric acid: 137.5 g 0.5 M EDTA (pH 8.0): 100 ml Deionized water: ad 5000 ml	Agarose gel electrophoresis, EMSA
Orange G loading dye	Glycerol 87.5%: 43.5 ml Orange G: 200 mg Ampuwa: Ad 100 ml	Loading buffer for agarose gel electrophoresis
5 M NaCl stock	NaCl: 292.2 g Ampuwa: ad 1000 ml Sterile filter + autoclave	Stock solution for biochemical buffers

2. Materials and Methods

Buffer/solution	Preparation	Application
1 M Tris pH 8 or pH 7.5 stock	Tris-base: 121.14 g HCl: to pH 8 or pH 7.5 Ampuwa: ad 1000 ml Sterile filter + autoclave	Stock solution for biochemical buffers
1 M $MgCl_2$ stock	$MgCl_2$ x $6H_2O$: 203.3 g Ampuwa: ad 1000 ml Sterile filter + autoclave	Stock solution for biochemical buffers
0.1 M $CaCl_2$	$CaCl_2$ x $2H_2O$: 14.7 g Ampuwa: ad 1000 ml Sterile filter	Preparation of calcium competent cells
0.1 M $CaCl_2$ + 15% glycerol	$CaCl_2$ x $2H_2O$: 14.7 g Glycerol: 150 g Ampuwa: ad 1000 ml Sterile filter	Preparation of calcium competent cells
0.5 M EDTA pH 8 stock	EDTA: 93 g NaOH: to pH 8 Ampuwa: ad 500 ml Sterile filter + autoclave	Stock solution for biochemical buffers
0.2 M EDTA pH 8	EDTA: 0.58 g NaOH: to pH 8 Nuclease-free water: ad 10 ml	DNase digest
1 M imidazole stock	Imidazole: 68.08 g Ampuwa: ad 1000 ml Sterile filter + autoclave	Stock solution for biochemical buffers
1 M DTT stock	DTT: 7.7125 g Ampuwa: ad 50 ml Sterile filter, store at -20°C	Stock solution for biochemical buffers
1 M IPTG stock	IPTG: 11.9151 g Ampuwa: ad 50 ml Sterile filter, store at -20°C	Induction of protein overexpresion
100 mM NAD^+	NAD^+: 6.63 g Ampuwa: ad 100 ml	Stock solution for Gibson buffer
10 mg/ml DNase I	DNase I: 10 mg Ampuwa: ad 1 ml	Stock solution for biochemical buffers
10 mg/ml lysozyme	Lysozyme: 10 mg Ampuwa: ad 1 ml	Stock solution for biochemical buffers
50 mM Tris, 150 mM NaCl, 25 mM imidazole, 1 mM DTT, pH 7.5	1 M Tris pH 8 stock: 50 ml 5 M NaCl stock: 30 ml 1 M imidazole stock: 25 ml 1 M DTT stock: 1 ml HCl: to pH 7.5 Ampuwa: ad 1000 ml Sterile filter	Protein purification, Ni^{2+}-NTA-affinity chromatography, reducing conditions
50 mM Tris, 150 mM NaCl, 25 mM imidazole, pH 7.5	1 M Tris pH 8 stock: 50 ml 5 M NaCl stock: 30 ml 1 M imidazole stock: 25 ml HCl: to pH 7.5 Ampuwa: ad 1000 ml Sterile filter	Protein purification, Ni-affinity chromatography
50 mM Tris, 150 mM NaCl, 25 mM imidazole, 1 mM DTT, pH 8	1 M Tris pH 8 stock: 50 ml 5 M NaCl stock: 30 ml 1 M imidazole stock: 25 ml 1 M DTT stock: 1 ml HCl: to pH 8 Ampuwa: ad 1000 ml Sterile filter	Protein purification, Ni^{2+}-NTA-affinity chromatography, reducing conditions

2. Materials and Methods

Buffer/solution	Preparation	Application
50 mM Tris, 150 mM NaCl, 25 mM imidazole, pH 8	1 M Tris pH 8 stock: 50 ml 5 M NaCl stock: 30 ml 1 M imidazole stock: 25 ml HCl: to pH 8 Ampuwa: ad 1000 ml Sterile filter	Protein purification, Ni^{2+}-NTA-affinity chromatography
50 mM Tris, 150 mM NaCl, 1 mM DTT, pH 7.5 (GST-A)	1 M Tris pH 8 stock: 50 ml 5 M NaCl stock: 30 ml 1 M DTT stock: 1 ml HCl: to pH 7.5 Ampuwa: ad 1000 ml Sterile filter	Protein purification, glutathione affinity chromatography, reducing conditions, dialysis
50 mM Tris, 150 mM NaCl, 10 mM reduced glutathione, pH 8 (GST-B)	1 M Tris pH 8 stock: 50 ml 5 M NaCl stock: 30 ml Reduced glutathione: 3.0732 g HCl: to pH 7.5 Ampuwa: ad 1000 ml Sterile filter	Protein purification, glutathione affinity chromatography, elution, reducing conditions
50 mM Tris, 150 mM NaCl, 20% glycerol, 1 mM DTT, pH 7.5	1 M Tris pH 8 stock: 100 ml 5 M NaCl stock: 60 ml Glycerol: 400 g 1 M DTT stock: 1 ml HCl: to pH 7.5 Ampuwa: ad 2000 ml Sterile filter	Dialysis
10 mM Tris, 200 mM NaCl, 25 mM imidazole, 5% glycerol, 1 mM DTT, pH 7.5	1 M Tris pH 8 stock: 10 ml 5 M NaCl stock: 40 ml 1 M imidazole stock: 25 ml Glycerol: 50 g 1 M DTT stock: 1 ml HCl: to pH 7.5 Ampuwa: ad 1000 ml Sterile filter	Protein purification, Ni^{2+}-NTA-affinity chromatography, reducing conditions
10 mM Tris, 200 mM NaCl, 25 mM imidazole, 5% glycerol, 1 mM DTT, pH 7.5	1 M Tris pH 8 stock: 10 ml 5 M NaCl stock: 40 ml 1 M imidazole stock: 25 ml Glycerol: 50 g 1 M DTT stock: 1 ml HCl: to pH 7.5 Ampuwa: ad 1000 ml Sterile filter	Protein purification, Ni^{2+}-NTA-affinity chromatography, reducing conditions
10 mM Tris, 200 mM NaCl, 5% glycerol, 1 mM DTT, pH 7.5	1 M Tris pH 8 stock: 10 ml 5 M NaCl stock: 40 ml Glycerol: 50 g 1 M DTT stock: 1 ml HCl: to pH 7.5 Ampuwa: ad 1000 ml Sterile filter	Dialysis, size-exclusion-chromatography
10x Duplex buffer (1 M KOAc, 300 mM HEPES)	KOAc: 9.815 g HEPES: 7.15 g NaOH: to pH 7.5 Ampuwa: ad 100 ml Sterile filter + autoclave	Annealing of oligos for EMSA
50 mM Tris, 150 mM NaCl, 20% glycerol, pH 7.5	1 M Tris pH 8 stock: 50 ml 5 M NaCl stock: 30 ml Glycerol: 200 g HCl: to pH 7.5 Ampuwa: ad 1000 ml Sterile filter	Protein storage buffer EMSA

2. Materials and Methods

Buffer/solution	Preparation	Application
Competitor buffer (50 mM KOAc, 15 mM HEPES)	10x Duplex buffer: 500 µl Ampuwa: ad 10 ml	EMSA
GST-pulldown buffer (50 mM Tris, 300 mM NaCl, 0.5%, Igepal CA-630, 2 mM DTT)	1 M Tris pH 8 stock: 50 ml 5 M NaCl stock: 60 ml Igepal CA-630: 5 ml 1 M DTT stock: 2 ml HCl: to pH 7.5 Ampuwa: ad 1000 ml Sterile filter	GST-pulldowns
10x GSH solution	Reduced glutathione: 0.0768 g 30% NaOH: to pH 7.5 GST-pulldown buffer: ad 1 ml	GST-pulldowns, elution of samples
His-pulldown buffer (50 mM Tris pH 7.5, 25 mM imidazole, 300 mM NaCl, 0.5% IGEPAL, 2 mM DTT	1 M Tris pH 8 stock: 50 ml 5 M NaCl stock: 60 ml Igepal CA-630: 5 ml 1 M imidazole stock: 25 ml 1 M DTT stock: 2 ml HCl: to pH 7.5 Ampuwa: ad 1000 ml Sterile filter	His-pulldowns
Phosphate buffer, pH 6, 100 mM	NaH_2PO_4 x H_2O: 5.965 g Na_2HPO_4 x 7 H_2O: 1.813 g Measure pH, potentially adjust Ampuwa: Ad 500 ml	Preparation of cefepime stock solution
Saturated sodium bicarbonate solution	$NaHCO_3$: > 1 g Ampuwa: 10 ml	Preparation of aztreonam stock solution
Phosphate buffer, pH 7.2, 10 mM	NaH_2PO_4 x H_2O: 0.3541 g Na_2HPO_4 x 7 H_2O: 0.6525 g Measure pH, potentially adjust Ampuwa: Ad 500 ml	Preparation of imipenem stock solution
Buffer K (50 mM triethanolamine pH 7.5, 250 mM sucrose)	Triethanolamine: 3.73 g Sucrose: 42.79 g Ampuwa: ad 500 ml	Lysis of bacterial cells
Buffer K supplemented (1 mM EDTA, 1 mM $MgCl_2$, 0.5% Triton X-100, 10 µg/ml DNase I, 20 µg/ml lysozyme, 1:100 c0mplete protease inhibitor cocktail)	Buffer K: 10 ml 0.5 M EDTA: 20 µl 1 M $MgCl_2$: 10 µl Triton-X100: 50 µl 10 mg/ml DNase I: 10 µl 10 mg/ml lysozyme: 20 µl 25x c0mplete protease inhibitor cocktail: 100 µl	Lysis of bacterial cells
300 mM sucrose	Sucrose: 102.7 g Ampuwa: Ad 1000 ml Sterile filter	Electroporation
50 mg/ml DAP	Dissolve in Ampuwa Sterile filter	Mutagenesis of *E. coli*
Colloidal coomassie solution	ROTI-Blue, 5x concentrate: 20 ml Methanol: 20 ml Ampuwa: 60 ml	Staining of protein gels for proteomics
5x Isothermal reaction buffer	1 M Tris, pH 7.5 stock: 2 ml 1 M $MgCl_2$ stock: 200 µl 10 mM dNTPs: 400 µl 1 M DTT: 200 µl PEG-8000: 1 g 100 mM NAD^+: 200 µl Ampuwa: ad 4 ml	Gibson assembly

2.1.6. Culture media

Table 6: Culture media used in this study and their preparation.

Medium	Preparation	Application
Luria Bertani (LB) medium, Miller modification	Tryptone: 10 g Yeast extract: 5 g NaCl: 10 g Deionized water: ad 1000 ml	Culturing of bacteria in liquid medium
LB agar	Tryptone: 10 g Yeast extract: 5 g NaCl: 10 g Agar: 15 g Deionized water: ad 1000 ml	Culturing of bacteria on solid medium
No salt LB agar (NSLB)	Tryptone: 10 g Yeast extract: 5 g Agar: 15 g Deionized water: ad 1000 ml	Culturing of bacteria on solid medium, mutagenesis
Mueller Hinton Broth, cation adjusted (MHB II)	BD BBL Mueller Hinton II Broth powder: 22 g Ampuwa: Ad 1000 ml	Antibiotic susceptibility testing
Super optimal broth with catabolite repression (SOC)	Tryptone: 20 g Yeast extract: 5 g NaCl: 0.5 g $MgSO_4$: 4.8 g Glucose: 3.6 g KCl: 0.186 g Deionized water: Ad 1000 ml	Growth of bacteria after transformation by heat shock

2.1.7. Antibiotic stock solutions

Table 7: Antibiotics used in this study and the preparation of their stock solutions.

Antibiotic	Stock concentration	Preparation of stock solution
Ciprofloxacin hydrochloride monohydrate (CIP)	5.12 mg/ml	Ciprofloxacin monohydrate: 11.92 mg Ampuwa: Ad 2 ml
Piperacillin sodium (PIP)	5.12 mg/ml	Piperacillin sodium: 26.69 mg Ampuwa: Ad 5 ml
Ceftazidime pentahydrate (CAZ)	5.12 mg/ml	Ceftazidime pentahydrate: 11.93 mg Na_2CO_3: ~1.1 mg Dissolve Na_2CO_3 in most of necessary water Dissolve ceftazidime pentahydrate in Na_2CO_3 solution Ampuwa: Ad 2 ml
Imipenem monohydrate (IPM)	5.12 mg/ml	Imipenem monohydrate: 10.85 mg Phosphate buffer, pH 7.2, 0.01 mol/L: Ad 2 ml
Aztreonam (AZT)	5.12 mg/ml	Aztreonam: 10.24 (adjust for given correction factor) Sat. $NaHCO_3$ solution: q.s. to dissolve aztronam Ampuwa: Ad 2 ml
Gentamicin (Genta)	10 mg/ml	Dissolve in Ampuwa, sterile filter
Kanamycin (Kan)	50 mg/ml	Dissolve in Ampuwa, sterile filter
Carbenicillin (Carb)	100 mg/ml	Dissolve in Ampuwa, sterile filter
Ampicillin (Amp)	100 mg/ml	Dissolve in Ampuwa, sterile filter
Tetracyclin hydrochloride (Tet)	10 mg/ml	Dissolve in Ampuwa, sterile filter
Irgasan (Irg)	25 mg/ml	Dissolve in EtOH, sterile filter
Azidothymidine	100 mg/ml	Dissolve in MeOH, sterile filter

2.1.8. Antibodies

Table 8: Antibodies used in this study and the dilutions used for Western blotting.

Antibody	Antigen	Raised in	Dilution	Manufacturer
Polyclonal rabbit anti-PaYgfB	YgfB from *P. aeruginosa* ID40 YgfB	Rabbit	1:500	Kristina Klein
HA-Tag (C29F4) Rabbit mAb	HA-tag	Rabbit	1:1000	Cell Signaling Technology, Danvers (USA)
Anti-*E. coli* RNA Polymerase β Antibody	*E. coli* RNA polymerase β-subunit	Mouse	1:1000	BioLegend, San Diego (USA)
Goat anti-Rabbit IgG (H+L) Secondary Antibody, HRP	Rabbit IgG	Goat	1:10,000	Thermo Fisher Scientific, Waltham (USA)
Rabbit anti-Mouse IgG (H+L) Secondary Antibody, HRP	Mouse IgG	Rabbit	1:2000	Thermo Fisher Scientific, Waltham (USA)

2.1.9. Bacterial strains

Table 9: Bacterial strains used in this study. Strain descriptions written in italics and marked with quotation marks are literally cited from Eggers et al. (2023). Strains described as "this work" were generated by me, strains described as Bohn lab were generated by coauthors or colleagues in the lab.

Name of strain	Info	Source/Published in
Pseudomonas aeruginosa		
ID40 strains		
ID40	*"Clinical bloodstream isolate, resistant against cefepime, ceftazidime, imipenem, ciprofloxacin, levofloxacin, piperacillin and piperacillin/tazobactam"*	Bohn lab (Eggers et al., 2023; Sonnabend et al., 2020; Willmann, Götting, et al., 2018)
ID40Δ*ygfB*	*"In-frame deletion mutant encoding the first and last 10 amino-acids of ygfB. For note: all following deletion mutants are in-frame deletion mutants"*	Bohn lab (Eggers et al., 2023; Sonnabend et al., 2020)
ID40Δ*ygfB*::rha-*ygfB*	*"ygfB deletion mutant complemented with pJM220-rha-ygfB carrying the ygfB coding sequence"*	Bohn lab (Eggers et al., 2023; Sonnabend et al., 2020)
ID40Δ*ampDh3*	*"ampDh3 deletion mutant"*	Bohn lab (Eggers et al., 2023)
ID40Δ*ampDh3*::rha-*ampDh3*	*"ampDh3 deletion mutant complemented with pJM220-rha-ampDh3 carrying the ampDh3 coding sequence"*	This work (Eggers et al., 2023)
ID40Δ*ygfB*Δ*ampDh3*	*"In frame deletion of both ygfB and ampDh3"*	Bohn lab (Eggers et al., 2023)
ID40::*ampDh3*-HiBiT	*"Knock-in mutant carrying a strep-Tag and the 11 amino acid HiBiT-tag at the C-terminal end of AmpDh3"*	This work (Eggers et al., 2023)
ID40Δ*ygfB*::*ampDh3*-HiBiT	*"ygfB deletion mutant with HiBiT tagged ampDh3"*	Bohn lab (Eggers et al., 2023)
ID40Δ*ygfB*::rha-*ygfB*:: *ampDh3*-HiBiT"	*"ygfB complementant with HiBiT tagged ampDh3"*	This work (Eggers et al., 2023)
ID40Δ*alpA*	*"In-frame deletion mutant of alpA encoding the first and last 10 amino-acids of alpA"*	Bohn lab (Eggers et al., 2023)

2. Materials and Methods

Name of strain	Info	Source/Published in
ID40Δ*alpA*::rha-*alpA*	*"alpA deletion mutant complemented with pJM220-rha-alpA carrying the alpA coding sequence"*	This work (Eggers et al., 2023)
ID40Δ*ygfB*Δ*alpA*	*"Double in-frame deletion mutant of ygfB and alpA"*	Bohn lab (Eggers et al., 2023)
ID40::*alpA*-HiBiT::HA-*alpR*	*"ID40 wildtype with HiBiT tagged alpA at the C-terminus and N-terminal HA-tagged alpR"*	Bohn lab (Eggers et al., 2023)
ID40Δ*ygfB*::*alpA*-HiBiT::HA-*alpR*	*"ygfB deletion mutant with HiBiT tagged alpA at the C-terminus and N-terminal HA-tagged alpR"*	This work (Eggers et al., 2023)
ID40 pBBR1-532-luc	*"ID40 wildtype with plasmid pBBR1-532-luc"*	Bohn lab (Eggers et al., 2023)
ID40Δ*ygfB* pBBR1-532-luc	*"ID40ΔygfB with plasmid pBBR1-532-luc"*	Bohn lab (Eggers et al., 2023)
ID40Δ*ygfB*::rha-SmBiT-*ygfB*	Deletion mutant of *ygfB*, carrying SmBiT-tagged *ygfB* under the control of a rhamnose inducible promoter inserted at the Tn7-site	Bohn lab
ID40Δ*ygfB*::rha-SmBiT-*ygfB* pBBR1_LgBiT	ID40Δ*ygfB*::rha-SmBiT-*ygfB* carrying a pBBR1 plasmid encoding for LgBiT	Bohn lab
ID40Δ*ygfB*::rha-SmBiT-*ygfB* pBBR1_LgBiT-*radA*	ID40Δ*ygfB*::rha-SmBiT-*ygfB* carrying a pBBR1 plasmid encoding for LgBiT fused to RadA	Bohn lab
ID40Δ*ygfB*::rha-SmBiT-*ygfB* pBBR1_LgBiT-*ubiH*	ID40Δ*ygfB*::rha-SmBiT-*ygfB* carrying a pBBR1 plasmid encoding for LgBiT fused to UbiH	Bohn lab
ID40Δ*ygfB*::rha-SmBiT-*ygfB* pBBR1_LgBiT-*zipA*	ID40Δ*ygfB*::rha-SmBiT-*ygfB* carrying a pBBR1 plasmid encoding for LgBiT fused to ZipA	Bohn lab
ID40Δ*ygfB*::rha-SmBiT-*ygfB* pBBR1_LgBIT-*uvrB*	ID40Δ*ygfB*::rha-SmBiT-*ygfB* carrying a pBBR1 plasmid encoding for LgBiT fused to UvrB	Bohn lab
ID40Δ*ygfB*::rha-SmBiT-*ygfB* pBBR1_LgBiT-*dinG*	ID40Δ*ygfB*::rha-SmBiT-*ygfB* carrying a pBBR1 plasmid encoding for LgBiT fused to DinG	Bohn lab
ID40Δ*ygfB*::rha-SmBiT-*ygfB* pBBR1_LgBiT-*mutL*	ID40Δ*ygfB*::rha-SmBiT-*ygfB* carrying a pBBR1 plasmid encoding for LgBiT fused to MutL	Bohn lab
ID40Δ*ygfB*::rha-SmBiT-*ygfB* pBBR1_LgBiT-*rhlE*	ID40Δ*ygfB*::rha-SmBiT-*ygfB* carrying a pBBR1 plasmid encoding for LgBiT fused to RhlE	Bohn lab
ID40Δ*ygfB*::rha-SmBiT-*ygfB* pBBR1_LgBiT-*recG*	ID40Δ*ygfB*::rha-SmBiT-*ygfB* carrying a pBBR1 plasmid encoding for LgBiT fused to RecG	Bohn lab
ID40Δ*ygfB*::rha-SmBiT-*ygfB* pBBR1_LgBiT-06036	ID40Δ*ygfB*::rha-SmBiT-*ygfB* carrying a pBBR1 plasmid encoding for LgBiT fused to TUEID40_06036	Bohn lab
ID40Δ*ygfB*::rha-SmBiT-*ygfB* pBBR1_LgBiT-*pslH*	ID40Δ*ygfB*::rha-SmBiT-*ygfB* carrying a pBBR1 plasmid encoding for LgBiT fused to PslH	Bohn lab
ID40Δ*ygfB*::rha-SmBiT-*ygfB* pBBR1_LgBiT-*rbsB*	ID40Δ*ygfB*::rha-SmBiT-*ygfB* carrying a pBBR1 plasmid encoding for LgBiT fused to RbsB	Bohn lab
ID40Δ*ygfB*::rha-SmBiT-*ygfB* pBBR1_LgBiT-05398	ID40Δ*ygfB*::rha-SmBiT-*ygfB* carrying a pBBR1 plasmid encoding for LgBiT fused to TUEID40_05398	Bohn lab

2. Materials and Methods

Name of strain	Info	Source/Published in
ID40Δ*ygfB*::rha-SmBiT-*ygfB* pBBR1_LgBiT-*pslB*	ID40Δ*ygfB*::rha-SmBiT-*ygfB* carrying a pBBR1 plasmid encoding for LgBiT fused to PslB	Bohn lab
ID40Δ*ygfB*::rha-SmBiT-*ygfB* pBBR1_LgBiT-*nirQ*	ID40Δ*ygfB*::rha-SmBiT-*ygfB* carrying a pBBR1 plasmid encoding for LgBiT fused to NirQ	Bohn lab
ID40Δ*ygfB*::rha-SmBiT-*ygfB* pBBR1_LgBiT-*waaG*	ID40Δ*ygfB*::rha-SmBiT-*ygfB* carrying a pBBR1 plasmid encoding for LgBiT fused to WaaG	Bohn lab
ID40Δ*ygfB*::rha-SmBiT-*ygfB* pBBR1_LgBiT-*mreB*	ID40Δ*ygfB*::rha-SmBiT-*ygfB* carrying a pBBR1 plasmid encoding for LgBiT fused to MreB	Bohn lab
ID40Δ*ygfB*::rha-SmBiT-*ygfB* pBBR1_LgBiT-*ygfB*	ID40Δ*ygfB*::rha-SmBiT-*ygfB* carrying a pBBR1 plasmid encoding for LgBiT fused to *YgfB*	Bohn lab
ID40Δ*ygfB*::rha-SmBiT-*ygfB* pBBR1_LgBiT-05668	ID40Δ*ygfB*::rha-SmBiT-*ygfB* carrying a pBBR1 plasmid encoding for LgBiT fused to TUEID40_05668	Bohn lab
ID40Δ*ygfB*::rha-SmBiT-*ygfB* pBBR1_LgBiT-*pleD*	ID40Δ*ygfB*::rha-SmBiT-*ygfB* carrying a pBBR1 plasmid encoding for LgBiT fused to PleD	Bohn lab
ID40Δ*ygfB*::rha-SmBiT-*ygfB* pBBR1_LgBiT-*relA*	ID40Δ*ygfB*::rha-SmBiT-*ygfB* carrying a pBBR1 plasmid encoding for LgBiT fused to RelA	Bohn lab
ID40Δ*ygfB*::rha-SmBiT-*ygfB* pBBR1_LgBiT-*srkA*	ID40Δ*ygfB*::rha-SmBiT-*ygfB* carrying a pBBR1 plasmid encoding for LgBiT fused to SrkA	Bohn lab
ID40Δ*ygfB*::rha-SmBiT-*ygfB* pBBR1_LgBiT-*ubiB*	ID40Δ*ygfB*::rha-SmBiT-*ygfB* carrying a pBBR1 plasmid encoding for LgBiT fused to UbiB	Bohn lab
ID40Δ*ygfB*::rha-SmBiT-*ygfB* pBBR1_LgBiT-*waaC*	ID40Δ*ygfB*::rha-SmBiT-*ygfB* carrying a pBBR1 plasmid encoding for LgBiT fused to WaaC	Bohn lab
ID40Δ*ygfB*::rha-SmBiT-*ygfB* pBBR1_LgBiT-*rpsE*	ID40Δ*ygfB*::rha-SmBiT-*ygfB* carrying a pBBR1 plasmid encoding for LgBiT fused to RpsE	Bohn lab
ID40Δ*ygfB*::rha-SmBiT-*ygfB* pBBR1_LgBiT-*hflD*	ID40Δ*ygfB*::rha-SmBiT-*ygfB* carrying a pBBR1 plasmid encoding for LgBiT fused to HflD	This work
ID40Δ*ygfB*::rha-SmBiT-*ygfB* pBBR1_LgBiT-*ibpA*	ID40Δ*ygfB*::rha-SmBiT-*ygfB* carrying a pBBR1 plasmid encoding for LgBiT fused to IbpA	This work
ID40Δ*ygfB*::rha-SmBiT-*ygfB* pBBR1_LgBiT-*asrA*	ID40Δ*ygfB*::rha-SmBiT-*ygfB* carrying a pBBR1 plasmid encoding for LgBiT fused to AsrA	This work
ID40Δ*ygfB*::rha-SmBiT-*ygfB* pBBR1_LgBiT-*lon*	ID40Δ*ygfB*::rha-SmBiT-*ygfB* carrying a pBBR1 plasmid encoding for LgBiT fused to Lon	This work
ID40Δ*ygfB*::rha-SmBiT-*ygfB* pBBR1_LgBiT-*hemL*	ID40Δ*ygfB*::rha-SmBiT-*ygfB* carrying a pBBR1 plasmid encoding for LgBiT fused to HemL	This work
ID40Δ*ygfB*::rha-SmBiT-*ygfB* pBBR1_LgBiT-*lpxB*	ID40Δ*ygfB*::rha-SmBiT-*ygfB* carrying a pBBR1 plasmid encoding for LgBiT fused to LpxB	This work
ID40Δ*ygfB*::rha-SmBiT-*ygfB* pBBR1_LgBiT-*ettA*	ID40Δ*ygfB*::rha-SmBiT-*ygfB* carrying a pBBR1 plasmid encoding for LgBiT fused to EttA	This work

2. Materials and Methods

Name of strain	Info	Source/Published in
ID40Δ*ygfB*::rha-SmBiT-*ygfB* pBBR1_LgBiT-*rpoC*	ID40Δ*ygfB*::rha-SmBiT-*ygfB* carrying a pBBR1 plasmid encoding for LgBiT fused to RpoC	This work
Other *Pa* strains		
PA14 (DSM No.19882)	*"Clinical isolate from a human burn patient"*	DSMZ Braunschweig
PA14 pBBR1-532-luc	PA14 carrying pBBR1-532-luc	Bohn lab (Eggers et al., 2023)
PA14Δ*ygfB*	*"In-frame deletion mutant encoding the first and last 10 amino-acids of ygfB"*	Bohn lab (Eggers et al., 2023)
PA14Δ*ygfB* pBBR1-532-luc	*"In-frame deletion mutant encoding the first and last 10 amino-acids of ygfB; with plasmid pBBR1-532-luc"*	Bohn lab (Eggers et al., 2023)
ID72	*"Clinical bloodstream isolate, MDR strain"*	Bohn lab (Klein et al., 2019; Willmann, Götting, et al., 2018)
ID72 pBBR1-532-luc	*"Clinical bloodstream isolate, with plasmid pBBR1-532-luc"*	This work (Eggers et al., 2023)
ID72Δ*ygfB*	*"In-frame deletion mutant encoding the first and last 10 amino-acids of ygfB"*	This work (Eggers et al., 2023)
ID72Δ*ygfB* pBBR1-532-luc	*"In-frame deletion mutant encoding the first and last 10 amino-acids of ygfB; with plasmid pBBR1-532-luc"*	This work (Eggers et al., 2023)
ID143	*"Clinical bloodstream isolate, MDR strain"*	(Eggers et al., 2023; Willmann, Götting, et al., 2018)
ID143 pBBR1-532-luc	*"Clinical bloodstream isolate, MDR strain; with plasmid pBBR1-532-luc"*	This work (Eggers et al., 2023)
ID143Δ*ygfB* pBBR1-532-luc	*"In-frame deletion mutant encoding the first and last 10 amino-acids of ygfB; ; with plasmid pBBR1-532-luc"*	This work (Eggers et al., 2023)
PAO1 DMSZ No.22644	*"Infectious wound"*	DMSZ Braunschweig
PAO1 pBBR1-532-luc	*PAO1 carrying pBBR1-532-luc*	Bohn lab (Eggers et al., 2023)
PAO1Δ*ygfB*	*"In-frame deletion mutant encoding the first and last 10 amino-acids of ygfB(...)"*	Bohn lab (Eggers et al., 2023)
PAO1Δ*ygfB* pBBR1-532-luc	In-frame deletion mutant of *ygfB* carrying pBBR1-532-luc	Bohn lab (Eggers et al., 2023)
Escherichia coli		
SM10 λ pir	*"thi thr leu tonA lacY supE recA::RP4-2-Tc::Mu Km λpir"*. Used for mobilization of plasmids in *P. aeruginosa* during mutagenesis	(Simon et al., 1983)
DH5α	*"Used for propagation of plasmids during cloning"*	Thermo Scientific
One Shot™ TOP10 Chemically Competent *E. coli*		Thermo Scientific
BL21 DE3	*"fhuA2 [lon] ompT gal (λ DE3) [dcm] ΔhsdS λ DE3 = λ sBamHIo ΔEcoRI-B int::(lacI::PlacUV5::T7 gene1) i21 Δnin5"*. Used for overexpression of proteins using plasmids under control of a T7 promoter	New England Biolabs (NEB)
Dh5α pir116	Used for propagation of plasmids carrying a R6Ky origin, able to propagate plasmids due to carrying pir gene	(Platt et al., 2000)
β2163	Auxotrophic for diamino pimelic acid (DAP),	(Demarre et al., 2005)
BW25113	*Δ(araD-araB)567, ΔlacZ4787(::rrnB-3), λ⁻, rph-1, Δ(rhaD-rhaB)568, hsdR514;* parent strain of the Keio single gene	CGSC, (Datsenko & Wanner, 2000)

Name of strain	Info	Source/Published in
	knockout collection, derivative of *E. coli* K12	
JW5473-1	Derivative of BW25113 from Keio collection, Δ*ygfB::kan,* deletion of *ygfB*, carrying a kanamycin resistance cassette in the CDS of *ygfB*	Brötz-Oesterhelt Lab, (Baba et al., 2006)
BW25113Δ*ygfB*	Cleaned up version of JW5473-1, kanamycin resistance cassette has been excised using pCP20 plasmid, carries insertion sequence in *flhDC* promoter leading to overexpression of flagella regulon	This work
BW25113Δ*ygfB*_new	In-frame deletion mutants of *ygfB,* containing the first and last 10 amino acids of *ygfB*, generated using the pSB890y plasmid	This work

2.1.10. Plasmids

Table 10: Plasmids used in this study. Plasmid descriptions written in italics and marked with quotation marks are literally cited from Eggers et al. (2023). Plasmids described as "this work" were generated by me, plasmids described as Bohn lab were generated by coauthors or colleagues in the lab.

Plasmid	Info	Source/Published in
pEXG2	*"Allelic exchange vector with pBR origin, Gm^R, $sacB^+$"*	(Rietsch et al., 2005)
pEXTK	*"Allelic exchange vector derived from pEXG2, sacB exchanged by thymidine-kinase; Gm^R, Tk+"*	Bohn lab (Eggers et al., 2023)
pEXG2Δ*ygfB*	*"pEXG2 derivative for the in-frame deletion of ygfB-CDS"*	Bohn lab (Eggers et al., 2023; Sonnabend et al., 2020)
pEXG2Δ*alpA*	*"pEXG2 derivative for the in-frame deletion of alpA-CDS"*	Bohn lab (Eggers et al., 2023)
pEXG2Δ*ampDh3*	*"pEXG2 derivative for the in-frame deletion of ampDh3-CDS"*	Bohn lab (Eggers et al., 2023)
pEXG2::*ampDh3*-HiBiT	*"pEXG2 derivative for the C-terminal knockin of Strep-HiBiT tag into ampDh3"*	Bohn lab, made by Genescript (Eggers et al., 2023)
pEXG2*::alpA*-HiBiT	*"pEXG2 derivative for the C-terminal knockin of HiBiT tag into alpA"*	Bohn lab, HiBiT tag obtained from Promega (Eggers et al., 2023)
pEXTKΔ*ygfB*	*"pEXTK derivative for the in-frame deletion of ygfB-CDS"*	Bohn lab (Eggers et al., 2023)
pEXTK::HA-*alpR*	*"pEXTK derivative for the N-terminal knockin of HA-tag into alpR"*	This work (Eggers et al., 2023)
pEXTK::*ampDh3*-HiBiT	*"pETK derivative for the C-terminal knockin of HiBiT into ampDh3"*	Bohn lab (Eggers et al., 2023)
pJM220	*"Mini-TN7 based vector with transcriptional terminators, rhamnose inducible promoter and MCS, Gm^R"*	(Meisner & Goldberg, 2016)
pJM220*ygfB*	*"pJM220 derivate for the complementation of the ygfB-CDS"*	Bohn lab (Eggers et al., 2023; Sonnabend et al., 2020)
pJM220*alpA*	*"pJM220 derivate for the complementation of the alpA-CDS"*	Bohn lab (Eggers et al., 2023)
pJM220*ampDh3*	*"pJM220 derivate for the complementation of the amppDh3-CDS* [sic]*"*	Bohn lab (Eggers et al., 2023)
pJM220_SmBiT-*ygfB*	pJM220 derivative for the introduction of SmBiT-tagged *ygfB* at the Tn7-site of ID40	Bohn lab

2. Materials and Methods

Plasmid	Info	Source/Published in
pTNS3	*"Amp^R, plasmid expressing tnsABCD from P1 and Plac"*	(Choi et al., 2008)
pFLP2	*"Cb^R/Amp$^{R;}$ sacB$^+$; Flp recombinase"*	(Hoang et al., 2000)
pGEX-4T3	*"Overexpression vector und* [sic] *control of a tac-promoter, N-terminal GST tag and a thrombin cleavage site; Amp$^{R"}$*	GE Healthcare
pETM-30	*"Overexpression vector under the control of a T7-promoter, N-terminal His-GST-tag, N-terminal TEV-cleavage site, Kan^R"*	EMBL Heidelberg
pETM-41	*"Overexpression vector under the control of a T7-promoter, N-terminal His-MBP-tag, Kan^R"*	EMBL Heidelberg
pGEX-4T3_*ygfB*	*Derivative of pGEX-4T3 for the overexpression of GST-YgfB derived from P. aeruginosa ID40"*	Bohn lab (Eggers et al., 2023)
pETM-30_*ygfB*	*"Derivative of pETM-30 for the overexpression of His-GST-YgfB"*	Bohn lab (Eggers et al., 2023)
pETM30_Ec_*ygfB*	Derivative of pETM30 for the overexpression of 6xHis-tagged YgfB derived from *E. coli* BW25113	This work
pETM30_stop	Derivative of pETM30, carrying a stop-codon after the coding sequence of His-GST. For purification of 6xHis-tagged GST	This work
pETM-41_*alpA*	*"Derivative of pETM-41 for the overexpression of His-MBP-AlpA"*	This work (Eggers et al., 2023)
pNL1.1	*"Promoterless basic vector encoding Nanoluc Luciferase"*	Promega
pVT77	*"Vector containing lacI-tdk cassette"*	(Trebosc et al., 2016)
pME6032	*"Modified pVS1-p15A shuttle vector including lacI^q-P$_{tac}$ promoter, Tc^r"*	(Heeb et al., 2002), (Heeb et al., 2000)
pBBR1-MCS-5	*"Broad host range vector, Gm^R"*	(Obranic et al., 2013)
pBBR1-532-luc	*"pBBR1-MCS-5 derivate containing ampDh3 promoter fragment bp -532 to -1 upstream of CDS fused to Nanoluc luciferase"*	Bohn lab (Eggers et al., 2023)
pBit1.1C	Amp^R, containing LgBiT with an N-terminal GS linker for generation of C-terminally LgBiT-tagged fusion proteins	Promega
pBBR1_LgBiT	pBBR1-MCS-5 derivate carrying LgBiT amplified from pBit1.1C under a lac promoter	Bohn lab
pBit1.1N	Amp^R, containing LgBiT with a C-terminal GS linker for generation of N-terminally LgBiT-tagged fusion proteins	Bohn lab
pBit1.1N_LgBiT_*ygfB*	Derivative of pBit1.1N carrying a N-terminally LgBiT-tagged YgfB, for amplification of LgBiT-*ygfB* CDS and cloning in pBBR1-MCS5	Bohn lab
pBBR1_LgBiT-*ygfB*	pBBR1-MCS-5 derivate carrying LgBiT-YgfB under a lac promoter, LgBiT-*ygfB* amplified from pBit1.1N_LgBiT-*ygfB*	Bohn lab
pBBR1_LgBiT-*radA*	pBBR1-MCS-5 derivate carrying LgBiT-RadA under a lac promoter	Bohn lab
pBBR1_LgBiT-*ubiH*	pBBR1-MCS-5 derivate carrying LgBiT-UbiH under a lac promoter	Bohn lab
pBBR1_LgBiT-*zipA*	pBBR1-MCS-5 derivate carrying LgBiT-ZipA under a lac promoter	Bohn lab
pBBR1_LgBiT-*uvrB*	pBBR1-MCS-5 derivate carrying LgBiT-UvrB under a lac promoter	Bohn lab
pBBR1_LgBiT-*dinG*	pBBR1-MCS-5 derivate carrying LgBiT-DinG under a lac promoter	Bohn lab
pBBR1_LgBiT-*mutL*	pBBR1-MCS-5 derivate carrying LgBiT-MutL under a lac promoter	Bohn lab

2. Materials and Methods

Plasmid	Info	Source/Published in
pBBR1_LgBiT-*recG*	pBBR1-MCS-5 derivate carrying LgBiT-RecG under a lac promoter	Bohn lab
pBBR1_LgBiT-*rhlE*	pBBR1-MCS-5 derivate carrying LgBiT-RhlE under a lac promoter	Bohn lab
pBBR1_LgBiT-06036	pBBR1-MCS-5 derivate carrying LgBiT-TUEID40_06036 under a lac promoter	Bohn lab
pBBR1_LgBiT-*pslH*	pBBR1-MCS-5 derivate carrying LgBiT-PslH under a lac promoter	Bohn lab
pBBR1_LgBiT-*rbsB*	pBBR1-MCS-5 derivate carrying LgBiT-RbsB under a lac promoter	Bohn lab
pBBR1_LgBiT-05398	pBBR1-MCS-5 derivate carrying LgBiT-TUEID40_05398 under a lac promoter	Bohn lab
pBBR1_LgBiT-*pslB*	pBBR1-MCS-5 derivate carrying LgBiT-PslB under a lac promoter	Bohn lab
pBBR1_LgBiT-*nirQ*	pBBR1-MCS-5 derivate carrying LgBiT-NirQ under a lac promoter	Bohn lab
pBBR1_LgBiT-*waaG*	pBBR1-MCS-5 derivate carrying LgBiT-WaaG under a lac promoter	Bohn lab
pBBR1_LgBiT-*mreB*	pBBR1-MCS-5 derivate carrying LgBiT-MreB under a lac promoter	Bohn lab
pBBR1_LgBiT-05668	pBBR1-MCS-5 derivate carrying LgBiT-TUEID40_05668 under a lac promoter	Bohn lab
pBBR1_LgBiT-*pleD*	pBBR1-MCS-5 derivate carrying LgBiT-PleD under a lac promoter	Bohn lab
pBBR1_LgBiT-*relA*	pBBR1-MCS-5 derivate carrying LgBiT-RelA under a lac promoter	Bohn lab
pBBR1_LgBiT-*srkA*	pBBR1-MCS-5 derivate carrying LgBiT-SrkA under a lac promoter	Bohn lab
pBBR1_LgBiT-*ubiB*	pBBR1-MCS-5 derivate carrying LgBiT-UbiB under a lac promoter	Bohn lab
pBBR1_LgBiT-*waaC*	pBBR1-MCS-5 derivate carrying LgBiT-WaaC under a lac promoter	Bohn lab
pBBR1_LgBiT-*rpsE*	pBBR1-MCS-5 derivate carrying LgBiT-RpsE under a lac promoter	Bohn lab
pBBR1_LgBiT-*hflD*	pBBR1-MCS-5 derivate carrying LgBiT-HflD under a lac promoter	This work
pBBR1_LgBiT-*ibpA*	pBBR1-MCS-5 derivate carrying LgBiT-IbpA under a lac promoter	This work
pBBR1_LgBiT-*asrA*	pBBR1-MCS-5 derivate carrying LgBiT-AsrA under a lac promoter	This work
pBBR1_LgBiT-*lon*	pBBR1-MCS-5 derivate carrying LgBiT-Lon under a lac promoter	This work
pBBR1_LgBiT-*hemL*	pBBR1-MCS-5 derivate carrying LgBiT-HemL under a lac promoter	This work
pBBR1_LgBiT-*lpxB*	pBBR1-MCS-5 derivate carrying LgBiT-LpxB under a lac promoter	This work
pBBR1_LgBiT-*ettA*	pBBR1-MCS-5 derivate carrying LgBiT-EttA under a lac promoter	This work
pBBR1_LgBiT-*rpoC*	pBBR1-MCS-5 derivate carrying LgBiT-RpoC under a lac promoter	This work
pSB890y	Suicide plasmid, derivate of pSB890, PstI restiction sites removed, Tet^R, R6Ky origin	(Weirich et al., 2017)
pSB890y_*ygfB*	Derivate of pSB890y containing the first and last 10 amino acids of *ygfB*, for mutagenesis of BW25113	This work
pCP20	Amp^R, temperature-dependent replication, thermal induction of FLP recombinase	(Cherepanov & Wackernagel, 1995)

2.1.11. Oligonucleotides

Table 11: Primers used for cloning and mutagenesis. Primer descriptions written in italics and marked with quotation marks are cited literally from Eggers et al. (2023).

Plasmid	Primer for Gibson Cloning/PCR/Sequencing	Sequence 5'–3'
pEXG2 derivates		
"Gibson assembly of linearized pEXG2 (template pEXG2) with up and down fragments (template ID40). Sequencing primers: 3pEXG2_seq_f and 4pEXG2_seq_r. For validation of mutants the primer GOI_seqF / GOI_seqR and GOI_seqF / GOI_seq_insideR were used"		
	gib_uni_pEXG2_f (linearization of vector)	aggtcgactctagaggatcc
	gib_uni_pEXG2_r (linearization of vector)	ttccggctcgtataatgtgt
	3pEXG2_seq_f	tactgtgttagcggtctg
	4pEXG2_seq_r	gatccggaacataatggtg
pEXG2Δ*alpA*	1572alpA_up_F	agctaattccacacattatacgagccggaaagtaccccgagcatccac
	1573alpA_up_R	aataccatgtttcaaagtaccgagcaggcggaggtggggatcgtgggc
	1574 alpA_dn_F	tttttagcgctcgcccacgatccccacctccgcctgctcggtactttg
	1575alpA_dn_R	tcgagcccggggatcctctagagtcgacctttgaagctgcgaatgcgc
	1578AlpA_seq_F	ttggctcggacatggatg
	1579alpA_seq_R	caagcgtccgtatatggg
	1580alpA_inside_R	ctgtcgaagagcaccctg
pEXG2Δ*ampDh3*	959 ampDH3_up_F	agctaattccacacattatacgagccggaaccaggtgatcctgtcgatg
	960 ampDH3_up_R	atgctgaccatcgactacaacagctatcgctacgctctgaacgagaaataccc
	961 ampDH3_dn_F	tcaggccgggtatttctcgttcagagcgtagcgatagctgttgtagtcgatg
	967ampDh3_dn_R	tcgagcccggggatcctctagagtcgacctttcatcctgaccctctgcg
	963ampDH3_seq_F	attcggccattcgatgag
	964ampDH3_seq_R	cggaggctttccatcatc
	965ampDH3_inside_R	gccttccagatgcatttcc
pEXG2::*alpA*-HiBiT	1620alpAHiBiT_up_F	agctaattccacacattatacgagccggaaggacttgccgcgctccagatc
	1621alpAHiBiT_up_R	ttcttgaacagccgccagccgctcactccactcgaaccaccgctcgagccgcgctcgcccacgatccc
	1622alpAHiBiT_dn_F	gagtgagcggctggcggctgttcaagaagattagctaaaaaaatttctgtatgaaaacgggttttccc
	1623alpAHiBiT_dn_R	gaattcgagctcgagcccggggatcctctagagtcgacctaggtgctcggcacgatac
	1624alpAHiBiT_seq_F	ggcgggatttcgtccttg
	1625alpAHiBiT_seq_R	gagcttggctcggacatg
	1081HiBiT_inside_R	tcttcttgaacagccgcc
pEXG2-*ampDh3*-HiBiT_up *"Gibson assembly of linearized pEXG2 with ampDh3_up fragment (ID40 as template) and strep-HiBiT fragment"*	1072 ampDh3_up_F	agctaattccacacattatacgagccggaaatgctgaccatcgactacaac
	1073ampDh3_up_R	cttctcaaattgaggatgactccacgcgctggccgggtatttctcgtt
	1074strep-HiBiT_F	ctctacgctctgaacgagaaataccggccagcgcgtggagtcatcc
	1075strep-HiBiT_R	tcgagcccggggatcctctagagtcgacctttagctaatcttcttgaacagccg

Plasmid	Primer for Gibson Cloning/PCR/Sequencing	Sequence 5‘–3‘
	1073ampDh3_up_R	cttctcaaattgaggatgactccacgcgctggccgggtatttctcgtt
pEXG2-*ampDh3*-HiBiT *“Gibson assembly of linearized pEXG2-ampDh3-HiBiT_up (pEXG2-ampDh3-HiBiT_up as template) and downstream fragment”*	1076peXG2-HiBiTup_lin_F (Linearization of vector)	ttagctaatcttcttgaacagccgccagccgctcactccactcgaaccac
	1077peXG2-HiBiTup_lin_R (Linearization of vector)	aaatcggccagcagttgcaggttcaggccgaggtcgactctagaggatccc
	1078ampDH3dn_F	ggctggcggctgttcaagaagattagctaagccattaaccgcgagcg
	1285ampDh3dn_R	tcgagcccggggatcctctagagtcgacctgctggtgaccctgctctac
	1080ampDH3_seq_F	gaaggaactctacgaggccg
	1081HiBiT_inside_R	tcttcttgaacagccgcc
	963ampDh3_seq_R	attcggccattcgatgag
pEXTK *“Gibson assembly with linearized pEXG2 and lacI-tdk fragment from pVT77;1375-1378 sequencing primer”*	1371pEXG2_lin_R	aaacgcaaaagaaaatgccg
	1372pexAZTlin_F	gcaggtaagctaattccacac
	1373lacI-tdK_F	cttccataatcggcattttcttttgcgtttttaatcgtggcgatgcctttc
	1374lacI-tdk_R	tcgtataatgtgtggaattagcttacctgcgacaccatcgaatggtgcaaaac
	1375pEXTKseq1_F	cttatgtcaattcgagaattacg
	1376pEXTKseq2_R	gagattcgtgcggaacatg
	1377pEXTKseq3_F	acctatacgcgaactgac
	1378pEXTKseq4_F	gttaacggcgggatataac
pEXTK derivates *“Gibson assembly of linearized pEXTK (template pEXTK) with up and down fragment (template ID40). Sequencing primers: 1388pEXT_seqF and 4pEXG2_seq_r For validation of mutants the primer GOI_seqF / GOI_seq_R and GOI_seq_F / GOI_inside_R were used”*		
	1gib_uni_pEXG2_F (linearization of pEXTK vector)	aggtcgactctagaggatcc
	1467gib_uni_pEXTK_R (linearization of pEXTK vector)	ttccggctcgtataatgtgtggaattagcttacctgc
	1388pEXT_seqF	accctgaattgactctcttcc
pEXTKΔ*ygfB* *“Template for ygfB insert derived from pEXG2ΔygfB”*	704pEXG2_ygfB_up_F	agctaattccacacattatacgagccggaagtagcagtcgatctcgcag
	707pEXG2_ygfB_dn_R	ctcgccgaggcggccatgccggtctcgccgccttcactgcactgaggtttc
	708ygfB_seq_F	catgaccttcacttcgttg
	709ygfB_seq_R	cttgtcgagaatctgcac
	710ygfB_inside_R	ggaagtcatggaatacctg
pEXTK-HA-*alpR*	1599HAalpR_up_F	agctaattccacacattatacgagccggaaggacatggatgactcccg
	1600HAalpR_up_R	gtaagcgtaatctggaacatcgtatgggtacataggtggaaagactaaggg
	1601HAalpR_dn_F	tacccatacgatgttccagattacgcttacccatacgatgttccagattacgctgaactca-aagatcgcatcaagg
	1602HAalpR_dn_R	tcgagcccggggatcctctagagtcgaccttcagaccagcaccgagtac

Plasmid	Primer for Gibson Cloning/PCR/Sequencing	Sequence 5‘–3‘
	1603HAlpR_seq_F	gcgaaacgcacggtcatc
	1604HAalpRseq_R	gcgctccagatcggaaatg
	1248 HA_inside_R	tggaacatcgtatgggtaagc
pEXTK-*ampDh3*-HiBiT *“Gibson assembly using linearized pEXTK and ampDh3-strep-HiBiT fragment (from pEXG2-HiBiT as template)”*	1072 ampDh3_up_F	agctaattccacacattatacgagccggaaatgctgaccatcgactacaac
	1285ampDh3_dn_R	tcgagcccggggatcctctagagtcgacctgctggtgaccctgctctac
	1080ampDH3_seq_F	gaaggaactctacgaggccg
	1081HiBiT_inside_R	tcttcttgaacagccgcc
	963ampDh3_seq_R	attcggccattcgatgag
pJM220 derivatives *“Gibson assembly of linearized pJM220 (template pJM220) with coding seqeunce of GOI. For validation of plasmids the primers 777pJM220_seq_f and 778pJM220_seq_r were used”*		
	777pJM220_seq_f	ttttcaagatacagcgtgaa
	778pJM220_seq_r	gcccaaacataacaggaaga
pJM220_*alpA* *“Gibson assembly of linearized pJM220 with alpA coding sequence of ID40 (template ID40)”*	773Gib_uni_pJM220_F (linearization of vector)	tacctcgcgaaggccttgca
	774Gib_uni_pJM220_R (linearization of vector)	aagcttctcgaggaattcctgc
	2074 pJM220_alpA_F	agtgctctgcaggaattcctcgagaagcttatgtttcaaagtaccgag
	2075pJM220_alpA_R	ctggttggcctgcaaggccttcgcgaggtattagcgctcgcccacgatc
pJM220_*ampDh3* “*Gibson assembly of linearized pJM220 with ampDh3 coding sequence of ID40 (template ID40)”*	773Gib_uni_pJM220_F (linearization of vector)	tacctcgcgaaggccttgca
	774Gib_uni_pJM220_R (linearization of vector)	aagcttctcgaggaattcctgc
	2072pJM220_ampDh3_F	agtgctctgcaggaattcctcgagaagcttatgctgaccatcgactacaac
	2073pJM220_ampDh3_R	ctggttggcctgcaaggccttcgcgaggtatcaggccgggtatttctcg
pJM220_SmBiT-*ygfB* SmBiT amplified using 1987/1988 using pBiT2.1C as template, pJM220_ygfB linearized using 1986/774	1986Gib_uni_pJM220-SmBiT-YgfB_lin-F	atgtccactcagaattccgcc
	774Gib_uni_pJM220_r	aagcttctcgaggaattcctgc
	1987Gib-pJM220-SmBiT-YgfB_F	ctctgcaggaattcctcgagaagcttgtgaccggctaccggctg
	1988Gib-pJM220-SmBiT-YgfB_R	ggcgctgtaggcggaattctgagtggacatacctgacgaccctccacctc
Others		
pGEX4T3_*ygfB* *“Gibson assembly of linearized pGEX4T3 with coding sequence of ygfB (template ID40); 847 and 848 sequencing primer”*	845Gib_pGEX4T3_R	ggaattcggggatccacgcg
	846Gib_pGEX4T3_F	cgggtcgactcgagcggc
	843Gib_pGEX4T3_ygfB_F	gatctggttccgcgtggatccccgaattccatgccggtctcgccggcc
	844Gib_pGEX4T3_ygfB_R	atcgtcagtcagtcacgatgcggccgctcgagtcgacccgtcagtgcagtgaaggcttgggagcgg
	847pGEX4T3_seq_F	atgttgtatgacgctcttga
	848pGEX4T3_seq_R	caagaattatacactccgct

Plasmid	Primer for Gibson Cloning/PCR/Sequencing	Sequence 5‘–3‘
	1693T7_prom	taatacgactcactataggg
	1694T7_term_sw	gctagttattgctcagcgg
pETM-41_*alpA* *“Gibson assembly of linearized pETM-41 with coding sequence of alpA (template ID40); 1693 and 1694 sequencing primer”*	1769_pETM41_lin_F	taatgaggtaccggatccgaattcgagc
	1770_pETM41_lin_R	gcccatggcgccctgaaaataaag
	1771_pETM41_MBP-AlpA-fw	gagaatctttattttcagggcgccatgggctttcaaagtaccgagcaggcg
	1772_pETM41_MBP-AlpA_rw	gagctcgaattcggatccggtacctcattattagcgctcgcccacgat
pETM-30_*ygfB* *“Gibson assembly of linearized pETM-30 with coding sequence of ygfB (template ID40); 1693 and 1694 sequencing primer”*	1824_pETM-30_linF	taaggtaccggatccgaattcg
	1825_pETM-30_linR	gccatggcgccctgaaaa
	1826_pETM-30_ygfB_insert_F	gagaatctttattttcagggcgccatggcgatgtccactcagaattccgcc
	1827_pETM-30_ygfB_insertR	acggagctcgaattcggatccggtaccttagtgcagtgaaggcttggg
pETM30_Ec_ygfB *“Gibson assembly using linearized pETM30 (1824/1825) and Ec_ygfB (template E. coli BW25113); Sequencing primer: 1693/1694”*	2508_pETM30_Ec-ygfB_f	gagaatctttattttcagggcgccatggcgatgtctatacagaacgaaatgcc
	2509_pETM30_Ec_ygfB_r	gacggagctcgaattcggatccggtaccttattagtgtagagtcggtttttgtac
pETM30_stop Gibson assembly of a pETM30 plasmid linearized with the shown primers, inserting a stop codon behind the GST coding sequence; Sequencing primer: 1693/1694	2607pETM30_stop_f	gagaatctttattttcagggcgccatggcgtaaggtaccggatccgaattcg
	2608pETM30_stop_r	acggagctcgaattcggatccggtaccttacgccatggcgccctgaaaa
pSB90y_*ygfB* Gibson assembly of the linearized pSB890y plasmid with up and down fragments of *ygfB,* Template: *E. coli* BW25113, plasmid was sequenced with 357/358, mutants were confirmed by PCR with 2232/2233 and 2232/2606	347_pSB890y_fwd (linearization of vector); from AG Schütz	caagctcaataaaaagccccac
	348_pSB890y_rev (linearization of vector); from AG Schütz	caagagggtcattatatttcgcg
	2602pSB890y_ygfB_up_f	gttattccgcgaaatataatgaccctcttgggtaatatcgccagcgtaac
	2603pSB890y_ygfB_up_r	atgtctatacagaacgaaatgcctggttacccagaagtacaaaaaccgactc
	2604pSB890y_ygfB_dn_f	ttagtgtagagtcggtttttgtacttctgggtaaccaggcatttcgttctg
	2605pSB890y_ygfB_dn_r	ccaccgcggtggggctttttattgagcttggcggatttcttgtcgggata
	357_p890seqF; from AG Schütz	cgtcaccaaatgatgttattcc
	358_p890seqR; from AG Schütz	gttgagaagcggtgtaagtg
	2232Keio_JW5473-1_ygfB_f	ggttaaacagaacgctgtgg
	2233Keio_JW5473-1_ygfB_r	gctgccttcgtctttagacc
	2606pSB890y_ygfB_inside_r	ggtcaatcacttcctgcttg

Plasmid	Primer for Gibson Cloning/PCR/Sequencing	Sequence 5‘–3‘
Screening clones after excision of kan^R by pCP20 2232 and 2233 were used as well as 2225	2225_Keio_proof_k1	cagtcatagccgaatagcct
Screening for insertion of IS-element in *flhDC* promoter	2485Ec_flhDC_ko_dnF	ttaaacagcctgtactctctgttcatccagaatgtgtttcagcaactcg
	2486Ec_flhDC_ko_dnR	ccaccgcggtggggctttttattgagcttgaagcgagagtaattaaactgatg
pBBR-532-luc *“Gibson assembly of linearized pBBR with ampDh3 promoter fragment -1 to -532 prior to CDS (template ID40) and nanoluc (template pNL1.1); Sequencing primer: 944 and 945 “*	946 pBBR1_lin_R	gcgttaatattttgttaaaattcgcg
	947 pBBR1_lin_F	gcctggggtgcctaatgag
	948 nanoluc pBBR-F	aacgcgaattttaacaaaatattaacgcttacgccagaatgcgttcg
	949nanoluc_pbbr R	ctttccatcatccgaaaaaaggtgaaaaccatggtcttcacactcgaagatttc
	950ampDH3_532_F	cccaacgaaatcttcgagtgtgaagaccatggttttcacctttttttcggatgatg
	951 ampDH3_532_R	gagttagctcactcattaggcaccccaggctagccgctctgtcgaggg
	944 pBBR1 seqF	cttattcaggcgtagcac
	945 pBBR1 seqR	cttattcaggcgtagcac
pBBR1_lgbit and derivates Sequencing primer for N-terminally LgBiT-tagged constructs made from PBBR1_LgBiT-*ygfB*: 2481 and 1757		
	2431 lgbit-x sequniF	gtaacagggaccctgtgg
	1757pBBRseqlgbitF	tcgcagtcggcctattgg
	1758pBBRseqlgbitR	gcaccccaggctttacac
pBBR1_lgbit Gibson assembly of linearized pBBR1-MCS5 with LgBiT-insert amplified from pBit1.1C Sequencing primer: 1757/1758	1753pBBRlaclinF (linearization of backbone)	catagctgtttcctgtgtgaaattg
	1754pBBRlaclinR (linearization of backbone)	gcgttaatattttgttaaaattcgcg
	1755pbbrlgbitF	ttaacgcgaattttaacaaaatattaacgcttagctgttgatggttactcggaaca
	1756pBBRlgbitR	gataacaatttcacacaggaaacagctatggtcttcacactcgaagatttcgttg
pBiT1.1N_LgBiT-ygfB Gibson cloning of linearized pBit1.1N and ygfb (Template ID40) Sequencing primer: 1743/1744	1773_lgBit-ygfB-for (linearization of backbone)	tccaccgctcgagcctcc
	1774_lgBit-ygfB-rev (linearizatio of backbone)	taagctagcagatcttctagagtcgggg
	1775_lgBit-ygfB-gib-for	ggcgggagcggaggtggaggctcgagcggtggatccactcagaattccgcctac
	1776_lgBit-ygfB-gib-rev	cgccccgactctagaagatctgctagcttagtgcagtgaaggcttggg
	1743p2.1NCseqF	ctcgaacaccgagcgacc
	1744p2.1NCseqR	agttgtggtttgtccaaactcatc
pBBBR1_LgBiT-ygfB Gibson assembly of linearized pBBR1-MCS5 (1753/1754) with LgBiT-*ygfB* insert amplified from pBiT1.1N_LgBiT-ygfB Seqencing primer: 1757/1758	1777_pBBRlgbit-ygfBgib-for	acgcgaattttaacaaaatattaacgcttagtgcagtgaaggcttggg
	1778 pBBRlgbit-ygfBgibRev	gataacaatttcacacaggaaacagctatgatggtcttcacactcgaagatttc
pBBR1_lgbit-radA Gibson assembly of linearized	1754pBBRlaclinR (linearization of backbone)	gcgttaatattttgttaaaattcgcg
	1773_lgBit-ygfB-for (linearization of backbone)	tccaccgctcgagcctcc

Plasmid	Primer for Gibson Cloning/PCR/Sequencing	Sequence 5‘–3‘
pBBR1_LgBiT-*ygfB* and insert amplified from ID40	1965 lgBitradA_F	gggagcggaggtggaggctcgagcggtggagccaaggccaagcgcatg
	1966 lgbitradA_R	ttaacgcgaattttaacaaaatattaacgctcactcgaagagggcgtc
pBBR1_lgbit-ubiH Gibson assembly of linearized pBBR1_LgBiT-ygfB and insert amplified from ID40	1971 lgbit ubiH-F	gggagcggaggtggaggctcgagcggtggaagcaaggtcaacctggcg
	1972 lgbit ubiH_R	ttaacgcgaattttaacaaaatattaacgcctacagcggccgcgcgcc
pBBR1_lgbit-zipA Gibson assembly of linearized pBBR1_LgBiT-ygfB and insert amplified from ID40	1969 lgbit zipA_F	gggagcggaggtggaggctcgagcggtggaatatcggtctgcgcgaatg
	1970 lgbit zipA_R	ttaacgcgaattttaacaaaatattaacgctcagcgcttctgcatcagg
pBBR1_lgbit-uvrB Gibson assembly of linearized pBBR1_LgBiT-ygfB and insert amplified from ID40	1967 lgbit uvrB_F	gggagcggaggtggaggctcgagcggtggagatacgttccaactcgactc
	1968 lgbit uvrB _R	ttaacgcgaattttaacaaaatattaacgctcagacgttgaccaggcg
pBBR1_LgBiT-dinG Gibson assembly of linearized pBBR1_LgBiT-ygfB and insert amplified from ID40	2076pBBRlgbitdinGF	gggagcggaggtggaggctcgagcggtggactcagcgccgaactcaag
	2077pBBRlgbitdinGR	ttaacgcgaattttaacaaaatattaacgctcaggcgatttcccgccg
	2088dingGseq1R	ttcaccagttccggcagc
	2089dingGseq2R	gaaatcgccgatctcttc
	2090dinGseq3R	ttcctgcagcagcacgtc
pBBR1_LgBiT-mutL Gibson assembly of linearized pBBR1_LgBiT-ygfB and insert amplified from ID40	2082pBBRlgbitmutlnewF	gggagcggaggtggaggctcgagcggtggaagtgaagcaccgcgtatc
	2083pBBRlgbitmutLnewR	ttaacgcgaattttaacaaaatattaacgctcagcgtccgcgcaggaa
pBBR1_LgBiT-recG Gibson assembly of linearized pBBR1_LgBiT-ygfB and insert amplified from ID40	2080pBBRlgbitrecG_F	gggagcggaggtggaggctcgagcggtggaaccgagctgtccagggtc
	2081pBBRlgbitrecG_R	ttaacgcgaattttaacaaaatattaacgctcacacttgaccgtattgctgg
	2084 recGseq1R	tggcaggtaagctcctcg
	2085recGseq2R	ccgaggttggcaaggaag
pBBR1_LgBiT-rhlE Gibson assembly of linearized pBBR1_LgBiT-ygfB and insert amplified from ID40	2078pBBRlgbitPA3950rhlE_F	gggagcggaggtggaggctcgagcggtggaacgttcgcttccctcggtc
	2079pBBRlgbitPA3950rhlE_R	ttaacgcgaattttaacaaaatattaacgcctatttgccggatggccg
	2086rhlseq1R	ttgtcgccatggatcgag
	2087rhlEseq2R	aaccaggaccagtgcacg
pBBR1_LgBiT-06036 Gibson assembly of linearized pBBR1_LgBiT-ygfB and insert amplified from ID40	2581lgbit06036	gggagcggaggtggaggctcgagcggtggaaagttcgaaggcacccagtcctacg
	2582lgbit06036	ttaacgcgaattttaacaaaatattaacgctcagcggctggcgcggc
pBBR1_LgBiT-pslH Gibson assembly of linearized	2519lgbitpslH F	ggagcggaggtggaggctcgagcggtggacgtattctctggatcctgccctac
	2520lgbit pslH R	ttaacgcgaattttaacaaaatattaacgcctatgcgcatgccggcg

Plasmid	Primer for Gibson Cloning/PCR/Sequencing	Sequence 5‘–3‘
pBBR1_LgBiT-ygfB and insert amplified from ID40		
pBBR1_LgBiT-rbsB	2536lgbitrbsBFwd	gggagcggaggtggaggctcgagcggtggaatgaagcgggtcgcttcc
Gibson assembly of linearized pBBR1_LgBiT-ygfB and insert amplified from ID40	2537lgbitrbsBRev	ttaacgcgaattttaacaaaatattaacgctcagggcgcggtcaccaa
pBBR1_LgBiT-05398	2432 lgbit 05398 Fwd	gggagcggaggtggaggctcgagcggtggagcggcgcctaccgacgc
Gibson assembly of linearized pBBR1_LgBiT-ygfB and insert amplified from ID40	2433 lgbit 05398 Rev	ttaacgcgaattttaacaaaatattaacgctcagcattggccggtctcctcg
pBBR1_LgBiT-pslB	2447 lgbit pslB Fwd	gggagcggaggtggaggctcgagcggtggaaacgccgtcgccccgct
Gibson assembly of linearized	2448 lgbit pslB Rev	ttaacgcgaattttaacaaaatattaacgctcaggctttcttctcgtcgctg
pBBR1_LgBiT-ygfB and insert amplified from ID40	2449 lgbit pslB Seq1	ttgcagaagaccttcctg
pBBR1_LgBiT-nirQ	2436 lgbit nirQ Fwd	ggagcggaggtggaggctcgagcggtggacgggacgcgacacccttc
Gibson assembly of linearized pBBR1_LgBiT-ygfB and insert amplified from ID40	2437lgbit nirQR	ttaacgcgaattttaacaaaatattaacgctcaggcgacatggagatcg
pBBR1_LgBiT-waaG	2443 lgbit waaG fwd	cgggagcggaggtggaggctcgagcggtggaaccctggcgttcatcctc
Gibson assembly of linearized pBBR1_LgBiT-ygfB and insert amplified from ID40	2444 lgbit waaG rev	ttaacgcgaattttaacaaaatattaacgctcatgaggcctccccgag
pBBR1_LgBiT-mreB	2566lgbitmreB Fwd	gggagcggaggtggaggctcgagcggtggattcaaaaaattgcgtggcatg
Gibson assembly of linearized pBBR1_LgBiT-ygfB and insert amplified from ID40	2567lgbitmreBrev	ttaacgcgaattttaacaaaatattaacgcttactcggtggagagcagg
pBBR1_LgBiT-05668	2440 lgbit 05668 fwd	gggagcggaggtggaggctcgagcggtggacgccgttggaatggctgg
Gibson assembly of linearized	2441 lgbit 05668 rev	ttaacgcgaattttaacaaaatattaacgctcagtcctgcagcagggtg
pBBR1_LgBiT-ygfB and insert amplified from ID40	2442 lgbit 05668 seq1	tcgctggagcgcatgaac
pBBR1_LgBiT-pleD	2578lgbitpleD fwd	gggagcggaggtggaggctcgagcggtggaatgaccgagcacgatgac
Gibson assembly of linearized	2579lgbitpleD rev	ttaacgcgaattttaacaaaatattaacgcttatcgagcgtcgggacg
pBBR1_LgBiT-ygfB and insert amplified from ID40	2580lgbitpleDseq1F	gcgatcgtcatggaagtc
pBBR1_LgBiT-relA	2429 pBBRlgbit rela FWD	gggagcggaggtggaggctcgagcggtggagtacaggtgagagcgcac
Gibson assembly of linearized	2430pBBR lgbit relA rev	ttaacgcgaattttaacaaaatattaacgctcaaggcgtacggttgcg

Plasmid	Primer for Gibson Cloning/PCR/Sequencing	Sequence 5‘–3‘
pBBR1_LgBiT-ygfB and insert amplified from ID40		
pBBR1_LgBiT-srkA	2564lgbitsrkA Fwd	gggagcggaggtggaggctcgagcggtggaccccatcccttcgaccaac
Gibson assembly of linearized pBBR1_LgBiT-ygfB and insert amplified from ID40	2565lgbit srkARev	ttaacgcgaattttaacaaaatattaacgctcagaacagccgcagcgg
pBBR1_LgBiT-ubiB	2585lgbitubiBFwd	gggagcggaggtggaggctcgagcggtggaaagctcctcgctgtccgc
Gibson assembly of linearized	2586lgbitubiBrev	ttaacgcgaattttaacaaaatattaacgcctagcggcgcaggatcag
pBBR1_LgBiT-ygfB and insert amplified from ID40	2587lgbitubiBseq1F	gacgaactcgacctgctc
pBBR1_LgBiT-waaC	2445 lgbit waaC fwd	gggagcggaggtggaggctcgagcggtggaagggtactgctggtcaaga
Gibson assembly of linearized pBBR1_LgBiT-ygfB and insert amplified from ID40	2446 lgbit waaC rev	ttaacgcgaattttaacaaaatattaacgctcatcggagggtctccg
pBBR1_LgBiT-rpsE	2568lgbit rpsE Fwd	gggagcggaggtggaggctcgagcggtggagcaaacaacgagcaaaag
Gibson assembly of linearized pBBR1_LgBiT-ygfB and insert amplified from ID40	2569lgbitrpseE Rev	ttaacgcgaattttaacaaaatattaacgcttagagaatctcctcgacgc
pBBR1_LgBiT-hflD	2774pBBr_lgbit-hflD_neu_f	gggagcggaggtggaggctcgagcggtggaagcgatccgcgacagcaac
Gibson assembly of linearized pBBR1_LgBiT-ygfB and insert amplified from ID40	2775pBBr_lgbit-hflD_neu_r	ttaacgcgaattttaacaaaatattaacgcggctggctcccggccatg
pBBR1_LgBiT-lpxB	2776pBBr_lgbit-lpxB_f	gggagcggaggtggaggctcgagcggtggagctgacggattgcgcgtag
Gibson assembly of linearized pBBR1_LgBiT-ygfB and insert amplified from ID40	2777pBBr_lgbit-lpxB_r	ttaacgcgaattttaacaaaatattaacgctcagcggcgctccaccag
pBBR1_LgBiT-rpoC	2778pBBr_lgbit-rpoC_f	gggagcggaggtggaggctcgagcggtggaaaagacttgcttaatctgttgaaaaacc
Gibson assembly of linearized pBBR1_LgBiT-ygfB and insert amplified from ID40	2779pBBr_lgbit-rpoC_r	ttaacgcgaattttaacaaaatattaacgcttagttaccgctcgagttcagc
pBBR1_LgBiT-ettA	2781pBBr_lgbit-ettA_f	gggagcggaggtggaggctcgagcggtggagctcagtacgtctacaccatg
Gibson assembly of linearized pBBR1_LgBiT-ygfB and insert amplified from ID40	2782pBBr_lgbit-ettA_r	ttaacgcgaattttaacaaaatattaacgcttacgccagtttcttgtagcg
pBBR1_LgBiT-hemL	2783pBBr_lgbit-hemL_f	gggagcggaggtggaggctcgagcggtggatcccgttccgaaacgctg
Gibson assembly of linearized	2784pBBr_lgbit-hemL_r	ttaacgcgaattttaacaaaatattaacgcgccgcgaagaggatcatttc

Plasmid	Primer for Gibson Cloning/PCR/Sequencing	Sequence 5‘–3‘
pBBR1_LgBiT-ygfB and insert amplified from ID40		
pBBR1_LgBiT-ibpA	2785pBBr_lgbit-ibpA_f	gggagcggaggtggaggctcgagcggtggaagcaacgctttttccctcg
Gibson assembly of linearized pBBR1_LgBiT-ygfB and insert amplified from ID40	2786pBBr_lgbit-ibpA_r	ttaacgcgaattttaacaaaatattaacgcttactggttgtccagtgccg
pBBR1_LgBiT-lon	2787pBBr_lgbit-lon_f	gggagcggaggtggaggctcgagcggtggaaaaacactcgtcgaattgccc
Gibson assembly of linearized pBBR1_LgBiT-ygfB and insert amplified from ID40	2788pBBr_lgbit-lon_r	ttaacgcgaattttaacaaaatattaacgcctaatgcgtgctaattcgctcc
pBBR1_LgBiT-asrA	2789pBBr_lgbit-AsrA_f	gggagcggaggtggaggctcgagcggtggaagcgaccaggacattaatccc
Gibson assembly of linearized pBBR1_LgBiT-ygfB and insert amplified from ID40	2790pBBr_lgbit-AsrA_r	ttaacgcgaattttaacaaaatattaacgctcaggccgggaacagcac

Table 12: Primers used for (RT)-qPCR.

Name	Sequence 5‘–3‘
Pa_rpoS_F	tgccgatccatgtggtcaag
Pa_rpoS_R	gttggcgatttcttcgggtg
Pa_gyrB_F	cgtaacctgaacaactacatcgag
Pa_gyrB_F	aagtacttgcccatctcctgttc
Pa_ygfB_F	tccatatagtccgtctcgcc
Pa_ygfB_R	gggtttcctcgccggttt
Ec_gyrB_F	gctgttctttgtcgttcagttc
Ec_gyrB_R	aatcgtatggagcgtcgttatc
Ec_ygfB_f	acgcaaccgaagctggataa
Ec_ygfB_r	cgtcttcgtcgtaacccagt

2.1.12. Software and web applications

Table 13: Software used in this study.

Name of software	Developer/Citation	Application
bcl2fastq v2.19.0.316	Illumina Inc, San Diego (US)	Demultiplexing RNAseq data
BioRender	Science Suite Inc., Toronto (CA)	Creation of figures
BLAST	Camacho et al. (2009)	Sequence analysis
BV-BRC	Olson et al. (2023)	Database of bacteria and viruses, information on genes and proteins
EnhancedVolcano v1.14.0	Blighe (2024)	Generation of volcano plots
fastp v0.20.1	Chen et al. (2018), Chen (2023)	Quality control of demultiplexed RNAseq data
ggplot2 v3.4.2	Wickham (2016)	Visualization of RNAseq data
Graphpad Prism v10.1.1	Graphpad Software LLC, Boston (US)	Statistical analysis, plotting of data
i-control v2.0.10.0	Tecan Group Ltd., Männedorf (CH)	Software to control Tecan Infinite 200 Pro
Illustrator CS6 v16.0.0	Adobe Systems Incorporated, San José (US)	Vector graphics editor
Image Studio v5.2.5	LI-COR Biosciences GmbH, Bad Homburg vor der Höhe	Software to control LI-COR Odyssey, image analysis
ImageJ v1.53e	Wayne Rasband (Schneider et al., 2012)	Image processing
KEGG	Kanehisa (2019), Kanehisa et al. (2023), Kanehisa and Goto (2000)	Database of information on genes
LabGuru	Biodata Inc., Westborough (US)	Electronic lab notebook, LIMS
LightCycler 480 Software v1.5.0	Roche Diagnostics, Rotkreuz (CH)	Software to control LightCycler 480, data analysis
MaxQuant v1.6.14.0	Cox Lab (Cox & Mann, 2008)	Analysis of mass-spectrometric data
Microsoft Office Professional Plus 2019	Microsoft, Redmond (US)	Word processing, presentations, data management
MultiQC v1.7	Ewels et al. (2016)	Visualization of RNAseq QC data
nf-core/rnaseq pipeline v3.11.2	Patel et al. (2023)	Analysis of RNAseq data
Perseus v2.0.10.0	Cox Lab (Tyanova, Temu, Sinitcyn, et al., 2016)	Analysis of mass-spectrometric datasets generated by MaxQuant
Photoshop CS6 v13.0.1	Adobe Systems Incorporated, San José (US)	Raster graphics editor
plotly v4.10.2	Plotly Technologies Inc. (2015)	Visualization of RNAseq data
R v4.3.2	R-Core Team (R Core Team, 2023)	Statistical analysis, plotting of data
Sequence Manipulation Suite	Stothard (2000)	Scrambling of sequences
SnapGene v4.2.11	GSL Biotech LLC, Boston (US)	Visualization and annotation of DNA and cloning procedures
STRING v12.0	Szklarczyk et al. (2023)	Enrichment analysis, analysis of protein networks
UniProt	The UniProt Consortium (2023)	Database of sequence and functional information on proteins
VolcaNoseR	Goedhart and Luijsterburg (2020)	Generation of volcano plots

2.2. Microbiological methods

2.2.1. Culturing of bacteria

Liquid cultures of bacteria were grown in Luria-Bertani medium (LB) at 37°C with shaking at 180-200 rpm unless otherwise specified. Antibiotics were added to the medium as needed in appropriate concentration. For growth on solid medium, bacteria were cultured on LB agar, supplemented with antibiotics as appropriate. Solid media were prepared by mixing LB medium with 1.5% agar and autoclaving the mixture. To prepare the plates, the LB agar was melted in a microwave and stirred intermittently using a stir bar and stirring plate. Once the agar was fully melted, medium was allowed to cool to about 50°C. Appropriate antibiotics were added to the desired concentration. The liquid agar was then poured into petri dishes and allowed to solidify with the lid open inside a laminar flow cabinet. The plates were then stored at 4°C for later use.

2.2.2. Turbidimetric determination of bacterial concentration

To measure the cell density of bacteria in a liquid culture, the optical density of the sample at 600 nm (OD_{600}) was measured. The photometer was blanked against the used medium. As an approximation of cell number, it was assumed that $OD_{600} = 1 = 10^9$ cells/ml.

2.2.3. Determination of colony forming units

To determine the actual number of living cells in a sample, the colony forming units (CFU) were counted on agar medium. The sample was serially diluted in either PBS or 0.9% NaCl solution. Following appropriate dilution steps that were previously determined via OD_{600} measurement, 100 µl were plated on LB agar plates and spread with a glass spreader. After 24-48 hours of growth, the colonies on the plate were counted. The actual cell number in the sample could then be calculated.

2.2.4. Long term storage of bacteria

For long term storage of bacteria, glycerol stocks were prepared. The bacteria were grown in 5 ml of LB medium overnight, harvested by centrifugation at 4000 x *g* for 10 minutes and re-suspended in 3 ml of LB medium containing 20% glycerol. For storage, 1 ml each was transferred to a cryotube yielding three individual stocks. One stock was used as a use-stock, while two were kept as a backup. The stocks were frozen at -80°C for long-term use.

2.2.5. Minimum inhibitory concentrations of antibiotics

Antibiotic susceptibility testing was done as described previously (Eggers et al., 2023): *"For antibiotic susceptibility testing by microbroth dilution, bacterial strains were grown overnight at 37°C in LB medium. Physiological NaCl solution was inoculated to a McFarland standard*

of 0.5. Subsequently 62.5 µl of the suspension were transferred into 15 ml MH broth and mixed well. According to the manufacturer´s instructions, 50 µl of the suspension was transferred into each well of a microbroth dilution microtiter plate (Sensititre™ GN2F, Sensititre™ EUX2NF (Thermo Fisher Scientific)). Microtiter plates were incubated for 18 h at 37°C and OD_{600} was measured using the Tecan Infinite® 200 PRO. Bacterial strains were considered as sensitive to the respective antibiotic concentration if an OD_{600} value below 0.05 was measured" (Eggers et al., 2023, p. 14). The adjustment to a McFarland standard of 0.5 was done using the Biomerieux Densicheck densitometer.

2.2.6. Checkerboard assays

To study the effect of antibiotic combinations, checkerboard assays were done. These are two-dimensional MIC assays, where two antibiotics are combined, each in log_2-fold dilutions. One antibiotic dilution is added along the abscissa of a 96-well plate, while the second dilution one is added along the ordinate of a 96-well plate. This yields a different concentration of each antibiotic in each well of the 96-well plate and after inoculation and overnight incubation the growth-inhibitory effect of each particular combination of concentrations could be studied.

Figure 4 shows a schematic workflow of a checkerboard assay done for a combination of ceftazidime and ciprofloxacin in the ID40 wildtype strain. After formatting the plate with antibiotics, each well except the sterility control was inoculated with the strain to be tested. After incubation for 20 hours at 37°C, the OD_{600} of each well was measured. For each well, the ratio of the well absorbance and the mean of the absorbance of the sterility control wells was calculated. For each antibiotic combination and each strain, at least two replicates were done. The mean of the signal/blank ratio was calculated and if this value was <1.5, this combination of antibiotics was considered to be growth inhibitory. Plotting the means of the ratios as a heatmap allowed reading of the MICs for each antibiotic alone or in combination with the second antibiotic.

2. Materials and Methods

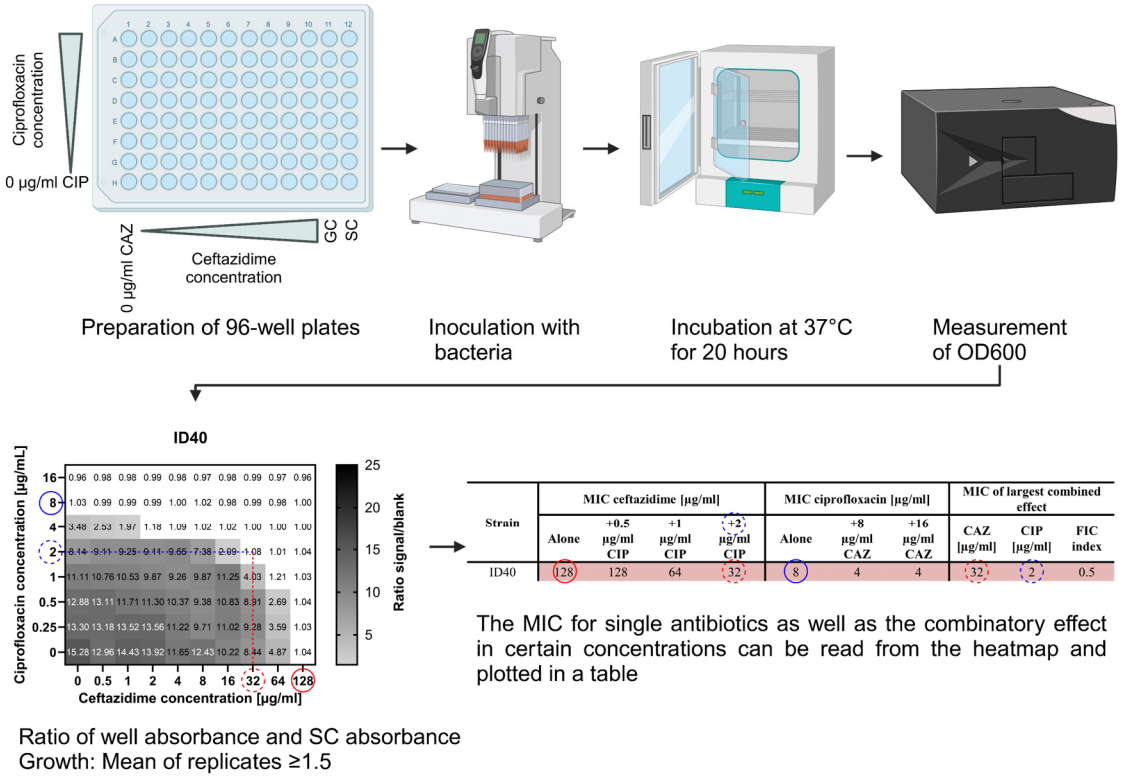

Figure 4: Schematic overview of workflow for the checkerboard assay. As an example, a combination of ciprofloxacin (CIP) and ceftazidime (CAZ) is used. Ceftazidime is added in log_2-fold dilutions in the abscissa of a 96-well plate and ciprofloxacin in log_2-fold dilutions in the ordinate of a 96-well plate. After inoculation with bacteria, the plate is incubated at 37°C for 20 hours and the OD_{600} is measured. The ratio of the turbidity of a particular well and the mean of the sterility control are calculated. If the mean of at least two replicates is <1.5, this particular antibiotic combination is classified as growth inhibitory. The MIC for a particular antibiotic alone and in combination can be read from a heatmap of the combinations and plotted in a table. In this example, the effect of a combination of CAZ with 2 µg/ml of CIP is highlighted. In this case, the combination of 32 µg/ml CAZ and 2 µg/ml of CIP is also the combination with the largest effect. In addition, FIC indices can be calculated as described in Equation 1. Created with BioRender.com.

The ratio of the MIC for antibiotic A in combination with antibiotic B and the MIC of antibiotic A alone allowed for calculation of the fractional inhibitory coefficient (FIC) for antibiotic A. Adding the FIC for antibiotic A and antibiotic B gave the FIC index, which is a measure for synergism, antagonisms, or additive effects of the antibiotic combination. FIC indices were calculated as shown in Equation 1:

Equation 1: Calculation of FIC indices. $MIC_{combination}$: MIC for a particular antibiotic in combination with a second one. MIC_{alone}: MIC of a particular antibiotic not combined with a second one. FIC: Fractional inhibitory coefficient.

$$\frac{MIC_{A,combination}}{MIC_{A,alone}} + \frac{MIC_{B,combination}}{MIC_{B,alone}} = FIC_A + FIC_B = FIC\ index$$

If a FIC index was ≤ 0.5, that antibiotic combination was considered synergistic. If the FIC index was between >0.5 and ≤ 1, the combination was considered additive, and, if the FIC index was between >1 and ≤ 4, indifferent. A FIC index of > 4 was considered antagonistic.

The method of the checkerboard was described in detail in Eggers et al. (2023). *"Stocks of antibiotics to test were prepared by dissolving them according to CLSI M100 Performance Standards for Antimicrobial Susceptibility Testing* (Clinical and Laboratory Standards Institute, 2018) *in the indicated solvent and diluent to a final concentration of 5.12 mg/ml. Salts were corrected for their mass. Used antibiotics: Ciprofloxacin hydrochloride monohydrate (Sigma-Aldrich; European Pharmacopoeia Reference Standard), piperacillin sodium (Sigma-Aldrich, analytical standard), imipenem (Sigma-Aldrich; European Pharmacopoeia Reference Standard), ceftazidime pentahydrate (Sigma-Aldrich; European Pharmacopoeia Reference Standard) and aztreonam (United States Pharmacopeia Reference Standard).*

Working stocks were then prepared by serial dilution in MHB II medium. Plates for checkerboards were prepared by adding 25 µl of each antibiotic at 4x the final concentration to be tested in the respective well in a flat bottom, transparent 96-well plate (Greiner). In one column a growth control was prepared by adding 50 µl of MHB II medium. A sterility control was prepared in a second column by adding 100 µl of MHB II medium. Inocula of the strain to be tested were prepared by inoculating physiological NaCl solution to a McFarland standard of 0.5 from overnight cultures. 125 µl of this solution were then added to 15 mL of MHB II medium and 50 µl of this inoculum added to the wells containing antibiotics as well as to the growth control wells. Plates were incubated for 20 hours at 37°C. After incubation the OD_{600} values were determined using a Tecan Infinite® 200 PRO. Each assay was prepared in duplicate. For each replicate, the ratio of signal for each well and the mean of the sterility control was calculated. The mean value of both replicates was calculated. If the value was smaller than 1.5, this concentration was considered to be inhibitive" (Eggers et al., 2023, pp. 14, 15).

2.2.7. Induction of DNA damage

"Induction of DNA-damage using ciprofloxacin was adapted from Peña et al. (Peña et al., 2021). *Overnight cultures were subcultured in LB for 3 h at 37°C and grown until exponential phase. The cultures were diluted to OD_{600} 0.5 and 32 µg/ml ciprofloxacin (Sigma-Aldrich) was added to the cultures if not otherwise stated. Cultures were incubated for two hours at 37°C and harvested by centrifuging appropriate cell numbers for the desired downstream analyses"* (Eggers et al., 2023, p. 14).

2.2.8. Determination of mutation frequency

The mutation frequency of bacteria was determined as described previously (Mandsberg, Ciofu, Kirkby, Christiansen, Poulsen, & Hoiby, 2009). Bacterial strains to be tested were directly loop-streaked from frozen glycerol stock onto LB agar to obtain single colonies. This was done to

later be able to assess that the single original colonies were susceptible to streptomycin. LB agar plates containing 500 µg/ml of streptomycin (STR) were prepared. To prepare the culture for the assessment of mutation frequency, a single colony from the LB agar plate was picked and streaked onto a LB + STR plate to assess susceptibility. The inoculation loop was then dipped into 20 ml of LB medium in a 100 ml flask. The liquid culture was incubated for 24 hours with shaking at 37°C. If the LB + STR plates had no growth on them the next day, the liquid cultures could be plated to count the CFU. First, the OD_{600} of the cultures was measured and subsequently, the entire 20 ml of liquid culture were centrifuged for 15 minutes at 4000 x *g* and the pellet was resuspended in 1 ml of 0.9% NaCl solution. A dilution series was prepared by adding 100 µl of the original suspension to 900 µl of 0.9% NaCl solution until a dilution of 10^{-11} was reached. 100 µl of the dilution steps 10^{0} and 10^{-1} were plated in triplicates on the LB + STR plates and 100 µl dilutions steps of 10^{-8} to 10^{-11} plated on LB agar in duplicates. After 48 hours of growth, the CFU on the plates were calculated. The mutation frequency was determined by dividing the CFU on the STR plates by the total CFU. The result is the ratio of bacteria that have spontaneously acquired resistance to STR by mutation.

2.2.9. Determination of persister fraction

The determination of the persister fraction was modified from Wilmaerts, Focant, et al. (2022). Overnight cultures of the bacterial strain to be tested were cultured in 5 ml of LB medium in 100 ml flasks. After overnight growth, bacteria were diluted 1:100 in 5 ml of LB medium and grown for another 16 hours. The CFU of the pre-treatment bacteria was counted by plating and the bacteria were subsequently treated with 10x their MIC of ciprofloxacin dissolved in sterile water or with sterile water as a vehicle control. The bacteria were incubated for 5 hours, allowing the ciprofloxacin to kill all bacteria except the persister cells. Subsequently, the bacteria were washed twice with PBS and plated to measure the CFU count. After 48 hours of incubation, the CFU on the plates was be counted. The persister fraction was calculated by dividing the post-treatment CFU by the pre-treatment CFU.

2.2.10. Preparation of electrocompetent bacteria

Electrocompetent bacteria were prepared by using the method of Choi et al. (2006). Overnight cultures of bacteria (*P. aeruginosa* or *E. coli*) to be transformed were harvested using centrifugation for 5 minutes at 4000 x *g*. The pellets were washed twice with 5 ml of 300 mM sterile filtered aqueous sucrose solution using centrifugation for 5 minutes at 4000 x *g*. After the second wash, the pellet was resuspended in 100 µl of 300 mM sucrose solution and stored on ice for electroporation. To save time if only one culture had to be prepared, the overnight culture

was distributed in four 1.5 ml reaction tubes. The cells were harvested by centrifugation at 10,000 x *g* for 1 minute and washed twice using 1 ml of 300 mM aqueous sucrose solution, again centrifuging at 10,000 x *g* for 1 minute after each wash step. After washing, the pellets were resuspended in a combined total of 100 µl of 300 mM sucrose and stored on ice for electroporation.

2.2.11. Preparation of chemically competent bacteria

Chemically competent *E. coli* cells were prepared by streaking cells on a LB agar plate and growing them overnight. A single colony was selected and grown in LB medium with shaking overnight. The overnight culture was diluted 1:100 in 400 ml of LB medium and grown until and OD_{600} of 0.4-0.6 was reached. 50 ml of the cells each were distributed in eight falcon tubes and stored on ice for 20 minutes. The cells were then harvested by centrifuging at 4°C at 4000 x *g* for 10 minutes. The supernatant was removed and the cells resuspended in 3 ml of ice cold 0.1 mM $CaCl_2$ per falcon tube and incubated on ice for 30 minutes. The cells were centrifuged at 4°C at 4000 x *g* for 10 minutes, the supernatant was discarded and the pellet resuspended in 6.4 ml of ice cold 0.1 M $CaCl_2$ containing 15% glycerol. 100 µl of the cells each were transferred in 1.5 ml reaction tubes stored on ice and frozen in liquid nitrogen. The competent cells were then stored at -80°C for later usage.

2.2.12. Transformation of bacteria by electroporation

For transformation by electroporation, 100 µl of the prepared electrocompetent bacteria were mixed with 100 ng of the plasmid to be transformed on ice. The bacteria were pulsed using a BioRad GenePulser II set to 2.5 kV, 200 Ω, 25 µF. Subsequently, 1 ml of LB medium was added and the mixture was incubated at 37°C with shaking for 1-2 hours. The bacteria were then harvested by centrifugation at 10,000 x *g* for 1 minute. The supernatant was discarded and the cells were resuspended in the remaining volume. Of this, 10 and 100 µl were plated on LB agar plates containing appropriate antibiotics and incubated at 37°C overnight to obtain single colonies. Transformants were confirmed by PCR.

2.2.13. Transformation of bacteria by heat shock

To transform chemically competent *E. coli* cells by heat shock, either 100 ng of plasmid or 8 µl of Gibson reaction was added to 100 µl of previously prepared competent cells. The mixture was incubated on ice for 20 minutes and subsequently heat shocked at 42°C for 30 seconds. The mixture was then incubated on ice for 2 minutes and 1 ml of SOC medium was added afterwards. The cells were incubated at 37°C with shaking for 1 hour and afterwards harvested

by centrifugation at 10,000 x *g* for 1 minute. The supernatant was removed and the cells resuspended in the remaining volume. Of this, 10 and 100 µl were plated on LB agar with appropriate antibiotics. Transformants were confirmed by PCR.

2.3. Biochemical methods

2.3.1. Preparation of whole cell lysates of bacteria

After appropriate treatment of bacteria, the OD_{600} was measured. 1 ml of bacterial culture was centrifuged at 10,000 x *g* for 1 minute and resuspended in water and 4x Laemmli buffer containing 10% β-mercaptoethanol. To calculate to volume of water and 4x Laemmli buffer, Equation 2 was used:

Equation 2: Equation used to calculate volume of water and 4x Laemmli buffer needed for preparation of whole cell lysates.

$$V\ [ml] = \frac{OD_{600} * 0.1}{2}$$

The volume calculated was used for the water and the 4x Laemmli buffer. This resulted in a final concentration of OD_{600} = 10 in the sample. The prepared sample was boiled at 95°C for 10 minutes and briefly centrifuged before loading.

2.3.2. SDS-PAGE

Appropriate volumes of protein samples prepared in 4x Laemmli buffer were loaded onto BioRad TGX precast protein gels used at appropriate concentrations according to the protein of interest. 1x SDS-PAGE running buffer was prepared from 5x stock using deionized water (DI-H_2O) and used as a running buffer for the SDS-PAGE. The SDS-PAGE was carried out at 110 V constant for 60-70 minutes. As a size marker, 4 µl of PageRuler Plus Prestained Protein Ladder was loaded onto one lane of the gel.

2.3.3. Coomassie staining

To do an unspecific staining of proteins separated on an SDS-PAGE gel, Coomassie staining was done. The gel was transferred into a plastic box and rinsed three times using warm tap water. Then, the gel was covered with water and heated in a microwave until boiling. The gel was again rinsed three times with warm water and subsequently covered with the Coomassie quick stain solution. Again, the gel was heated in a microwave until the Coomassie quick stain solution came to a boil. The gel was then incubated on a shaker while still covered with the staining solution for 10 minutes. The staining solution was poured off to be reused and the gel rinsed several times with warm water. The gel was covered with water and a tissue was placed

in the water. The gel was then left on a shaker overnight to destain. The next day the gel was imaged using a Vilber Fusion Solo S.

2.3.4. Western blot

Western blots were done by first separating the proteins in a sample by SDS-PAGE. The proteins were then transferred onto a nitrocellulose membrane using a tank blotting system. The transfer buffer was prepared by mixing one part 10x blotting buffer with two parts methanol and seven parts cool water for injection (Ampuwa). The transfer was carried out at 350 mA constant for 60 minutes at 4°C. After the transfer, the membrane was reversibly stained with Ponceau S to confirm that the proteins had been successfully transferred to the membrane. For that, the membrane was rinsed with DI-H_2O and covered for 10 minutes with the Ponceau staining solution. Subsequently, the stain was washed off with DI-H_2O and the gel was imaged using the Vilber Solo Fusion S imager. The marker was then labeled using a pencil and the membrane was cut into several pieces in case multiple proteins were to be detected. The membrane was transferred to a petri dish and covered with a known volume of 1x BlueBlock to block unspecific binding of antibodies to the membrane. The membrane was incubated in 1x BlueBlock for 1 hour at room temperature or overnight at 4°C. Afterwards, the primary antibody was added at an appropriate dilution and incubated for 1 hour at room temperature or overnight at 4°C. The membrane was then washed three times using TBS-T, each time shaking for 3-5 minutes. The membrane was again covered with a known volume of 1x BlueBlock and the secondary antibody coupled to horseradish peroxidase was added at an appropriate concentration. The membrane was again incubated for 1 hour at room temperature or overnight at 4°C. Afterwards, the membrane was again washed three times with TBS-T as described above and a final time with PBS. ECL substrate was added to the membrane to generate chemiluminescence. To image the Western blot, first a white light image was taken to record the marker and then an image recording the chemiluminescence was taken to detect the specific proteins against which the antibodies were directed. The imaging was again done using a Vilber Solo Fusion S imager.
In case the protein to be detected was a HiBiT-tagged protein, detection was performed using the Nano-Glo HiBiT Blotting System, making use of a split-luciferase system. HiBiT, together with the protein LgBiT forms an active luciferase that generates chemiluminescence when the substrate furimazine is added. The kit was used according to the instructions of the manufacturer. First, after the transfer and the Ponceau stain, the membrane was transferred into a petri dish containing TBS-T. Then the Nano-Glo HiBiT Blotting Reagent was prepared by diluting the 10x Nano-Glo Blotting Buffer with water and adding the 200x concentrated LgBiT protein

to a final concentration of 1x each. The TBS-T was removed from the petri dish and the Nano-Glo HiBiT Blotting Reagent was added and the membrane was incubated for 1 hour at room temperature or overnight at 4°C. The Nano-Glo Luciferase Assay Substrate was then diluted 500-fold in the reagent and mixed by rocking the petri dish. The membrane was incubated for 5 minutes and afterwards the chemiluminescent signal imaged as described above. Quantification of Western blots using ImageJ was done as described in Stael et al. (2022), normalizing the intensities to a loading control.

2.3.5. Overexpression of proteins

To overexpress proteins and to further purify them, the CDS of the protein of interest was cloned in an appropriate expression vector. This yielded a fusion protein with the protein of interest tagged with an affinity tag for purification (i.e. a hexa-histidine-tag or a GST-tag) and possibly, a solubility tag such as a maltose-binding protein (MBP)-tag.

The expression vectors used in this study carry the CDS under control of a T7 promoter flanked by a LacO site, as well as the *lacI* gene. The chemically competent T7 expression strains *E. coli* BL21(DE3) were transformed with the expression vectors. These strains carry the gene for the T7-polymerase under control of a *lacUV5* promoter. LacI binds to the LacO site, preventing the T7-polymerase from binding to its promoter and expressing the protein of interest. By addition of IPTG to the culture, binding of LacI to LacO is inhibited and expression of the T7-polymerase is induced. This allows the induced T7-polymerase to transcribe the CDS downstream of the T7 promoter site. (Dubendorff & Studier, 1991)

Cultures of the expression strains were prepared by diluting overnight cultures to an OD_{600} of 0.1-0.2 in desired volumes of LB medium supplemented with appropriate antibiotics. Usually, 1000 or 2000 ml of medium were used. Expression cultures were grown at 37°C with shaking until an OD_{600} of 0.6-0-8 was reached. If the expression was carried out at 37°C, IPTG was now added at an appropriate concentration, usually 1 mM. If the expression was to be done at lower temperatures, the cultures were shifted to the desired temperature and equilibrated for 30 minutes. After equilibration, IPTG was added to a desired final concentration, usually 1 mM. Before addition of IPTG, the OD_{600} was measured and a sample for SDS-PAGE was taken as described in 2.3.1. Expression was carried out for a desired duration, usually overnight if expression was done at lower temperatures, and for 3 h if expression was done at 37°C.

After expression, a sample for SDS-PAGE was taken as described before. The success of the expression was then analyzed by SDS-PAGE.

2.3.6. Lysis of bacterial cells by sonication

To lyse bacteria in order to produce whole cell lysates for pulldown assays, or to purify proteins that were overexpressed, the bacteria were pelleted by centrifugation at 6000 x *g* for 10 minutes and resuspended in an appropriate volume of lysis buffer that was supplemented with DNase I, lysozyme, Triton X-100, and "c0mplete" protease inhibitor. The resuspended cells were then lysed by sonication with the sonicator set to 20% output and 50% duty cycle. Depending on the size of the pellet, different sonicator heads and tips were used as well as different sonication times. The lysates were stored on ice in between sonication steps. Subsequently, the lysates were centrifuged at 35,000 x *g* to remove cell debris and the supernatant was sterile filtered with a 0.22 µM syringe filter prior to further use.

Samples were taken for the total resuspended pellet, the slurry after lysis, and the supernatant after centrifugation by adding 10 µl of sample to 20 µl of 4x Laemmli buffer supplemented with β-mercaptoethanol. SDS-PAGE was done to analyze whether the protein of interest remained soluble after lysis.

2.3.7. Ni^{2+}-NTA affinity chromatography

Ni^{2+}-NTA affinity chromatography was used to purify proteins that carried a hexa-histidine tag (6xHis). For Ni^{2+}-NTA affinity chromatography, 5 ml of Ni^{2+}-NTA beads per 1 l of initial expression culture were added to a gravity flow column. The beads were washed with 4x the column volume of water for injection (i.e. 20 ml for a 5 ml column), and then equilibrated with 4x the column volume of sterile filtered lysis buffer without supplements, i.e. the same buffer that was used for lysis by sonication but without DNase I, lysozyme, protease inhibitor, or Triton X-100. The lysis buffer usually contained 15-25 µM of imidazole to reduce unspecific binding of proteins to the beads.

The sterile filtered supernatants of the cell lysates from the lysis step were then added to the column and incubated for 15 minutes at 4°C on a rolling mixer. This allowed the 6xHis-tagged proteins to bind to the beads. Subsequently, the column was fixed in a laboratory stand and the valve of the column opened to collect the flow through that contained the proteins that had not bound to the beads. The flow through was collected in a 50 ml plastic tube and kept on ice.

The beads were then washed with one column volume of lysis buffer and the first wash fraction collected in a 50 ml plastic tube and kept on ice. Then, a second wash step was done with up to five column volumes of lysis buffer. To monitor the second washing step, a benchtop Bradford assay (Hammond & Kruger, 1988) was done. For this purpose, a 5x Bradford reagent was diluted 5-fold with water for injection and 100 µl of this reagent were added to each well of a

transparent 96-well plate. To monitor the amount of protein in the wash fractions, 10 µl of sample was taken from the tip of the column and added to one well with Bradford reagent. The intensity of the blue color then allowed an estimation of the amount of protein present in the sample. Washing of the beads was done until no more protein could be detected in the Bradford assay or until a volume of 5 column volumes for the second wash fraction was reached. The second wash fraction was also collected in a 50 ml plastic tube and kept on ice.

To elute the proteins from the column, an elution buffer was prepared by mixing 15 ml of 1 M aqueous imidazole solution with 30 ml of lysis buffer. The elution buffer was added carefully to the column and the protein concentration was monitored using the benchtop Bradford assay. The first elution fraction was collected in a 50 ml plastic tube until the protein amount seen in the Bradford assay dropped visibly. Then, a second elution fraction was collected until there was barely any protein detected in the Bradford assay.

Samples for SDS-PAGE were prepared by adding 10 µl of sample to 20 µl of 4x Laemmli buffer supplemented with β-mercaptoethanol for the flow through samples, and 20 µl of sample to 10 µl of 4x Laemmli buffer supplemented with β-mercaptoethanol for the wash and elution samples, and boiled at 95°C for 5 minutes. Success of the purification was then analyzed by SDS-PAGE.

2.3.8. Reverse-Ni^{2+}-NTA affinity chromatography

Reverse Ni2+-NTA affinity chromatography was done to separate 6xHis-tagged TEV-protease, the 6xHis-tag itself, or the 6xHis-tagged fusion protein from the cleaved, now untagged protein of interest (see 2.3.13).

The Ni2+-NTA column was prepared as described in 2.3.7, but after incubation with the proteins, the flow through was collected for further usage down the line as it contained all non-6xHis-tagged proteins, i.e. the protein of interest but not the 6xHis-TEV-protease or 6xHis-tagged solubility tags.

2.3.9. Glutathione affinity chromatography

Glutathione-S-transferase (GST)-tagged proteins were purified by glutathione affinity chromatography. For this, a GSTrap 4B column (column volume = 1 ml) was connected to a peristaltic pump and washed with 5 column volumes (CV) water and equilibrated with 5 CV GST-A buffer. Subsequently, the lysates containing the GST-tagged protein were loaded on the column and the column was then washed with 5 CV GST-A buffer. The GST-tagged proteins were eluted from the column using 5 CV GST-B buffer, containing 10 mM reduced glutathione. The column was regenerated with 3 CV of GST-A buffer and the flow through of the first loading

step was loaded again on the column, followed by the steps described above. Samples for SDS-PAGE were taken as described in 2.3.7.

2.3.10. Upconcentration by ultrafiltration

Proteins were upconcentrated using Amicon Ultra Centrifugal Filters. Protein solution was added to a filter at an appropriate molecular weight cutoff and centrifuged for 5 minutes at 4000 x *g* at 4°C. The flow through was collected and the filter was rinsed with a pipette using the protein solution to improve filter efficiency. The procedure was repeated until a desired volume was reached or until visible precipitation by protein was seen.

2.3.11. Size exclusion chromatography

Size exclusion chromatography (SEC) was done to separate proteins by size. This allowed further clean-up of proteins that were purified by affinity chromatography or to remove cleavage products after a proteolytic digest. For this purpose, an ÄKTAprime plus (GE Healthcare) system was used together with HiLoad Superdex prep grad columns (Cytivia). Depending on the size of the protein of interest and the volume of protein solution to be injected, different pore sizes and column volumes were chosen. For proteins with a molecular mass between 8 and 50 kDa, a Superdex 75 pg resin was chosen, and for a molecular mass of 30 and 250 kDa a Superdex 200 pg resin was chosen. Column sizes in this study were always 16/600, providing a column volume of 120 ml.

For purification of proteins, first the ÄKTA system, the tubing and the column were washed with water and equilibrated with sterile filtered running buffer. The protein solution was upconcentrated using Amicon Ultra centrifugal filters as described in 2.3.10 to a volume of 2% of the column volume. In case precipitates formed before an appropriate volume of sample was reached, two separate runs had to be done. Prior to injection, the protein sample was centrifuged at 20,817 x *g* (maximum speed) for 10 minutes and the supernatant withdrawn using a syringe with a needle, avoiding the collection of the pellet. A sample for SDS-PAGE analysis was taken by mixing 20 µl protein sample with 10 µl 4x Laemmli buffer and boiled at 95°C for 5 minutes. Air was removed from the syringe and the protein solution was injected into the sample loop of the ÄKTA system. The method for SEC is shown in Table 14.

Table 14: Method for SEC. Fractions of 1 ml were collected between 40 ml and 90 ml elution volume.

Breakpoint	Volume	Concentration running buffer	Flow	Fractionation	Valve position
1	0 ml	100%	0.5 ml/min	No	Inject
2	20 ml	100%	1 ml/min	No	Load
3	40 ml	100%	1 ml/min	1 ml fractions	Load
4	90 ml	100%	1 ml/min	No	Load
5	150 ml	100%	1 ml/min	No	Load

Fractions of 1 ml were collected between 40 ml and 90 ml of elution volume. Elution was monitored by measurement of UV-absorbance at 280 nm. According to the chromatogram, samples of the elution fractions were taken by mixing 20 µl of sample with 10 µl of 4x Laemmli buffer and boiling at 95°C followed by SDS-PAGE analysis. Fractions that had the pure protein of interest were pooled and used for downstream applications.

2.3.12. Dialysis

To exchange the buffer in which a protein was stored, dialysis was done. For this, an appropriate volume of dialysis buffer (for details see method of purification of specific protein) was prepared that allowed for a large enough concentration gradient of the component that was to be removed or introduced by dialysis. The protein solution was transferred into a ZelluTrans dialysis tube (Roth) with a cutoff of 3,500 Da. The tube containing the protein solution was then allowed to float in a large beaker containing the dialysis buffer and a stir bar. The dialysis was carried out with stirring overnight at 4°C.

2.3.13. TEV-protease digest

In case a tag or fusion protein had to be removed from the protein of interest, a TEV-cleavage site was inserted between the tag and the protein of interest. This amino acid sequence is highly specific for the TEV-protease (Parks et al., 1994). This protease can then be used to separate the protein of interest and the tag. For this purpose, 1 ml of purified 6xHis-tagged TEV-protease at a concentration of 0.5 mg/ml was added to the protein solutions to be treated during dialysis. To separate the reaction products, either reverse Ni^{2+}-NTA affinity chromatography or size exclusions chromatography was done.

2.3.14. Photometric quantification of proteins

Protein concentrations were measured using a NanoDrop spectrophotometer. The UV-absorbance at 280 nm was measured in triplicates with the spectrophotometer blanked with the buffer in which the protein was stored. The mean of the triplicates was calculated and inserted in the equation of the Lambert-Beer-Law (Equation 3), where A is the absorbance measured by the nanodrop and ε is the molar absorbance coefficient, calculated for each protein to measure by ExPASy ProtParam (Wilkins et al., 1999). The pathlength l was set to 1 cm as the nanodrop automatically normalized the absorbance to 1 cm. This gave the molar concentration c of protein.

Equation 3: Equation of Lambert-Beer-Law used to calculate protein concentrations. $\boldsymbol{A}$ = absorbance measured, $\boldsymbol{\varepsilon}$ = molar absorbance coefficient of the proteins at 280 nm [l/(mol*cm)], $\boldsymbol{c}$ = molar concentration [mol/l], $\boldsymbol{l}$ = pathlength [cm]

$$A = \varepsilon * c * l$$

2.3.15. Storage of proteins

Proteins were diluted to desired concentrations after photometric quantification using the appropriate buffer and aliquoted in appropriate volumes. Aliquots were snap frozen by dropping the tubes in liquid N_2 and stored at -80°C.

2.3.16. Expression and purification of His-MBP-AlpA and His-MBP

"For purification of His-MBP-AlpA and His-MBP, expression cultures of 1 liter LB medium were inoculated at an OD_{600} of 0.15 with starter cultures of E. coli BL21 carrying either pETM-41_AlpA or pETM-41_stop. Expression cultures were grown until an OD_{600} of 0.6–0.8 at 37 °C. The cultures were then shifted to 20 °C and equilibrated for 30 min. IPTG was added to a final concentration of 1 mM and expression was carried out at 20 °C for 18 h. Cultures were harvested by centrifuging at 6000 × g for 10 min at 4 °C. Pellets were resuspended in 35 ml lysis buffer (50 mM Tris, 150 mM NaCl, 25 mM imidazole, pH 7.5) supplemented with lysozyme, Triton X-100, DNase and cOmplete protease inhibitor cocktail (Roche). Bacteria were lysed by sonication for 3 × 1 min on ice at 20% amplitude and 50% duty cycle. Cell debris was removed by centrifuging the lysate at 35,000 × g for 1 h at 4 °C. The supernatant was sterile filtered through a 0.22 µm syringe filter (Millipore) and affinity-purified in a gravity flow column using Ni^{2+}-NTA-agarose beads (Qiagen). After binding of the His-tagged proteins to the columns, columns were washed with lysis buffer and proteins were eluted using elution buffer (lysis buffer + 350 mM imidazole). Fractions were analyzed via SDS-PAGE and Coomassie staining. Elution fractions were dialyzed in 3 liter dialysis buffer (50 mM Tris, 150 mM NaCl, 20% V/V glycerol at pH 7.5) using Slide-A-Lyzer dialysis cassettes (ThermoFisher) with 20 kDa cutoff and 12-30 ml volume. Pure protein was aliquoted and stored at –80 °C after snap freezing with liquid nitrogen" (Eggers et al., 2023, p. 15).

His-MBP-AlpA had a final concentration of 24.4 µM in 15 ml of protein solution. This added up to a final yield of 23.63 mg of protein per liter of culture. His-MBP had a final concentration of 297.4 µM in 10 ml of protein solution and a final yield of 132.4 mg of protein per 1 liter of expression culture. SDS-PAGE gels from the purification are shown in Figure 32 in the appendix.

2.3.17. Expression of GST

"Expression and purification were performed as above [2.3.16] *, using the strain E. coli BL21 carrying* […] *carrying pGEX4T3_stop* […]. *Differing from above* [2.3.16]*, the expression was carried out at 25 °C. For resuspension and lysis of the bacterial pellet, GST-A buffer (50 mM Tris, 150 mM NaCl, 1 mM DTT, pH 7.5) supplemented with lysozyme, Triton X-100, DNase and*

protease inhibitor was used. For purification, a GSTrap™ HP 1 ml column (Cytiva) connected to a peristaltic pump was used. After loading the column and collecting the flow through the column was washed using GST-A buffer and the protein eluted using GST-B-buffer (50 mM Tris, 150 mM NaCl, 10 mM reduced glutathione, pH 8). After column regeneration, the flow through was loaded on the column once again and also washed and eluted. The obtained eluate fractions were pooled and dialysed against 10 liter of PBS pH 7.4 and 0.5 mM DTT using a ZelluTrans (Roth) dialysis tube with a 3.4 kDa cutoff and frozen in dialysis buffer. Analysis by SDS-PAGE and protein storage was done as described above" (Eggers et al., 2023, p. 15).

The obtained protein had a final yield of 152.1 µM GST in 9 ml. This corresponded to a final yield of 34.9 mg protein per liter of expression culture. SDS-PAGE gels from the purification are shown in Figure 33 in the appendix.

2.3.18. Expression and purification of YgfB

"Expression and purification were performed similar to as described for His-MBP and His-MBP-AlpA, using the strain E. coli BL21 carrying pETM30_YgfB, however, the expression was carried out at 25 °C. This purification step yielded His-GST-TEV-YgfB. Then, His-tagged TEV-protease was added to the elution fraction containing His-GST-TEV-YgfB and dialyzed in 2 l dialysis buffer (50 mM Tris, 150 mM NaCl, 1 mM DTT at pH 7.5) using a ZelluTrans (Roth) dialysis tube with a 3.4 kDa cutoff over night at 4 °C.

The yielded cleavage product was purified using reverse Ni^{2+}-affinity chromatography using Ni^{2+}-NTA-agarose beads equilibrated with sterile filtered dialysis buffer and the flow through containing only YgfB was collected, aliquoted and stored as above. Fractions were analyzed via SDS-PAGE and Coomassie staining" (Eggers et al., 2023, p. 15).

In total, 22 ml of YgfB at a concentration of 123.3 µM was recovered. This corresponds to a yield of 53.4 mg of protein per liter of expression culture. SDS-PAGE gels from the purification are shown in Figure 34 in the appendix.

2.3.19. Expression and purification of His-GST-EcYgfB and His-GST

The CDS of *ygfB* derived from BW25113 was cloned in the plasmid pETM30, yielding pETM30_Ec_*ygfB*. After transforming *E. coli* BL21(DE3) cells with this plasmid, they could be used for purification of the fusion protein His-GST-EcYgfB. The protein was purified in two steps, with a Ni^{2+}-NTA affinity chromatography step followed by SEC. The expression was induced with 1 mM IPTG in 1 liter of LB medium and the protein was expressed overnight at 25°C with shaking. After harvesting the cells, the pellet was resuspended in supplemented lysis buffer (50 mM Tris pH 7.5, 150 mM NaCl, 25 mM imidazole, 1 mM DTT) as described in

2.3.6. After centrifugation, the 6xHis-tagged construct was purified by Ni^{2+}-NTA-affinity chromatography. Figure 35 in the appendix shows a Coomassie stained gel of the purification fractions. Elution fraction 1 was further dialyzed against 1 liter of dialysis buffer (50 mM Tris pH 7.5, 150 mM NaCl, 10% (m/V) glycerol, 1 mM DTT) overnight. As the elution fraction after the Ni^{2+}-NTA affinity chromatography showed some contaminations, the protein was further purified by SEC. The dialyzed protein was concentrated using a 30 kDa Amicon Ultra Centrifugal Filter and loaded on a HiLoad 16/600 Superdex 75 pg size exclusion column with 50 mM Tris pH 7.5, 150 mM NaCl, 10% glycerol (m/V) and 1 mM DTT as a running buffer. The chromatogram of the SEC is shown in Figure 36a in the appendix. Fractions were collected and loaded on an SDS-PAGE gel and stained with Coomassie for analysis (Figure 36b in the appendix). Fractions 8-20 were pooled, which resulted in 12 ml of protein solution at a final concentration of 52.3 µM. This corresponded to a final yield of 31.5 mg of protein per 1 liter of expression culture.

His-GST was purified in the same manner as His-GST-EcYgfB using the plasmid pETM30_stop. Since the SDS-PAGE analysis of the fraction of the Ni^{2+}-NTA purification step (Figure 37 in the appendix) showed a much cleaner product than the His-GST-EcYgfB purification, no SEC step was done after dialysis. The purification yielded 15 ml of 84.3 µM of His-GST, which corresponded to 36.7 mg of protein per 1 liter of culture.

2.3.20. Pulldown assay with cell lysates

"Day cultures were inoculated at an OD_{600} of 0.1 in 500 ml of LB with overnight cultures of ID40Δygfb::alpA-HiBiT::HA-alpR and grown for 5 h at 37 °C. Cultures were harvested by centrifuging for 10 min at 6000 × g. Cell pellets were resuspended in 5 ml pulldown-buffer (50 mM Tris pH 7.5, 300 mM NaCl, 0.5% IGEPAL, 2 mM DTT) supplemented with cOmplete protease inhibitor cocktail, DNase I, lysozyme and Triton-X 100. Cells were lysed by sonification, cell debris removed by centrifugation and supernatants were used for downstream application after sterile filtration.

1 ml of recombinant GST or GST-YgfB protein at a concentration of 10 µM was incubated with 100 µl 50% MagneGST (Promega) bead-slurry equilibrated with pulldown-buffer for 45 min at 4 °C and washed two times with 500 µl pulldown-buffer. The beads were then incubated with 1 ml of cell lysate for 45 min at 4 °C. After washing the beads three times with 700 µl pulldown-buffer, the bound proteins were eluted from the beads using 100 µl pulldown-buffer supplemented with 25 mM glutathione. 33 µl of 4x Laemmli buffer was added to the eluate and the samples were boiled for 10 min at 95 °C. For the input samples, 10 µl of GST-tagged protein

was mixed with 10 µl of cell lysate. In total, 20 µl 4x Laemmli buffer was added and samples were boiled at 95 °C for 10 min. Samples were analysed by SDS-PAGE and Western Blot using the Nano-Glo HiBiT blotting system (Promega)" (Eggers et al., 2023, pp. 15, 16).

Pulldown with cell lysates of *E. coli* were done the same as for *P. aeruginosa*. In case LC-MS/MS analysis was done downstream of the pulldown, samples prepared in Laemmli buffer as described above were used.

2.3.21. Pulldown assay with recombinant proteins

Pulldown assays done with recombinant proteins were done to study direct interactions between two proteins. *"1 ml of recombinant His-MBP-AlpA and His-MBP at a concentration of 10 µM was incubated with 100 µl MagneHis™ Ni Particles (Promega) equilibrated with pulldown-buffer (50 mM Tris pH 7.5, 25 mM imidazole, 300 mM NaCl, 0.5% IGEPAL, 2 mM DTT) for 45 min at 4 °C and washed 2 times with 500 µl pulldown-buffer. In total, 1 ml of recombinant YgfB at a concentration of 10 µM was added to the beads and incubated for 45 min at 4 °C. After washing the beads three times with 700 µl pulldown-buffer, the bound proteins were eluted with 75 µl pulldown-buffer supplemented with 350 mM imidazole. In total, 25 µl 4x Laemmli buffer were added to the eluate and the samples were boiled for 10 min at 95 °C. For the input samples, 10 µl of His-tagged protein was mixed with 10 µl of rYgfB. After addition of 20 µl 4x Laemmli buffer the samples were boiled at 95 °C for 10 min. Proteins were detected by SDS-PAGE and Western blot as described above"* (Eggers et al., 2023, p. 16).

2.3.22. Electrophoretic mobility shift assay (EMSA)

Electrophoretic mobility shift assays (EMSA) were done to study the binding of His-MBP-AlpA to the *ampDh3* promoter, namely the stretch of the promoter that contained the AlpA binding element (ABE). Near-infrared labeled DNA probes (IRDye 700 by LI-COR) were incubated with proteins and resolved on a non-denaturing polyacrylamide gel. The migration of the labeled probes could be detected by using the LI-COR Odyssey Imaging System using the 700 nm channel. When proteins bound to the DNA probe, the migration of the probe in the polyacrylamide gel was retarded due to the larger size of the DNA:protein-complex. This is called a band-shift. If another protein, such as YgfB, would inhibit the interaction of the DNA-binding protein and the DNA-probe, then the shift intensity would be reduced or completely abrogated. Figure 5 shows a schematic depiction of the EMSA done in this study. In addition, as a negative control probe, the DNA sequence of the DNA-probe was scrambled using the Sequence Manipulation Suite (Stothard, 2000).

2. Materials and Methods

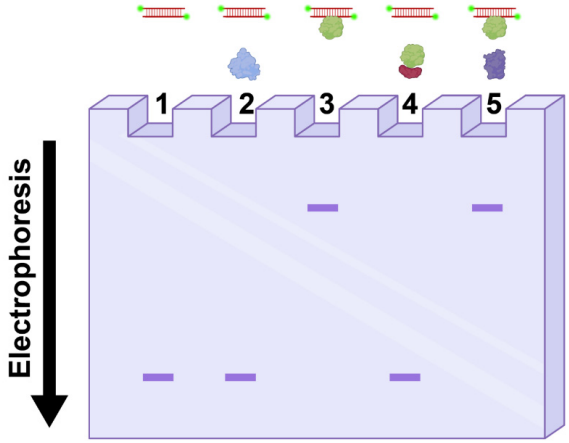

Figure 5: Schematic overview of the EMSA experiments done in this study. In 1, only fluorescently labeled DNA probe is loaded on the gel, while in 2 a non-DNA-binding protein is added to the probe. In both conditions, the labeled probe migrates to the bottom of the gel in the electrophoresis. In 3, a DNA-binding protein is added to the probe, leading to a change in migratory behavior of the DNA probe. This leads to a band shift. In 4, a second protein that interacts with the DNA-binding protein is added to the reaction mix. The DNA-binding protein can no longer bind to the DNA and no band shift appears. In 5, a second protein that does not interact with the DNA-binding protein is added to the mix. The DNA-binding protein can bind to the DNA and a band shift can be seen. The figure was created with BioRender.com.

DNA-labeled probes were generated by ordering 5'-IRDye 700-labeled oligonucleotides from IDT. Sequences for the labeled oligos were as follows (for the oligos that contain the ABE, the ABE is marked with asterisks):

Sense oligonucleotide containing the ABE: 5′-CGG TGT TGC ACG CGG *CGG GAC GCT CGC GGT AGT TTT* TTC CCA TGA TCA CG-3′

Antisense oligonucleotide containing the ABE: 5′-CGT GAT CAT GGG AAA *AAA CTA CCG CGA GCG TCC CGC CGC* GTG CAA CAC CG-3′

Scrambled sense oligonucleotide: 5′-GTT TAC TAG GTC GAG GTA CTT CGA CGC GCG CCG TCT GCT AGC GCG GTC TG-3′ and

Scrambled antisense oligonucleotide: 5′-CA GAC CGC GCT AGC AGA CGG CGC GCG TCG AAG TAC CTC GAC CTA GTA AAC-3′

"The oligonucleotides were annealed by mixing them in equimolar amounts in duplexing buffer (100 mM Potassium Acetate; 30 mM HEPES, pH 7.5) and heating to 100 °C for 5 min in a PCR cycler. The cycler was then turned off and the samples were allowed to cool to room temperature while still inside the block. The annealed product was then diluted with water to 6.25 nM for EMSA experiments" (Eggers et al., 2023, p. 16).

Binding reactions for EMSAs were prepared by mixing DNA probes at a final concentration of 0.3125 nM with proteins in 20 µl of reaction mix per reaction. The final buffer composition in each reaction mix consisted of 32.5 mM Tris, 67.5 mM NaCl, 9% glycerol, 12.5 mM KOAc, 3.75 mM HEPES, 50 mM KCl, 3.5 mM DTT, 0.25% Tween 20, and 0.025 µg/ml (0.5 µg total)

of sheared salmon sperm DNA as a blocking agent of unspecific protein-DNA-interactions. His-MBP and His-MBP-AlpA were added to a final concentration of 1.25 µM and YgfB or BSA added to a final concentration of either 5 µM or 12.5 µM, depending on the condition. Binding reactions were prepared by first mixing buffer components, then adding YgfB or BSA and subsequently His-MBP or His-MBP-AlpA. After preincubation of the proteins for 10 min at 20°C to allow protein-protein-binding to take place, the fluorophore-labeled DNA-probes were added. The binding reactions were then incubated in the dark for 30 min at 20°C. *"For resolving the reactions, 4% polyacrylamide gels containing 30% triethylene glycol were cast (For two gels: 2 ml ROTIPHORESE®Gel 30 37.5:1 (Roth), 4.5 ml triethylene glycol (Sigma-Aldrich), 1.5 ml 5x TBE-buffer, 7 ml ddH2O, 15 µl TEMED, 75 µl 10% APS). The gels were preequilibrated for 30 min at 130 V in 0.5x TBE-buffer. Samples with added 10x orange dye were then loaded onto the gel at 4 °C and the voltage set to 300 V until the samples entered the gel completely. The voltage was then turned down to 130 V and the gel was run until the migration front reached the end of the gel. The gels were imaged using the Licor Odyssey imaging system using the 700 nm channel. For generation of the figures, the scanned image was converted to greyscale and brightness and contrast adjusted"* (Eggers et al., 2023, p. 16).

2.3.23. Split-luciferase assays

"Subcultures were harvested by centrifuging at 5000 × g for 10 min. Cell pellets were washed once by resuspending in 1 ml PBS and centrifuged at 10,000 × g for 1 min. The pellet was resuspended 1 ml PBS and the OD_{600} was measured. Bacteria corresponding to an OD_{600} = 1 were harvested by centrifugation at 10,000 × g for 1 min. The pelleted bacteria were resuspended in 500 µl buffer K adapted from Dietsche et al. (Dietsche et al., 2016) *(50 mM triethanolamine pH 7.5, 250 mM sucrose, 1 mM EDTA, 1 mM $MgCl_2$, 0.5% Triton-X 100, 10 µg/ml DNase, 20 µg/ml lysozyme, 1:100 cOmplete protease inhibitor cocktail) and incubated on ice for 30 min. For quantification of HiBiT-tagged proteins, 50 µl Nano-Glo HiBiT Lytic Reagent containing 1 µl furimazine and 2 µl recombinant LgBiT were added to 50 µl lysate in a white flat-bottom 96-well plate (Greiner) in technical triplicates. Plates were incubated for 10 min and chemiluminescence was measured using a Tecan Reader Infinite 200 Pro plate reader (500 ms integration time)"* (Eggers et al., 2023, p. 15).

2.3.24. Sample preparation for proteomics

Samples in 4x Laemmli buffer were prepared for proteomics using a short gel run. 25 µl per sample were loaded on a Protean Mini TGX gel with 10 wells, 30 µl per well. The gel was run with SDS-PAGE running buffer for 10 minutes at 110 V constant until the samples entered the

gel about 1 cm. The gel was stained overnight with colloidal Coomassie, then destained with water by shaking for 5 minutes and imaged. The gels were then transferred to the proteome center for analysis.

2.3.25. NanoLC-MS/MS analysis

NanoLC-MS/MS analysis as well as data processing was done by Dr. Mirita Franz-Wachtel of the Proteome Center Tübingen. The following section was written by Dr. Mirita Franz-Wachtel of the Proteome Center Tübingen.

"Proteins in Coomassie-stained gel pieces were digested in gel with trypsin (Borchert et al., 2010), and extracted peptides were desalted (Rappsilber et al., 2007) and finally analyzed on an Easy-nLC 1200 system coupled to a Q Exactive HF mass spectrometer (all Thermo Fisher Scientific) as described previously (Aly et al., 2023) with slight modifications: peptides were separated using a 57 minute segmented gradient from 10-33-50-90% of HPLC solvent B (80% acetonitrile in 0.1% formic acid) in HPLC solvent A (0.1% formic acid) at a flow rate of 200 nl/min. The mass spectrometer was operated in data-dependent mode, collecting MS spectra in the Orbitrap mass analyzer (60,000 resolution, 300-1750 m/z range) with an AGC target and a maximum ion injection time set to 3x106 and 25 ms, respectively. The 7 most intense precursor ions were sequentially fragmented with a normalized collision energy of 27 in each scan cycle using higher energy collisional dissociation (HCD) fragmentation. In all measurements, sequenced precursor masses were excluded from further selection for 30 s. MS/MS spectra were recorded with a resolution of 60,000, whereby AGC target and fill time were set to 105 and 220ms, respectively."

2.3.26. MS data processing

The following section was written by Dr. Mirita Franz-Wachtel of the Proteome Center Tübingen.

"Processing of MS spectra were performed with MaxQuant software package version 1.6.14.0 (Cox & Mann, 2008) with integrated Andromeda search engine (Cox et al., 2011). The respective MS datasets were searched against a *P. aeruginosa* PAO1 (UP000002438) and/or an *Escherichia coli* K12 (UP000000625) databases, both obtained from UniProt (uniprot.org, last accesses: UP000002438: 07.10.2020 UP000000625: 30.11.2023), whereby the sequence of YgfB was removed from the *Escherichia coli* database, and against a database of 286 commonly

observed contaminants. Trypsin was defined as protease with a maximum of two missed cleavages. Oxidation of methionine, and protein N-terminal acetylation were specified as variable modifications, and carbamidomethylation on cysteine was set as fixed modification. Mass tolerance was set to 4.5 parts per million (ppm) for precursor ions and 20 ppm for fragment ions. Peptide, protein and modification site identifications were reported at a false discovery rate (FDR) of 0.01, estimated by the target-decoy approach (Elias & Gygi, 2010). iBAQ (Intensity Based Absolute Quantification) and LFQ (Label-Free Quantification) values were calculated, and the "match between runs" option was enabled (Tyanova, Temu, & Cox, 2016)."

2.3.27. Protein-fragment complementation assay

Protein-fragment complementation assays (PCA) were used to screen for potential *in vivo* protein-protein interactions. For each protein of interest (POI) to be tested, the corresponding coding sequence of the gene of interest (GOI) encoding the POI was cloned to generate the plasmid pBBR1_LgBiT-GOI. This plasmid allowed to express the POI with an N-terminal LgBiT tag. The strain ID40Δ*ygfB*::rha-SmBiT-*ygfB* was transformed with the plasmid. The strain lacked *ygfB* at the native locus but had it reintroduced under a rhamnose inducible promoter at the Tn7-site with an N-terminal SmBiT tag as described in 2.4.15. SmBiT and LgBiT are parts of a split-luciferase with a low affinity to each other that form a functional luciferase only if they come in close proximity. Therefore, if the POI and YgfB interacted on a physical level, the luciferase was reconstituted and could, upon addition of the substrate furimazine, generate chemiluminescence.

The ID40Δ*ygfB*::rha-SmBiT-*ygfB* strains that harbored the respective pBBR1_LgBiT-POI plasmid were grown overnight in LB medium with 75 µg/ml of gentamicin and 0.1% rhamnose to induce expression of the LgBiT-GOI fusion protein. The next day, day cultures were prepared by 1:20 dilution in LB medium with 75 µg/ml of gentamicin and 0.1% rhamnose and grown for 2-3 hours. The OD_{600} was measured and the bacterial cultures were diluted to an OD_{600} of 0.2 in 1 ml of medium. 50 µl of each culture was added in triplicates to a white 96-well plate, resulting in 10^7 bacteria per well. The Nano-Glo Luciferase Assay reagent was prepared by mixing 1 µl of Nano-Glo Luciferase Assay Substrate with 49 µl Nano-Glo Luciferase Assay Buffer per reaction. 50 µl of the reagent was then added to each well that contained 50 µl of bacteria. The plate was then shaken for 5 minutes on a plate shaker and chemiluminescence was measured using a Tecan Infinite 200 Pro plate reader.

2.4. Molecular biological methods

2.4.1. Polymerase chain reaction (PCR) to generate fragments for cloning

Polymerase chain reaction was done to either amplify certain stretches of genes as inserts for cloning, to generate linearized plasmid backbones for cloning, or to confirm successful cloning or mutants during mutagenesis. To generate PCR fragments to be used for further cloning, usually the KAPA HiFi PCR kit by Roche was used. Alternatively, the Phusion High-Fidelity DNA polymerase was used, when amplification by KAPA polymerase was unsuccessful. For either polymerase, the GC-rich buffers were used if the GC-content of the target sequence was ~60% or higher. The compositions of the master mixes are shown below. These were added in the order as written, the master mix was mixed by pipetting up and down and the volume for one reaction each was distributed in PCR tubes. The final volume of one reaction was 25 µl for KAPA and 20 µl for Phusion. Table 15 shows the composition of the master mix for KAPA PCR and Table 16 the composition for Phusion PCR.

Table 15: Composition of master mix for KAPA PCR. Reagents were added in the order as written.

Reagent	Volume for 1 reaction	Final concentration
Nuclease-free water	Ad 25 µl	-
5x KAPA HiFi Buffer (Fidelity or GC)	5 µl	1x
10 mM KAPA dNTP Mix	0.75 µl	0.3 mM
10 µM forward primer	0.75 µl	0.3 µM
10 µM reverse primer	0.75 µl	0.3 µM
Template DNA	As needed	20 ng per reaction for PCR with gDNA, 2 ng per reaction for PCR with plasmid
1 U/µl KAPA HiFi DNA polymerase	0.5 µl	0.5 U

Table 16: Composition of master mix for Phusion PCR. Reagents were added in the order as written.

Reagent	Volume for 1 reaction	Final concentration
Nuclease-free water	Ad 20 µl	-
5x Phusion HF Buffer or 5x GC Buffer	4 µl	1x
10 mM dNTP	0.4 µl	0.2 mM
10 µM forward primer	1 µl	0.5 µM
10 µM reverse primer	1 µl	0.5 µM
Template DNA	As needed	50 ng per reaction for PCR with gDNA, 4 ng per reaction for PCR with plasmid
Phusion High-Fidelity DNA Polymerase	0.2 µl	0.02 U/µl

The prepared PCR tubes were placed in a thermocycler, and depending on the polymerase, melting temperature of the primers, and length of the amplicon, the cycling protocol was adapted. For amplification of fragments for cloning, the annealing was usually done with a

temperature gradient, allowing different annealing temperatures per reaction. With this approach unspecific amplification could be minimized. The cycling protocol for KAPA PCR is shown in Table 17 and the protocol for Phusion PCR in Table 18.

Table 17: Cycling protocol for KAPA PCR.

Step	Temperature	Duration	Cycles
Initial denaturation	95°C	5 min	1
Denaturation	95°C	30 s	25-35
Annealing	52°C-72°C	30 s	
Extension	72°C	30 s/kb	
Final extension	72°C	5 min	1

Table 18: Cycling protocol for Phusion PCR.

Step	Temperature	Duration	Cycles
Initial denaturation	98°C	30 s	1
Denaturation	98°C	10 s	25-35
Annealing	52°C-72°C	30 s	
Extension	72°C	30 s/kb for genomic DNA, 15 s/kb for plasmid DNA	
Final extension	72°C	5 min	1

2.4.2. Colony PCR to screen mutants or transformants

For confirmation of successful cloning or mutagenesis by colony PCR, MangoMix was used. This is a ready-to-use PCR mix containing all components except water template and primers, and already includes loading dye. For ease of use when checking colonies, some material was taken from to colony with a pipette tip and added to the prepared MangoMix PCR reaction. The cells were then lysed during denaturation and template DNA was released into the mix. The PCR reactions were set up as described in Table 19.

Table 19: Composition of master mix for MangoMix PCR.

Reagent	Volume for 1 reaction	Final concentration
Nuclease-free water	Ad 15 µl	-
2X MangoMix	7.5 µl	1x
10 µM forward primer	0.5 µl	0.333 µM
10 µM reverse primer	0.5 µl	0.333 µM
Template	Small amount of material from colony	

The cycling conditions for the MangoMix PCR were adapted to ensure complete lysis of the bacteria added to the mix. For this the initial denaturation was longer than usual. The cycling conditions are shown in Table 20.

Table 20: Cycling protocol for MangoMix PCR.

Step	Temperature	Duration	Cycles
Initial denaturation	95°C	8 min	1
Denaturation	95°C	30 s	30
Annealing	2°C below lowest melting temperature of primers	30 s	
Extension	72°C	30 s/kb	
Final extension	72°C	5 min	1

2.4.3. Agarose gel electrophoresis

To analyze PCR reactions or to check integrity of purified RNA, agarose gel electrophoresis was done. This allows separation of various DNA fragments by size. To prepare a gel, first 0.5x TBE buffer was prepared by adding one part 5x TBE buffer to nine parts deionized water. Agarose was weighed in and 0.5x TBE buffer was added to a final concentration of 1% agarose. The mixture was heated in a microwave until the agarose dissolved. The desired volume of agarose gel was poured into a fresh flask and allowed to cool. MIDORI Green Xtra DNA stain was then added in a dilution of 1:20,000 and mixed. The liquid agarose was then poured into a gel tray with a comb with an appropriate well number that was fitted into a casting stand. The gel was allowed to solidify and transferred into the electrophoresis chamber filled with 0.5x TBE buffer. Then, the comb was removed and the gel was loaded by mixing 5µl of the PCR product with 2 µl of orange G loading dye in case of amplification by KAPA or Phusion PCR or directly loading 5 µl per well in case of PCR with MangoMix. The gel was run at 110 V constant for 30 minutes and then imaged using a FastGene FAS-V imaging system.

To check the integrity of purified RNA, 1 µl of RNA sample was mixed with 3 µl of Orange G loading buffer. The entire sample was loaded on a 1% agarose gel and ran at 110 v constant for 20 minutes. The RNA was assumed as intact if clear bands for the 16S- and 23S-rRNA could be seen.

2.4.4. Isolation of PCR products

In case PCR was done to generate fragments for downstream cloning, the PCR products were purified using the Wizard SV Gel and PCR Clean-Up System by Promega. For this, the PCR reactions that had the least unspecific products as seen in agarose gel electrophoresis were selected and pooled. The purification was then done as described by the manufacturer.

2.4.5. Isolation of plasmids

To isolate plasmids, *E. coli* strains carrying the plasmid to be isolated were grown overnight in LB medium containing appropriate antibiotics. The cultures were centrifuged and plasmid was

isolated using the Monarch Plasmid Miniprep Kit (New England Biolabs) according to the instruction of the manufacturer. Depending on the copy number of the plasmid, the volume of liquid culture had to be adapted. For high-copy plasmids, 5 ml of liquid culture was sufficient. If the plasmid had a low copy number, the bacteria were grown in 20 ml of liquid culture. For isolation, the culture was split in two parts and two isolations were done in parallel. Additionally, twice the volume as specified by the manufacturer was used per parallel-isolation for the alkaline lysis. This is because the upper limit of the kit as specified by the manufacturer is 5 ml of liquid culture per isolation. The column-based purification step was then done with the normal volumes as specified. The plasmid was eluted in 50 µl of elution buffer.

2.4.6. Isolation of genomic DNA

Genomic DNA (gDNA) was isolated using the DNeasy UltraClean Microbial Kit by Qiagen. Bacteria were grown overnight in LB medium and gDNA was isolated according to the manufacturer.

2.4.7. Isolation of total RNA

Total RNA was isolated using the ZymoBiomics RNA Miniprep Kit. For this purpose, after the treatment of interest, OD_{600} was measured. $OD_{600} = 1$ was pelleted by centrifugation and washed twice with 500 µl ice cold PBS. The cells were then resuspended in 100 µl of ice-cold PBS and transferred to a ZR BashingBead Lysis Tube. 750 µl of DNA/RNA shield was added and the tubes were fixed in a Multi-Tube Holder fixed to a Vortex Genie 2. The samples were then processed at maximum speed for 20 minutes. The samples could be kept frozen at -80°C previous to further isolation. To further isolate the total RNA, the samples homogenized in DNA/RNA shield were thawed and RNA was isolated according to the instructions of the manufacturer. The DNase digest as described by the manufacturer was done as described.

After isolation a second DNase digest was done using the Roche DNase I. For this, a master mix was prepared by mixing 5 µl of 10x buffer per reaction with 1 µl of DNase I per reaction. Of this mixture, 6 µl of master mix were added to each sample. The samples were incubated at 37°C for 30 minutes. To stop the DNase I digest, 2 µl of 0.2 M EDTA were added per sample and the samples were incubated at 72°C for 10 minutes.

The product of the DNase digest was further purified using the RNA Clean & Concentrator-5 kit by Zymo Research as described by the manufacturer. The samples were eluted in a final volume of 20 µl DNase/RNase-free water.

Subsequently, the concentration of isolated total RNA was determined using a Qubit fluorometer with the Qubit RNA BR Assay-Kit. The integrity of the isolated RNA was checked by

agarose gel electrophoresis. The RNA was deemed intact, if clear bands for the 16S- and 23S-rRNA could be seen.

Successful digestion of DNA by DNase I was controlled by quantitative PCR (qPCR) as well as reverse-transcription quantitative PCR (RT-qPCR). Targets that were amplified were house-keeping genes such as *gyrB* or *rpoS* as well as genes that were potentially deleted. This gave information whether there was still DNA present in the sample that could interfere with down-stream applications such as RNAseq and if gene deletions were successful.

2.4.8. Photometric quantification of nucleic acids

Nucleic acid concentrations were determined using a Nanodrop One. The Nanodrop was blanked against the medium in which the nucleic acid was dissolved.

2.4.9. Fluorometric quantification of nucleic acids

Fluorometric quantification of nucleic acids was done using a Qubit fluorometer. Depending on the type of nucleic acid (RNA or DNA) a different kit was used. The fluorometer was used according to the instructions of the manufacturer (ThermoFisher Scientific).

2.4.10. Gibson assembly for cloning of plasmids

Recombinant plasmids were generated by Gibson assembly (Gibson et al., 2009). This method allows the joining of multiple overlapping pieces of DNA in one reaction. *"For this purpose, vector fragments and inserts were amplified by PCR using the KAPA HIFI PCR Kit (Roche) and assembled using a Gibson Mix for 30 min at 50 °C. The reaction product was transformed in E. coli Dh5α and selected on LB agar plates with appropriate antibiotics"* (Eggers et al., 2023, p. 13).

If KAPA PCR was unsuccessful, Phusion PCR was alternatively used. Usually, 30 overlapping bases between fragments were enough to yield successful reaction products. The composition of the Gibson Mix is shown in Table 21.

Table 21: Composition of Gibson mix used in this study.

Reagent	Volume for 1 reaction	Final concentration
5x Isothermal reaction buffer	2 µl	1x
Taq DNA Ligase 40 U/µl	1 µl	4 U/µl
T5 Exonuclease 10 U/µl	0.004 µl	0.004 U/µl
Phusion DNA Polymerase 2 U/µl	0.0125	0.025 U/µl
Nuclease-free water	ad 10 µl	-

Chemically competent *E. coli* Dh5α or Top10 were transformed with the reaction product of the Gibson assembly by heat shock. The cells were plated in LB agar plates containing appropriate antibiotics. The obtained colonies carrying the recombinant plasmids were screened by

colony PCR. Positive clones were grown for plasmid preparation and confirmed by Sanger sequencing.

2.4.11. Excision of the kanamycin resistance cassette from Keio strains

Excision of the *kan*^{R} cassette from the strains of the Keio collection (Baba et al., 2006) was done as described by Cherepanov and Wackernagel (1995), using the protocol of Jeffrey Barrick published on the website barricklab.org (Barrick et al., 2023). Overnight cultures of the respective strains were transformed with the plasmid pCP20, carrying an ampicillin resistance cassette *amp*^{R}, and encoding a FLP recombinase, by electroporation. As the plasmid has a temperature sensitive origin of replication and encodes the FLP recombinase under a temperature-dependent promoter, the incubation steps after the electroporation were done at 30°C instead of 37°C. Single colonies were picked and grown in LB medium containing 50 µg/ml kanamycin overnight at 43°C to induce production of the FLP recombinase as well as to select for a loss of pCP20. The overnight culture was then diluted 10^6-fold and 50 µl were plated on LB agar. The plates were incubated at 30°C overnight. Single colonies were than patched on LB plates containing either kanamycin (50 µg/ml), or carbenicillin (200 µg/ml), and LB plates without antibiotic and grown overnight with the LB and LB + kanamycin plates grown at 37°C and the LB + carbenicillin plates grown at 30°C.

Clones that were susceptible to both antibiotics were confirmed by PCR and stored as glycerol stocks for long term usage.

2.4.12. Sanger sequencing of plasmids

To confirm plasmids were correct after cloning, Sanger sequencing was done by Eurofins Genomics. Appropriate primers for sequencing were designed to cover about 800-1000 bp of DNA sequence of interest. The plasmids were isolated and diluted to 50-100 ng/µl. 15 µl of plasmid were mixed with 2 µl of sequencing primer per reaction and sent to Eurofins for sequencing.

2.4.13. Whole plasmid sequencing

Whole plasmid sequencing was done with Eurofins Genomics to confirm that plasmids were correct after cloning. Whole plasmid sequencing was used in case the inserts were too large to be covered properly by Sanger sequencing or to confirm the correctness of the backbone sequence of a plasmid. Plasmids were isolated and diluted to 30 ng/µl. At least 10 µl of plasmid were sent to sequencing.

2.4.14. Mutagenesis of *P. aeruginosa* by homologous recombination

In-frame deletion mutants of *P. aeruginosa* were generated by allelic exchange as described previously (Eggers et al., 2023; Hmelo et al., 2015; Klein et al., 2019; Sonnabend et al., 2020). For this, between 800 and 900 bp upstream of the gene containing the first 30 bases, including the start codon, and 800 to 900 bases downstream of the gene of interest, including the stop codon, were amplified by PCR using genomic DNA as a template. Overhangs were introduced by PCR to allow for joining of the fragments. The fragments were cloned into the suicide plasmids pEXTK or pEXG2 by Gibson assembly. These plasmids are able to replicate in *E. coli*, but not in *P. aeruginosa*, and thus are only able to propagate when inserted into the genome of *P. aeruginosa* by homologous recombination. These plasmids were transformed into the conjugative *E. coli* strain SM10λpir and mobilized into *P. aeruginosa* by conjugation. Conjugation was done by bi-parental mating, mixing 200 µl of overnight culture of the donor stain and 400 µl of overnight culture of the recipient strain. The mixture was centrifuged at 10,000 x *g* for one minute, the supernatant discarded and the pellet resuspended in the remaining liquid. The cells were then spotted on a LB plate and incubated at 37°C overnight. The next day, the cells were resuspended in 2 ml of LB medium and 20 µl and 100 µl of the slurry was plated on LB agar plates containing 75 µg/ml gentamicin and 15 µg/ml irgasan. This allowed for the selection of *P. aeruginosa* clones that have integrated the plasmids by homologous recombination, as the plasmid contains a gentamicin resistance cassette but does not replicate in *P. aeruginosa*. The *E. coli* cells are killed by the irgasan. Of these clones, four were picked and streaked overnight on LB agar plates, allowing for a second crossover, resulting either in deletion mutants or a reversion back to wildtype. To counter select the clones that underwent a successful second crossover event, all the clones that still carried the integrative plasmid had to be killed. For this, the plasmid pEXG2 encodes a *sacB* cassette derived from *Bacillus subtilis*, encoding for levansucrase. Levansucrase produces a toxic product from sucrose, thus conferring sucrose sensitivity (Hmelo et al., 2015; Ried & Collmer, 1987; Steinmetz et al., 1983). To select for double crossover exconjugants, of each of the four clones streaked on LB medium, a liquid culture in LB medium containing 20% sucrose was prepared and grown overnight with shaking at 37°C. Of this culture a three-loop-streak was done on NSLB agar plates containing 15% sucrose and incubated overnight at 37°C. From these plates, single colonies were picked and patched on LB agar containing 75 µg/ml gentamicin and on LB agar without antibiotics to screen for gentamicin susceptible clones. After overnight incubation, gentamicin susceptible clones were screened by colony PCR using primers flanking the gene of interest, as well as

primers that bind inside the region to be deleted. Positive clones were grown in 5 ml of LB medium and the next day, genomic DNA was isolated and the PCR was repeated. The mutants were then stored as glycerol stocks. In case the plasmid pEXTK was used, the procedure was the same, but the counter selection after the second cross over was different. *"In pEXTK, the sacB gene is replaced by a thymidine kinase gene. If pEXTK based mutator plasmids were used in the mutagenesis procedure, the positive selection to obtain a second crossover was performed by incubating merodiploidic clones for 3 h in 5 ml LB medium containing IPTG (1 mM). Subsequently, bacteria were positively selected by streaking bacteria on LB agar plates containing 200 µg/ml azidothymidine (Acros Organics) and 1 mM IPTG"* (Eggers et al., 2023, p. 13).

Figure 6 shows a schematic overview of the mutagenesis procedure.

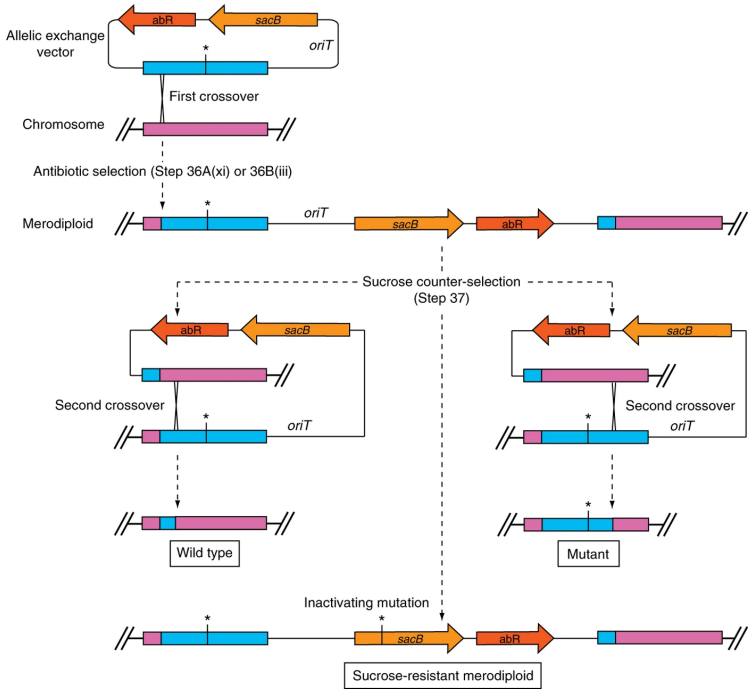

Figure 6: Principle of allelic exchange utilized in this study. The allelic exchange vector is mobilized into *P. aeruginosa* by conjugation. A first crossover happens by homologous recombination at one of the flanking regions of the shortened gene of interest. As the allelic exchange vector cannot replicate in *P. aeruginosa*, only merodiploids that have integrated the vector into their genome remain viable after antibiotic selection. Utilizing *sacB* or a thymidine kinase, a counter selection is done. This forces a second crossover, reverting the bacterium back to wildtype or to a mutant. The figure was reproduced unaltered from Figure 1 in Hmelo et al. (2015). Reproduced with permission from Springer Nature.

2.4.15. Complementation of *P. aeruginosa* by Tn7-insertion

Rhamnose-inducible complementant strains of ID40 were generated as described by Choi and Schweizer (2006). The CDS of the gene of interest to complement was PCR-amplified using genomic DNA as a template and inserted by Gibson assembly into the miniTn7 element (Gm^R) present on the plasmid pJM220 (Meisner & Goldberg, 2016). The CDS was inserted down-

stream of a rhamnose-inducible promoter that was also located on the miniTn7-element. *P. aeruginosa* strains to complement were transformed with the pJM220 plasmid and the helper plasmid pTNS3 by electroporation. pTNS3 harbors a Tn7 transposase, allowing insertion of the miniTn7-constructs at the attTn7 site of *P. aeruginosa*. The insertion of the miniTn7 construct was verified by PCR. The gentamicin resistance cassette was then excised by transforming the *P. aeruginosa* strains with the FLP-recombinase expressing plasmid pFLP2 (Cb^R, sac^+) by electroporation. The strains were streaked on NSLB agar containing 15% sucrose to cure them from the pFLP2 vector. Loss of the plasmid and the gentamicin resistance cassette was tested by patching colonies on LB agar containing either 200 µg/ml carbenicillin or 75 µg/ml gentamicin and on NSLB agar containing 15% sucrose. Finally, colonies were verified by PCR.

2.4.16. Mutagenesis of *E. coli* by homologous recombination

E. coli BW25113 strains were mutated by allelic exchange using the suicide plasmid pSB890y. Due to its origin R6Kγ, pSB890y is not able to replicate in *E. coli* BW25113 except when integrated in the genome. For cloning, the *E. coli* strain Dh5αpir116 was used that carries the *pir* gene, encoding for the π-protein. This protein is required for replication of plasmids carrying the R6Kγ plasmid (Germino & Bastia, 1982; Shafferman et al., 1982; Stalker et al., 1982). Same as before, the gene of interest was cloned in a truncated version with 800 bp upstream and downstream of the scar site. As described before, the pSB890y plasmid carries a *sacB* gene for counterselection.

For conjugation in *E. coli* BW25113 strains, chemically competent *E. coli* β2163Δnic35 were transformed with the plasmid and grown in 5 ml of LB medium containing 6 µg/ml tetracycline and 50 µg/ml diaminopimelic acid (DAP), as the *E. coli* β2163Δnic35 is auxotroph for DAP (Babic et al., 2008). *E. coli* β2163Δnic35 is able to transfer its plasmid by mating (Babic et al., 2008) and thus was used to transfer the suicide plasmid to *E. coli* BW25113.

For this purpose, 900 µl of the prepared culture of *E. coli* β2163Δnic35 carrying the pSB890y plasmid and 900 µl of overnight culture of BW25113 were mixed, pelleted by centrifugation at 5000 x *g* for 1 minute, washed twice with 1 ml of LB medium without supplements, and finally resuspended in 100 µl of LB medium supplemented with 50 µg/ml DAP. The slurry was then spotted on a LB agar plate containing 50 µg/ml DAP and incubated overnight at 37°C. The next day, the spot was scraped off and resuspended in 1 ml LB medium. The suspension was diluted 1:100 with LB medium and 100 µl were plated on LB agar plates containing 12.5 µg/ml tetracycline. As the donor strain is unable to grow without DAP and the plasmid itself does not

replicate in *E. coli* BW25113, except when integrated by homologous recombination, this allowed for the selection of the merodiploid clones that had the plasmid integrated in the genome by homologous recombination. Two merodiploids were picked and grown in 5 ml LB medium overnight at 37°C to allow for a second crossover. The next day, a counter selection was done using sucrose, as the plasmid encodes a *sacB* gene that allows for counter selection using sucrose due to the production of a toxic product from sucrose by levansucrase, the gene product of *sacB* (Ried & Collmer, 1987; Steinmetz et al., 1983). For the counter selection, 1.5 µl of the prepared overnight cultures were diluted in 1 ml LB medium and plated on a LB agar plate containing 15% sucrose and incubated at 37°C overnight. The next day, the success of the second crossover was tested by screening for tetracycline susceptible clones by patching on LB agar plates containing 12.5 µg/ml tetracycline and of LB agar plates without antibiotics. After overnight incubation at 37°C, tetracycline susceptible clones were screened by colony PCR for the correct size of the truncated gene of interest. Positive clones were grown in liquid culture, genomic DNA was isolated and the PCR repeated. Mutants were stored as glycerol stocks for long term usage at -80°C.

2.4.17. Quantitative polymerase chain reaction

Quantitative polymerase chain reaction (qPCR) was done using the QuantiFast SYBR Green PCR Kit by Qiagen. qPCR was mainly done to control for successful digestion of DNA by DNase I to avoid DNA interfering with the downstream application. As target genes, either of the housekeeping genes *gyrB* or *rpoS* was used. The master mix was used according to the instructions of the manufacturer and transferred to a 96 well PCR plate. The samples were diluted to an RNA concentration of 50 ng/µl and 1 µl of sample was added per reaction. The PCR plates were sealed with transparent foil and the qPCR reaction was carried out in a LightCycler 480 II (Roche). The qPCR protocol is listed in Table 22. Primers used for qPCR are listed in Table 12.

2.4.18. Reverse-transcription quantitative polymerase chain reaction

Reverse-transcription quantitative polymerase chain reaction (RT-qPCR) was done to quantify the abundance of mRNA in a sample. For this, the QuantiFast SYBR Green RT-PCR Kit (Qiagen) was used, a one-step RT-qPCR kit. The master mix was prepared as described by the manufacturer and 24 µl were added to the wells of a 96 well PCR plate. The samples were diluted to 50 ng of RNA per µl using RNase-free water and 1 µl was added to the master mixes. RT-qPCR was carried out with primers for the genes of interest as well as for either of the housekeeping genes *gyrB* or *rpoS*. The RT-qPCR was done in a LightCycler 480 II (Roche)

with the cycling conditions shown in Table 22. Primers used for RT-qPCR are listed in Table 12. A melting curve was recorded to see if the amplified PCR product consisted of one species or if there were several products due to unspecific binding of primers. Samples of biological replicates were always run in technical duplicates.

Table 22: Cycling conditions for qPCR and RT-qPCR. For qPCR the reverse transcription step was done to keep conditions equal between both methods and to increase comparability.

Step	Target temperature	Ramp rate	Hold	Cycles	Acquisition mode
Reverse transcription	50°C	4.4 °C/s	10 min	1	None
Initial denaturation	95°C	4.4 °C/s	5 min	1	None
Denaturation	95°C	4.4 °C/s	10 s	40	None
Annealing	60°C	2.2 °C/s	10 s		None
Extension	72°C	4.4 °C/s	30 s		Single
Melt curve	95°C	4.4 °C/s	5 min	1	None
	46°C	4.4 °C/s	10 s	1	None
	95°C	0.06 °C/s	-	1	Continuous (10 acquisitions per °C)
Cool	40°C	2.2 °C/s	20 s		None

The data analysis was done using the LightCycler 480 software, using the second derivative max method for absolute quantification. The obtained values for the crossing point (Cp), the PCR cycle at which the fluorescence signal crosses above the background threshold, were then used to calculate the gene expression according to Pfaffl (2001). The Pfaffl method requires the knowledge of the amplification efficiency of each primer pair, i.e. if indeed there is a doubling of the amplicon in each cycle of the PCR. An efficiency of 2 displays that this particular primer pair indeed doubles the amount of generated amplicon in each cycle. To obtain the efficiency of a primer pair, a serial dilution was done by diluting a chosen sample in two-fold steps and run in duplicates. The primer efficiency could then be calculated by the LightCycler software by selecting the runs as a standard curve. The mean of the Cp values of the technical duplicates was calculated and then the mean of the Cp values of the biological replicates of the control was calculated for the gene of interest as well as for the reference gene. The individual Cp values and the efficiency of each sample was then inserted in Equation 4 with the control being the mean of the control samples for each gene. The individual values of the control condition were also treated as a sample.

Equation 4: Equation for calculation of relative gene expression as described by Pfaffl (2001). Ratio = relative expression, E = primer efficiency, Cp = crossing-point value

$$ratio = \frac{(E_{target})^{\Delta Cp target(control-sample)}}{(E_{ref})^{\Delta Cp_{ref}(control-sample)}}$$

This gave the relative expression of each gene of interest in the different conditions. The relative expression could then be further plotted and analyzed.

2.4.19. Library preparation for RNA sequencing

Library preparation of RNA samples for RNAseq was done by Christina Engesser of the NGS Competence Center Tübingen (NCCT) together with me.

As a first quality control step prior to library preparation, the concentration of total RNA was measured using the Qubit RNA BR Assay Kit. For library preparation (depletion of ribosomal RNA, fragmentation, cDNA synthesis, poly(A)-tailing, adapter ligation and specific amplification of adapter-ligated cDNA by PCR), the kit Illumina Stranded Total RNA Prep with Ribo-Zero Plus was used according to the instruction of the manufacturer with an initial input of 200 ng of total RNA per sample.

After library preparation, the quality of the individual libraries was controlled by Bioanalyzer using the Bioanalyzer High sensitivity DNA Kit. The libraries were then pooled in two pools, one for each species of bacteria tested, with a concentration of 8 nM of cDNA per pool. The concentration of the pools was measured using the Qubit DS DNA HS assay Kit and quality of the pools was controlled by Bioanalyzer using the Bioanalyzer High Sensitivity DNA Kit.

2.4.20. RNA sequencing

Sequencing of the pooled libraries was done in two batches by Christina Engesser (NCCT) on an Illumina NextSeq 500 with a MidOutput Flowcell v2.5, 2×75 bp (runmode 74, 10, 10, 74) with a final input of 1 pM and a PhiX spike-in of 1%.

The data analysis was done by Jennifer Müller of the NCCT. The following section was written using information provided by Jennifer Müller.

The sequencing was demultiplexed with bcl2fastq (v2.19.0.316) and quality was checked with fastp (v0.20.1) and visualized using MultiQC (v1.7). The analysis of the RNAseq was then performed with the nf-core/rnaseq pipeline (v.3.11.2), using hisat2 as an aligner. The default settings were used for the analysis, except for the *featurecounts_group_type*, which was set to *gene_id.* The *featurecounts_feature_type* was set to *transcript.* The featurecounts tables were used for downstream analysis and visualization. The *deseq2_qc.R* script was adapted and the data were visualized with EnhancedVolcano (v1.14.0), ggplot2 (v3.4.2), plotly (v4.10.2), and the VolcaNoseR web application (Goedhart & Luijsterburg, 2020). Genes with an adjusted *p* value of ≤0.01 and a $\log_2$ fold change of ≥2 or ≤-2 were considered differentially expressed.

2.4.21. AmpDh3 promoter activity assay

"To determine the activity of the ampDh3-promoter, various ampDh3-promoter-luciferase reporter constructs such as the plasmid pBBR-ampDh3-532-nanoluc were transformed into Pseudomonas aeruginosa strains via electroporation according to the protocol of Choi et al. (Choi et al., 2006) […] *Overnight cultures were subcultured for 3 h in 5 ml LB containing 75 µg/ml gentamicin. OD_{600} was measured and cultures were diluted to an OD_{600} of 0.2 in 1 ml LB. 50 µl were transferred into a white flat bottom 96-well plate in triplicates and 50 µl of Promega NanoGlo Luciferase assay reagent (Promega) prepared according to the manufacturer's instructions was added to the wells. The plate was then shaken for 10 min at RT and chemiluminescence was measured using a Tecan Infinite Pro 200 plate reader"* (Eggers et al., 2023, p. 13).

2.5. Statistical methods

Statistical analysis of RNAseq data as well as of raw NanoLC-MS/MS data is described in the respective chapter (2.4.20 and 2.3.25)

2.5.1. Definitions of replicates and sample size

A biological replicate *n* was defined as a distinct biological entity, i.e., a distinct bacterial culture. Technical replicates were repeated measurements prepared from the same biological replicate. The mean of technical replicates was calculated to obtain the value of a biological replicate. The sample sizes in this study ranged from $n = 1$ to $n = 19$. Statistical analysis was only done, when a condition had at least $n = 3$ biological replicates.

2.5.2. Welch's *t* test

Two-tailed Welch's *t* test was done to compare exactly two groups that had unequal variances in GraphPad Prism v10.1.1. The data were tested for normality using Shapiro-Wilks test as well as by graphical analysis using Q-Q-plots. The test was done with a confidence level α of 95%.

2.5.3. One-way ANOVA

One-way ANOVA was done to compare three or more unmatched groups that were affected by one factor. GraphPad Prism v10.1.1 was used for the analysis. Normality was analyzed by Shapiro-Wilks test as well as by graphical analysis using Q-Q-plots. If the data were not normally distributed, a $\log_{10}$ transformation was done, and checked again. The groups were tested for equal variances by Brown-Forsythe test. One-way ANOVA was then done with the post-hoc test being adapted to the comparisons made. In all cases, an α threshold of 0.05 was chosen. If all groups were compared to each other, Tukey's multiple comparisons test was done. If all

groups were compared to a control group, Dunnett's multiple comparison test was done and if only preselected pairs of groups were compared, Šídák's multiple comparisons test was done.

2.5.4. Two-way ANOVA

Two-way ANOVA was done to compare the means of three or more unmatched groups that were influenced by two factors using GraphPad Prism v10.1.1. As before, normality was analyzed by Shapiro-Wilks test as well as by graphical analysis using Q-Q-plots. Heteroscedasticity was tested by Spearman's rank correlation coefficient test. Two-way ANOVA was then done with an appropriate post-hoc test as described in 2.5.3, with an α threshold of 0.05.

2.5.5. Data analysis of pulldown-MS data using Perseus

Analysis of the pulldown-MS data was done using the Perseus software platform v2.0.10.0 (Tyanova, Temu, Sinitcyn, et al., 2016) on LFQ intensity values that were obtained from MaxQuant as described in section 2.3.26. Data were cleaned by removing proteins that were "only identified by site" by MaxQuant, i.e. identification only by peptides with modified amino acids, as these identifications are typically irrelevant. In addition, for pulldown assays done in *P. aeruginosa* ID40, all proteins that were annotated as *E. coli* proteins, as these were likely contaminants from the purification of GST or GST-YgfB.

The matrix was imported into Perseus and LFQ intensity values were categorically annotated into groups of replicates. To check for variations between groups and replicates, a principal component analysis was done. The LFQ intensity values were then $\log_2$ transformed and filtered based on valid values. All rows that had three valid values in at least one group were kept, while the rest was discarded. This ensured that only unambiguous measurements were kept for analysis. Missing values were then replaced with values sampled from a normal distribution with a width of 0.3 and a down shift of 1.8, with the mode set to "Total matrix" to sample from the entire matrix and not from each column. Multi scatter plots of the data were then created and the Pearson correlation was calculated to estimate the degree of correlation between the replicates. Additionally, histograms of the data $\log_2$ transformed LFQ intensity values were created to verify a normal distribution of the data and to control that the imputed values fell within this normal distribution. The data were then analyzed by two-sided two-sample *t* test with an S0 of 2 and an FDR of 0.01. FDR was calculated by permutation-based FDR with the number of randomizations set to 250.

Proteins that had a *q* value of ≤ 0.01 and a positive $\log_2$ fold change when comparing the GST-YgfB condition with the GST control were considered as interactors.

2. Materials and Methods

In the *P. aeruginosa* dataset, proteins that derived from the purification of GST or GST-YgfB could be excluded previously to the analysis in Perseus, as these were annotated as *E. coli* proteins. For the *E. coli* BW25113 condition, this was not possible. Therefore, pulldowns were not only done with whole cell lysates as bait, but also with pulldown buffer as a mock condition. All proteins that were present in the mock-pulldown condition except GST or GST-YgfB could be considered as contaminants. To perform statistical analysis for interactors of YgfB in BW25113, the data had to be cleaned by removing purification contaminants. For this, the "GST-YgfB + Lysate" and GST + Lysate" conditions were compared by two-sided multiple *t* test with the "GST-YgfB + Mock" and "GST + Mock", respectively, with an S0 of 2 and an FDR of 0.01. Proteins that had significant differences and were enriched in the "+Lysate" condition vs. the "+Mock" condition in either the GST-YgfB or the GST comparison were categorized as potential interactors of either GST or GST-YgfB and could be ruled out as contaminants. Statistical analysis by multiple *t* test comparing "GST-YgfB + Lysate" vs. "GST + Lysate" was then done as described above using the cleaned dataset of potential interactors of either protein. To be classified as an interactor of GST-YgfB, a protein had to be significantly enriched in the "GST-YgfB + Lysate" vs. "GST + Lysate" comparison as well as in the "GST-YgfB + Lysate" vs. "GST-YgfB + Mock" comparison. The data was visualized using the VolcaNoseR web application (Goedhart & Luijsterburg, 2020).

3. Results

Declaration of contributions

Parts of the results shown in chapter 3.1 and 3.2 have been published in Eggers et al. (2023). Some passages have been cited literally from this publication. These citations were formatted in italics and are marked with quotation marks. The publication Eggers et al. (2023) was mainly written by PD Dr. Erwin Bohn and me. Figures in the results section of this work that were adopted, adapted or modified from Eggers et al. (2023) have originally been created by me, with the exception of Figure 7a, which was created together with PD Dr. Monika Schütz. The data originally published in Eggers et al. (2023) that are presented in the results section of this work were generated by me or under my supervision.

The RNAseq as well as the data evaluation shown in 3.3.1 were done in collaboration with the NGS Competence Center Tübingen (NCCT). Sequencing was done by Christina Engesser and data analysis by Jennifer Müller.

The NanoLC-MS/MS analysis of the interactome, including sample preparation of protein samples that were provided in a gel by me and the generation of LFQ data shown in 3.3.2 were done by Dr. Mirita Franz-Wachtel of the Proteome Center Tübingen.

All other data shown in this work were generated by me or under my supervision.

3.1. Regulation of AmpC and β-lactam resistance by YgfB

As described in the introduction, it has previously been shown that deletion of *ygfB* increases expression levels of *ampDh3*, which in turn leads to a shift in cell wall metabolic products. This shift in cell wall products modulates the activity of the regulator of *ampC*, AmpR, and thus AmpC levels and resistance to β-lactam antibiotics. This relationship has been shown by transcriptomic analysis as well as by RT-qPCR. AlpA has been shown to be a transcription factor of *ampDh3* and to be essential for transactivation of *ampDh3* upon deletion of *ygfB*.

3.1.1. Validation of transcriptome on the protein level

To validate the findings of the RNAseq, as well as of the RT-qPCR experiments on a proteomic level, we investigated the production of YgfB and AmpDh3. For this purpose, strains that had the *ampDh3* gene exchanged with *ampDh3* fused to a HiBiT-tag were generated by homologous recombination. HiBiT is an eleven amino acid tag and part of a split-NanoLuc luciferase. Adding the second part of the split-luciferase, LgBiT, reconstitutes NanoLuc to form a working luciferase generating chemiluminescence upon addition of the substrate furimazine.

Using this system allowed the levels of AmpDh3 to be measured by Western blot, as well as by 96-well plate-based measurement. We genomically tagged *ampDh3* with a sequence encoding the HiBiT tag in ID40 wildtype, *ygfB* deletion background, as well as in a conditional *ygfB* deletion mutant where *ygfB* had been reinserted under the control of a rhamnose inducible promoter at the Tn7-site of *P. aeruginosa*. This yielded the strains ID40::*ampDh3*-HiBiT, ID40Δ*ygfB*::*ampDh3*-HiBiT, and ID40Δ*ygfB*::rha-*ygfB*::*ampDh3*-HiBiT, respectively. These strains were then used to track AmpDh3 production as a response to *ygfB* deletion and/or induction. The data shown in this section have been published in Eggers et al. (2023).

3.1.1.1. Concentration-dependent relationship between *ygfB* and *ampDh3*

To validate the influence of *ygfB* deletion, the AmpDh3-HiBiT production in the ID40 wildtype, *ygfB* deletion, and complementation background was analyzed by Western blotting. The strains were grown in LB medium and whole cells lysates were prepared (Figure 7). For the complemented strain, rhamnose was added to the medium in different concentrations (0%, 0.001%, 0.01%, and 0.1%) to induce expression of *ygfB*. Figure 7a shows the Western blot of a dataset representative of three individual experiments, while Figure 7b and Figure 7c show a semi-quantification of the band intensities of three independent replicate sets. *"It should be noted that the antibodies we used for detection of YgfB produced an unspecific band very close to YgfB but at a slightly higher molecular weight and that YgfB and AmpDh3 were detected on separate blots"* (Eggers et al., 2023, p. 3).

Deletion of *ygfB* strongly increased the levels of AmpDh3-HiBiT. Increasing the levels of rhamnose added to the complemented strains clearly correlated with increasing protein levels of YgfB, while the levels of AmpDh3-HiBiT were negatively correlated with the levels of rhamnose added to the medium.

3. Results

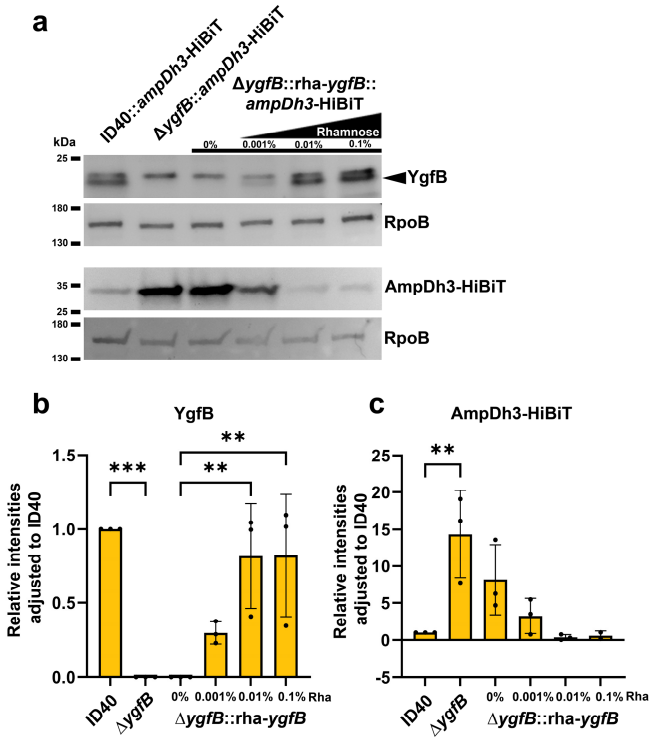

Figure 7: Western blot to validate data of RNAseq and RT-qPCR. a) *"Whole cell lysates of the indicated strains were used for SDS-PAGE and Western blots. The detection of YgfB and AmpDh3 was done on separate Western blots, each with RpoB as a loading control. As primary antibodies, anti-YgfB or as a loading control anti-RpoB antibodies and as secondary antibody anti-IgG-HRP antibodies were used and detection was done using ECL. For determination of AmpDh3, recombinant LgBiT was used. LgBiT binds to HiBiT resulting in a functional luciferase. The cleavage of the substrate furimazine leads to detectable chemiluminescence. Data are representative of three independent experiments"* (Eggers et al., 2023, p. 4). Rhamnose was added in the indicated concentrations to medium of the complemented strain to induce production of YgfB. **b + c)** Quantification of Western blot band intensity using ImageJ of the blots shown in **a)** as well as two other replicates. **b)** shows the quantification of YgfB and **(c)** the quantification of AmpDh3-HiBiT. Asterisks indicate significant differences, comparing either the wildtype and *ygfB*-deletion strain or the 0% rhamnose condition with the increasing rhamnose conditions. ns: not significant, $^{**}p<0.01$, $^{***}p<0.001$, one-way ANOVA, Šídák's multiple comparisons. Plotted are mean and standard deviation as well as individual data points from $n = 3$ individual experiments. The figure has been adapted from Eggers et al. (2023) under CC BY 4.0 (https://creativecommons.org/licenses/by/4.0/).

To further quantify the levels of AmpDh3-HiBiT, split-luciferase assays that allowed measurement of protein levels using a plate reader were done (Figure 8). ID40, ID40Δ*ygfB,* and ID40Δ*ygfB*::rha-*ygfB*::*ampDh3*-HiBiT were grown in LB medium as before. ID40 and ID40Δ*ygfB* were additionally treated with 0.1% rhamnose, while 0%, 0.001%, 0.01%, or 0.1% rhamnose was added to ID40Δ*ygfB*::rha-*ygfB*::*ampDh3*-HiBiT to induce increasing levels of *ygfB* expression. Cells were lysed and recombinant LgBiT and substrate were added to the lysates that contained the HiBiT-tagged protein.

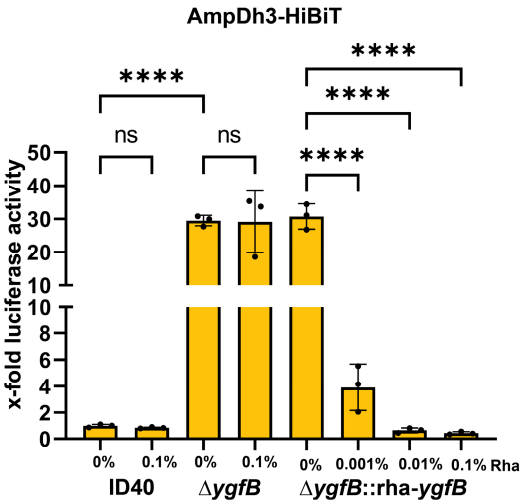

Figure 8: Quantification of AmpDh3-HiBiT levels. To quantify the levels of AmpDh3-HiBiT, ID40::*ampDh3*-HiBiT, ID40Δ*ygfB*::*ampDh3*-HiBiT, and ID40Δ*ygfB*::rha-*ygfB*::*ampDh3*-HiBiT were grown for 3 hours in LB medium and then chemically lysed. Addition of recombinant LgBiT to the lysates containing the HiBiT-tagged proteins led to the reconstitution of a working luciferase. Addition of furimazine as a substrate generated chemiluminescence that could be measured using a plate reader, giving information on the levels of HiBiT-tagged protein present in the lysate. Rhamnose was added to the culture at the indicated concentrations. Plotted are the relative levels of luciferase activity normalized to ID40 wildtype without added rhamnose. Comparisons were done by one-way ANOVA comparing the conditions as indicated by the brackets, using Šídák's multiple comparisons as a post-hoc test. ****p<0.0001. Plotted are the mean and standard deviation as well as individual data points of n = 3 biological replicates. The figure has been adapted from Eggers et al. (2023) under CC BY 4.0 (https://creativecommons.org/licenses/by/4.0/).

The levels of AmpDh3-HiBiT were strongly increased (~28-fold) in the ID40Δ*ygfB* strain compared to the wildtype. Addition of increasing concentrations of rhamnose to the complemented strain carrying rhamnose-inducible *ygfB* reduced the levels of AmpDh3-HiBiT about 8-fold, 48-fold, and 70-fold, respectively, as compared to the condition without rhamnose. In addition, there was no significant difference between AmpDh3-HiBiT production in ID40 wildtype and ID40Δ*ygfB* when rhamnose was added, highlighting that the effect on AmpDh3-HiBiT by addition of rhamnose was indeed due to an increased production of YgfB and not due non-specific effects of rhamnose. These results could further solidify the inverse relationship between YgfB and AmpDh3 and as such, also on downstream effects of AmpDh3.

3.1.1.2. Time-dependent relationship between *ygfB* and *ampDh3*

The temporal relationship of *ygfB*-induction and subsequent *ampDh3* expression observed on a transcriptomic level was also validated on the protein level. For this, the strain ID40Δ*ygfB*::rha-*ygfB*::*ampDh3*-HiBiT was grown in LB medium and 0.1% rhamnose was added at time point 0 min. At this time point and every subsequent 30 min for 180 min in total, a sample was taken from the growing culture and whole cell lysates were prepared for Western blotting. Figure 9a shows a Western blot representative of three independent Western blots. In Figure 9b and c, a semi-quantification of the Western blot band intensities that was done using ImageJ is shown.

3. Results

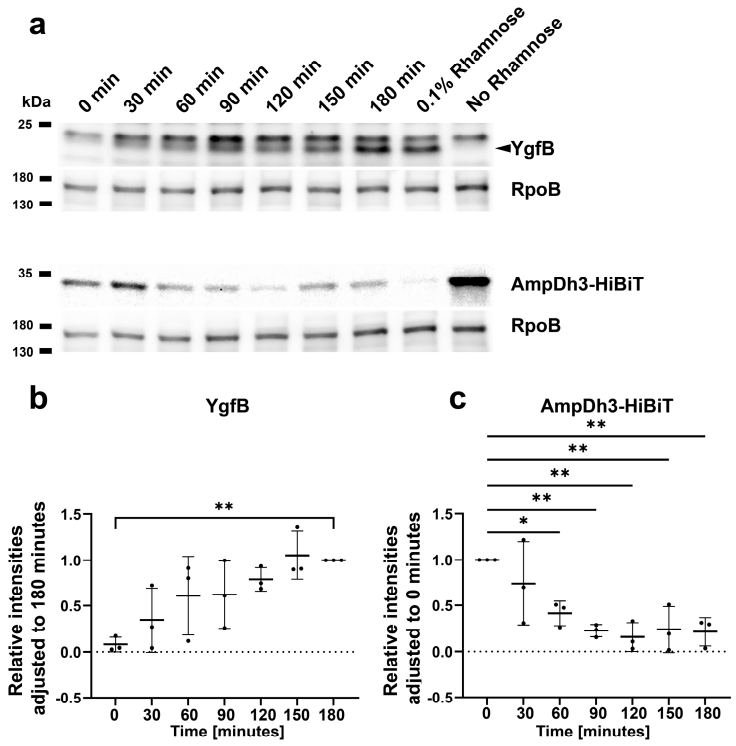

Figure 9: Western blot time course to track YgfB and AmpDh3-HiBiT production. a) *"The expression of ygfB in ID40ΔygfB::rha-ygfB::ampDh3-HiBiT was induced with 0.1% rhamnose at time point zero and samples were taken from the growing culture in LB medium at the indicated time points. Then, whole cell lysates were prepared and used for SDS-PAGE and Western blots. The 0.1% condition depicts a strain grown under constant rhamnose supplementation. The detection of YgfB and AmpDh3 was done on separate Western blots, each with RpoB as a loading control. As primary antibodies, anti-YgfB or anti-RpoB antibodies and as secondary antibody anti-IgG-HRP antibodies were used, and detection was done using ECL. For determination of AmpDh3, recombinant LgBiT was used. LgBiT binds to HiBiT resulting in a functional luciferase. The cleavage of the substrate furimazine leads to detectable chemiluminescence. Data are representative of three independent experiments"* (Eggers et al., 2023, p. 5). **b and c)** Western blot band intensities of three independent experiments were semi-quantified using ImageJ. Plotted are the loading control-normalized intensities of YgfB (**b**) and AmpDh3-HiBiT (**c**) compared to time point 180 min and time point 0 min, respectively. In **(b)**, all relative intensities were compared with the time point 180 min using one-way ANOVA and Dunnett's multiple comparisons as a post-hoc test. In **(c)**, all relative intensities were compared to the 0 min time point using one-way ANOVA and Dunnett's multiple comparisons as a post-hoc test. *p<0.05, **p<0.01. Plotted are mean and standard deviation as well as the individual data points of n = 3 biological replicates. Figure has been adapted from Eggers et al. (2023) under CC BY 4.0 (https://creativecommons.org/licenses/by/4.0/).

While YgfB levels were strongly increased already after 30 min and continued to rise throughout the experiment, levels of AmpDh3-HiBiT remained constant after 30 minutes and then dropped off sharply. Quantification of the band intensities of three independent Western blots using independently samples could confirm this impression.

Again, a split-luciferase assay was used to further measure the levels of AmpDh3-HiBiT in the cells upon induction of YgfB. As for the Western Blot, the same strain and setup were used, but at the sampling time points a fixed volume was taken from the growing culture, washed using PBS, and 10^9 cells (OD_{600} = 1) were harvested by centrifugation. The pellets were then frozen in liquid nitrogen and chemically lysed only once all samples had been collected to avoid protein degradation by lysing at different time points. The levels of AmpDh3-HiBiT in the

lysate were then measured by a luciferase assay as shown in Figure 10. This assay allowed a more exact tracking of the levels of AmpDh3-HiBiT following induction of *ygfB* expression, and again a sharp decline could be observed after 60 minutes.

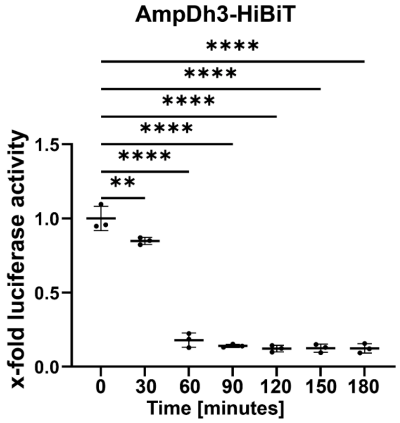

Figure 10: Time course analysis of AmpDh3-HiBiT levels following *ygfB*-induction by split-luciferase assay. 0.1% rhamnose was added to cultures of the strain ID40Δ*ygfB*::rha-*ygfB*::*ampDh3*-HiBiT at time point 0 min to induce production of YgfB. Levels of AmpDh3-HiBiT were then measured by taking samples every 30 minutes, freezing the pellets, and later lysing the cells by chemical lysis. The levels of AmpDh3-HiBiT could then be quantified by adding recombinant LgBiT, leading to a reconstituted luciferase that, upon addition of furimazine as a substrate, produced chemiluminescence. Luciferase activity at each time point was normalized to the time point 0 min. Time points were analyzed by one-way ANOVA, with Dunnett's multiple comparisons as a post-hoc test, comparing each time point to time point 0 min. Plotted are means, standard deviations, as well as individual data points of $n = 3$ biological replicates. $^{**}p<0.01$, $^{****}p<0.0001$. Figure was adapted from Eggers et al. (2023) under CC BY 4.0 (https://creativecommons.org/licenses/by/4.0/).

Together, the data of the Western blot and of the split-luciferase assay show that there is a temporal connection between levels of YgfB and AmpDh3, further solidifying the evidence that AmpDh3-levels are regulated by YgfB. In concert with the previous experiments on mRNA expression and β-lactamase activity, as well as analysis of PG recycling products that was described in the introduction, we were able to show that *ygfB* clearly regulates expression of *ampC,* and therefore resistance via repression of *ampDh3*. The repression of *ampDh3* affects the composition of muropeptides, leading to *ampC*-induction.

3.1.2. Regulation of *alpA* and *ampDh3* by ciprofloxacin and *ygfB*

It has been previously described that DNA damage leads to autocleavage of the repressor AlpR, whose main function is to repress the expression of the regulatory protein AlpA (McFarland et al., 2015). AlpA acts as an antiterminator and as such regulates expression of the *alpBCDE* self-lysis cluster as well as of the amidase *ampDh3* (Peña et al., 2021). The fluoroquinolone ciprofloxacin has long been known to induce DNA damage by binding to the DNA-gyrase and topoisomerase IV and inducing single- and double-strand breaks as reviewed in Drlica and Zhao (1997). This leads to activation of the SOS-response by autocleavage of LexA as well as autocleavage of LexA-like repressors such as AlpR (McFarland et al., 2015).

3. Results

As we had previously found that AlpA is essential for YgfB to regulate *ampDh3* expression and furthermore that YgfB regulates the *ampDh3* promoter at the same site that was described for AlpA by Peña et al. (2021), we figured that there is a possible relationship between YgfB and AlpA in the regulation of *ampDh3* and as such AmpC. To further investigate this relationship, the influence of ciprofloxacin-induced DNA damage and presence or absence of YgfB on the protein levels of AmpDh3, AlpA and AlpR was investigated.

3.1.2.1. Effect of ciprofloxacin and *ygfB* on AmpDh3 production

To confirm the findings of Peña et al. (2021), we first aimed to determine the abundance of AmpDh3 after exposure to suprainhibitory levels of ciprofloxacin. Additionally, we were interested in how YgfB levels were affected by ciprofloxacin, and if YgfB modulated the effect of ciprofloxacin on AmpDh3. After two hours of incubation with 32 µg/ml (4x MIC) of ciprofloxacin, the cultures of ID40::*ampDh3*-HiBiT and ID40Δ*ygfB*::*ampDh3*-HiBiT were harvested for preparation of whole cell lysates and analyzed by Western blot (Figure 11). Levels of YgfB remained unchanged upon induction of DNA damage by addition of ciprofloxacin, while a strong upregulation of the levels of AmpDh3-HiBiT could be observed. Deletion of *ygfB* increased the protein levels of AmpDh3-HiBiT as expected, while concurrent deletion of *ygfB* and addition of ciprofloxacin increased the levels of AmpDh3-HiBiT even further.

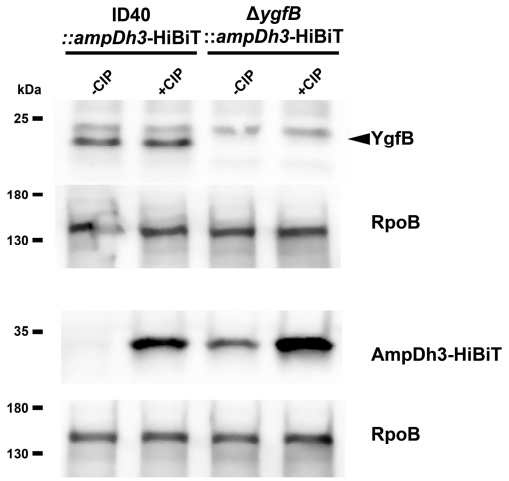

Figure 11: Western blot showing protein levels of AmpDh3-HiBiT and YgfB upon addition of suprainhibitory levels of ciprofloxacin. Cultures of ID40::*ampDh3*-HiBiT and ID40Δ*ygfB*::*ampDh3*-HiBiT were grown to OD_{600} = 0.5. 32 µg/ml (4x MIC) of ciprofloxacin was added to the +CIP condition to induce DNA damage. The cultures were incubated for 2 hours and then harvested for preparation of whole cell lysates and Western blotting. AmpDh3-HiBiT and YgfB were each detected on separate Western blot membranes and thus each have their own loading control (RpoB) shown. Detection of AmpDh3-HiBiT was done using the Nano-Glo HiBiT Blotting System. YgfB and RpoB were detected by α-YgfB and α-RpoB antibodies, HRP-conjugated secondary antibodies and ECL substrate respectively. Blots shown are representative of three individual experiments.

With this data we were able to confirm that the effect of DNA damage on AmpDh3 production described by Peña et al. (2021) could also be observed in the clinical isolate ID40. DNA damage

induced by ciprofloxacin did not seem to affect the levels of YgfB, suggesting DNA damage acting on AmpDh3-levels downstream of YgfB. Concurrent deletion of *ygfB* and induction of DNA damage seemed to have slight additive effects on the levels of AmpDh3-HiBiT, which led us to hypothesize that YgfB might modulate the AmpDh3-inducing effects of DNA damage.

3.1.2.2. Effect of ciprofloxacin and *ygfB* on AlpA and AlpR production

As Peña et al. (2021) described the effect of DNA damage on *alpBCDE* and *ampDh3* expression to be due to antitermination by AlpA, we investigated whether there was an interconnection between the regulation of *ampDh3* by YgfB and by AlpA or AlpR. For this purpose, the strains ID40::HA-*alpR*::*alpA*-HiBiT and ID40Δ*ygfB*::HA-*alpR*::*alpA*-HiBiT were created by homologous recombination. This allowed us to track the levels of HA-AlpR and AlpA-HiBiT by Western blotting. 32 µg/ml ciprofloxacin (4x MIC) were added to cultures of the respective strains to induce DNA damage. This should lead to autocleavage of AlpR and production of AlpA as described previously (McFarland et al., 2015; Peña et al., 2021). Figure 12a depicts a representative Western blot, showing again no effect of DNA damage on the levels of YgfB. HA-AlpR levels were reduced in the +CIP conditions, confirming that AlpR is cleaved upon induction of DNA damage in ID40. HA-AlpR levels were, however, not affected by the deletion of YgfB. Additionally, AlpA-HiBiT levels were increased upon induction of DNA damage by ciprofloxacin as described previously. Similarly, AlpA-HiBiT levels were also increased upon deletion of *ygfB*, however, the effect was smaller to that observed upon the addition of CIP. Interestingly, concurrent *ygfB* deletion and addition of CIP did not increase the levels of AlpA-HiBiT further in comparison to either single treatment condition. As the changes in AlpA-HiBiT levels were rather small, which made them hard to detect on a Western blot, we additionally quantified the AlpA-HiBiT levels using a split-luciferase assay. This allowed us to track also subtle changes in protein levels with higher confidence. The results of this experiment are shown in Figure 12b. Again, we observed a similar effect on the levels of AlpA-HiBiT, namely that CIP treatment and *ygfB* deletion both increased the levels of AlpA-HiBiT, while a combination of both conditions did not have an additive effect on AlpA-HiBiT levels. These data have been published in been published in Eggers et al. (2023).

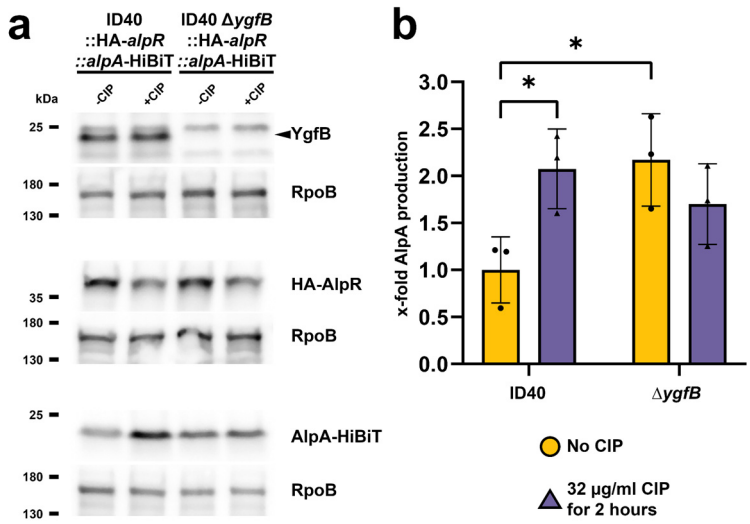

Figure 12: Western blot and split-luciferase assay showing YgfB, AlpR and AlpA levels in ID40 upon deletion of *ygfB* and addition of suprainhibitory levels of ciprofloxacin. a) *"Whole cell lysates of the indicated strains were used for Western blot analyses. +CIP conditions were treated with 32 µg/ml of ciprofloxacin for 2 h. The detection of YgfB, AlpR and AlpA was done on separate Western blots, each with RpoB as a loading control. As primary antibodies, anti-HA, anti-YgfB or anti-RpoB antibodies and as secondary antibody anti-IgG-HRP antibodies were used and detection was done using ECL. For detection of AlpA-HiBiT, recombinant LgBiT was used. LgBiT binds to HiBiT resulting in a functional luciferase. The cleavage of the substrate furimazine leads to detectable chemiluminescence. Data are representative of three independent experiments"* (Eggers et al., 2023, p. 11). **b)** The strains ID40::HA-*alpR*::*alpA*-HiBiT and ID40Δ*ygfB*::HA-*alpR*::*alpA*-HiBiT were treated as in **(a)**. *"Quantification of AlpA by measuring luciferase activity of AlpA-HiBiT in lysed cell extracts. Conditions not treated with CIP depicted as yellow circle, conditions with added CIP depicted as purple up-pointing triangle"* (Eggers et al., 2023, p. 11). The data shows mean and *SD* of x-fold luciferase activity relative to ID40 -CIP. Significant differences calculated by two-way ANOVA with Dunnett's multiple comparisons as a post-hoc test comparing all groups to ID40 -CIP as a control group are indicated by asterisks. *0.05. n = 3. The figure has been adapted from Eggers et al. (2023) under CC BY 4.0 (https://creativecommons.org/licenses/by/4.0/).

The fact that AlpR seemed to be only affected by CIP exposure, while AlpA seemed to be modulated by both CIP-induced DNA damage as well as by the presence of *ygfB* suggested that YgfB might predominantly regulate *ampDh3* expression by acting on the levels of AlpA.

3.1.3. YgfB interacts with AlpA to repress *ampDh3*

As YgfB seemed to regulate *ampDh3* expression via AlpA or AlpR, we hypothesized that YgfB interacts with AlpR or AlpA. We figured that an interaction with AlpA is more likely than an interaction with AlpR as deletion of YgfB did not affect the levels of AlpR but increased the levels of AlpA. If YgfB interacted with AlpR and, for example, stabilized it, preventing autocleavage, levels of AlpR should be reduced in the Δ*ygfB* condition and even more so in the Δ*ygfB* +CIP condition. However, as levels of HA-AlpR were unaffected by deletion of *ygfB*, a protein-protein interaction with AlpA downstream of AlpR was more likely.

Another indicator that an interaction of YgfB with AlpA would hypothetically be more likely than with AlpR, is the net charge of the three proteins at pH 7.4. AlpA is positively charged with a theoretical pI of 9.78, while AlpR is negatively charged (theoretical pI = 5.79). As YgfB

is also strongly negatively charged with a theoretical pI of 4.30, an interaction of the negatively charged YgfB with the positively charged AlpA is more likely than with the negatively charged AlpR.

3.1.3.1. GST-pulldown assays

To test the hypothesis that YgfB interacts with AlpA, the strain ID40Δ*ygfB*::HA-*alpR*::*alpA*-HiBiT was generated. This strain allowed us to perform pulldown assays from cell lysates using recombinantly purified GST-YgfB derived from ID40 as well as GST as a control. The tagged proteins (HA-tagged AlpR and HiBiT-tagged AlpA) could then be detected using Western blotting. GST-YgfB had been purified previously by members of our group while GST was purified in this work (2.3.17 in the method section, Figure 33 in the appendix).

Assay establishment

A first experimental setup consisted of cell lysates prepared from overnight cultures of ID40Δ*ygfB*::HA-*alpR*::*alpA*-HiBiT lysed by sonication in pulldown buffer containing 50 mM Tris pH 7.5, 150 mM NaCl, and 2 mM DTT. To improve the lysing conditions, the pulldown buffer was additionally supplemented with Triton X-100, lysozyme, DNase and protease inhibitor. The insoluble proteins and cell debris were removed by centrifugation. GST or GST-YgfB at a concentration of 10 µM were bound to washed magnetic GSH-beads and subsequently washed with pulldown buffer. The cell lysates were then added, incubated with the proteins bound to the beads and again washed with pulldown buffer. To elute the bound proteins from the beads, the beads were boiled in 4x Laemmli buffer.

To test the planned experimental setup, we performed a pilot pulldown assay as described above. The results of this test assay are shown in Figure 13. The assay conditions are described in more detail than typical to further highlight the modifications done during assay optimization.

3. Results

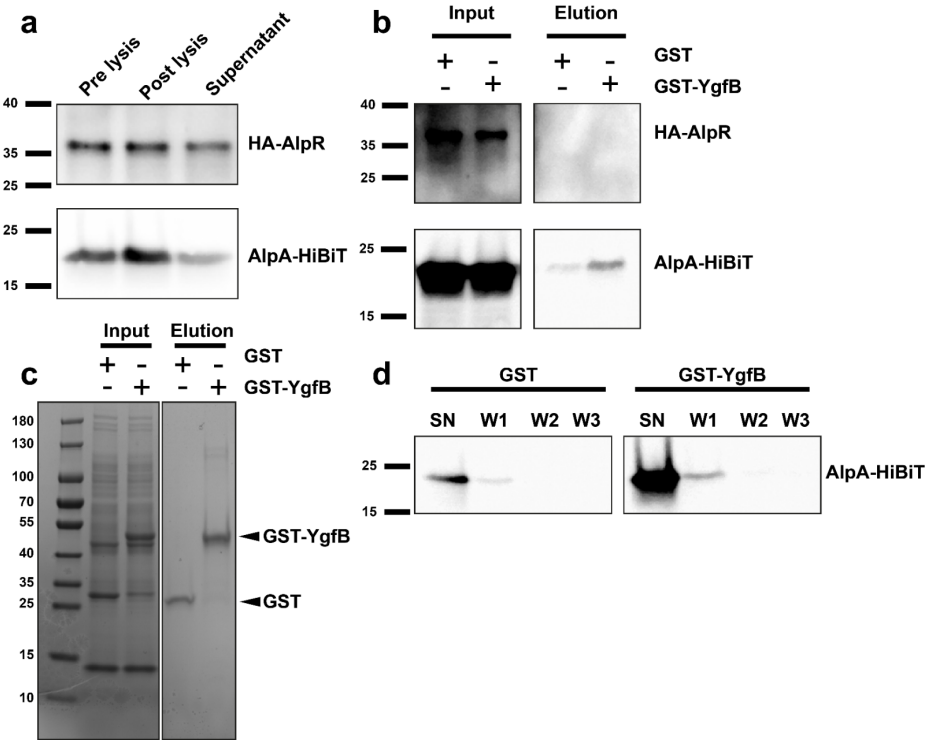

Figure 13: Results of a pilot GST-pulldown assay using GST-YgfB or GST as bait and whole cell lysates of ID40Δ*ygfB* as prey. Lysates of ID40Δ*ygfB*::HA-*alpR*::*alpA*-HiBiT were prepared by sonication in pulldown buffer (50 mM Tris pH 7.5, 150 mM NaCl, 2 mM DTT) supplemented with Triton X-100, DNase, lysozyme, and protease inhibitor. GST or GST-YgfB at a concentration of 10 µM were bound to 50 µl of magnetic beads and washed with pulldown buffer. Cell lysates were added to the proteins bound to the beads and again washed three times with pulldown buffer. To elute the bound proteins, the beads were boiled in 4x Laemmli buffer. To prepare the input samples, 10 µl of bait proteins were mixed with 10 µl of cell lysates and boiled with 20 µl 4x Laemmli buffer. **a)** Western blotting shows that both HA-AlpR and AlpA-HiBiT remain intact during lysis and are soluble in the supernatant fraction (the fraction of soluble protein after removing cell debris by centrifugation) that is added to the beads. **b)** Western blot of the input and elution fraction for HA-AlpR and AlpA-HiBiT shows that AlpA-HiBiT but not HA-AlpR seems to interact with GST-YgfB. The images of the blot were adjusted by changing brightness and saturation in an attempt to get the intensities for HA-AlpR and AlpA-HiBiT as similar as possible without creating too high of a background. **c)** SDS-PAGE and Coomassie stain of the input and elution samples. GST (27.8 kDa) and GST-YgfB (45.9 kDa) have been indicated by arrows. **d)** Western blot analysis of the supernatants and wash fractions after addition of prey proteins. SN: Supernatant of the beads containing all proteins that have not bound to either the beads or the bait proteins. W1-3: Wash fractions after the beads were incubated with prey cell lysates and then washed using pulldown buffer. These fractions contain lightly bound proteins and Western blot analysis shows sufficient washing conditions. **a-d)** Images of gels or blots were trimmed and lanes removed that were not needed to make a sufficient point. This is indicated by boxes around the blots or gels. AlpA-HiBiT and HA-AlpR were always detected on separate blots. Brightness and contrast were always adjusted for the entire gel/blot and trimming was always done after adjustment. AlpA-HiBiT was detected using the Nano-Glo HiBiT Blotting kit, and the HA-tag was detected by primary antibodies directed against HA and HRP conjugated secondary antibodies by ECL.

To screen whether the proteins of interest remained soluble in the supernatant, a Western blot was done using samples taken before the lysis, after the lysis and of the supernatant after centrifugation (Figure 13a). Both HA-AlpR as well as AlpA-HiBiT remained soluble in the supernatant, indicating that in theory a potential interaction between either protein could be detected. Figure 13b shows a Western blot of the input and elution fraction detecting HA-AlpR and AlpA-HiBiT and Figure 13c an SDS-PAGE gel with subsequent Coomassie staining. For the input fraction, 10 µl of whole cell lysates and 10 µl of recombinant bait protein were mixed and

prepared in 4x Laemmli buffer. The elution fraction consisted of the supernatant of the beads boiled in 4x Laemmli buffer. In Figure 13b, no band can be seen for HA-AlpR in the elution fraction for neither the GST, nor the GST-YgfB condition. This suggests no interaction between YgfB and HA-AlpR. When looking at AlpA-HiBiT, a band for AlpA-HiBiT can be detected in the GST and GST-YgfB condition. The AlpA-HiBiT band in the GST-YgfB condition is stronger than in the GST condition, suggesting an interaction between YgfB and AlpA-HiBiT, while there is some background of AlpA-HiBiT binding to either GST or the beads.

As shown in Figure 13c, the interacting proteins could not be detected by Coomassie staining. However, Coomassie staining served as a good control for the purity of the bead-bound proteins. In Figure 13d, the wash conditions were evaluated by Western blot detecting AlpA-HiBiT. The wash conditions seem sufficient, as after three washes no more protein could be detected. Interestingly, the band for AlpA-HiBiT in the supernatant (i.e. the fraction of proteins that have not bound to either of the bait proteins) of the GST-YgfB condition is much more intense than in the GST-condition. This is counterintuitive as one would expect a depletion of AlpA-HiBiT in the supernatant after binding to GST-YgfB.

The pilot pulldown assay indicated that YgfB might interact with AlpA. However, we also observed a band for AlpA-HiBiT in the GST control. This might be due to several causes such as unspecific interactions of AlpA-HiBiT with GST or the magnetic glutathione beads. Because of this, further optimization of the assay conditions was required.

As described above, an interaction of YgfB with AlpR was unlikely, due to the effect of YgfB and ciprofloxacin on the levels of AlpR. As we did not see an interaction between AlpR and YgfB in the pilot pulldown assay either, we did not further investigate a potential interaction between YgfB and AlpR but concluded that AlpA is a more likely interaction partner of YgfB.

YgfB and AlpA interact on a protein-protein level

After a successful pilot assay, we further optimized the conditions for the GST-pulldown assay to reduce background binding of AlpA-HiBiT to GST (data of optimization tests not shown here). We finally continued with assay conditions as described in the Methods section (2.3.20). In short, we prepared day cultures to harvest the cell lysates for the pulldowns instead of using overnight cultures as the ID40Δ*ygfB*::HA-*alpR*::*alpA*-HiBiT produced large amounts of biofilm in overnight cultures, which made handling quite difficult. Additionally, we increased the NaCl concentration to 300 mM to reduce unspecific electrostatic interactions between GST and AlpA-HiBiT and added 0.5% Igepal CA-630 as a non-ionic, non-denaturing detergent to further reduce unspecific interactions. Additionally, instead of eluting the proteins from the beads by boiling them in 4x Laemmli buffer, we used an elution buffer that consisted of pulldown buffer

supplemented with 250 mM reduced glutathione. The purpose of this was to exclude proteins that interacted directly with the beads or precipitated by selectively eluting GST or GST-YgfB and their binding partners by high glutathione conditions.

Figure 14a shows results from pulldown assays with the established assay conditions using GST and GST-YgfB as bait and cell lysates of ID40Δ*ygfB*::HA-*alpR*::*alpA*-HiBiT as prey. A clear band for AlpA-HiBiT in the GST-YgfB condition can be observed in the elution fraction, while no background band is present in the GST condition. The bands for AlpA-HiBiT in the elution fraction runs slightly higher when compared to the input fraction. This is most likely due to a change in buffer condition in the elution fraction when compared to the input fraction. Figure 14b shows an SDS-PAGE gel stained with Coomassie where the pulldown fractions as well as just GST-YgfB itself has been loaded on the gel. We also observed a slightly different migration of the GST-YgfB protein alone when not mixed with the lysates. This provided further hints that the difference in migration is due to different buffer systems.

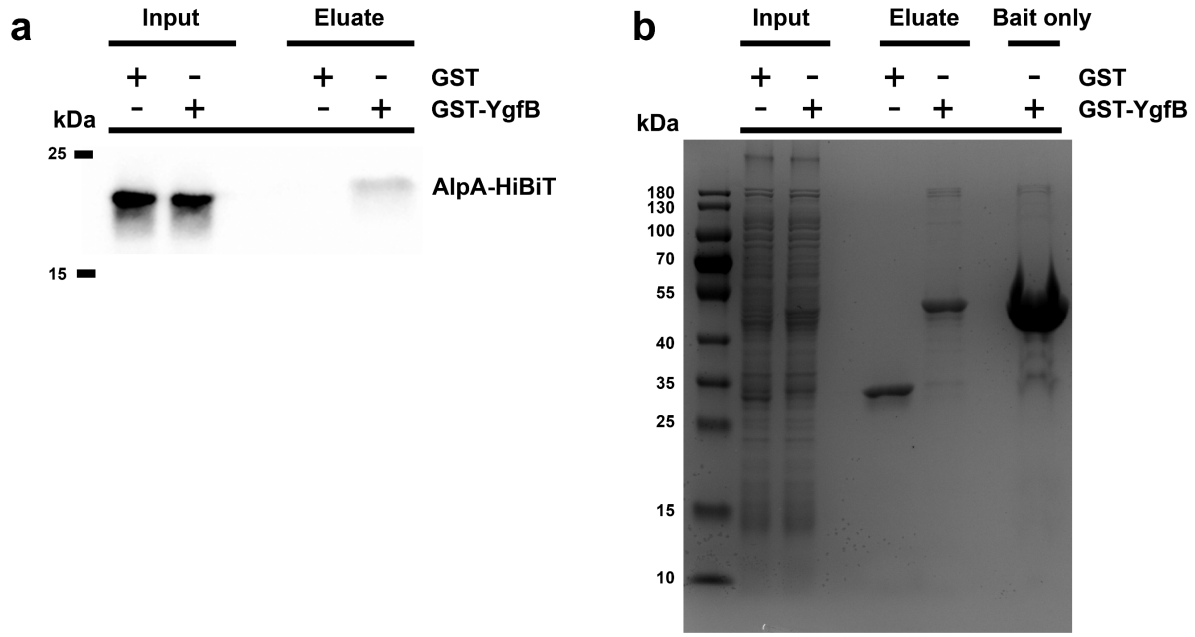

Figure 14: GST-pulldown assay with GST or GST-YgfB as bait and cell lysates of ID40Δ*ygfB*::HA-*alpR*::*alpA*-HiBiT as prey. Lysates of ID40Δ*ygfB*::HA-*alpR*::*alpA*-HiBiT were prepared by sonication in pull-down buffer (50 mM Tris pH 7.5, 300 mM NaCl, 0.5% Igepal, 2 mM DTT) supplemented with protease inhibitor, Triton X-100, DNase, and lysozyme after growth in 500 ml of day culture for 5 hours. After removal of the cell debris by centrifugation, the supernatant was used as prey for the pulldown. GST or GST-YgfB (10 µM) were coupled to 100 µl of magnetic glutathione beads, washed and incubated with the prey lysates. After further washing, the glutathione coupled proteins were eluted from the beads by resuspending in pulldown buffer containing 250 mM reduced glutathione. The elution fractions were then prepared for SDS-PAGE and Western blotting using 4x Laemmli buffer. For the input samples, 10 µl of bait and 10 µl of prey protein were mixed and prepared in 4x Laemmli buffer. **a)** Western blot analysis of the input and elution fraction detecting AlpA-HiBiT using the Nano-Glo Blotting System. The Western blot is representative of five experiments. The figure has been adapted from Eggers et al. (2023) under CC BY 4.0 (https://creativecommons.org/licenses/by/4.0/). **b)** SDS-PAGE analysis with Coomassie staining of the input and elution fraction. GST-YgfB was loaded to control for buffer effects in the migratory behavior of the protein.

The pulldown assay provided evidence that AlpA-HiBiT and GST-YgfB interact at the protein-protein level. This data has been published in Eggers et al. (2023). The fact that no band corresponding to AlpA-HiBiT could be observed in the GST condition, indicates that the interaction seen between GST-YgfB and AlpA-HiBiT is most likely due to an interaction between the YgfB part of the fusion protein. While unlikely, it cannot be ruled out that the interaction might be due to the HiBiT-tag carried by AlpA interacting with YgfB. However, the pulldown experiment cannot distinguish, whether the interaction between YgfB and AlpA is direct or mediated by a second, or even third binding partner as part of a larger protein complex. For this purpose, pulldowns using recombinantly purified proteins were needed.

3.1.3.2. His-pulldowns using purified proteins show a direct interaction between His-MBP-AlpA and YgfB

To further validate the previously seen interaction between YgfB and AlpA (3.1.3.1), we performed His-pulldowns using recombinantly expressed and purified His-MBP or His-MBP-AlpA as bait and recombinant purified YgfB as prey (method section 2.3.16 and 2.3.18, appendix Figure 32 and Figure 34). In these experiments, either His-MBP or His-MBP-AlpA were coupled to magnetic Ni^{2+}-NTA beads and YgfB was added as prey.

This allowed to further exclude potential confounders in the GST-pulldowns, such as an unspecific interaction of AlpA-HiBiT with the beads or a potential interaction between GST-YgfB and the HiBiT-tag itself that was carried by AlpA. Most importantly, however, the assay allowed to gain insights into whether the interaction between YgfB and AlpA was direct, or if there was a third or even more potential bridging factors that facilitated a protein-protein interaction as part of a larger complex. As these potential factors are present in cell lysates that were used in the GST-pulldown assay but should not be present when both interactors were expressed recombinantly and purified, an interaction seen in this assay should provide evidence for a direct protein-protein interaction. In addition, reversing the bait and prey proteins would further underline the strength of the evidence for an interaction

Figure 15 shows a Western blot that was done with the input and eluate fractions of the recombinant His-pulldown. This data has been published in Eggers et al. (2023).

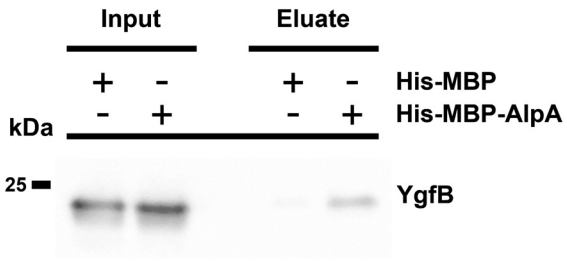

Figure 15: Recombinant His-pulldowns using His-MBP or His-MBP-AlpA as bait and YgfB as prey. 1 ml of recombinant His-MBP or His-MBP-AlpA at a concentration of 10 µM was coupled to magnetic Ni^{2+}-NTA beads and washed with pulldown buffer. 1 ml of recombinant YgfB at a concentration of 10 µM was added to the beads and incubated. After further washing steps, the Ni^{2+}-NTA bound His-tagged proteins were eluted with a high imidazole buffer and samples for Western blotting were prepared. The input samples were prepared by mixing 10 µl of bait and prey protein each and preparing samples in 4x Laemmli buffer. YgfB was detected by a α-YgfB antibody and an HRP-conjugated secondary antibody using ECL. The figure has been adapted from Eggers et al. (2023) under CC BY 4.0 (https://creativecommons.org/licenses/by/4.0/).

In the His-MBP condition, a very light band can be observed for YgfB. The much more intense band corresponding to YgfB in the His-MBP-AlpA condition, however, points to a clear enrichment of YgfB.

In summary, the pulldown assay using recombinantly expressed and purified proteins provided further evidence for an interaction between YgfB and AlpA. The GST-pulldown assay could be reproduced with the bait and prey proteins reversed and using a different method for capturing the bait protein. Furthermore, the usage of only two recombinant proteins provided evidence for a direct interaction between YgfB and AlpA

The next question now was, how the interaction between YgfB and AlpA affected the regulation of the *ampDh3* promoter and therefore the composition of muropeptides, AmpC levels and finally the resistance to β-lactam antibiotics.

3.1.3.3. Electrophoretic mobility shift assays

We hypothesized that YgfB interacts with AlpA and that this interaction might inhibit the capacity of AlpA to bind to the *ampDh3* promoter. This would explain why in the *ygfB* deletion strain of ID40, levels of AmpDh3 are increased, as more AlpA would be able to bind to the AlpA binding element of the *ampDh3* promoter and facilitate antitermination, resulting in increased expression of *ampDh3*.

To test this hypothesis, electrophoretic mobility shift assays (EMSA) were done. EMSAs allow to study interactions of proteins with DNA by tracking the migration of labeled DNA (the probe) by gel-electrophoresis. DNA that has no protein bound migrates faster than DNA that is bound by a protein, as this larger complex is less mobile. This leads to a band shift of the labeled DNA when an interacting protein is added to the DNA.

3. Results

We used this method to study the binding of His-MBP-AlpA to a fragment of the *ampDh3* promoter that contained the ABE, the site of the *ampDh3* promoter where AlpA has been described to bind (Peña et al., 2021) and where both AlpA and YgfB have been shown to regulate the expression of *ampDh3*. More precisely, 5'-IRDye 700 labeled double stranded DNA fragments that contained the ABE, the -35 and -10 elements, as well as the transcription start site (TSS), were used as probes. These fluorescent probes could be detected using the LI-COR Imaging System in the 700 nm near-infrared channel. Adding YgfB to the reaction mix could provide evidence that the interaction of AlpA and YgfB reduces the capacity of AlpA to bind to the ABE.

Figure 16 shows a representative EMSA where 1.25 µM His-MBP or His-MBP-AlpA were added to 0.3125 nM of IRDye 700-labeled DNA-probe containing the part of the *ampDh3* promoter described above. As a control, an IRDye 700-labeled probe was used, where the DNA sequence of the probe containing the ABE was scrambled, i.e. bases were randomly switched. YgfB or bovine serum albumin (BSA) were added to His-MBP-AlpA at final concentrations of 5 µM or 12.5 µM to investigate if an interaction between AlpA and YgfB could abrogate the shift seen for His-MBP-AlpA and if this effect was specific for YgfB or could also be abrogated by other proteins. The binding reactions were loaded on a 4% polyacrylamide gel containing TBE as a buffer system. In addition, the gels contained 30% triethyleneglycol to stabilize protein-DNA interactions (Sidorova et al., 2010). After resolving the reactions on the gel, the IRDye 700-labeled probes were imaged using the LI-COR system. This data has been published in Eggers et al. (2023).

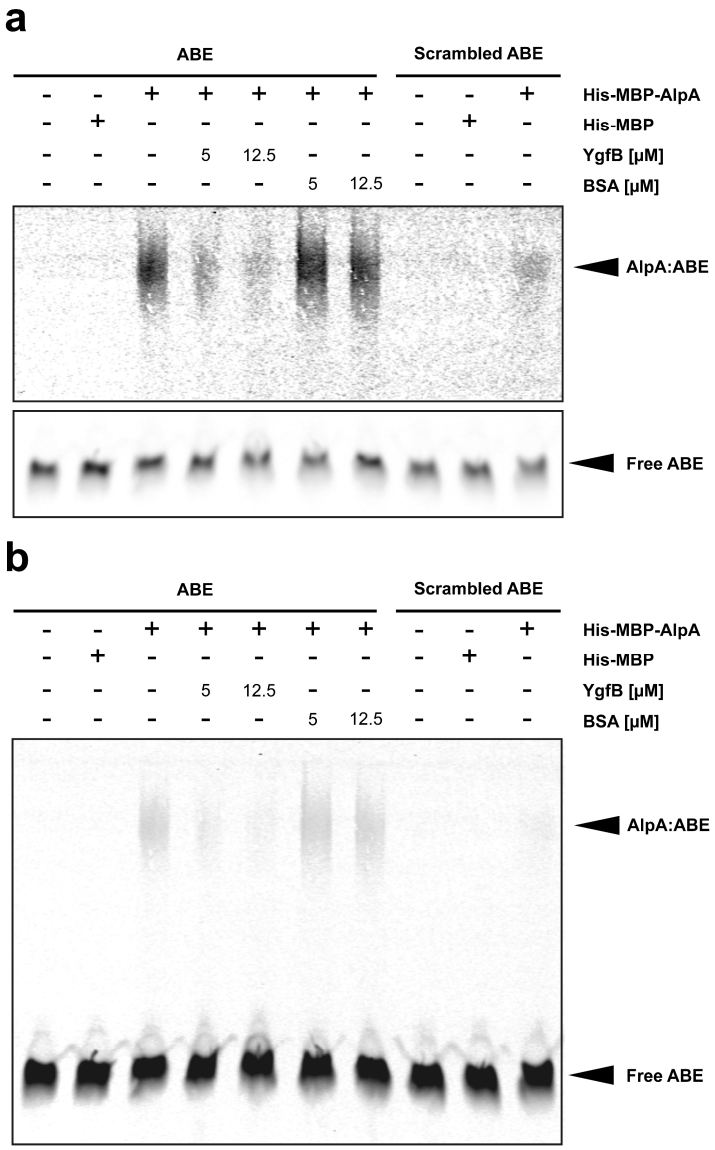

Figure 16: Electrophoretic mobility shift assays show that YgfB interferes with AlpA binding to the AlpA binding element of the *ampDh3* promoter. IRDye 700-labeled DNA probe or scrambled IRDye 700-labeled DNA-probe was incubated at room temperature with 1.25 µM of His-MBP or His-MBP-AlpA. As a control, a reaction mix was prepared where no protein was added to the DNA-probes. In addition, YgfB or BSA at final concentrations of 5 µM or 12.5 µM was added to the binding mix. The binding reactions were loaded on a 4% polyacrylamide gel with TBE as a buffering system and electrophoresis was carried out at 4°C. After electrophoresis, the labeled DNA-probes were imaged using the LI-COR Odyssey imaging system. Free ABE denotes free probe containing the AlpA binding element, while AlpA:ABE denotes the shift in migration of the DNA-probe due to an interaction between AlpA and the DNA-probe. The figure is representative of five individual experiments. **a)** To increase the dynamic range and improve the interpretability of the EMSA, the free labeled probe and band shifts by protein-DNA-interactions were recorded separately. **b)** The entire gel was imaged to record free and shifted DNA-probe simultaneously. The figure has been reproduced unchanged from Eggers et al. (2023) under CC BY 4.0 (https://creativecommons.org/licenses/by/4.0/).

As seen by the band shift in the His-MBP-AlpA condition, His-MBP-AlpA but not His-MBP binds to the stretch of the *ampDh3* promoter that was used as a probe, here labeled as ABE as it contains the AlpA-binding element. When the probe was scrambled, a slight background

binding of His-MBP-AlpA to the scrambled probe could be observed, pointing to some unspecific protein-DNA interactions. This could confirm the findings of Peña et al. (2021) that AlpA interacts with the *ampDh3* promoter. When YgfB was added to the binding reaction, the intensity of the shift seen for His-MBP-AlpA was reduced to the levels of the unspecific DNA-interaction between His-MBP-AlpA and the scrambled probe, while this was not the case when BSA was added in equal concentrations. The band shift observed in the EMSA experiments, when His-MBP-AlpA was added to the IRDye 700-labeled DNA probe, was always rather weak but highly reproducible, pointing to a transient or weak interaction between AlpA and the DNA. This could be due to the nature of the interaction itself or due to the size of the His-MBP-AlpA fusion protein. Attempts to purify AlpA without any tags, however, were unsuccessful. As the pETM41 expression vector also contains a cleavage site for the protease derived from the *tobacco etch virus* (TEV protease) (Parks et al., 1994) between the His-MBP-tag and the protein of interest downstream of His-MBP (AlpA in this case), we attempted to cleave off the His-MBP tag by digesting the protein using the TEV protease (2.3.13). However, several different buffer conditions and downstream purification methods to separate His-MBP and the TEV protease from -AlpA such as reverse Ni^{2+}-NTA affinity chromatography (2.3.8) or size exclusion chromatography (2.3.11) did not yield any soluble -AlpA protein but rather, aggregated protein.

3.1.4. The effect of *ygfB* on β-lactam resistance applies to other MDR *P. aeruginosa* strains

"To investigate whether the prominent role of YgfB in β-lactam resistance holds true also for other MDR P. aeruginosa strains, ygfB was deleted in the clinical blood stream infection isolates ID143 and ID72 as well as in the more sensitive strains PAO1 and PA14. As depicted in Table 23*, β-lactam resistance was also decreased in the investigated P. aeruginosa strains, indicating that the presence of YgfB seems to be of general importance to achieve higher resistance of P. aeruginosa to β-lactam antibiotics"* (Eggers et al., 2023, p. 11).

Table 23: Effect of *ygfB* deletion in other *P. aeruginosa* strains. ID143 and ID72 are MDR clinical isolates, PAO1 and PA14 are susceptible lab strains. MIC values are given as µg/ml, classification is according to EUCAST. Values written in bold indicate a reduction in MIC compared to the wildtype. Green cells indicate that the strain is classified as susceptible or susceptible at an increased dosage according to EUCAST, while red cells indicate that the strain is resistant according to EUCAST. Some MIC values lie in between the window between resistance and susceptibility. Such values classify the corresponding strain as susceptible at an increased dosage. For *P. aeruginosa*, some antibiotics do not have a classification of susceptibility, but strains are always classified as susceptible at an increased dosage. For these antibiotics, the breakpoint for susceptibility has been replaced by the placeholder value 0.001 µg/ml. MEM: meropenem, IPM: imipenem, FEP: cefepime, CAZ: ceftazidime, PIP: piperacillin, TZP: piperacillin + tazobactam, AZT: aztreonam, CIP: ciprofloxacin

	Carbapenems		**Cephalosporins**		**Penicillins**		**Mono-bactams**	**Fluoro-quinolones**
	MEM	**IPM**	**FEP**	**CAZ**	**PIP**	**TZP**	**AZT**	**CIP**
MIC S≤	**2**	**0.001**	**0.001**	**0.001**	**0.001**	**0.001**	**0.001**	**0.001**
MIC R>	**8**	**4**	**8**	**8**	**16**	**16**	**16**	**0.5**
ID143 WT	32	32	16	32	>128	>128	>32	>4
ID143Δ*ygfB*	**2-4**	**2**	**8**	**<2-2**	**<16**	**8**	**4**	>4
ID72 WT	16	32	32	>32	>128	>128	32	<0.125
ID72Δ*ygfB*	**2**	**4**	**2**	**4**	**<16**	**<8**	**8**	0.125
PAO1	<0.5!	8	2	<1-2	<16	<4	4	<0.125
PAO1Δ*ygfB*	<0.5!	**<1**	2	<1-2	<16	<4	**2**	<0.125
PA14 WT	<0.5!	<1	<1	2	<4	nd	4-8	<0.125
PA14Δ*ygfB*	<0.5!	<1	<1	2	<4	nd	**4**	<0.125

A comparison of the typical *ampC*-overexpression associated genes *dacB*, *ampD,* and *ampR* of ID72 and ID143 with those of PAO1, revealed that ID72 carries five point mutations in *ampD* and ID143 carries a 15-bp deletion in the *ampD* gene. While the *dacB* gene of ID143 is intact, ID72 carries two point mutations in the *dacB* gene. ID143 carries three point mutations in the *ampR* genes while *ampR* of ID72 was the same as PAO1.

The effect of *ygfB* deletion seemed especially pronounced in the MDR strains ID72 and ID143, where deletion of *ygfB* was able to break resistance towards all tested β-lactam antibiotics. This is in contrast to ID40, where deletion of *ygfB* reduced resistance, but not below the resistance breakpoint (Eggers et al., 2023; Sonnabend et al., 2020). With the exception of the MIC of imipenem in PAO1, the effect of *ygfB* deletion in the susceptible strains PA14 and PAO1 seemed to be less pronounced, however, as the MIC values were close to the limit of detection of the MIC assay plates used, conclusions on whether the effect of *ygfB* is smaller in more susceptible strains and more pronounced in resistant strains could not be made.

To further generalize the previously observed effect of *ygfB* deletion on *ampDh3,* we tested the influence of *ygfB* deletion on the promoter activity of *ampDh3* in the strains used in the MIC assay and ID40 (Figure 17a). For this purpose, the strains were transformed with the plasmid pBBR1-532-luc as a reporter. On this plasmid, the promoter of the *ampDh3* gene is fused to the luciferase NanoLuc. When the promoter is active, NanoLuc is expressed and in presence of the

substrate furimazine, chemiluminescence is generated that can be quantified using a plate reader. In addition to the effect of *ygfB* deletion in each strain, the basal levels of *ampDh3* promoter activity are shown in Figure 17b.

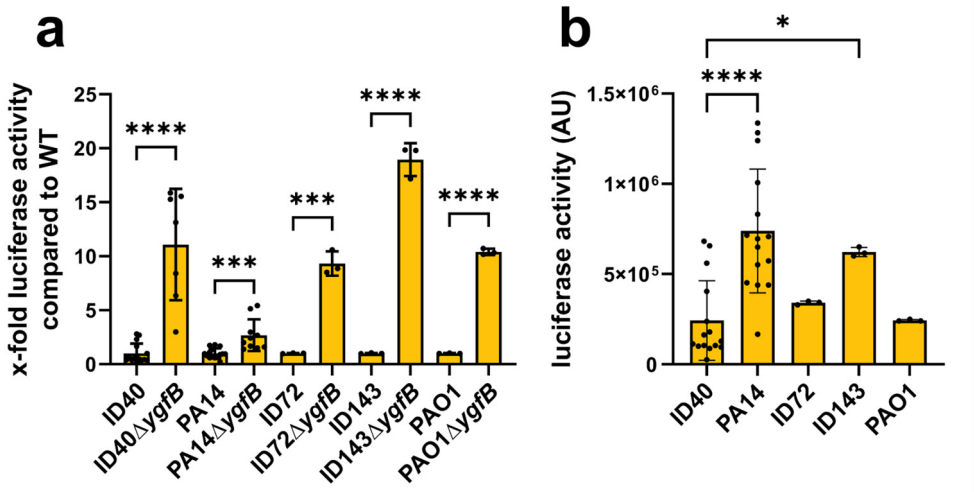

Figure 17: Deletion of *ygfB* leads to increased *ampDh3* promoter activity in other *P. aeruginosa* strains. a and b) *"ampDh3 promoter activity was determined as described in the materials and methods for the indicated strains using the plasmid pBBR harboring the reporter construct ampDh3-532-luc comprising the ampDh3 promoter fragment between position -532 and -1 upstream of the CDS of Nanoluc. Data depict mean and SD"* (Eggers et al., 2023, Figure legend Supplementary Fig. 7). **a)** *"Luciferase activity of ygfB deletion strains relative to the "wildtype" is shown using data from n=3-15 individual experiments. Asterisks indicate significant differences compared to the "wildtype" strain (*p<0.05, **p<0.1 ***p<0.001, ****p<0.0001; two-tailed Welch's t-test)"* (Eggers et al., 2023, Figure legend Supplementary Fig. 7). **b)** *"Basal promoter activity is shown for the indicated strains using data from n=3-15 individual experiments. Asterisks indicate significant differences compared to ID40 (*p<0.05, ****p<0.0001; one-way ANOVA, Dunnett's multiple comparisons comparing to ID40)"* (Eggers et al., 2023, Figure legend Supplementary Fig. 7). The figure has been reproduced unchanged from Eggers et al. (2023) under CC BY 4.0 (https://creativecommons.org/licenses/by/4.0/).

In all tested strains, deletion of *ygfB* increased the activity of the *ampDh3* promoter. Basal levels of *ampDh3* promoter activity did not seem to be predictive of the resistance to β-lactam antibiotics, as the susceptible strain PAO1 and the resistant strain ID40 have similar basal promoter activity, while in the susceptible strain PA14 the promoter activity for *ampDh3* was much higher compared to ID40. The resistant strain ID143, however, had a higher basal activity of the *ampDh3* promoter when compared to ID40. The data shown in this section have been published in Eggers et al. (2023).

3.2. Influence of YgfB on β-lactam/ciprofloxacin combinations

As shown previously, deletion of *ygfB* and the resulting upregulation of *ampDh3* expression led to reduced resistance to β-lactam antibiotics in ID40 and other MDR *P. aeruginosa* strains. As ciprofloxacin also had the effect of increasing the levels of AmpDh3, we wondered if this might be a potential pathway by which the fluoroquinolone ciprofloxacin and β-lactam antibiotics had synergistic effects. In addition, since YgfB inhibits activity of AlpA on the *ampDh3*

promoter, we were interested to find out how the presence of YgfB affected a combination of ciprofloxacin and β-lactam antibiotics.

3.2.1. Achievable serum levels of ciprofloxacin break resistance to β-lactam antibiotics in ID40

To test if ciprofloxacin influenced the resistance towards β-lactam antibiotics in ID40, we planned to expose ID40 to subinhibitory levels of ciprofloxacin and to determine the levels of AmpDh3 as well as the MIC towards different antipseudomonal β-lactam antibiotics. In a first step, we needed to determine an appropriate concentration of ciprofloxacin to use for these experiments.

3.2.1.1. Pharmacokinetic considerations to mimic serum levels achievable in high dose ciprofloxacin regimens

To study the combinatory effect of ciprofloxacin and β-lactam antibiotics, we wanted to expose ID40 to levels of ciprofloxacin that could theoretically be reached in the serum of patients but would still be subinhibitory. ID40 is resistant to β-lactam antibiotics (MIC: 8 µg/ml, cutoff according to EUCAST: 0.5 µg/ml (The European Committee on Antimicrobial Susceptibility Testing, 2024)), and deletion of *ygfB* itself does not affect resistance towards ciprofloxacin in ID40 (Sonnabend et al., 2020). To determine an appropriate concentration to be used for the experiments, common dosing regimens as well as published pharmacokinetic data were considered.

The document "Dosages (v 14.0)" by EUCAST that is part of the clinical breakpoint tables v 14.0 (The European Committee on Antimicrobial Susceptibility Testing, 2024), as well as the professional information for "Ciprobay® 400 mg, 400 mg/200 ml, Infusionslösung", a ciprofloxacin infusion of 400 mg per infusion (Bayer Vital GmbH, 2023), define an increased dosage for ciprofloxacin as 400 mg of intravenously administered ciprofloxacin three times daily (400 mg q8h i.v.). Bioequivalent to this is the oral administration of 750 mg of ciprofloxacin twice every 12 hours, i.e. twice daily. For infections with *P. aeruginosa*, increased dosages of ciprofloxacin are recommended, which reflects itself in the EUCAST breakpoints for ciprofloxacin that generally report all *P. aeruginosa* MICs as susceptible at an increased dosage but never as susceptible (The European Committee on Antimicrobial Susceptibility Testing, 2024). Pharmacokinetic data on ciprofloxacin administered intravenously as well as orally have been published in the FDA approved prescribing information for "CIPRO® IV (ciprofloxacin) injection, for intravenous use" by Bayer Healthcare (Bayer HealthCare Pharmaceuticals Inc., 2022). While the intravenous CIPRO® product by Bayer has been discontinued from marketing, the

prescribing information still provides insights into the pharmacokinetics and the same information is also contained in the prescribing information of CIPRO® for oral use (Bayer HealthCare Pharmaceuticals Inc., 2021). The prescribing information gives steady-state state pharmacokinetic parameters for the area under the concentration-time curve of the serum concentration of ciprofloxacin over 24 hours in steady-state ($AUC_{(0\text{-}24h),ss}$) in [(µg*h)/ml] as well as maximal serum concentrations in steady-state $C_{max,ss}$ in [µg/ml]. $AUC_{(0\text{-}24h),ss}$ for ciprofloxacin administered at 400 mg i.v. q8h is 32.9 (µg*h)/ml and $C_{max,ss}$ is 4.07 µg/ml.

Next to official documents by the marketing authorization holders, several studies have reported on the pharmacokinetics of ciprofloxacin administered in the high dose intravenous regimen (400 mg i.v. q8h).

For example, Lipman et al. (1998) reported pharmacokinetic data of 16 patients without any renal dysfunction that suffered from severe sepsis. Patients were treated with intravenous ciprofloxacin 400 mg q8h for infections with multiple bacterial species. Levels of ciprofloxacin were measured by HPLC in plasma samples drawn at day 0, day 2, and between day 6 and day 8 for steady-state parameters. In steady-state, the mean AUC over 8 hours ($AUC_{0\text{-}8h,ss}$) was 15.5 ± 4.7 (µg*h)/ml and the $C_{max,ss}$ value was 6.45 ± 1.54 µg/ml. When multiplying the $AUC_{0\text{-}8h,ss}$ value with 3, we obtained the AUC_{ss} over 24 hours, which would be $AUC_{0\text{-}24h,ss}$ = 46.5 (µg*h)/ml.

Shah et al. (1995) reported a mean plasma $AUC_{0\text{-}8h,ss}$ value of 14.6 (µg*h)/ml and a plasma $C_{max,ss}$ value of 5.85 µg/ml in 12 younger female and male patients aged 18 to 40 years. In 12 elderly female and male patients (>65 years), they reported mean values of $AUC_{0\text{-}8h,ss}$ = 19.0 (µg*h)/ml and $C_{max,ss}$ = 6.83 µg/ml. Multiplying the area under the curve for 8 hours with 3 to get to the AUC for 24 hours results in $AUC_{0\text{-}24h,ss}$ = 43.8 (µg*h)/ml for young patients and an $AUC_{0\text{-}24h,ss}$ = 57 (µg*h)/ml in elderly patients.

In another study by Shah et al. (1994), mean serum $AUC_{0\text{-}24h,ss}$ values of 32.9 ± 8.83 (µg*h)/ml were determined. These are the same as the data published by Bayer in the prescribing information, potentially due to the prescribing information being informed by this study.

In Table 1 of their publication, Schlender et al. (2018) have provided an overview of the literature regarding pharmacokinetic properties of ciprofloxacin for different dosages as well as different regimens. As expected, pharmacokinetic properties of ciprofloxacin are highly variable depending on the patient collective.

To study the effect of subinhibitory concentrations of ciprofloxacin on the resistance to β-lactams in ID40, we wanted to use a concentration that was relatively high to see the largest effect

while still being physiologically relevant. As serum levels of drugs have peak and through levels due to the levels rising during infusion and then being excreted after, which leads to decreasing concentrations, the levels are never constant. As this cannot, or only with much effort be mimicked in our experiments, we had to settle for a constant concentration to use as a compromise. This constant concentration should ideally have the same area under the curve as that which could be therapeutically reached over 24 hours.

To approximate an achievable $AUC_{0\text{-}24h,ss}$ in a constant concentration of ciprofloxacin, we settled for an exposure of the bacteria to 2.5 µg/ml of ciprofloxacin over 18 hours. 18 hours as an exposure duration was chosen as this is the minimum time prescribed for incubation of the Sensititre MIC plates used for determination of the MICs towards antipseudomonal β-lactam antibiotics. This allowed to increase the actual concentration of ciprofloxacin while still keeping the AUC constant. As shown in Equation 5, this constant concentration given over 18 hours corresponds to an $AUC_{0\text{-}24h,ss}$ of 45 (µg*h)/ml that can be obtained in some patients as described above.

Equation 5: Exposing bacteria to 2.5 µg/ml of ciprofloxacin over 18 hours results in the same AUC of ciprofloxacin as that obtained in 24 hours in the serum of some patients treated with the 400 mg i.v. q8h high dose regimen of ciprofloxacin. $AUC_{0\text{-}24h,ss}$: Area under the concentration-time curve of ciprofloxacin in 24 hours in steady-state in serum. c_{test}: Concentration of ciprofloxacin used for further experiments.

$$AUC_{0-24h,ss} = 45\,\frac{\mu g * h}{ml}$$

$$c_{test} = \frac{AUC_{0-24h,ss}}{exposure\ time} = \frac{45\,\frac{\mu g * h}{ml}}{18\,h} = 2.5\,\frac{\mu g}{ml}$$

Forrest et al. (1993) have shown that the main relevant parameter predicting successful treatment of bacterial infections with ciprofloxacin was the ratio of the AUC in serum/plasma over 24 hours and the MIC of the bacterium ($AUC_{0\text{-}24h}$/MIC, AUIC). If this ratio was >125 SIT^{-1} * h (inverse serum inhibitory titer integrated over time), significantly better outcomes could be observed for the parameters likelihood of clinical cure, likelihood of microbiological cure, and time to bacterial eradication. This classified the AUIC as a critical breakpoint in treatment of ciprofloxacin. They suggested an AUIC <125 SIT^{-1} * h to be representing inadequate antimicrobial activity, AUIC of 125 to 250 SIT^{-1} * h to be acceptable, and an AUIC of 250 to 500 SIT^{-1} * h to be optimal.

As ID40 has a MIC of 8 µg/ml for ciprofloxacin and the $AUC_{0\text{-}24h}$ in our subsequent experiments was 45 (µg*h)/ml, the AUIC would be 5.625 SIT^{-1} * h. Obviously, this is well below the breakpoint of >125 SIT^{-1} * h, which in this case was actually desired, as we wanted to study the effect of subinhibitory ciprofloxacin exposure on the resistance towards β-lactam antibiotics.

This is obviously only a very rough approximation of the processes that take place in actual patients, as concentrations of antibiotics are never constant and concentrations at the site of infection differ from those in serum/plasma. However, in order to mechanistically study the effects of subinhibitory ciprofloxacin on the resistance of ID40 to β-lactam antibiotics, this approximation was enough to continue with the experiments.

3.2.1.2. Subinhibitory levels of ciprofloxacin and deletion of YgfB have an additive effect on AmpDh3 production

First, we wanted to study the effect of subinhibitory ciprofloxacin over a longer period of time on AmpDh3 production. We were interested to investigate if in these conditions, AmpDh3 production would be increased by ciprofloxacin and also if the DNA damage induced by ciprofloxacin together with a *ygfB*-deletion had additive effects on the levels of AmpDh3. The strains ID40::*ampDh3*-HiBiT and ID40Δ*ygfB*::*ampDh3*-HiBiT were grown overnight in LB medium. The next day, inocula of the strains were prepared the same as for MIC assays, i.e. by adjusting to a McFarland of 0.5 in 0.9% NaCl solution. 25 µl of the inoculum were added to 6 ml of LB medium, ciprofloxacin was added to the +CIP conditions in a final concentration of 2.5 µg/ml and the cultures were grown with shaking for 18 hours. The next day, whole cell lysates were prepared and the production of AmpDh3-HiBiT and YgfB was determined by Western blot. Figure 18 shows a representative Western blot of three individual experiments. These data have been published in Eggers et al. (2023).

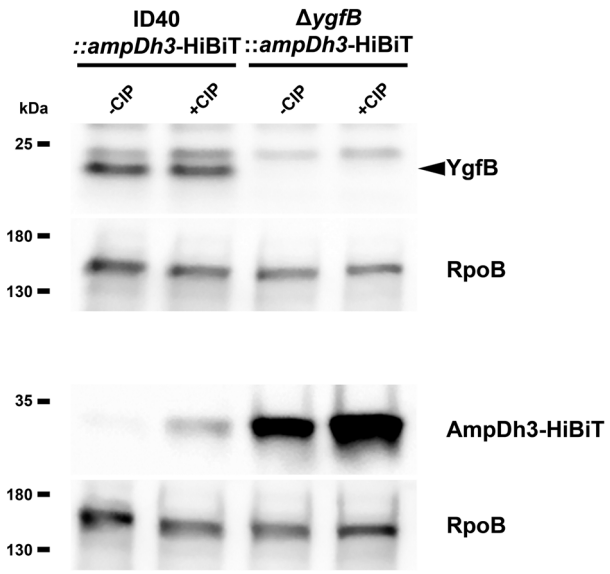

Figure 18: Subinhibitory levels of ciprofloxacin lead to increased AmpDh3 abundance. To monitor the effect of subinhibitory levels of ciprofloxacin over a longer period of time, overnight cultures of ID40::*ampDh3*-HiBiT and ID40Δ*ygfB*::*ampDh3*-HiBiT were adjusted to a McFarland standard of 0.5 in 0.9% NaCl solution. 25 µl were added to 6 ml of LB medium together or not with 2.5 µg/ml of ciprofloxacin (+CIP or –CIP, respectively). The cultures were incubated with shaking for 18 hours and the next day harvested for preparation of whole lysates and Western blotting. AmpDh3-HiBiT and YgfB were each detected on separate Western blot membranes and thus each have their own loading control (RpoB) shown. Detection of AmpDh3-HiBiT was done using the Nano-Glo HiBiT Blotting System. YgfB and RpoB were detected by α-YgfB and α-RpoB antibodies, HRP-conjugated secondary antibodies and ECL substrate respectively. Blots shown are representative of three individual experiments. The figure has been adapted from Eggers et al. (2023) under CC BY 4.0 (https://creativecommons.org/licenses/by/4.0/).

As previously seen for suprainhibitory concentrations of ciprofloxacin in 3.1.2.1, also subinhibitory ciprofloxacin concentrations induce the production of AmpDh3-HiBiT in ID40 wildtype and ID40Δ*ygfB*. The increase in production of AmpDh3-HiBiT in the wildtype +CIP condition is less than when comparing the increase in ID40Δ*ygfB*. Concurrent deletion of *ygfB* and treatment with subinhibitory ciprofloxacin resulted in a strong increase of AmpDh3-HiBiT production. This should theoretically also be associated with a stronger reduction in β-lactam resistance.

3.2.1.3. Minimum inhibitory concentrations of β-lactams are reduced when ID40 is exposed to physiologically achievable concentrations of ciprofloxacin

To test if the ciprofloxacin-induced DNA damage that led to increased production of AmpDh3 was associated with a reduced resistance to β-lactam antibiotics, the MIC of several different mutants towards different antipseudomonal β-lactam antibiotics was determined as described in 2.2.5 using Sensititre EUX2NF and GN2F MIC plates. In the +CIP condition, ciprofloxacin was added to a final concentration of 2.5 µg/ml to the MHB II broth. After 18 hours of incubation at 37°C, the MICs were determined.

3. Results

Table 24 lists the MIC towards antipseudomonal β-lactams and ciprofloxacin for the strains ID40 wildtype, ID40Δ*ygfB*, ID40Δ*ampDh3,* and ID40Δ*alpA,* as well as the double deletion mutants ID40Δ*ygfB*Δ*ampDh3* and ID40Δ*ygfB*Δ*alpA* with and without 2.5 µg/ml ciprofloxacin in the medium.

Table 24: MIC assay of ID40 strains with and without 2.5 µg/ml ciprofloxacin. MICs of the indicated antibiotics for the indicated strains were either determined in the presence (+CIP) or absence (-CIP) of 2.5 µg/ml of ciprofloxacin in the medium. MIC values are given as µg/ml, classification is according to EUCAST. Values written in bold indicate a reduction in MIC compared to the wildtype without ciprofloxacin. Green cells indicate that the strain is classified as susceptible or susceptible at an increased dosage according to EUCAST, while red cells indicate that the strain is resistant according to EUCAST. Some MIC values lie in between the window between resistance and susceptibility. Such values classify the corresponding strain as susceptible at an increased dosage. For *P. aeruginosa*, some antibiotics do not have a classification of susceptibility, but strains are always classified as susceptible at an increased dosage. For these antibiotics, the breakpoint for susceptibility has been replaced by the placeholder value 0.001 µg/ml. MICs were measured after 18 h of incubation at 37°C. MEM: meropenem, IPM: imipenem, FEP: cefepime, CAZ: ceftazidime, PIP: piperacillin, TZP: piperacillin + tazobactam, AZT: aztreonam, CIP: ciprofloxacin

		Carbapenems		**Cephalosporins**		**Penicillins**		**Mono-bactams**	**Fluoro-quin-olones**
		MEM	**IPM**	**FEP**	**CAZ**	**PIP**	**TZP**	**AZT**	**CIP**
MIC S≤		**2**	**0.001**	**0.001**	**0.001**	**0.001**	**0.001**	**0.001**	**0.001**
MIC R>		**8**	**4**	**8**	**8**	**16**	**16**	**16**	**0.5**
ID40 WT	-CIP	8-16	64	32	>32	128	128	>32	>4
ID40Δ*ampDh3*	-CIP	**8**	64	32	>32	128	>128	>32	>4
ID40Δ*alpA*	-CIP	**8**	64	32	>32	**64**	>128	**32**	>4
ID40 WT	+CIP	**2**	**32**	**4**	**8**	**32**	**32**	**4**	**4**
ID40Δ*ampDh3*	+CIP	**2**	**32**	**8**	**16**	**32**	**16**	**8**	**2**
ID40Δ*alpA*	+CIP	**2**	**32**	**<1**	**8**	**32**	**16-32**	**4**	**2**
ID40Δ*ygfB*	-CIP	**4**	**16**	**16**	**32**	**64**	**32-64**	**16**	>4
ID40Δ*ygfB*Δ*ampDh3*	-CIP	**8**	64	32	>32	**>128**	128	**32**	>4
ID40Δ*ygfB*Δ*alpA*	-CIP	**8**	**32**	**16**	>32	**>128**	128	**32**	>4
ID40Δ*ygfB*	+CIP	**1-2**	**4**	**4**	**4-8**	**<16**	**<4**	**2**	**4**
ID40Δ*ygfB*Δ*ampDh3*	+CIP	**2-4**	**32**	**4**	**8-16**	**64**	**16-32**	**4**	**4**
ID40Δ*ygfB*Δ*alpA*	+CIP	**1-2**	**32**	**<1**	**8**	**32**	**16-32**	**4**	**2**

The single gene deletions of either *ampDh3* or *alpA* did not have a marked effect on the resistance to any of the tested antibiotics. For some antibiotics and combinations, the resistance was reduced 2-fold, which might be an effect but could also be well within the noise of the assay leading to fluctuations.

When exposing ID40 wildtype or the Δ*ampDh3,* or Δ*alpA* mutants to 2.5 µg/ml of ciprofloxacin, the resistance towards all of the tested antibiotics was reduced 2-fold to 64-fold for all tested β-lactams. The resistance towards meropenem, cefepime, ceftazidime, and aztreonam could even be broken by combination with 2.5 µg/ml ciprofloxacin. Concurrent deletion of *ampDh3* was able to increase resistance for cefepime, ceftazidime and aztreonam. This effect

was again not large (2-fold increase) and could again be well within random fluctuations of the assay. Deletion of *alpA* did not have the same effect as *ampDh3*, however, and in one condition, the MIC in the Δ*alpA* strain was even reduced to below 1 µg/ml.

The ID40Δ*ygfB* deletion mutant displayed reduced resistance against all tested antipseudomonal β-lactam antibiotics as expected. Concurrent deletion of either *ampDh3* or *alpA* reverted the resistance phenotype seen for the *ygfB* deletion mutant back to the wildtype, or almost back to the wildtype for some conditions. This further emphasized the importance of *alpA* and *ampDh3* in the *ygfB*-mediated resistance to β-lactam antibiotics.

If *ygfB* was deleted and the strains were exposed to subinhibitory levels of ciprofloxacin however, resistance to all tested β-lactam antibiotics was broken. Concurrent deletion of *ampDh3* or *alpA* increased the resistance to β-lactam antibiotics in most conditions back to the levels of ID40 wildtype exposed to ciprofloxacin. However, in the absence of ciprofloxacin, the double deletion was not able to restore the resistance to the levels of ID40 wildtype. Interestingly, again the deletion of *ampDh3* had a more general effect in reverting the Δ*ygfB* phenotype, while deletion of *alpA* was able to increase resistance only for some antibiotics. This suggests that *alpA* might not be the only factor regulating for the expression of *ampDh3* as its deletion does not phenocopy the *ampDh3* deletion.

Together, these data suggest that presence of YgfB might inhibit additive effects of β-lactam antibiotics and ciprofloxacin. In the deletion mutant of *ygfB*, the combination of β-lactam antibiotics and ciprofloxacin had a much larger effect, which seemed partly mediated by AlpA-induced AmpDh3 production. However, this effect does not seem to be monocausal for the combined action of the antibiotics, but other factors might also play a role.

3.2.2. Checkerboard assays give further insights in the additive effects of ciprofloxacin and β-lactam antibiotics

Performing MIC assays in combination with a constant dose of ciprofloxacin provided a one-dimensional view of the interplay of β-lactam antibiotics and ciprofloxacin in the various mutants. To gain better insights into how the antibiotics interact in combination, checkerboard assays were done. Essentially, this is a two-dimensional MIC assay, where two antibiotics are combined in different concentrations. One antibiotic is added in $\log_2$-fold dilutions along the abscissa of a 96-well plate and the other one in $\log_2$-fold dilutions against the ordinate of a 96-well plate. As one row or column always contains only the $\log_2$-fold dilutions series of one antibiotic without any second antibiotics added, this assay also allows to determine the MIC for each antibiotic tested individually, as well as the inhibitory effect of the antibiotic combination

at specific concentrations. The methods of the checkerboard assay, as well as the calculation of the FIC index as measure for synergism, additive effects, or antagonism, are explained in detail in the methods section under heading 2.2.6 on page 56. The classification of synergism according to the FIC index was done as follows: FIC index ≤ 0.5: synergism, FIC index between > 0.5 and ≤ 1: additive effect, FIC index between > 1 and ≤ 4: indifferent effect, and FIC index > 4: antagonism.

Table 25, Table 26, Table 27, and Table 28 plot the results of checkerboard assays using ceftazidime (CAZ), piperacillin (PIP), imipenem (IPM), and aztreonam (AZT), each in combination with ciprofloxacin. These β-lactam antibiotics were chosen, as each of them represents a different subclass of β-lactam antibiotics, i.e. ceftazidime is a cephalosporin, piperacillin a penicillin, imipenem a carbapenem, and aztreonam a monobactam.

The effect of these combinations was tested for the ID40 wildtype as well as in the deletion strains ID40Δ*ygfB*, ID40Δ*ampDh3*, ID40Δ*ygfB*Δ*ampDh3,* ID40Δ*alpA,* and ID40Δ*ygfB*Δ*alpA*. Additionally, the effect of the antibiotic combinations was tested in the conditional, rhamnose-inducible deletion mutants ID40Δ*ygfB*::rha-*ygfB*, ID40Δ*ampDh3*::rha-*ampDh3,* and ID40Δ*alpA*::rha-*alpA*.

For each antibiotic combination, the MIC for one antibiotic alone and in combination with the second one is plotted. The MIC of the first antibiotic in combination is always plotted with the second one at a concentration at the resistance breakpoint as well as a concentration one $\log_2$ step above the breakpoint according to EUCAST. (The European Committee on Antimicrobial Susceptibility Testing, 2024). Additionally, the values in combination with 2 µg/ml of CIP are shown to allow comparison with the results of 3.2.1.3 where 2.5 µg/ml of CIP were combined with the β-lactam antibiotics. In addition, the combination that had the largest combined effect is shown, i.e. the combination of antibiotics in which each concentration had the highest relative difference to the MIC of a single antibiotic. This in essence minimizes the FIC value of each antibiotic, and therefore also the FIC index. From this largest effect, in addition the FIC index was calculated and is also shown. MIC values that are written in bold show a decrease in MIC in respect to the wildtype. Cells of the table with a red background indicate that the particular MIC in that cell is above the defined resistance breakpoint. Cells with a green background indicate that the MIC is below the resistance breakpoint. The checkerboard assay data have been published in Eggers et al. (2023).

Table 25: Results of checkerboard assays combining ceftazidime and ciprofloxacin. The effect of the antibiotic combination was tested in the indicated strains of ID40. In the +0.1% rha conditions, 0.1% rhamnose has been added to the medium to induce production of the complemented gene. MIC values are given in µg/ml, values written in bold indicate a decrease of the MIC value compared to ID40 wildtype. Cells colored red: resistant. Cells colored green: susceptible or susceptible at an increased dosage. Resistance breakpoints according to EUCAST for ceftazidime: resistant >8 µg/ml, susceptible at an increased dosage ≤8 µg/ml. Resistance breakpoints according to EUCAST for ciprofloxacin: resistant >0.5 µg/ml, susceptible at an increased dosage ≤0.5 µg/ml. FIC index ≤ 0.5: synergism, FIC index between > 0.5 and ≤ 1: additive effect, FIC index between > 1 and ≤ 4: indifferent effect, and FIC index > 4: antagonism.

Strain	0.1% rha	MIC ceftazidime [µg/ml]				MIC ciprofloxacin [µg/ml]			MIC of largest combined effect		
		Alone	+0.5 µg/ml CIP	+1 µg/ml CIP	+2 µg/ml CIP	Alone	+8 µg/ml CAZ	+16 µg/ml CAZ	CAZ [µg/ml]	CIP [µg/ml]	FIC index
ID40	-	128	128	64	32	8	4	4	32	2	0.5
ID40Δ*ygfB*	-	**32**	**32**	**16**	**8**	8	**2**	**1**	**8**	2	0.5
ID40Δ*ampDh3*	-	**64**	**64**	64	**16**	8	4	**2**	**16**	2	0.5
ID40Δ*ygfB*Δ*ampDh3*	-	128	128	64	32	8	4	4	32	2	0.5
ID40Δ*alpA*	-	128	128	64	**16**	8	4	**2**	**16**	2	0.375
ID40Δ*ygfB*Δ*alpA*	-	128	128	64	**16**	8	4	**2**	**16**	2	0.375
ID40Δ*ygfB*::rha-*ygfB*	-	**32**	**32**	**16**	**8**	8	**2**	**1**	**8**	2	0.5
	+	128	**64**	64	32	8	4	4	32	2	0.5
ID40Δ*ampDh3*::rha-*ampDh3*	-	**64**	**64**	64	32	8	4	4	**8**	4	0.625
	+	**32**	**32**	**32**	32	8	4	4	**0.5**	4	0.516
ID40Δ*alpA*::rha-*alpA*	-	128	128	128	32	8	4	4	32	2	0.5
	+	**64**	**32**	**32**	**16**	8	4	**2**	**16**	2	0.5

3. Results

Table 25 shows the results of the checkerboard assay for the combination of ceftazidime and ciprofloxacin. Deletion of *ygfB* alone reduced the MIC for ceftazidime alone 4-fold. Concurrent deletion of *ygfB* and either *ampDh3* or *alpA* was able to restore the susceptibility phenotype back to the wildtype level. The same effect was observed with 0.5 µg/ml and 1 µg/ml of ciprofloxacin (CIP) in combination with ceftazidime (CAZ). Deletion of *ygfB* did not affect resistance to ciprofloxacin alone. However, when combined with 8 µg/ml ceftazidime, resistance to ciprofloxacin was reduced by 2-fold, and with 16 µg/ml, it was reduced by 4-fold. Concurrent deletion of *alpA* or *ampDh3* partially rescued this phenotype. When having one antibiotic of the combination fixed at the resistance breakpoint or one step above, resistance in the second antibiotic could not be broken. However, in the combination with 2 µg/ml of CIP in ID40Δ*ygfB*, the resistance for CAZ could be broken, which was also the largest combined effect. FIC indices indicated that the combination of ceftazidime and ciprofloxacin was synergistic in ID40, but only barely so (Synergism: FIC index ≤ 0.5). The deletion of genes did not affect the FIC index, except for *alpA*, where it was reduced to 0.375. The effect of the combination with 2 µg/ml CIP was lower than in the previous experiment where the effect of 2.5 µg/ml of CIP was tested. Here, 2.5 µg/ml of CIP was enough to reduce the MIC of ID40 wildtype towards CAZ to 8 µg/ml, breaking resistance, while in the checkerboard assay resistance could only be broken with 2 µg/ml of CIP when *ygfB* was deleted. The conditional deletion mutants without added rhamnose showed similar behavior as the in-frame deletion counterparts. In the *ygfB* complementant strain, the resistance phenotype was restored to the wildtype upon addition of *ygfB*, while the *ampDh3* and *alpA* conditional deletion mutants showed a more susceptible phenotype upon addition of rhamnose.

Table 26: Results of checkerboard assays combining piperacillin and ciprofloxacin. The effect of the antibiotic combination was tested in the indicated strains of ID40. In the +0.1% rha conditions, 0.1% rhamnose has been added to the medium to induce production of the complemented gene. MIC values are given in µg/ml, values written in bold indicate a decrease of the MIC value compared to ID40 wildtype. Cells colored red: resistant. Cells colored green: susceptible or susceptible at an increased dosage. Resistance breakpoints according to EUCAST for piperacillin: resistant >16 µg/ml, susceptible at an increased dosage ≤16 µg/ml. Resistance breakpoints according to EUCAST for ciprofloxacin: resistant >0.5 µg/ml, susceptible at an increased dosage ≤0.5 µg/ml. FIC index ≤ 0.5: synergism, FIC index between > 0.5 and ≤ 1: additive effect, FIC index between > 1 and ≤ 4: indifferent effect, and FIC index > 4: antagonism.

Strain	0.1% rha	MIC piperacillin [µg/ml]				MIC ciprofloxacin [µg/ml]			MIC of largest combined effect		
		Alone	+0.5 µg/ml CIP	+1 µg/ml CIP	+2 µg/ml CIP	Alone	+16 µg/ml PIP	+32 µg/ml PIP	PIP [µg/ml]	CIP [µg/ml]	FIC index
ID40	-	256	256	256	64	4	4	4	64	2	0.75
ID40Δ*ygfB*	-	**128**	**64**	**32**	**8**	4	**2**	**1**	**32**	**1**	0.5
ID40Δ*ampDh3*	-	256	256	**128**	64	4	4	4	64	2	0.75
ID40Δ*ygfB*Δ*ampDh3*	-	256	256	**128**	64	4	4	4	64	2	0.75
ID40Δ*alpA*	-	512	256	256	**32**	8	4	**2**	**32**	2	0.312
ID40Δ*ygfB*Δ*alpA*	-	512	256	**128**	64	8	4	4	64	2	0.312
ID40Δ*ygfB*::rha-*ygfB*	-	**64**	**64**	**64**	**8**	4	**2**	**2**	**8**	2	0.625
	+	256	256	256	64	4	4	4	64	2	0.75
ID40Δ*ampDh3*::rha-*ampDh3*	-	256	256	**128**	64	4	4	4	64	2	0.75
	+	**64**	**64**	**64**	**32**	4	4	**2**	**32**	2	1
ID40Δ*alpA*::rha-*alpA*	-	512	512	256	64	4	4	4	64	2	0.75
	+	**128**	**64**	**32**	**16**	8	**2**	**1**	**32**	1	0.375

Table 26 shows the results of the piperacillin (PIP)/ciprofloxacin combination. Deletion of *ygfB* reduced resistance to piperacillin alone by 2-fold compared to the wildtype and combination with 0.5 µg/ml or 1 µg/ml of ciprofloxacin reduced the resistance in the Δ*ygfB* mutant 4-fold or 8-fold respectively, while not breaking resistance. In combination with 2 µg/ml of CIP, resistance to PIP could be broken in the ID40Δ*ygfB* strain. The effect of Δ*ygfB* could again be rescued by concurrent deletion of *ampDh3* or *alpA*. Looking at the MICs for ciprofloxacin, resistance to ciprofloxacin alone was not affected by deletion, except for *alpA*, where resistance was increased. However, the values for the MIC of ciprofloxacin varied between 4 µg/ml and 8 µg/ml in these assays. Thus, the increase of the CIP MIC was likely due to variation. In combination with 16 or 32 µg/ml PIP, the MIC for ciprofloxacin was not affected in the wildtype, while deletion of *ygfB* reduced the MIC values in combination 2- and 4-fold. As before, the concurrent deletion of *alpA* or *ampDh3* reverted the phenotype to the wildtype levels. Looking at the largest combined effect, deletion of *ygfB* reduced the combination from 64 µg/ml piperacillin together with 2 µg/ml of ciprofloxacin to 32 µg/ml of piperacillin together with 1 µg/ml of ciprofloxacin. Concurrent deletion of either *alpA* or *ampDh3* was able to abrogate the effect of *ygfB* deletion. The FIC index was reduced from 0.75 to 0.5 (from additive to synergistic) upon deletion of *ygfB* in the wildtype. In a Δ*ampDh3* or Δ*alpA* background, deletion of *ygfB* did not alter the FIC index. Overall, the results of the checkerboard assay were similar to the results of the MIC assay with 2.5 µg/ml CIP, in which a break of resistance for PIP was only possible in the *ygfB* deletion mutant in combination with 2.5 µg/ml of CIP. In the conditional deletion mutants in the absence of rhamnose, the resistance phenotype was similar to the respective deletion mutants. Expression of *ygfB* by addition of rhamnose restored the phenotype back to the wildtype, while complementation of *ampDh3* and *alpA* reduced resistance.

Table 27: Results of checkerboard assays combining imipenem and ciprofloxacin. The effect of the antibiotic combination was tested in the indicated strains of ID40. In the +0.1% rha conditions, 0.1% rhamnose has been added to the medium to induce production of the complemented gene. MIC values are given in µg/ml, values written in bold indicate a decrease of the MIC value compared to ID40 wildtype. Cells colored red: resistant. Cells colored green: susceptible or susceptible at an increased dosage. Resistance breakpoints according to EUCAST for imipenem: resistant >4 µg/ml, susceptible at an increased dosage ≤4 µg/ml. Resistance breakpoints according to EUCAST for ciprofloxacin: resistant >0.5 µg/ml, susceptible at an increased dosage ≤0.5 µg/ml. FIC index ≤ 0.5: synergism, FIC index between > 0.5 and ≤ 1: additive effect, FIC index between > 1 and ≤ 4: indifferent effect, and FIC index > 4: antagonism.

Strain	0.1% rha	MIC imipenem [µg/ml]				MIC ciprofloxacin [µg/ml]			MIC of largest combined effect		
		Alone	+0.5 µg/ml CIP	+1 µg/ml CIP	+2 µg/ml CIP	Alone	+4 µg/ml IPM	+8 µg/ml IPM	IPM [µg/ml]	CIP [µg/ml]	FIC index
ID40	-	64	64	64	32	8	8	8	16	4	0.75
ID40Δ*ygfB*	-	**16**	**16**	**16**	**8**	8	**4**	**2**	**1!**	4	0.56
ID40Δ*ampDh3*	-	64	64	**32**	32	**4**	**4**	**4**	32	**1**	0.75
ID40Δ*ygfB*Δ*ampDh3*	-	64	64	64	32	8	8	8	16	4	0.75
ID40Δ*alpA*	-	64	64	64	32	8	8	**4**	**8**	4	0.625
ID40Δ*ygfB*Δ*alpA*	-	64	64	64	32	8	8	**4**	**8**	4	0.625
ID40Δ*ygfB*::rha-*ygfB*	-	**32**	**32**	**16**	**16**	8	**4**	**4**	**4**	4	0.625
	+	64	64	64	32	8	8	8	16	4	0.75
ID40Δ*ampDh3*::rha-*ampDh3*	-	64	64	64	32	8	8	8	16	4	0.75
	+	**32**	**32**	**32**	**16**	8	**4**	**4**	**1**	4	0.531
ID40Δ*alpA*::rha-*alpA*	-	64	64	64	32	8	8	8	16	4	0.75
	+	**32**	**32**	**32**	32	8	**4**	**4**	**1**	4	0.531

For imipenem (IPM) and ciprofloxacin (Table 27), a similar pattern to that seen for CAZ and PIP was observed for both single and combined antibiotics. Deletion of *ygfB* reduced resistance to both IPM alone and in combination with CIP. Concurrent deletion of either *ampDh3* or *alpA* rescued the *ygfB*-mediated phenotype. In this combination, resistance to IPM could only be broken in the Δ*ygfB* strain when combined with 4 µg/ml of CIP, unlike before, where 2 µg/ml of CIP was enough to break resistance. This suggests a higher baseline level of resistance of ID40 towards imipenem. For the combination, deletion of *ygfB* in the wildtype background reduced the FIC index from 0.75 to 0.5625. In a Δ*ampDh3* or Δ*alpA* background, deletion of *ygfB* again did not alter the FIC index. When combined with 2.5 µg/ml of CIP, resistance to IPM was broken in the ID40Δ*ygfB* strain, suggesting that the concentration of CIP needed to break resistance to IPM may lie between 2 and 2.5 µg/ml of CIP. As before, the conditional deletion mutants in the absence of rhamnose behaved similarly to the single deletion mutant counterparts, with addition of rhamnose rescuing the *ygfB* phenotype and increasing susceptibility in the *ampDh3* and *alpA* complementant strain.

Table 28: Results of checkerboard assays combining aztreonam and ciprofloxacin. The effect of the antibiotic combination was tested in the indicated strains of ID40. In the +0.1% rha conditions, 0.1% rhamnose has been added to the medium to induce production of the complemented gene. MIC values are given in µg/ml, values written in bold indicate a decrease of the MIC value compared to ID40 wildtype. Cells colored red: resistant. Cells colored green: susceptible or susceptible at an increased dosage. Resistance breakpoints according to EUCAST for aztreonam: resistant >16 µg/ml, susceptible at an increased dosage ≤16 µg/ml. Resistance breakpoints according to EUCAST for ciprofloxacin: resistant >0.5 µg/ml, susceptible at an increased dosage ≤0.5 µg/ml. FIC index ≤ 0.5: synergism, FIC index between > 0.5 and ≤ 1: additive effect, FIC index between > 1 and ≤ 4: indifferent effect, and FIC index > 4: antagonism.

Strain	0.1% rha	MIC aztreonam [µg/ml]				MIC ciprofloxacin [µg/ml]			MIC of largest combined effect		
		Alone	+0.5 µg/ml CIP	+1 µg/ml CIP	+2 µg/ml CIP	Alone	+16 µg/ml AZT	+32 µg/ml AZT	AZT [µg/ml]	CIP [µg/ml]	FIC index
ID40	-	64	64	32	16	8	2	1	16	2	0.5
ID40Δ*ygfB*	-	**16**	**16**	**16**	**4**	8	-	-	**4**	2	0.5
ID40Δ*ampDh3*	-	**32**	**32**	**16**	**8**	8	**1**	**-!**	**8**	2	0.5
ID40Δ*ygfB*Δ*ampDh3*	-	64	**32**	32	**32**	8	4	**0.5**	**2**	4	0.531
ID40Δ*alpA*	-	**32**	**32**	32	**8**	8	2	**0.5**	**8**	2	0.5
ID40Δ*ygfB*Δ*alpA*	-	128	**32**	32	**16**	16	2	**0.5**	16	2	0.25
ID40Δ*ygfB*::rha-*ygfB*	-	**16**	**16**	**8**	**4**	8	-	-	**4**	2	0.5
	+	**32**	**32**	32	16	8	2	**0.5**	16	2	0.75
ID40Δ*ampDh3*::rha-*ampDh3*	-	**32**	**32**	32	16	8	2	-	16	2	0.75
	+	**16**	**16**	**16**	**8**	8	-	-	**0.5**	4	0.531
ID40Δ*alpA*:: rha-*alpA*	-	64	64	32	16	8	2	1	16	2	0.5
	+	**16**	**16**	**16**	**8**	8	-	-	**0.5**	4	0.531

Similar results as before could be observed for the combination of aztreonam and ciprofloxacin (Table 28). However, unlike before, deletion of *ygfB* itself was able to break resistance to aztreonam alone, with the effect being partially rescued by simultaneous deletion of *ampDh3* or *alpA*. The combination with 0.5 µg/ml or 1 µg/ml of ciprofloxacin did not reduce the resistance any further. When looking at ciprofloxacin, deletion of *ygfB* itself did not affect resistance against ciprofloxacin alone. In combination, 16 µg/ml of aztreonam was enough to inhibit growth, and thus no MIC values for ciprofloxacin in combination with 16 µg/ml or 32 µg/ml of aztreonam could be measured. Combination with 2 µg/ml of ciprofloxacin, which also resulted in the largest combined effect for most mutants, was enough to break resistance for all strains. The effect was again potentiated by deletion of *ygfB* and rescued by double deletion of *alpA* or *ampDh3*. The FIC index for the combination was not markedly affected by any gene deletion. The checkerboard assay results were consistent with those of the MIC assay using 2.5 µg/ml of CIP. Complementation experiments showed the same behavior as in the other combinations. The *ygfB* phenotype was rescued upon addition of rhamnose and the susceptibility was increased upon addition of rhamnose to the *ampDh3* or *alpA* complemented strain. The effect of *ygfB* deletion on reduction of resistance seemed to be most pronounced for aztreonam.

"*Measurement of MIC values for ID40, ΔampDh3 or ΔalpA showed that the combination of ciprofloxacin and β-lactam antibiotics reduced MIC values for the tested antibiotics in all three strains compared to single treatment in a similar manner. Deletion of ygfB further decreased the MIC values by two to three log2 steps as compared to ID40 depending on the β-lactam antibiotic used* (Table 25, Table 26, Table 27, Table 28). *This can be explained by the AlpA-induced AmpDh3 production, as additional deletion of either alpA or ampDh3 restored the resistance to β-lactam antibiotics to the levels of ID40 wildtype*" (Eggers et al., 2023, p. 10).
In the ID40 wildtype strain, resistance to either antibiotic could not be broken in combination. When *ygfB* was deleted, resistance to β-lactam antibiotics could only be broken when the antibiotic was combined with ciprofloxacin at a concentration above the resistance breakpoint according to EUCAST (2 µg/ml in this case, 4-fold increase to EUCAST breakpoint). This reflects the results from chapter 3.2.1, in which 2.5 µg/ml of ciprofloxacin was able to break resistance to all tested β-lactams in the ID40Δ*ygfB* strain.
"In the absence of rhamnose, the conditional deletion mutants responded to treatment with various β-lactams, alone or in combination with ciprofloxacin, like the corresponding single deletion mutants as confirmed by comparison of the MIC values. Upon rhamnose supplementation the MIC values of antibiotics measured for the conditional ygfB deletion mutant were

similar to the MIC values for the ID40 wildtype. In contrast, the conditional ampDh3 and alpA deletion mutants showed lower β-lactam resistance upon rhamnose treatment. This indicates, that under these conditions, the effect of YgfB can be overridden" (Eggers et al., 2023, p. 10). Taken together, the checkerboard experiments with the various mutants as well as with the conditional mutants underline the repressing role of *ygfB* in the AlpA-mediated activation of *ampDh3* resulting in resistance to combinations of ciprofloxacin and β-lactams. YgfB seems to inhibit a potential crosstalk between ciprofloxacin and β-lactams by inhibiting the DNA damage-induced effect of AlpA on *ampDh3* expression. However, deletion of *ampDh3* or *alpA* itself did not seem to reduce the combinatory effect of ciprofloxacin and β-lactam antibiotics, suggesting that next to this pathway, there are other factors at play that lead to an additive effect of antibiotic combination.

3.3. Further studies on the role of YgfB and ciprofloxacin in *P. aeruginosa* and *E. coli*

In the previous chapters, the molecular action of YgfB affecting resistance towards β-lactam antibiotics as well as towards a combination of β-lactams and ciprofloxacin in *P. aeruginosa* was described, leading to a working model of the interrelationship between YgfB, AlpA, and AmpDh3 and consequences on resistance to β-lactam antibiotics that will be discussed later.
As shown in the introduction, *ygfB* is present in many γ-proteobacteria while *alpA* is only found in *P. aeruginosa* as confirmed by Nucleotide BLAST and Protein BLAST (Camacho et al., 2009). Searching for orthologs of AmpDh3 in other γ-proteobacteria yielded many results such as AmiD in *E. coli.* However, when directly comparing *E. coli* AmiD with AmpDh2 and AmpDh3 of *P. aeruginosa*, the sequence seemed to have more similarity to AmpDh2 than AmpDh3. Nevertheless, orthologs of AmpDh3 seem to be present in some other γ-proteobacteria. Due to the lack of AlpA and the limited presence of AmpDh3, we speculated that YgfB might have also a more general function in γ-proteobacteria, while the repression of the AlpA-induced *ampDh3* expression might be a unique feature of *P. aeruginosa*.

As we have shown that *ygfB* might modulate the AlpR-AlpA-dependent response to ciprofloxacin in *P. aeruginosa*, we hypothesized that the main regulatory role of *ygfB* only comes into effect under the stimulus of ciprofloxacin-induced DNA damage, explaining why the differentially expressed gene set upon deletion of *ygfB* was rather limited.

We therefore initially asked the following questions:

(i) Does YgfB transcriptionally regulate a distinct gene set in other species such as *E. coli*?

(ii) Is *ygfB* mainly relevant as a transcriptional regulator in a DNA damage-induced state?

3.3.1. The *ygfB*-modulated transcriptomic response to ciprofloxacin

To answer these questions, RNAseq was done with the *P. aeruginosa* strain ID40 and the *E. coli* strain BW25113. For each species, four conditions were tested in triplicate. Triplicate overnight cultures of the wildtype strain and a *ygfB* deletion mutant were grown by preparing two subcultures from each overnight culture in parallel. The subcultures were grown to OD_{600} 0.5 and ciprofloxacin at 4x the MIC was added to the medium of one of the parallel subcultures (+CIP condition). The cultures were incubated for 2 hours with shaking at 37°C, after which RNA was isolated and RNAseq was performed. Differential expression analysis of the different conditions was done to identify genes that respond to the different stimuli.

3.3.1.1. The *ygfB* modulated ciprofloxacin response in *P. aeruginosa* ID40

To study the *ygfB* modulated response to ciprofloxacin in ID40, samples were prepared for RNAseq as described above. 32 µg/ml of ciprofloxacin was added to the medium of the +CIP conditions of ID40 and ID40Δ*ygfB*.

Effect of *ygfB* deletion

We have previously shown the effect of *ygfB* deletion in ID40 using transcriptomics (Eggers et al., 2023). Comparing the ID40Δ*ygfB* and ID40 conditions allowed validation of the previously described transcriptomic analysis. Unexpectedly, the differential expression analysis resulted in a different expression profile in ID40Δ*ygfB* vs. ID40 in this experiment as compared to before (Figure 19). All significantly differentially expressed genes are also listed in Table 34 in the appendix.

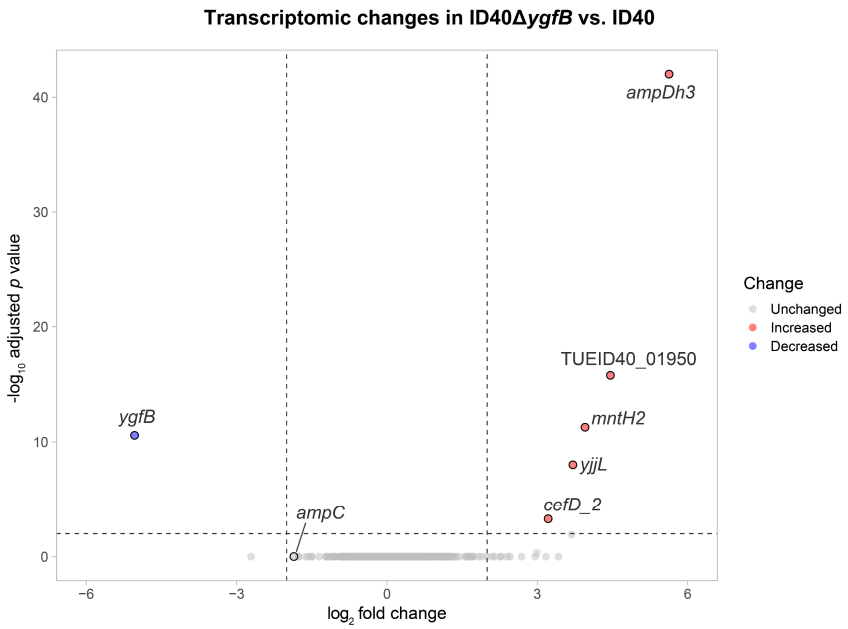

Figure 19: Transcriptome comparing ID40Δ*ygfB* with ID40. Upregulated genes (red): $\log_2$ fold change ≥2, adjusted *p* value ≤0.01; downregulated genes (blue): $\log_2$ fold change ≤-2, adjusted *p* value ≤0.01. Data analysis as described in the methods. *n* = 3. All differentially expressed genes and in addition *ampC* are labeled.

While *ampDh3* was still strongly upregulated upon deletion of *ygfB*, neither the gene in the same operon as *ampDh3*, TUEID40_01954 ($\log_2$ fold change of 2.99, adjusted *p* value of 0.48), nor the *alpBCDE* self-lysis cluster was significantly upregulated ($\log_2$ fold change between 1.25 and 2.15, however, non-significant adjusted *p* values). Similarly, TUEID40_01945 had a non-significant $\log_2$ fold change of 2.27 (*p*adj. = 1). *ampC* had a $\log_2$ fold change of -1.86 with an adjusted *p* value of 1. In contrast to the first differential expression analysis of ID40Δ*ygfB* vs. ID40, next to *ampDh3* now also the genes *cefD_2, yjjl, mntH2,* and TUEID40_01950 were upregulated. Interestingly, these genes lie downstream of *ampDh3* and have been shown to be upregulated upon ectopic overexpression of *alpA* in PAO1 (Peña et al., 2021). This could be explained by reduced inhibition of the action of AlpA upon deletion of *ygfB*.

Response to ciprofloxacin

The differentially expressed genes in the ID40 +CIP vs. the ID40 condition represented the transcriptomic response to DNA damage induced by ciprofloxacin. In total, 160 out of 6544 genes were differentially expressed in ID40 upon exposure to 32 µg/ml CIP for 2 hours, with 157 being upregulated and 3 genes being downregulated. 65 of the differentially expressed genes had orthologs in PAO1, while 84 differentially expressed genes had similarity to genes found in phages infecting *P. aeruginosa*. For two genes, orthologs only in other *P. aeruginosa* strains could be found and for nine genes, no ortholog could be assigned.

The genes were searched in UniProt (The UniProt Consortium, 2023), KEGG (Kanehisa, 2019; Kanehisa et al., 2023; Kanehisa & Goto, 2000), and the BV-BRC database (Olson et al., 2023)

to assign functions. The genes that were differentially expressed upon exposure to 32 µg/ml of ciprofloxacin were mostly the same as previously described by Cirz et al. (2006). Most of the genes were associated with DNA-metabolism and repair (*recA*, *recN*, *imuB, lexA*), DNA-replication (*gyrB*), nucleotide metabolism (*ndrA, ndrB*), pyocin synthesis (*prtN*, *pys2, pys2_2, ptrB* TUEID40_04251), and LexA-controlled genes of the SOS-response (*imuB, sulA2,* TUEID40_00205*, lexA, sulA, yebG, TUEID40_05264, recA, recN*). Additionally, we and Cirz et al. (2006) found *alpA, ampDh3,* and the *alpBCDE* cluster upregulated upon addition of 32 µg/ml ciprofloxacin.

As the focus of this study was not to elucidate the ciprofloxacin response *per se* and the response itself has been thoroughly described, it will not be further discussed here. The significantly differentially expressed genes are listed in Table 35 in the appendix.

The *ygfB* modulated ciprofloxacin response in ID40

To identify genes that were part of the *ygfB* modulated CIP response, the conditions ID40Δ*ygfB* + CIP and ID40 +CIP were compared. This comparison would allow to identify genes that are only regulated by *ygfB* in response to DNA damage. A volcano plot of differentially expressed genes in the comparison with an adjusted *p* value of ≤0.01 and a $\log_2$ fold change of ≥2 or ≤-2 is shown in Figure 20. In addition, all significantly differentially expressed genes with the respective $\log_2$ fold changes and adjusted *p* values are listed in Table 36 in the appendix.

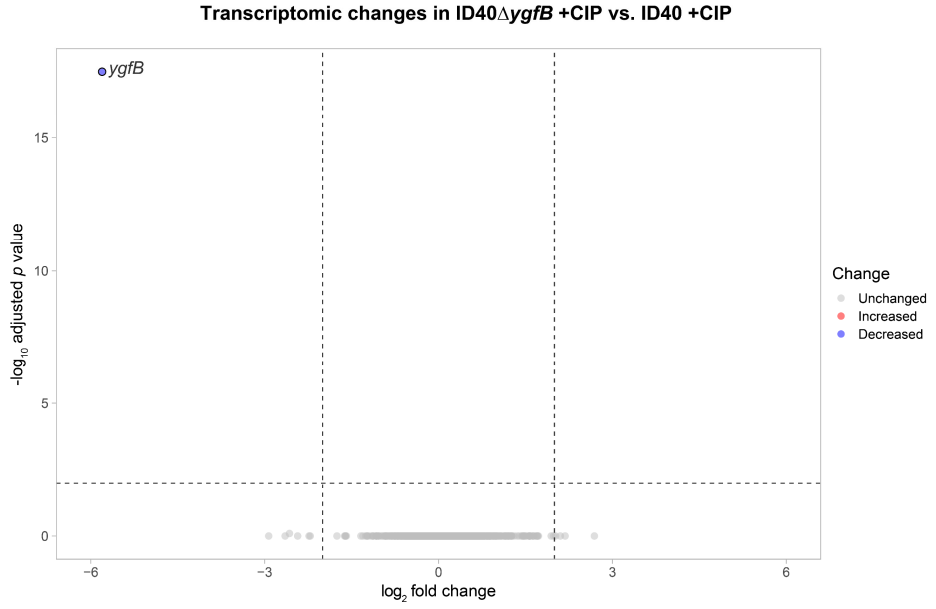

Figure 20: Differentially expressed genes in the comparison ID40Δ*ygfB* +CIP vs. ID40 +CIP. The conditions ID40Δ*ygfB* +CIP and ID40 +CIP were compared. In the +CIP condition, 32 µg/ml of ciprofloxacin was added for 2 hours. Upregulated genes (red): $\log_2$ fold change ≥2, adjusted *p* value ≤0.01; downregulated genes (blue): $\log_2$ fold change ≤-2, adjusted *p* value ≤0.01. Data analysis as described in the methods. *n* = 3.

Except *ygfB*, no genes were differentially expressed in the comparison. Interestingly, also genes that were shown to be differentially expressed by *ygfB* deletion such as *ampDh3* were non-significantly differentially expressed in this comparison (*ampDh3*: $\log_2$ fold change of 1.70 with an adjusted *p* value of 1).

Nevertheless, it was previously shown that the AmpDh3 protein abundance is increased slightly in the *ygfB* deletion mutant exposed to ciprofloxacin in comparison to the wildtype exposed to ciprofloxacin (Figure 11, page 97). As summarized in Table 29, the pattern observed for AmpDh3 seems to hold true for all genes that were found to be repressed by *ygfB* either in this study or previously (Eggers et al., 2023). The expression was increased either upon exposure to ciprofloxacin or deletion of *ygfB*. Furthermore, the concurrent deletion of *ygfB* and exposure to ciprofloxacin demonstrated a tendency towards elevated expression levels compared to wildtype exposed to ciprofloxacin, although the results were not statistically significant (Figure 20). Therefore, many AlpA-regulated genes (Peña et al., 2021) seem to be also regulated by *ygfB* and concurrent deletion of *ygfB* and exposure to ciprofloxacin seems to have slight additive effects. Interestingly, *ampC* expression was neither affected by exposure to ciprofloxacin in the wildtype nor the *ygfB* deletion background.

Table 29: $\log_2$ fold expression relative to ID40 WT -CIP for *ygfB* regulated genes. Values written in bold: Significant difference compared to ID40 WT-CIP with an adjusted *p* value of <0.01.

Locus tag	Gene name	$\log_2$ fold change relative to ID40 -CIP			
		ID40		ID40Δ*ygfB*	
		-CIP	+CIP	-CIP	+CIP
TUEID40_03245	*ygfB*	0	1.14	**-5.03**	**-4.67**
TUEID40_04486	*ampC*	0	0.93	-1.86	-1.64
TUEID40_01955	*ampDh3*	0	**6.86**	**5.63**	**8.56**
TUEID40_01954	TUEID40_01954	0	2.61	2.99	**4.19**
TUEID40_01840	*alpB*	0	**5.77**	1.72	**6.61**
TUEID40_01839	*alpC*	0	**5.76**	1.99	**6.71**
TUEID40_01838	*alpD*	0	**6.72**	2.15	**7.63**
TUEID40_01837	*alpE*	0	**5.67**	1.26	**6.56**
TUEID40_01945	TUEID40_01945	0	2.53	2.28	**3.92**
TUEID40_01949	*cefD_2*	0	**3.5**	**3.21**	**5.2**
TUEID40_01950	TUEID40_01950	0	**5.02**	**4.46**	**6.7**
TUEID40_01951	*yjjL*	0	**4.35**	**3.71**	**5.93**
TUEID40_01953	*mntH2*	0	**4.21**	**3.95**	**5.77**

3.3.1.2. The *ygfB*-modulated ciprofloxacin response in *E. coli* BW25113

To identify a potential role of *ygfB* in *E. coli* and to see if *ygfB* modulates a response to ciprofloxacin in *E. coli*, the experiment done in ID40 was repeated in the K12 derivative BW25113 (Datsenko & Wanner, 2000). BW25113 is the parent strain of the Keio collection, a library of knockouts of all non-essential genes in *E. coli* (Baba et al., 2006). To obtain a clean *ygfB* deletion mutant, the Keio strain JW5473-1, a BW25113 strain that contains a disruption of the *ygfB* gene by a kanamycin resistance cassette was used. The kanamycin resistance cassette was excised using the plasmid pCP20 as described in 2.4.11, yielding the clean, in-frame *ygfB* deletion mutant BW25113Δ*ygfB*.

To study the *ygfB* modulated response of BW25113 to ciprofloxacin, the strains were exposed to 4x the MIC of ciprofloxacin. To determine the MIC of BW25113 and BW25113Δ*ygfB* to ciprofloxacin, a simple microbroth dilution assay was done, which yielded an MIC for ciprofloxacin of 0.03125 µg/ml in the BW25113 wildtype and *ygfB* deletion mutant.

Cultures were grown and treated with ciprofloxacin as described in 3.3.1.1 for ID40 except that 0.125 µg/ml of ciprofloxacin was added for 2 hours in the +CIP condition. Again, RNA was isolated and RNAseq was done. Differential expression analysis gave information on the genes responding to the different stimuli.

Effect of *ygfB* deletion

As YgfB can also be found in *E. coli*, but the genes that were shown to be affected by YgfB in *P. aeruginosa* (*alpA* and *ampDh3*) are not, we wanted to elucidate the role of YgfB in *E. coli.* To identify genes regulated by *ygfB* in BW25113, the transcriptome of BW25113Δ*ygfB* and BW25113 was compared. Genes with an adjusted p value of ≤ 0.01 and a $\log_2$ fold change of ≥ 2 or ≤ -2 were considered differentially expressed. Figure 21 shows a volcano plot of the results of the differential expression analysis. In addition, all significantly differentially expressed genes are listed in Table 37 in the appendix.

3. Results

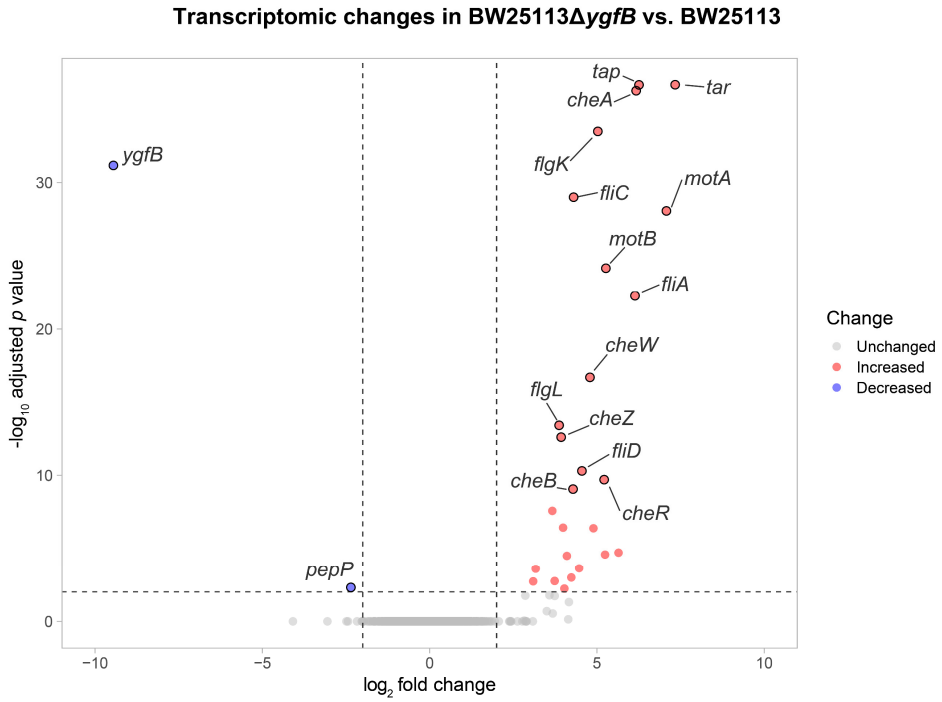

Figure 21: Transcriptome comparing BW25113Δ*ygfB* with BW25113. Upregulated genes (red): $\log_2$ fold change ≥2, adjusted *p* value ≤0.01; downregulated genes (blue): $\log_2$ fold change ≤-2, adjusted *p* value ≤0.01. Data analysis as described in the methods. *n* = 3. The top 15 differentially expressed genes as well as *pepP* were labeled.

Surprisingly, all upregulated genes were part of the flagellar regulon. This is a large network of genes that is regulated in a hierarchical fashion and contains most, if not all, structural as well as regulatory genes of flagella synthesis and motility. The flagellar regulon is regulated by the master regulator $FlhD_4C_2$, which acts as a transcription factor and is responsible for activating all regulatory and structural components of the flagellar machinery. $FlhD_4C_2$ activates class 2 promoters of the flagellar regulon directly, including expression of the sigma factor *fliA*. FliA in turn activates a class 3 promoter of the regulon, expressing late genes of flagellar synthesis. (Fitzgerald et al., 2014)

The only downregulated gene was *pepP,* which is a downstream neighbor of *ygfB* on the same operon.

This finding led to the hypothesis that YgfB might inhibit the transcriptional activator function of $FlhD_4C_2$ by protein-protein interaction, similarly to its interaction with AlpA in *P. aeruginosa*. However, Parker et al. (2019) described that the Keio collection carries high levels of secondary mutations in the promoter region of the master regulator of the flagellar regulon, *flhDC*, leading to stable overexpression of the master regulator and the regulon and therefore, increased motility compared to the poorly motile BW25113 parent strain. They described insertion sequence (IS) elements in the promoter of *flhDC.* Therefore, the BW25113 wildtype and BW25113Δ*ygfB* strains were checked for such an IS element by PCR (Figure 22).

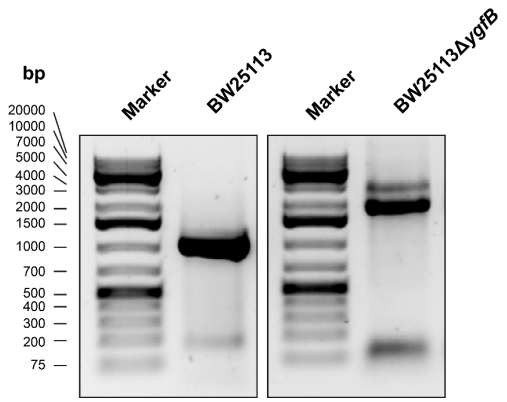

Figure 22: PCR for the *flhDC* promoter. Primers binding on the *flhD* ORF and on the *uspC* ORF upstream of *flhD* were used to amplify the promoter region of *flhDC*. Size of the amplicon without any IS element in the promoter: 990 bp.

The PCR indicated that the BW25113Δ*ygfB* strain likely carries an IS element in the promoter of the *flhDC* operon, leading to overexpression. Further analysis by Sanger sequencing of the *flhDC* promoter of BW25113 and BW25113Δ*ygfB* annealed the traces in BW25113Δ*ygfB* to the IS1A insertion sequence. This insertion sequence has a size of 772 bp (Patel & Matange, 2021), which correlated to the size difference seen in PCR. As a result, we concluded that the difference in expression of flagellar genes in BW25113Δ*ygfB* is not due to an actual effect of *ygfB* deletion, but rather due to a secondary mutation by an insertion element, which was further underlined by our futile attempts to complement the apparent *ygfB* phenotype in BW25113Δ*ygfB* (not shown).

To test if the upregulation of flagella genes might have skewed the analysis of the transcriptomic experiment somehow and masked a differential regulation, which could otherwise have been seen, the upregulated genes of the *flhDC* regulated flagellar regulon were excluded in the data analysis. Figure 23 shows a volcano plot of the results of the new analysis with a significance threshold of *p*adj. ≤0.01 and a $\log_2$ fold change of ≥2 or ≤-2. Table 38 in the appendix additionally shows all significantly differentially expressed genes.

3. Results

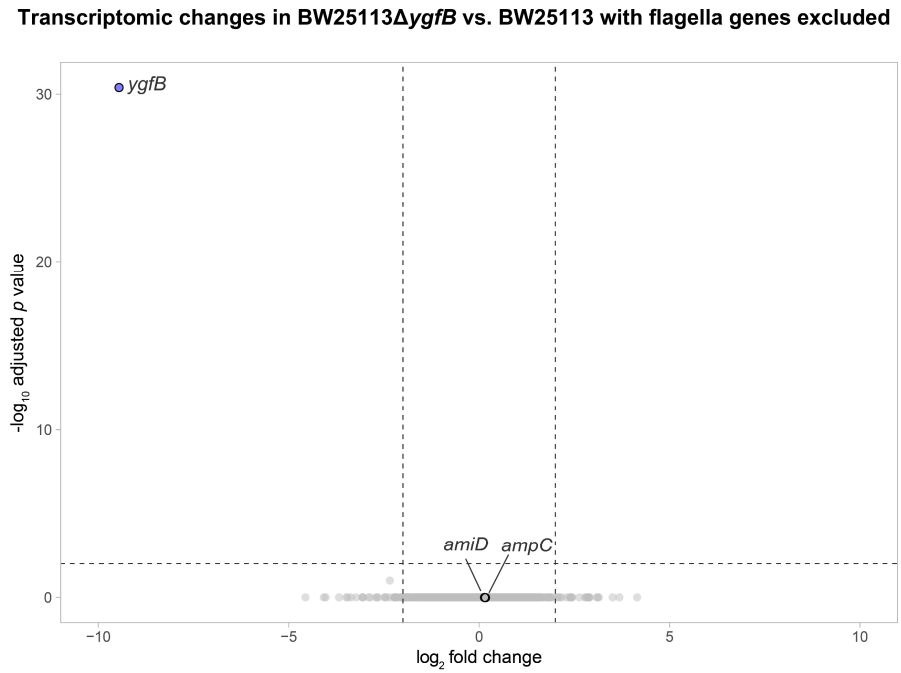

Figure 23: Transcriptomic analysis of genes differentially expressed in BW25113Δ*ygfB* vs. BW25113 with flagella genes upregulated by IS element in *flhDC* promoter removed. Upregulated genes: $\log_2$ fold change ≥2, adjusted *p* value ≤0.01; downregulated genes: $\log_2$ fold change ≤-2, adjusted *p* value ≤0.01. Data analysis as described in the methods. *n* = 3. The genes *ampC* and *amiD* (the next closest homolog to *ampDh3*) have been labeled.

When the flagella genes were removed, no genes except *ygfB* were significantly differentially expressed. *pepP*, which was previously downregulated and is not a part of the flagella regulon, was now non-significantly downregulated ($\log_2$ fold change of -2.35, adjusted *p* value of 0.1). The genes *ampC* and *amiD,* which are labeled in the figure, were not differentially expressed. *ampC* encodes for the β-lactamase that is regulated by YgfB in *P. aeruginosa* and *amiD* encodes for a paralog of AmpD and is the gene most closely related to *ampDh3*. Comparing *amiD* with *ampDh2* and *ampDh3* of *P. aeruginosa* shows closer similarity of *amiD* to *ampDh2*, suggesting that it is the ortholog of *ampDh2* rather than *ampDh3*. From this experiment, we concluded that *ygfB* most likely has no transcriptional effects in *E. coli*.

Response to ciprofloxacin in BW25113

Comparison of the BW25113 +CIP with the BW25113 condition yielded the differentially expressed genes upon exposure to 0.125 µg/ml of ciprofloxacin (4x MIC).

In total, 49 genes out of 4490 genes were upregulated with a threshold of a $\log_2$-fold change of ≥2 and an adjusted *p* value of ≤0.01 and 10 genes of 4490 genes were downregulated with a $\log_2$-fold change of ≤-2 and an adjusted *p* value of ≤0.01.

Searching the differentially expressed gene in UniProt (The UniProt Consortium, 2023), KEGG (Kanehisa, 2019; Kanehisa et al., 2023; Kanehisa & Goto, 2000), and the BV-BRC database (Olson et al., 2023) provided information on the function of the genes. Similarly, as in ID40,

most genes were related to the DNA. Ten upregulated genes were involved in DNA repair (*dinB, dinI, lexA, recX, recA, polB, recN, umuC, umuD, yebG*), two in nucleotide metabolism (*nrdA, nrdB*), and four genes involved in translesion repair (*dinB, umuC, umuD, recA*), with *umuC* and *umuD* forming the DNA-polymerase V complex (Kato & Shinoura, 1977). As in ID40, many genes that were upregulated are part of the LexA-regulated SOS-response (*sulA, dinB, dinD, dinF, dinI, yebG, umuC, umuD, recA, recN, lexA, polB, tisB*), as well as LexA-independent response (*recX)* (Courcelle et al., 2001; Simmons et al., 2008).

Previous studies had also looked at the transcriptomic response of *E. coli* to ciprofloxacin. Bie et al. (2023) treated K-12 MG1655 with subinhibitory ciprofloxacin and Sun et al. (2020) treated K-12 MG1655 with a suprainhibitory concentration. Both groups then performed RNAseq to identify the differentially expressed genes. Both groups found mostly overlapping genes to the ones we identified in the transcriptome.

Like in ID40, the ciprofloxacin response of BW25113 was not the main interest of this study and will not be discussed further here. Table 39 in the appendix shows the entirety of significant differentially expressed genes in BW25113 upon exposure to 0.125 µg/ml of ciprofloxacin for 2 hours.

The *ygfB* modulated response to ciprofloxacin in BW25113

To identify genes that might be part of a *ygfB* modulated ciprofloxacin response in BW25113, the conditions BW25113Δ*ygfB* +CIP and BW25113 +CIP were compared. Figure 24 shows a volcano plot of the $\log_2$ fold change and the $-\log_{10}$ adjusted *p* values of each gene. In Figure 24a, a volcano plot with all genes, including the flagella genes, is shown, while in Figure 24b the flagella genes that were upregulated due to the IS1A element in the *flhDC* promoter were removed. In addition, significantly differentially expressed genes that include the flagella genes are listed in Table 40, and significantly differentially expressed genes without the genes of the flagellar regulon are listed in Table 41.

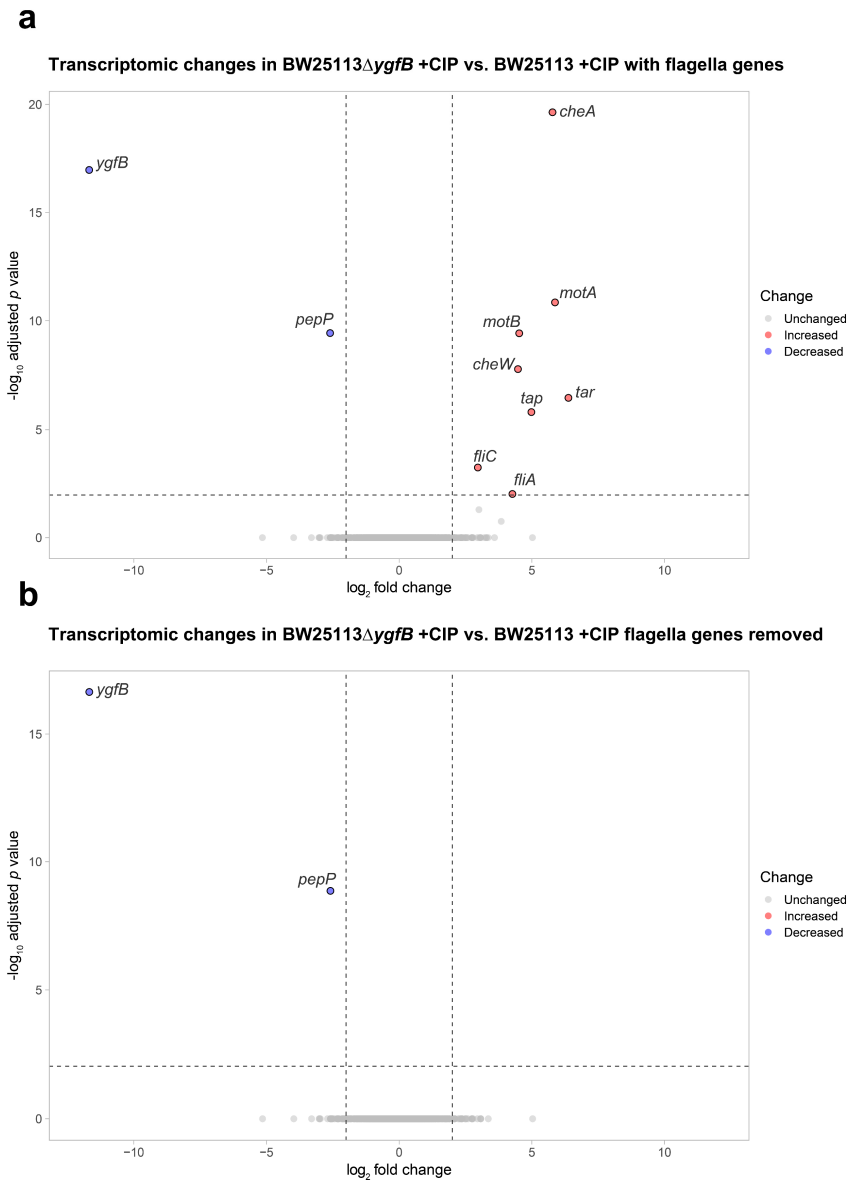

Figure 24: Transcriptome of the *ygfB* modulated response to ciprofloxacin in *E. coli* BW25113. The conditions BW25113Δ*ygfB* +CIP and BW25113 +CIP were compared. In the +CIP condition, 0.125 µg/ml of ciprofloxacin was added for 2 hours. **a)** All genes were analyzed. **b)** Flagella genes that were upregulated due to IS1A element in *flhDC* promoter were removed from the analysis. **a + b)** Upregulated genes (red): $\log_2$ fold change ≥2, adjusted *p* value ≤0.01; downregulated genes (blue): $\log_2$ fold change ≤-2, adjusted *p* value ≤0.01. Data analysis as described in the methods. $n = 3$.

When the upregulated *flhDC* flagellar genes were included in the analysis, 9 genes were differentially expressed upon deletion of *ygfB* in a +CIP background. The flagellar genes *cheA, cheW, fliA, fliC, motA, motB, tap,* and *tar* were upregulated, while *ygfB* and *pepP* were downregulated. When removing the flagellar genes from the analysis, only *ygfB* and *pepP* were differentially expressed, with both being downregulated. As *pepP* neighbors *ygfB* downstream on the same operon, we figured that the differential expression of *pepP* was likely due to expression being affected by the mutagenesis and not due to an actual effect of the gene deletion.

Together, like in *P. aeruginosa* ID40, *ygfB* did not seem to modulate a response to ciprofloxacin in *E. coli* BW25113. Unlike in ID40, *ygfB* deletion itself did not affect expression of any genes in BW25113.

3.3.2. The interactome of YgfB in *P. aeruginosa* and *E. coli*

By transcriptome analysis, we have shown that the role of *ygfB* on a transcriptional level is rather limited. In *P. aeruginosa,* YgfB regulates expression of *ampDh3* and potentially of *alpBCDE* by interacting with the transcriptional regulator of these genes, AlpA. In *E. coli* however, *ygfB* does not seem to regulate any genes on the transcriptional level. Unpublished proteomic data of our group also shows that upon deletion of *ygfB* in ID40, many more proteins are differentially abundant in comparison to differentially produced transcripts.

This suggests that YgfB might play a different cellular role, potentially by interacting with other proteins. To identify such putative interaction partners of YgfB, pulldown-MS experiments were done in *P. aeruginosa* and *E. coli*. Here, the entire fraction of interacting proteins in a pulldown assay was analyzed by NanoLC-MS/MS, providing an overview of the entirety of the interactome. We hoped that this could provide an insight into the further role of YgfB and give information on a conserved function in *P. aeruginosa* and *E. coli*.

3.3.2.1. Interactome of YgfB in *P. aeruginosa*

First, we set out to determine the interactome of YgfB in *P. aeruginosa* ID40. For this, the pulldown was repeated using whole cell lysates of cells grown for 5 hours as described in the methods section under 2.3.20, and as shown in Eggers et al. (2023) and in the results section of this work under 3.1.3.1.

Pulldowns were done in triplicates using GST or GST-YgfB as a bait. The eluate fraction of the pulldown was then analyzed by NanoLC-MS/MS at the Proteome Center Tübingen. The LFQ values for each condition were then used as raw data for analysis using Perseus as described in 2.5.5 in the methods section. In short, the quantity of proteins found in the GST-YgfB condition was compared with the quantity of proteins found in the GST condition by multiple *t* test analysis with a false discovery rate (FDR) of 0.01. Proteins that were significantly enriched in the GST-YgfB condition with a *q* value (multiplicity adjusted *p* value) of ≤0.01 were classified as potential interaction partners.

Figure 25 shows a volcano plot of the $\log_2$ fold change of protein abundance in the GST-YgfB vs. GST comparison as well as the $-\log_{10} p$ value of each comparison. Of note, the $-\log_{10} p$ value and not the *q* value as a multiplicity adjusted *p* value is plotted, as the program Perseus that was

used for the statistical analysis rounded *q* value that were low enough to 0, making them impossible to plot. Proteins that were significantly more abundant with a *q* value of ≤0.01 are labeled in red and classified as potential interactors. Proteins that were significantly less abundant are marked in blue and were not further analyzed. Table 42 in the appendix shows all interactors of YgfB in ID40.

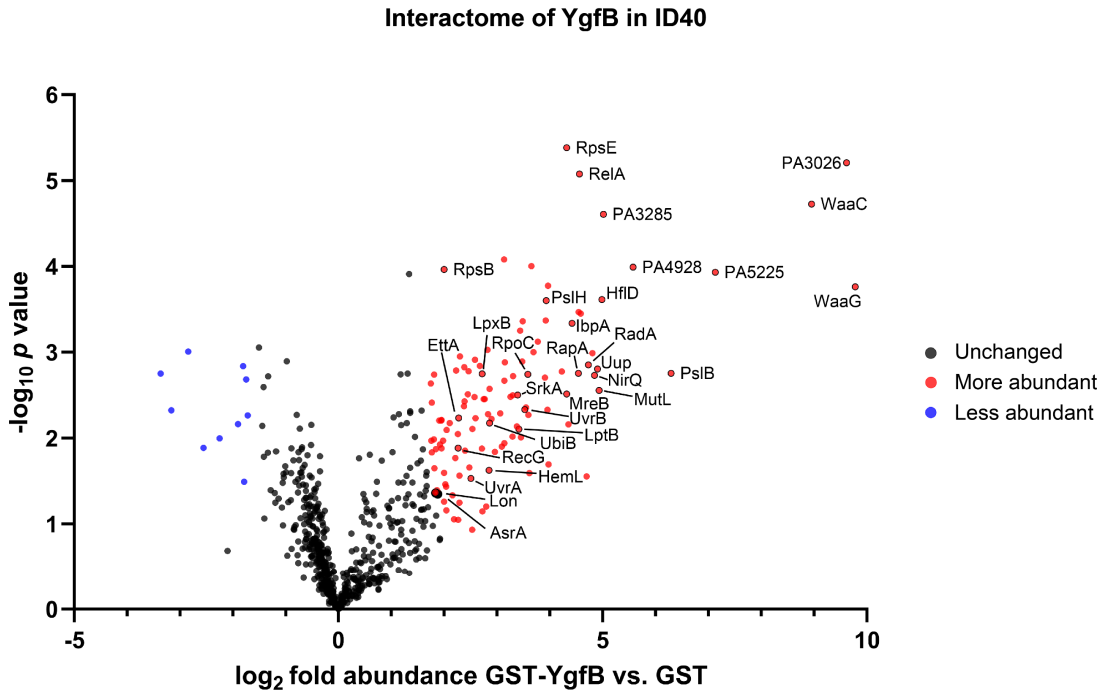

Figure 25: Interactome of YgfB in *P. aeruginosa* ID40. Plotted is the $\log_2$ fold abundance of proteins in the eluate fraction, comparing the GST-YgfB vs. GST conditions, as well as the $-\log_{10}$ *p* value of this comparison. Comparisons were done by two-sided multiple *t* test with an FDR of 0.01. *n* = 3. Proteins marked red were more abundant in the GST-YgfB condition and had a *q* value of ≤0.01. These are classified as interactors. Proteins marked blue were less abundant with a *q* value of ≤0.01. $-\log_{10}$ *p* values instead of *q* values (multiplicity adjusted *p* values) are plotted because the program Perseus that was used for data analysis, rounded low *q* values to 0, making them impossible to plot. Selected interactors were labeled.

In total, 118 proteins could be identified as potential interacting proteins of YgfB in *P. aeruginosa* ID40. Searching for the function of the proteins in various databases, such as UniProt (The UniProt Consortium, 2023), KEGG (Kanehisa, 2019; Kanehisa et al., 2023; Kanehisa & Goto, 2000), or the BV-BRC database (Olson et al., 2023) provided information on functional associations of the interacting proteins. The interactome included eleven proteins that were related to DNA repair (DnaB, DnaX, UvrA, UvrB, RdgC, RecA, RecG, DnaE, RadA, MutL, MfD). In addition, five proteins were associated with translation (LepA, RpsB, RpsE, RplS, SelB). Five proteins were associated with synthesis of lipopolysaccharide (WaaC, WaaU, LpxB, LptB, LptD) and interestingly, YgfB seemed to interact also with GyrB and ParE, the B-subunits of both bacterial type II topoisomerases, gyrase and topoisomerase IV (Aldred et al.,

2014). Also, two proteins that are involved in the biosynthesis of phenazine as precursors of PQS were found as interactors of YgfB (PqsC, PqsD).

To enable the identification of distinct cellular functions of protein-protein interactions involving YgfB, an enrichment analysis of gene ontology terms of biological processes (Table 30) was carried out using STRING (Szklarczyk et al., 2023).

Table 30: Enrichment analysis of biological processes using STRING. Analysis was done on GO terms of biological processes of all proteins identified in the interactome. Analysis was done with an FDR (false discovery rate) of ≤0.05, a minimum strength of ≥0.01, and a minimum count in the network of 2. Observed count is the number of proteins that have the associated GO term in the interactome and background count the total number of proteins in the entire proteome that carry this GO term. Strength is the $\log_{10}$ ratio of the observed number proteins with an associated term vs. the expected number of proteins with an associated term in a random dataset of the same size and is a measure of the strength of the enrichment effect. FDR is a measure of the significance of the enrichment as multiplicity adjusted *p* values by Benjamini-Hochberg procedure.

term ID	term description	observed count	background count	strength	FDR
GO:0006289	Nucleotide-excision repair	3	4	1.55	2.39E-02
GO:0006401	RNA catabolic process	4	9	1.32	1.06E-02
GO:0034605	Cellular response to heat	4	9	1.32	1.06E-02
GO:0009266	Response to temperature stimulus	5	15	1.2	5.30E-03
GO:0051276	Chromosome organization	6	30	0.98	8.40E-03
GO:0009628	Response to abiotic stimulus	6	44	0.81	3.99E-02
GO:0006259	DNA metabolic process	15	136	0.72	8.34E-05
GO:0006281	DNA repair	8	72	0.72	1.95E-02
GO:0033554	Cellular response to stress	15	143	0.69	1.30E-04
GO:0009605	Response to external stimulus	9	98	0.64	2.75E-02
GO:0090304	Nucleic acid metabolic process	26	365	0.53	2.21E-05
GO:0044260	Cellular macromolecule metabolic process	30	471	0.48	2.21E-05
GO:0006139	Nucleobase-containing compound metabolic process	31	554	0.42	1.00E-04
GO:0051716	Cellular response to stimulus	23	429	0.4	5.30E-03
GO:0043170	Macromolecule metabolic process	45	875	0.39	3.99E-06
GO:0046483	Heterocycle metabolic process	34	707	0.36	6.10E-04
GO:0050896	Response to stimulus	27	561	0.36	5.40E-03
GO:0034641	Cellular nitrogen compound metabolic process	43	901	0.35	2.72E-05
GO:1901360	Organic cyclic compound metabolic process	35	758	0.34	9.50E-04
GO:0006725	Cellular aromatic compound metabolic process	34	735	0.34	1.20E-03
GO:0044238	Primary metabolic process	64	1513	0.3	1.88E-06
GO:0006807	Nitrogen compound metabolic process	58	1440	0.28	2.21E-05
GO:0044249	Cellular biosynthetic process	38	940	0.28	5.30E-03
GO:0009058	Biosynthetic process	39	988	0.27	5.90E-03
GO:1901576	Organic substance biosynthetic process	37	945	0.27	1.06E-02
GO:0071704	Organic substance metabolic process	72	1858	0.26	1.88E-06
GO:0044237	Cellular metabolic process	69	1811	0.25	5.31E-06
GO:0008152	Metabolic process	74	2078	0.23	1.31E-05
GO:0009987	Cellular process	90	2891	0.17	2.21E-05

The top three most enriched clusters in the interactome of YgfB in ID40 were “Nucleotide-excision repair” (UvrA, UvrB, Mfd), “RNA catabolic process” (DeaD, RhlB, Rph, and Rne),

as well as “Cellular response to heat” (AsrA, ClpA, Lon, PA2725). The “Response to temperature stimulus” cluster contained the same proteins as the “Cellular response to heat” cluster, with DeaD being also present here. A cluster that contained many proteins that seemed relatively specific was the “Cellular response to stress” cluster (AsrA, ClpA, DeaD, Lon, Mfd, MutL, PA2725, PA3019, Ppx, RadA, RecA, RecG, RelA, UvrA, and UvrB).

In addition, an analysis for enrichment of local STRING network clusters (Szklarczyk et al., 2023) was done (Table 31). Local STRING network clusters are protein clusters that were computationally calculated using the full STRING network of *P. aeruginosa*. Enrichment of proteins that belonged to these clusters was then tested.

Table 31: Enriched local STRING network clusters in interactome of YgfB in ID40. Analysis was done on local STRING network clusters. Analysis was done with an FDR (false discovery rate) of ≤0.05, a minimum strength of ≥0.01, and a minimum count in the network of 2. Observed count is the number of proteins that have the associated cluster term in the interactome and background count the total number of proteins in the entire proteome that carry this cluster term. Strength is the $\log_{10}$ ratio of the observed number proteins with an associated term vs. the expected number of proteins with an associated term in a random dataset of the same size and is a measure for the strength of the enrichment effect. FDR is a measure of the significance of the enrichment as multiplicity adjusted *p* values by Benjamini-Hochberg procedure.

term ID	term description	observed count	background count	strength	FDR
CL:662	SOS response, and Mismatch repair	5	14	1.23	0.0072
CL:660	DNA repair	6	22	1.11	0.0048
CL:658	DNA repair, and Mismatch repair	9	43	0.99	0.0012
CL:653	Catalytic activity, acting on DNA, and Regulation of DNA metabolic process	10	65	0.86	0.0018

In the local STRING network enrichment, most clusters were related to DNA repair. The highest enriched cluster was the SOS response and mismatch repair cluster (MutL, RadA, RecA, UvrA, and UvrB) followed by the DNA repair cluster (all of the above and RdgC). Next followed the DNA repair and mismatch repair cluster, which contained all of the proteins above as well as DnaB, DnaE, and DnaX. The last enriched cluster was the “Catalytic activity, acting on DNA, and Regulation of DNA metabolic process” cluster, which contained all of the proteins above as well as HepA.

The functional analyses further underlined the notion that YgfB in *P. aeruginosa* mostly seemed to interact with proteins involved in DNA repair, as terms that are involved with this function had the highest enrichment strength. In addition, RNA catabolism, heat response, as well as a general stress response seemed to be of importance.

Validation of interactome *in vivo*

To validate candidates of the interactome experiment *in vivo*, protein-fragment complementation assays (PCA) were done. For this purpose, the strain ID40Δ*ygfB*::rha-SmBiT-*ygfB* was generated. The strain lacked *ygfB* at the native locus but had it reintroduced at the Tn7-site

carrying a SmbiT tag under the control of a rhamnose-inducible promoter. Unlike the HiBiT tag used previously in this work, which has a high affinity for LgBiT, SmBiT is part of the NanoLuc split-luciferase but has a low affinity for its counterpart LgBiT. The CDS of proteins of interest (POI) was cloned in the plasmid PBBR1_LgBiT (LgBiT-GOI), yielding LgBiT-POI-fusion proteins. If the POI and YgfB interacted, SmBiT and LgBiT would come in proximity leading to a reconstituted luciferase, which would generate chemiluminescence upon addition of the substrate furimazine. This allowed validation of the candidates identified in the interactome experiment in the native environment of the cell and might give further information on whether the interaction seen in the pulldown is biologically relevant.

In total, 15 candidates that were identified as potential interactors by the analysis described in this work (UvrB, RpsE, WaaC, RecG, MutL, PslH, RadA, PslB, NirQ, WaaG, MreB, RapA UbiB, RelA and SrkA), as well as 8 other candidates that had already previously been selected based on alternative analyses of the data (RhlE, UbiH, ZipA, DinG, TUEID40_06036, RbsB, TUEID40_05398, TUEID40_05668) were screened by PCA. The results of the PCA are shown in Figure 26. Luciferase activity relative to a LgBiT control that carried no POI is shown.

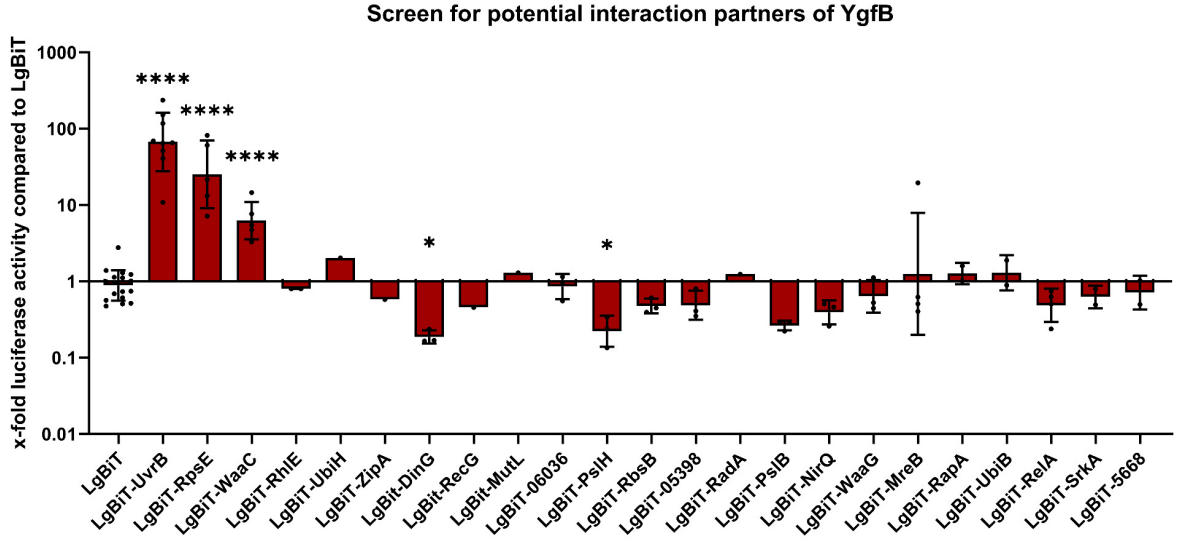

Figure 26: Screening for interacting proteins of YgfB. The strain ID40Δ*ygfB*::rha-SmBiT-*ygfB* was transformed with pBBR1-LgBiT-GOI plasmids where the LgBiT-GOI is constitutively expressed. The transformants were grown in LB medium overnight with 0.1% rhamnose to induce production of SmBiT-YgfB. After subculturing for 2-3 hours, 50 µl of culture containing 10^7 bacteria were added to a white 96 well plate in triplicates. 50 µl of luciferase detetion reagent was added and the chemiluminescence was measured. Plotted are the mean and *SD* of the $\log_{10}$ transformed data relative to a LgBiT control where no POI was fused to LgBiT, as well as individual data points. Asterisks indicate significant differences to the LgBiT control by one-way ANOVA done with the $\log_{10}$ transformed data. Dunnett's multiple comparisons test was used as a post-hoc test. *p<0.05, ****p<0.0001. n = 1-19 biological replicates.

In the screen for potential interaction partners, three candidates that were identified in the interactome of YgfB in ID40 could be validated *in vivo*. These included the protein UvrB, which is part of the UvrABC repair complex, responsible for DNA repair by nucleotide excision repair

(NER) and is particularly important for sensing DNA damage (Verhoeven et al., 2002). Another interactor was the small ribosomal subunit protein uS5, encoded by the gene *rpsE*. The protein will be referred to as RpsE throughout the rest of this work and has been described to play an important role in translational accuracy in *E. coli* (Kirthi et al., 2006; Takyar et al., 2005). Lastly, we could also validate the Lipopolysaccharide heptosyltransferase 1, encoded by the gene *waaC*. As for RpsE, the protein will be called WaaC throughout this work. WaaC is important in the biosynthesis of the inner core region of lipopolysaccharide (LPS), which tethers the O-antigen to the membrane bound Lipid A (de Kievit & Lam, 1997). The relatively low percentage of interacting proteins that could be validated *in vivo* suggested that the interactome produced a rather large number of false positive hits, potentially due to the non-native environment during the pulldown. Additionally, the protein tags in the fusion proteins might affect their functions, leading to an effect on interaction.

YgfB does not affect mutation frequency or persister formation in ID40

As UvrB could be validated to interact with YgfB *in vivo* with the strongest effect, the mutation frequency decline protein MfD seemed to be a potential interactor of YgfB (although not tested in the PCA, as due to the large number of potential interactors, only a limited selection of proteins could be screened), and lastly because DNA repair seemed to be the most prominent biological function of the interactors of YgfB in ID40, we asked whether YgfB interacting with UvrB or other proteins that are involved in DNA repair might affect the mutation frequency of ID40. We hypothesized this, as Mfd-mediated recruitment of NER was described to be involved in higher mutation rates in *B. subtilis* (Million-Weaver et al., 2015).

The mutation frequency was tested as described in 2.2.8 by growing a streptomycin (500 µg/ml) susceptible colony of both ID40 and ID40Δ*ygfB* in 20 ml of LB medium over 24 hours to allow mutations to accumulate. The entirety of this culture was then serial diluted and plated on LB agar plates as well as on LB agar plates containing 500 µg/ml streptomycin to count CFU for each condition. The ratio between the colonies that grew on the streptomycin plates (the colonies that had acquired resistance to streptomycin by mutation) and the total CFU in the culture represented the mutation frequency. Figure 27a shows the results of the mutation frequency assay.

Next to mutation frequency, we also tested whether *ygfB* had an effect on the number of persister cells emerging upon treatment with ciprofloxacin in ID40. UvrB and other components of the NER were described to be important in persister cell survival in *E. coli* due to the cells relying on NER to repair accumulated oxidative DNA damage (Wilmaerts, Govers, et al., 2022). The fraction of persister cells was determined as described in 2.2.9. For this, stationary

cultures of the strains ID40 and ID40Δ*ygfB* treated with 10x the MIC of ciprofloxacin in liquid culture for 5 hours to induce persister cell formation, as well as with water as a vehicle control. CFU were counted before and after treatment to determine the fraction of cells that went into persister state and that could be awakened from persistence after antibiotic removal. The ratio of CFU before and after ciprofloxacin treatment reflects the persister fraction and is a measurement of the combined effect of persistence entry as well as awakening. Results from the determination of the persister fraction are shown in Figure 27b.

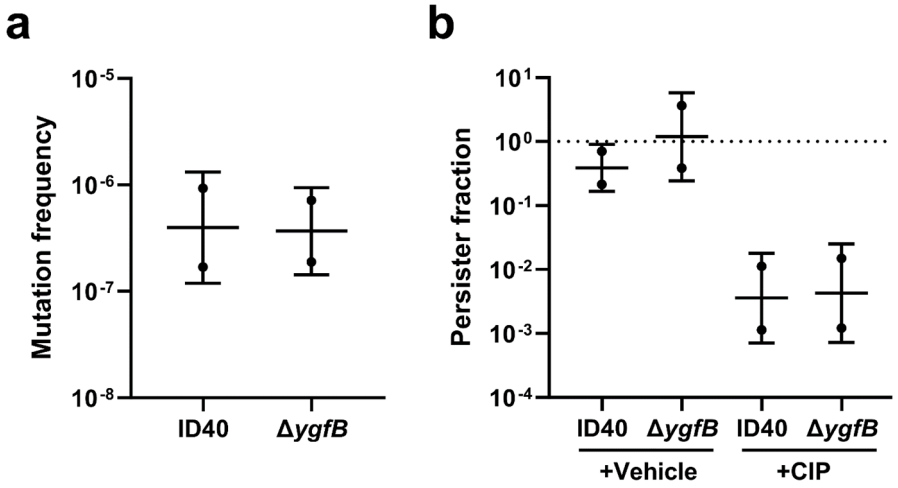

Figure 27: Mutation frequency and persister fraction in ID40 wildtype and ID40Δ*ygfB*. a) Mutation frequency was determined by growing a streptomycin susceptible colony of each strain in 20 ml of LB medium for 24 hours to allow natural mutations to accumulate. The cultures were then serial diluted and plated on LB medium to count the total number of cells, as well as on LB agar plates containing 500 µg/ml of streptomycin to count the colonies that had acquired resistance to streptomycin by mutation. The mutation frequency is the ratio of the colonies counted on the streptomycin plate and the LB plate, respectively. Plotted are the mean and *SD* of the $\log_{10}$ transformed data. $n = 2$ **b)** The persister fraction was determined by exposing stationary cultures of ID40 or ID40Δ*ygfB* to either water as a vehicle control or 10x the MIC of ciprofloxacin for 5 hours. The CFU before and after the treatment were counted by plating serial dilutions. The persister fraction is the ratio of CFU after the treatment and before the treatment. Plotted are the mean and *SD* of the $\log_{10}$ transformed data. $n = 2$.

Neither mutation frequency nor the persister fraction upon exposure to ciprofloxacin seemed to be affected by deletion of *ygfB*. The mutation frequency was about $5x10^{-6}$ in both ID40 and ID40Δ*ygfB*. The persister fraction was around $5x10^{-2}$ in ID40 wildtype and the *ygfB* deletion mutant while the vehicle control behaved as expected, meaning no change in cell numbers in the stationary culture for the 5-hour duration. These findings suggested that *ygfB* had no effect on either the mutation frequency nor the persister fraction emerging upon treatment with ciprofloxacin in ID40.

3.3.2.2. Interactome of YgfB in *E. coli* BW25113

The interactome experiment of YgfB in *P. aeruginosa* ID40 yielded a large number of potential interaction partners of which only a small part could be validated. We therefore tried to refine our search for interaction partners. As YgfB is also present in *E. coli*, but no function is known

so far, we figured that a conserved function in *P. aeruginosa* and *E. coli* might be mediated by a common interaction partner. Repeating the pulldown in *E. coli* and then searching for proteins that interacted with YgfB in both species might provide further information on the role of YgfB. We chose the *E. coli* K12 derivative BW25113 for these experiments. As in the experiments with *P. aeruginosa* ID40, a *ygfB* deletion background was needed for the pulldown assay. Since the BW25113Δ*ygfB* strain, which we used previously for transcriptomic analysis, carried an insertion sequence in the *flhDC* promoter, leading to an overactive flagella regulon, the strain BW25113Δ*ygfB*_new was generated by homologous recombination as described in 2.4.16 in the methods section. The *flhDC* promoter of this deletion mutant was also confirmed by PCR to be the same as the wildtype.

His-GST-EcYgfB derived from BW25113 and His-GST were purified as bait for the pulldown assay (method section 2.3.19, Figure 36 and Figure 37 in the appendix). With the purified proteins as bait, the pulldown interactome experiment was repeated with whole cell lysates of *E. coli* BW25113Δ*ygfB* as a prey. The pulldown was carried out in the same fashion as for *P. aeruginosa* ID40 i.e. using magnetic GSH-beads for binding the bait proteins, the same buffers, volumes etc. In this experiment, two additional conditions were included besides adding cell lysates to the bead-bound His-GST or His-GST-EcYgfB proteins. Pulldown buffer was added to His-GST or His-GST-EcYgfB as a mock condition to determine contaminants in the bait proteins that resulted from the purification process. These controls were particularly important as the proteins were purified in *E. coli* and the pulldown was also performed with lysates from *E. coli*, which prevented the preselection of contaminant proteins as it was done in the *P. aeruginosa* ID40 pulldown.

The pulldown assays were done in triplicates and the elution fractions were analyzed by NanoLC-MS/MS at the Proteome Center Tübingen to determine the interactome. As previously, the LFQ values were used for analysis using the software Perseus (Tyanova, Temu, Sinitcyn, et al., 2016) as described in 2.5.5. Unlike to the analysis in ID40, contaminators had to be removed from the dataset prior to analyzing the difference in protein abundance between the His-GST and His-GST-EcYgfB condition. Therefore, the LFQ values of the bait protein + lysate was compared with the bait protein + mock condition for each His-GST and His-GST-EcYgfB. The analysis was done with a two-sided multiple *t* test with an FDR of 0.01 and an S0 of 2. Proteins that were significantly more abundant in the lysate condition vs. the mock condi-

tion could be classified as potential interactors of either construct, while non-significant or significantly less abundant proteins could be classified as contaminants that stemmed from the purification process.

Therefore, all proteins that were significantly more abundant in either condition were kept, while the others were discarded from the further analysis. With the cleaned dataset, a comparison between His-GST-EcYgfB + Lysate and His-GST + Lysate could be done. Again, this comparison was done with a two-sided multiple *t* test with an FDR of 0.01 and an S0 of 2. All proteins that were significantly more abundant in this comparison (His-GST-EcYgfB + Lysate vs. His-GST + Lysate) and significantly more abundant in the comparison of His-GST-EcYgfB + Lysate vs. His-GST-EcYgfB + Mock were considered as potential interactors. Figure 28 shows as volcano plot of the His-GST-EcYgfB + Lysate vs. His-GST + Lysate comparison. All proteins that are marked red were classified as potential interactors of YgfB in BW25113.

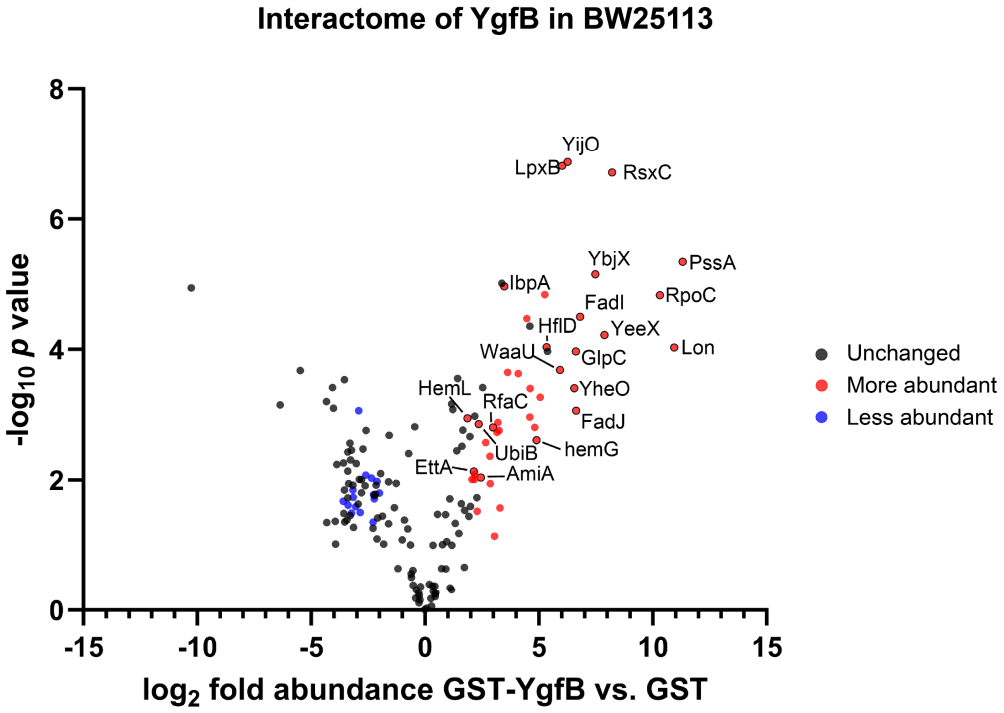

Figure 28: Interactome of YgfB in *E. coli* BW25113. Plotted is the $\log_2$ fold abundance of proteins in the eluate fraction, comparing the "His-GST-EcYgfB + Lysate vs. His-GST + Lysate" conditions as well as the $-\log_{10}$ *p* value of this comparison. Comparisons were done by two-sided multiple *t* test with an FDR of 0.01 and an S0 of 2 on the contamination-cleaned background. $n = 3$. Proteins marked in red are classified as interactors as they were significantly enriched in the "His-GST-EcYgfB + Lysate vs. His-GST + Lysate" comparison as well as in the "His-GST-EcYgfB + Lysate vs. His-GST-EcYgfB + Mock" comparison with a *q* value of ≤0.01. Proteins marked in blue were less abundant with a *q* value of ≤0.01. Proteins that were more abundant but not marked in red had no significant enrichment in the His-GST-YgfB + Lysate vs. His-GST-YgfB + Mock" comparison. $-\log_{10}$ *p* values instead of *q* values (multiplicity adjusted *p* values) are plotted because the program Perseus, which was used for data analysis, rounded low *q* values to 0, making them impossible to plot. Selected interactors were labeled.

In total, 41 proteins met the criteria to classify them as an interactor. These are also listed in Table 43 in the appendix. Searching for functions of the interacting proteins of YgfB in

BW25113 in the databases UniProt (The UniProt Consortium, 2023), KEGG (Kanehisa, 2019; Kanehisa et al., 2023; Kanehisa & Goto, 2000), and the BV-BRC database (Olson et al., 2023) provided information on the interacting proteins. Eight proteins were involved in the biogenesis of LPS (LpxB, WaaB, RfaC/WaaC, WaaU, WaaY, WbbK, WecF, YibB), three were part of the ribosomal large subunit (RplF, RplK, RplX), with TypA also being important for assembly of the large ribosomal subunit. YgfB in BW25113 also seemed to potentially interact with the RNA-polymerase, as both the DNA-directed RNA polymerase subunit beta (encoded by *rpoB*) and the DNA-directed RNA polymerase subunit beta' (encoded by *rpoC*) could be identified in the interactome. FadI and FadJ are involved in the degradation of long-chain fatty acids and have been annotated in KEGG to be involved in degradation of geraniol, valine, leucine, isoleucine, and benzoate degradation. HemG and HemL were also found to potentially interact with YgfB in BW25113 and have been annotated as playing a role in biosynthesis of porphyrins. Analysis of local cluster enrichment in STRING (Szklarczyk et al., 2023) provided further information on enrichment of certain functional classifications in the interactome (Table 32)

Table 32: Local cluster enrichment of STRING clusters in interactome of YgfB in BW25113. Analysis was done on local STRING network clusters. Analysis was done with an FDR (false discovery rate) of ≤0.05, a minimum strength of ≥0.01 and a minimum count in the network of 2. Observed count is the number of proteins that have the associated cluster term in the interactome and background count the total number of proteins in the entire proteome that carry this cluster term. Strength is the $\log_{10}$ ratio of the observed number proteins with an associated term vs. the expected number of proteins with an associated term in a random dataset of the same size and is a measure for the strength of the enrichment effect. FDR is a measure of the significance of the enrichment as multiplicity adjusted *p* values by Benjamini-Hochberg procedure.

term ID	term description	observed count	background count	strength	FDR
CL:3565	Galactosyltransferase activity, and Acetylglucosaminyltransferase activity	3	5	1.78	0.0126
CL:3561	Lipopolysaccharide core region metabolic process	4	17	1.38	0.0126
CL:3520	Lipopolysaccharide biosynthesis, and Lipopolysaccharide transport	6	38	1.2	0.0032
CL:3397	Polysaccharide biosynthetic process, and Lipopolysaccharide transport	8	120	0.83	0.0126
CL:37	Translation, and Protein export	9	161	0.75	0.0126

The cluster that was most strongly enriched was a cluster that contained proteins that had galactosyltransferase activity and acetylglucosaminyltransferase activity (WaaB, WaaU, WaaY). The “Lipopolysaccharide core region metabolic process” cluster contained WaaB, RfaC/WaaC, WaaU, and WaaY, which could also be found in the “Lipopolysaccharide biosynthesis, and Lipopolysaccharide transport” cluster, where additionally also LpxB and YibB were found. The “Polysaccharide biosynthetic process, and Lipopolysaccharide transport” contained all aforementioned protein but also WecF and WbbK. As all these clusters were related to LPS biogenesis, this seemed to be the most important function of interactors of YgfB in *E. coli*. Lastly, the

"Translation, and Protein export" cluster was also enriched, comprising the proteins EttA, GlyQ, RplF, RplK, RplX, RpoB, RpoC, SecA, and TypA.

3.3.2.3. Common interacting proteins in ID40 and BW25113

To further refine the search for interacting proteins of YgfB in *P. aeruginosa* ID40 and *E. coli* BW25113, interactors of YgfB in BW25113 were searched for homologs in PAO1 by protein BLAST (Camacho et al., 2009). Comparison of the interactome of YgfB in ID40 and BW25113 then revealed common interacting proteins of YgfB. These are listed in Table 33. In total, ten proteins could be identified as common interactors of YgfB in ID40 and BW25113. The common interactors entailed EttA, HemL, HflD, IbpA, Lon, AsrA (an alternative Lon protease in *P. aeruginosa*), LpxB, RpoC, UbiB, and WaaC, also known as RfaC in *E. coli*.

Table 33: Common interacting proteins of YgfB in *P. aeruginosa* ID40 and *E. coli* BW25113. Shown are the $\log_2$ fold abundance value in the GST-YgfB condition vs. the GST control. The *q* value (adjusted *p* value) of multiple two-sided *t* test is shown.

***P. aeruginosa* ID40**					***E. coli* BW25113**				
Gene names	**Majority protein ID**	**Protein names**	**$\log_2$ fold abundance GST-YgfB vs. GST**	***q* value**	**Gene names**	**Majority protein ID**	**Protein names**	**$\log_2$ fold abundance GST-YgfB vs. GST**	***q* value**
ettA	Q9HVJ1	Energy-dependent translational throttle protein EttA	2.28	2.88E-03	*ettA*	P0A9W3	Energy-dependent translational throttle protein EttA	2.15	2.39E-03
hemL	P48247	Glutamate-1-semialdehyde 2,1-aminomutase (GSA)	2.85	0	*hemL*	P23893	Glutamate-1-semialdehyde 2,1-aminomutase	1.87	3.31E-03
hflD	Q9I0L1	High frequency lysogenization protein HflD homolog	4.99	0	*hflD*	P25746	High frequency lysogenization protein HflD	5.34	0
ibpA	Q9HZ98	Heat-shock protein IbpA	4.42	0	*ibpA*	P0C054	Small heat shock protein IbpA	3.49	0
lon (PA1803)	Q9I2T9	Lon protease	1.84	9.14E-03	*lon*	P0A9M0	Lon protease	10.94	0
lon; asrA (PA0779)	Q9I5F9	Lon protease	1.88	7.20E-03					
lpxB	Q9HXY8	Lipid-A-disaccharide synthase	2.72	0	*lpxB*	P10441	Lipid-A-disaccharide synthase	6.02	0
rpoC	Q9HWC9	DNA-directed RNA polymerase subunit beta'	3.58	0	*rpoC*	P0A8T7	DNA-directed RNA polymerase subunit beta	10.31	0
ubiB	Q9HUB8	Probable protein kinase UbiB	2.86	0	*ubiB*	P0A6A0	Probable protein kinase UbiB	2.35	0
waaC	Q9HUF5	Heptosyltransferase I	8.95	0	*rfaC*	P24173	Lipopolysaccharide heptosyltransferase 1	2.99	1.55E-03

3. Results

To test if the common interacting proteins could be validated *in vivo*, pBBR1_LgBiT-GOI constructs with the CDS of the ID40 genes were generated. As previously, the strain ID40Δ*ygfB*::rha-SmBiT-*ygfB* was transformed with the construct and PCAs were done. PCA with LgBiT-UvrB was also done as a positive control and as a negative control, LB medium was mixed with luciferase reagent. The results of the PCA are shown in Figure 29.

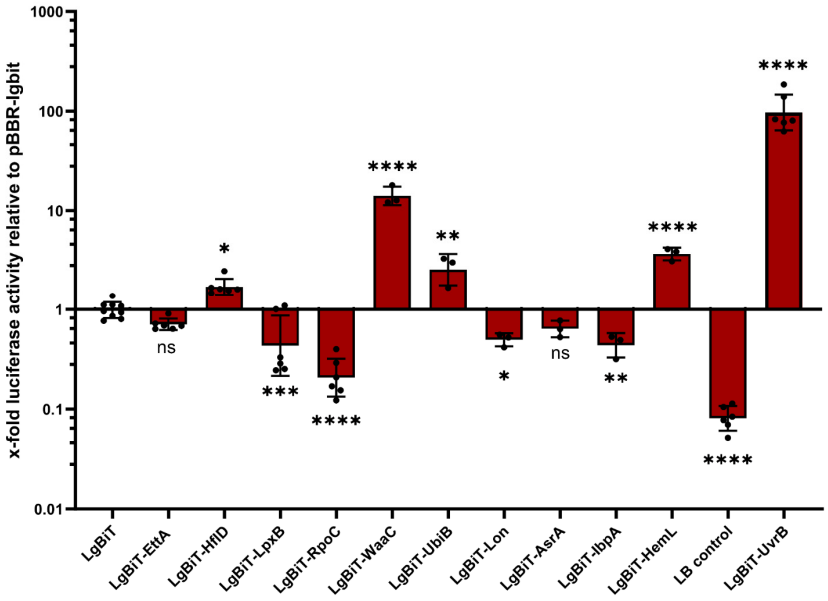

Figure 29: PCA of common interacting proteins in ID40 and BW25113 in ID40. The strain ID40Δ*ygfB*::rha-SmBiT-*ygfB* was transformed with pBBR1-LgBiT-GOI plasmids where the LgBiT-GOI is constitutively expressed. The transformants were grown in LB medium overnight with 0.1% rhamnose to induce production of SmBiT-YgfB. After subculturing for 2-3 hours, 50 µl of culture containing 10^7 bacteria were added to a white 96-well plate in triplicates. 50 µl of luciferase detetion reagent was added and the chemiluminescence was measured. In addition, an LB control where LB medium was mixed with luciferase detection reagent is shown as a negative control and LgBiT-UvrB is shown as a positive control. Plotted are the mean and *SD* of the $\log_{10}$ transformed data relative to a LgBiT control where no POI was fused to LgBiT, as well as individual data points. Asterisks indicate significant differences to the LgBiT control by one-way ANOVA done with the $\log_{10}$ transformed data. Dunnett's multiple comparisons test was used as a post-hoc test. *p<0.05, **p<0.01, ***p<0.001, ****p<0.0001. n = 3-9 biological replicates.

Of the 10 tested constructs, four showed increased luciferase activity compared to the LgBiT background and therefore these candidates could be validated *in vivo*. These were HflD, WaaC, UbiB and HemL. WaaC had been tested before in the general screen and the findings could therefore be reproduced. Luciferase activity of LgBiT-UbiB was increased in the previous large-scale screen non-significantly, but could now be successfully validated. Interestingly, four proteins also showed a significantly lower luciferase activity when compared to the LgBiT control (LpxB, RpoC, Lon, IpbA). As the LgBiT control theoretically represents stochastic assembly of SmBiT and LgBiT, one could argue that reduced luciferase activity to this control might also be due to a protein-protein interaction, although as part of a larger complex that prevents

LgBiT and SmBiT from interacting by keeping them spatially separated. If one takes this assumption, eight out of ten screened candidates could be validated *in vivo*, making the search for a common interactome very successful.

Combining the proteins that produced a significantly higher signal in the PCA done with the common interaction partners and those identified in the larger screen that was done previously, we were able to validate a total of six interaction partners of YgfB in ID40. These were HemL, HflD, RpsE, UbiB, UvrB, and WaaC. These interaction partners might inform further studies on the generalizable cellular function of YgfB in the future.

4. Discussion

Declaration of contribution

Certain parts of the discussion are cited literally from Eggers et al. (2023). These citations were formatted in italics and are marked with quotation marks. The publication Eggers et al. (2023) was mainly written by PD Dr. Erwin Bohn and me.

4.1. The role of YgfB in β-lactam resistance in *P. aeruginosa*

4.1.1. Molecular regulation of resistance by YgfB

It has previously been shown in the MDR clinical *P. aeruginosa* isolate ID40 that deletion of *ygfB* reduces the resistance towards most antipseudomonal β-lactam antibiotics by reducing expression of the β-lactamase AmpC (Sonnabend et al., 2020). As described in the introduction, previous data of our group showed that deletion of *ygfB* led to increased expression of the cell wall amidase *ampDh3*, which degrades anhMurNac-peptides by removing the peptide moiety (Juan et al., 2006).

It is known that in *P. aeruginosa, ampC* is regulated by muropeptides that arise during peptidoglycan recycling and *de novo* synthesis. These muropeptides bind to the transcriptional regulator of *ampC*, AmpR. The soluble peptidoglycan precursor UDP-MurNAc-pentapeptide binds to AmpR and represses *ampC* expression, while anhMurNAc-peptides, cell wall catabolites that arise early in the peptidoglycan recycling pathway, replace UDP-MurNAc-pentapeptides from AmpR and induce *ampC* expression via a conformational change in AmpR (Hanson & Sanders, 1999; Jacobs et al., 1997; Jacobs et al., 1994; Torrens et al., 2019). YgfB modulates the composition of peptidoglycan recycling products in an *ampDh3*-dependent manner and by this pathway leads to increased expression of *ampC*. The goal of this study was to elucidate the molecular mechanism by which YgfB regulates *ampDh3*.

We were able to show that YgfB represses *ampDh3* not only on the mRNA level, but also on the protein level, providing further evidence for this inverse relationship. Using pulldown assays, we have shown that YgfB interacts directly with the antiterminator AlpA, which is a transcriptional regulator of *ampDh3,* and by this direct interaction interferes with AlpA binding to the AlpA binding element (ABE) on the *ampDh3* promoter. Furthermore, ciprofloxacin-induced DNA damage leads to increased expression of *alpA* and *ampDh3*. This process is, however, dampened by YgfB interacting with AlpA. Lastly, it was possible to provide evidence that

the effect of *ygfB* seems also present in other *P. aeruginosa* strains, providing evidence for a generalized effect.

It was previously shown that in PAO1, the antiterminator AlpA regulates expression of the *ampDh3*-PA0808 operon (PA0808 = TUEID40_01954) and the *alpBCDE* self-lysis cluster (Peña et al., 2021). It was proposed that AlpA binds to the promoter of the *alpBCDE* and *ampDh3* genes and subsequently to the RNA polymerase (RNAP), allowing RNAP to read over intrinsic terminators that are positioned downstream of the transcription start site of *alpBCDE* and *ampDh3* (Peña et al., 2021; Wen et al., 2022). Expression of *alpA* is regulated by the LexA-like repressor AlpR, which is autocleaved upon DNA damage that can, for example, be induced by the fluoroquinolone ciprofloxacin (McFarland et al., 2015). Autocleavage of AlpR leads to derepression of *alpA* and therefore to increased expression of *ampDh3* and *alpBCDE*. Previous data generated by our group also showed that presence of *alpA* was essential for *ygfB* to repress the promoter activity of *ampDh3*. In addition, the minimal promoter region needed for YgfB to repress the activity of the *ampDh3* promoter was the same minimal region that was described by Peña et al. (2021) to be needed for positive regulation of *ampDh3* by AlpA.

As there seemed to be an interplay between *ygfB, alpR, alpA,* and *ampDh3*, we analyzed the protein expression of AmpDh3, AlpA and AlpR upon exposure to suprainhibitory levels of ciprofloxacin and studied the impact *ygfB* had on the system (Figure 11, Figure 12). Both ciprofloxacin-induced DNA damage as well as deletion of *ygfB* increased the abundance of AmpDh3. Concurrent deletion of *ygfB* and exposure to ciprofloxacin only increased the abundance of AmpDh3 slightly in comparison to exposure to ciprofloxacin in the wildtype. We observed no effect of *ygfB* deletion on AlpR, while the levels of AlpR were reduced upon exposure to ciprofloxacin, as expected, due to autocleavage of AlpR. Abundance of AlpA behaved similarly to that of AmpDh3, but with a smaller effect size. AlpA levels were increased both upon exposure to ciprofloxacin and deletion of *ygfB*, but concurrent exposure to ciprofloxacin and deletion of *ygfB* did not increase the AlpA levels further when compared to either condition alone.

This suggested that the effects of ciprofloxacin and *ygfB* intersect at the AlpR/AlpA-mediated regulation of *ampDh3*. However, why were AmpDh3 and AlpA levels not increased (much) further by exposure to ciprofloxacin in a Δ*ygfB* background? It was described previously that *alpR* is an essential gene and that loss of *alpR* induces *alpA* expression, which results in *alpBCDE*-mediated cell lysis (McFarland et al., 2015). Additionally, Peña et al. (2021) described that ectopic overexpression of *alpA* is toxic even in the absence of the *alpBCDE* genes.

Consequently, this could indicate that there is a maximum tolerable level of AlpA for the individual bacterial cell. This might explain why AlpA and AmpDh3 levels were not significantly elevated in the ciprofloxacin-treated *ygfB* deletion mutant as compared to the ciprofloxacin-treated wildtype (AmpDh3 and AlpA) or the untreated deletion mutant (AlpA). It can be postulated that any cell in which the abundance of the proteins encoded by the *alpABCDE* operon exceeds a certain threshold undergoes lysis. However, at this point, there is no evidence to support this hypothesis.

As YgfB seemed to regulate the expression of *ampDh3* via the AlpR-AlpA-pathway, we hypothesized that YgfB interacts with either AlpR or AlpA and represses *ampDh3* this way. Employing pulldown assays using whole cell lysates as well as purified proteins as prey, we were able to show that YgfB interacts directly with the antiterminator AlpA (Figure 14, Figure 15). The fact that the pulldown assays were reproducible when switching the bait proteins (pulldown 1: GST-YgfB as a bait and whole cell lysates as prey, pulldown 2: His-MBP-AlpA as a bait and purified YgfB as a prey), further strengthened the evidence that YgfB and AlpA interacted directly.
We did not observe an interaction between YgfB and AlpR. While a potential interaction of YgfB with AlpR could have been disrupted by the N-terminal HA-tag that was fused genomically to the coding sequence of *alpR*, an interaction of YgfB with AlpA was more likely than with AlpR based on previous data. For one, the levels of AlpA were affected by deletion of *ygfB*, while those of AlpR were not. If one were to hypothesize about a potential effect of YgfB on AlpR, one could imagine that YgfB might stabilize AlpR, preventing autocleavage. As levels of AlpR without and with ciprofloxacin were not affected by deletion of *ygfB,* however, this could be ruled out. Additionally, YgfB as well as AlpR are negatively charged at pH 7.4 with a theoretical pI of 4.30 and 5.79, respectively, as calculated by ProtParam (Wilkins et al., 1999). AlpA, however, is positively charged with a theoretical pI of 9.78, further indicating that an interaction between AlpA and YgfB is more likely than an interaction between AlpR and YgfB. The fact that the levels of AlpA were increased when *ygfB* was deleted in ID40, might be explained by a potential destabilization of AlpA that is bound by YgfB, while free AlpA might be more stable. This is, however, obviously very hypothetical and further evidence would be required to even make a lightly confident statement about this matter.

As we have provided evidence that YgfB interacts directly with AlpA, we hypothesized that YgfB represses *ampDh3* production by preventing AlpA from binding to the AlpA-binding

element on the *ampDh3* promoter. We employed EMSAs to study the binding of AlpA to the *ampDh3* promoter and to investigate if YgfB prevented this binding by protein-protein interaction (Figure 16).

We were able to replicate the findings of Peña et al. (2021) using a His-MBP-AlpA fusion protein, as we were unable to purify native AlpA without any solubility tag. The band shift we observed for the interaction of His-MBP-AlpA with a DNA-probe containing the AlpA binding element (ABE) was, however, rather weak and smeary, albeit specific for His-MBP-AlpA, as no band shift was observed in the His-MBP control. We hypothesized that the observed weak shift intensity could be explained by the nature of the interaction between AlpA and the ABE: *"The model proposed suggests that AlpA first binds to the promoter at the putative ABE, and then to the RNA polymerase (RNAP), allowing RNAP to bypass the intrinsic terminator positioned downstream* (Peña et al., 2021; Wen et al., 2022)*. Recently, Wen et al. confirmed these data by solving the AlpA-loading complex consisting of a nucleic acid scaffold corresponding to the positions -31 to 31 of the P_{alpB} promoter together with RNAP, σ^{70}, and AlpA by cryo-EM* (Wen et al., 2022)*. These data might suggest that for a robust binding of AlpA to the ABE, stabilization by RNAP and σ^{70} seems to be required. In contrast to Wen et al., we did not succeed in obtaining native AlpA and therefore used a His-MBP tag to solubilize AlpA. We speculate that the addition of the His-MBP tag to the AlpA in combination with the lack of the other components of the AlpA-loading complex such as RNAP and σ^{70} is very likely the reason why we ended up with a highly reproducible but only weak binding of AlpA to the ABE"* (Eggers et al., 2023, p. 12).

When adding YgfB to the His-MBP-AlpA:ABE binding reaction, the band shift intensity observed for the AlpA:ABE interaction was reliably reduced to the level of an unspecific interaction between His-MBP-AlpA and a scrambled DNA-probe. Adding BSA as a control instead of YgfB did not reduce the shift intensity observed, pointing towards a specific effect of YgfB. While not the most robust, the EMSA data provide further evidence for YgfB interfering with AlpA binding to the *ampDh3* promoter and controlling the levels of *ampDh3* by this route.

To gain further insights into the role of *ygfB* in *P. aeruginosa* in general, the MIC of the wildtype strain and *ygfB* deletion mutants was determined in the MDR *P. aeruginosa* strains ID72 and ID143 as well as in the susceptible laboratory strains PA14 and PAO1 (Table 23). Additionally, the activity of the *ampDh3* promoter was analyzed (Figure 17).

In general, all tested strains showed increased *ampDh3* promoter activity as a response to deletion of *ygfB*, suggesting that the repressive action of *ygfB* on *ampDh3* expression is not a special

feature limited to ID40 but can rather be seen as a general asset present in *P. aeruginosa.* Interestingly, the basal levels of *ampDh3* promoter activity were not associated with the resistance of a particular strain, suggesting that *ampDh3* expression *per se* is not predictive of β-lactam resistance.

In the resistant strains ID143 and ID72, deletion of *ygfB* led to a highly pronounced reduction of resistance. Unlike in ID40, deletion of *ygfB* was able to break resistance to all tested β-lactam antibiotics in these strains. In the susceptible strains PA14 and PAO1, a pronounced reduction in MIC could, however, not be observed upon deletion of *ygfB*. Several reasons for this could be discussed. On the one hand, the MIC assay plates used to determine the MICs only have a limited range of concentrations for each antibiotic to be tested. As the MICs for some antibiotics in PA14 and PAO1 were already close to the limit of detection for the MIC plate and the rest, being out of range, could not be measured at all, it might just be that one would need to repeat the MIC assay using other plates with lower concentration to observe an effect of *ygfB* deletion. The impact of *ygfB* deletion on the strains ID72 and ID143 will be discussed in 4.1.3.

Combining several lines of data, i.e. the fact that YgfB and AlpA regulate the *ampDh3* promoter at the same minimal responsive element (Eggers et al., 2023), the direct protein-protein interaction between YgfB and AlpA, the EMSA data suggesting that presence of YgfB seems to interfere with AlpA binding to the ABE, and the previous data provided by Peña et al. (2021) and Wen et al. (2022) led us to develop the following model of the effect of YgfB on the regulation of the *ampDh3* promoter.

a) When no AlpA is present, the RNA polymerase (RNAP) starts transcription at the transcription start site (TSS). Transcription is, however, terminated by an intrinsic terminator positioned downstream of the TSS and upstream of the CDS of *ampDh3* and TUEID40_01954. Expression of *ampDh3* is therefore suppressed.
b) AlpA is able to bind to the AlpA binding (ABE) on the *ampDh3* promoter that is located between the -35 and -10 region as described by Peña et al. (2021), forming the AlpA-loading complex together with RNAP and σ^{70} (Wen et al., 2022). After the AlpA-loading complex is formed, AlpA is then able to load onto the RNAP by interacting with the RNA exit channel, forming the AlpA-loaded complex. Due to the position of AlpA in the RNA exit channel and its structure forming a nozzle, RNA hairpin formation inside the exit channel by an intrinsic terminator is prevented. This steric hindrance by AlpA therefore leads to resistance of RNAP to intrinsic terminators in the AlpA-loaded state (Wen et al., 2022).

The RNAP in the intrinsic terminator-resistant state is now able to transcribe *ampDh3* downstream of the intrinsic terminator.

c) YgfB interacts with AlpA and prevents it from binding to the ABE and entering the AlpA-loading complex. No AlpA-loaded complex can therefore be formed, RNAP remains susceptible to intrinsic terminators, and transcription of *ampDh3* inhibited.

Figure 30 shows a graphic overview of our proposed model for the effect of YgfB on *ampDh3*.

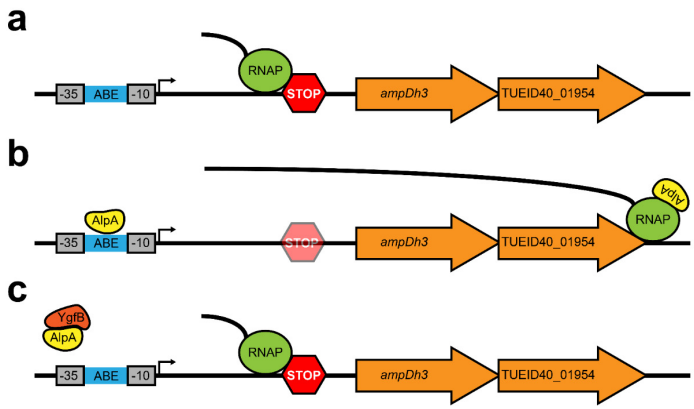

Figure 30: Proposed model of the effect of YgfB on *ampDh3* expression. a) In absence of AlpA, the RNAP starts transcription at TSS but transcription is terminated due to an intrinsic terminator in the promoter of *ampDh3* (STOP sign). RNAP is released, leading to a stop of transcription. **b)** As described by Peña et al. (2021), AlpA binds to the AlpA binding element (ABE) in the promoter of *ampDh3* (blue). This allows AlpA to load onto RNAP and allows it to read over the intrinsic terminator that is located upstream of the CDS of *ampDh3*. This results in transcription of the *ampDh3*-gene. **c)** YgfB interacts directly with AlpA. This prevents AlpA from binding to the ABE and from facilitating antitermination. Presence of YgfB thus reduces the levels of AmpDh3 by inhibiting the antitermination activity of AlpA. The figure was adapted and modified from Fig. 7 in Peña et al. (2021) under CC BY 4.0 (https://creativecommons.org/licenses/by/4.0/).

As the mechanism of antitermination by AlpA for the *alpBCDE* genes should theoretically be identical as for *ampDh3*, expression of *alpBCDE* could be expected to also be controlled by YgfB. Indeed, in the differential expression analysis using RNAseq comparing ID40Δ*ygfB* and ID40 done in Eggers et al. (2023), the *alpBCDE* genes were upregulated upon deletion of *ygfB*. Attempts to validate these data by RT-qPCR were, however, unsuccessful. Additionally, a pilot experiment not shown in this work using an *alpB* promoter fused to NanoLuc showed no increased *alpB* promoter activity upon deletion of *ygfB* in ID40. The promoter activity of *alpB* was, however, increased in the *P. aeruginosa* strains PAO1, ID72 and ID143, suggesting potential strain by strain differences. Furthermore, the EMSA was repeated in the same manner as it was shown in this work but using the *alpB* promoter as a probe. Here, similar results to the *ampDh3* probe were observed, suggesting a potential effect of YgfB also on *alpB*. As these experiments were not in the scope of this project, focusing mainly on *ampDh3* and the influence

on resistance, no further follow-up experiment was performed. Due to a limited number of repetitions, they were not shown in this work and do not provide enough evidence to make any claims on the effect of YgfB on *alpB*. Nevertheless, it might remain interesting to investigate how the regulation of *alpBCDE* and *ampDh3* by YgfB differs and if there are any factors mediating potential differences. Additionally, it would be interesting to determine the molecular basis of potential differences in transcriptional activity of the *ampDh3* and *alpB* promoter.

Cai et al. (2022) have found that *ampDh3*-PA0808 and the genes *alpDE* are positively regulated by the extracytoplasmic function sigma factor (ECFσ) HxuI in PAO1. This sigma factor is highly conserved in *P. aeruginosa* and part of the Hxu cell-surface-signaling pathway that has recently been described to be part of the response to host heme molecules (Cai et al., 2022; Otero-Asman et al., 2019). *hxuI* mRNA levels were also increased upon exposure to various host stress conditions such as iron limitation, oxidative stress by H_2O_2, anoxic conditions or nitric oxide stress conditions (Cai et al., 2022). To identify genes regulated by the Hxu system, Cai et al. (2022) performed RNAseq using an *hxuI* overexpression construct in PAO1. Among metabolic and virulence pathways important for infection of the host, the regulon of HuxI includes the *ampDh3* operon as well as the genes *alpDE* as part of the *alpBCDE* operon. These findings were validated using promoter-*lacZ* fusion constructs. Interestingly, a *lacZ*-fusion of the DNA sequence 500 bp upstream of the *alpD* CDS showed increased galactosidase activity upon *hxuI* overexpression, suggesting a promoter of the *alpDE* genes that is independent of the *alpB* promoter (Cai et al., 2022; Peña et al., 2021). In addition, overexpression of *hxuI* increased colonization of PAO1 in several murine infection models, including a murine sepsis model (Cai et al., 2022; Yang et al., 2022).

How HxuI regulates *ampDh3* and *alpDE,* and if it also regulates the complete *alpBCDE* operon is so far unknown. Cai et al. (2022) were able to define a consensus sequence for a HxuI-binding site in several promoters, however, the promoters of *ampDh3* and *alpDE* do not contain this consensus sequence, suggesting indirect regulation. As AlpA regulates both the *ampDh3* operon and the *alpBCDE* operon by antitermination (Peña et al., 2021), it might be interesting to see if the response of these genes to Hxu inductors is dependent on *alpA* or regulated independently. As AlpA activity is stimulated by the stringent response (Peña et al., 2021), genes of the HxuI regulon might modulate AlpA activity in a similar way or even via the stringent response itself, therefore facilitating increased antitermination. As we have shown that YgfB represses *ampDh3* expression and potentially *alpBCDE* expression by interacting with AlpA, it would be interesting to study if YgfB modulates the Hxu response of these genes. In addition,

it might be possible that regulation by HxuI takes place at the second, AlpA- and YgfB-unregulated promoter of *ampDh3* described in 1.4.3. As *ampDh3* and *ygfB* play a role in *ampC* overexpression, Hxu inductors might also reduce β-lactam resistance in AmpC overexpressing strains such as ID40.

4.1.2. The role of YgfB in combination of β-lactam antibiotics and ciprofloxacin

Combinations of β-lactam antibiotics with other antibiotics have been used empirically in the treatment of drug resistant *P. aeruginosa* strains (Johnson et al., 2011). In recent times, combination therapy has, however, been subject of debate with respect to its efficacy (Paul et al., 2004; Paulsson et al., 2017; Tamma et al., 2012; Vardakas et al., 2013) and, in the case of ciprofloxacin, could even been associated with increased emergence of drug resistant strains (Vestergaard et al., 2016).

As YgfB inhibits a potential synergistic pathway for the combination of β-lactam antibiotics, i.e. the DNA damage-induced activation of *ampDh3* production via AlpA leading to hypothetically reduced *ampC* expression and YgfB inhibiting the activity of AlpA, we investigated the role of *ygfB* in antibiotic combinations.

Initially, to study the effect of ciprofloxacin on the resistance to β-lactam antibiotics in ID40, MIC assays in combination with one fixed concentration of ciprofloxacin were done (3.2.1). This concentration was chosen in a way to approximate the area under the concentration-time curve of the serum concentration of ciprofloxacin over 24 hours in steady-state ($AUC_{(0\text{-}24h),ss}$) that could be found in some patients, resulting in the used concentration of 2.5 µg/ml ciprofloxacin. This concentration is obviously just an approximation for *in vitro* studies and is unlikely to reflect on pharmacodynamics and kinetics taking place in the actual human body.

To then gain further insights into the relationship between β-lactam antibiotics and ciprofloxacin, checkerboard assays were done (3.2.2). These assays allow studying the effect of two antibiotics on the growth inhibition in different concentration and can be used to quantify antibiotic combinations into synergistic, additive, indifferent and antagonistic based on the fraction inhibitory coefficient index (FIC index) (Berenbaum, 1978). The calculation of the FIC index is described in 2.2.6, but in short, the FIC index is a measurement of the degree of combinatory effect, whereas a lower value indicates a higher combinatory effect. For classification of FIC indices we applied the following cutoffs in accordance with previous studies (Sopirala et al., 2010; Walsh et al., 1995; White et al., 1996): FIC index ≤ 0.5: synergism, FIC index between

> 0.5 and ≤ 1: additive effect, FIC index between > 1 and ≤ 4: indifferent effect, and FIC index > 4: antagonism.

Combination of commonly used antipseudomonal β-lactam antibiotics with ciprofloxacin led to a dose-dependent reduction of resistance to β-lactam antibiotics. The effect on reduced resistance by addition of ciprofloxacin was not or only weakly affected by deletion of *ampDh3* or *alpA* in a wildtype background, suggesting that the AlpA-AmpDh3 pathway is not relevant for antibiotic crosstalk in the wildtype. In a *ygfB* deletion strain, combination of ciprofloxacin with β-lactams reduced resistance to all tested antibiotics in an *alpA*- and *ampDh3*-dependent manner as the effect of *ygfB* deletion was nullified upon additional deletion of *alpA* and *ampDh3*. Therefore, subinhibitory levels of ciprofloxacin can reduce the resistance to several β-lactam antibiotics in ID40, even breaking resistance in high enough concentrations. In absence of *ygfB*, this effect was partially mediated by the AlpR-AlpA pathway, but presence of *ygfB* seemed to be a factor preventing combinatory effects of β-lactam antibiotics and ciprofloxacin in ID40.

For none of the combinations and strains, except for aztreonam and ciprofloxacin, where Δ*ygfB* itself already broke resistance towards aztreonam, it was possible to break resistance towards both combinations of antibiotics at once (e.g. a combination of 8 µg/ml of ceftazidime and 0.5 µg/ml of ciprofloxacin would inhibit growth) by deletion of *ygfB*. This highlights that while the DNA damage induced pathway of AlpA leading to increased AmpDh3 production is a potential pathway of a combined action of ciprofloxacin and β-lactams, and this pathway is inhibited by *ygfB*, the effect of *ygfB* deletion on cross-resistance in ID40 is not large enough to sensitize ID40 to this antibiotic combination.

The FIC indices calculated for the different combinations varied between additive (>0.5, imipenem and piperacillin in ID40 wildtype) and synergistic (≤0.5, ceftazidime and aztreonam in ID40 wildtype). Deletion of *ygfB* reduced the FIC indices in the combinations of ciprofloxacin with imipenem and piperacillin in an *ampDh3*-dependent manner. The effect was furthermore dependent on *alpA* in the imipenem/ciprofloxacin combination. While one might interpret these results as *ygfB* preventing synergism of imipenem/aztreonam in combination with ciprofloxacin, the FIC indices likely vary too much for an appropriate interpretation.

Next to the potential cross resistance mechanism mediated by YgfB, other cross resistance pathways in *P. aeruginosa* might exist. One of these factors is, for example, overexpression of the

mexEF-oprN regulator *mexT*. As described above, fluoroquinolones are substrates of these efflux pumps. In addition, *mexT* negatively regulates the porin *oprD* that is important for the entry of carbapenems (Köhler, Epp, et al., 1999; Maseda et al., 2000; Ochs et al., 1999). *mexT* is therefore a potential cross-resistance factor to a combination of imipenem and ciprofloxacin. Unpublished data of our group did not experimentally confirm this notion in ID40, however, there is also no alteration in *mexT* or its promoter in ID40 in comparison to PA14 and *mexT* is also not overexpressed.

As ciprofloxacin likely induces several error prone polymerases in *P. aeruginosa* (Cirz et al., 2006), exposure to subinhibitory levels of ciprofloxacin over a longer period has been associated with a higher rate of mutator strains (Wassermann et al., 2016), and combinations of ciprofloxacin and β-lactam antibiotics were described to select for MDR strains (Vestergaard et al., 2016). The gained knowledge of these experiments is obviously limited to basic research and understanding regulatory connections in *P. aeruginosa*. The actual feasibility of trying to resensitize β-lactam resistant *P. aeruginosa* strains by combining a β-lactam with ciprofloxacin and a *ygfB* inhibitor is therefore limited by potential emergence of resistance, increased toxicity in a patient exposed to polypharmacy and also simply a lack of effect strength.

4.1.3. Working model of the role of *ygfB*

Tying together the data generated in this study regarding the molecular regulation of *ampDh3* by YgfB and regarding the effects of ciprofloxacin on β-lactam resistance with the data generated previously, it was possible to generate a working model of the action of YgfB and how it affects the crosstalk between ciprofloxacin, AmpDh3 and AmpC.

In the absence of YgfB, AlpA is able to bind to the ABE on the *ampDh3* promoter. This results in antitermination, leading to expression of *ampDh3*. Increased levels of AmpDh3 facilitate increased degradation of anhMurNAc-peptides by cleaving off the peptide stem from the muropeptides, yielding anhMurNAc and peptide. This changes the balance between anhMurNAc-peptides and UDP-MurNAc-5P towards the UDP-MurNAc-pentapeptide side. Both anhMurNAc-peptides and UDP-MurNAc-5P can bind to AmpR, but binding of anhMurNAc-peptides to AmpR stimulates *ampC* expression while binding of UDP-MurNAc-5P represses *ampC* expression. Consequently, increased levels of AmpDh3 result in reduced *ampC* production.

If YgfB is present, AlpA is bound by YgfB and can no longer bind to the ABE on the *ampDh3* promoter. This results in reduced *ampDh3* expression as the RNAP can no longer read over the intrinsic terminator in the *ampDh3* promoter. Reduced levels of AmpDh3 lead to an accumulation of anhMurNAc-peptides and activation of *ampC* expression by increased interaction of

anhMurNAc-peptides with AmpR. As a result, AmpC levels and thereby β-lactam resistance is increased.

The expression of AlpA is stimulated by DNA damage that can be induced by ciprofloxacin (McFarland et al., 2015; Peña et al., 2021) . The repressor of AlpA, AlpR, is autocleaved upon DNA damage and AlpA is derepressed. This results in increased expression of *ampDh3* and in reduced resistance to β-lactam antibiotics, potentially by downregulation of *ampC*. YgfB seems to have a dampening role in this pathway, potentially blocking overboarding activity of AlpA that might result in unfavorable outcomes.

Figure 31 depicts a graphic representation of the working model generated.

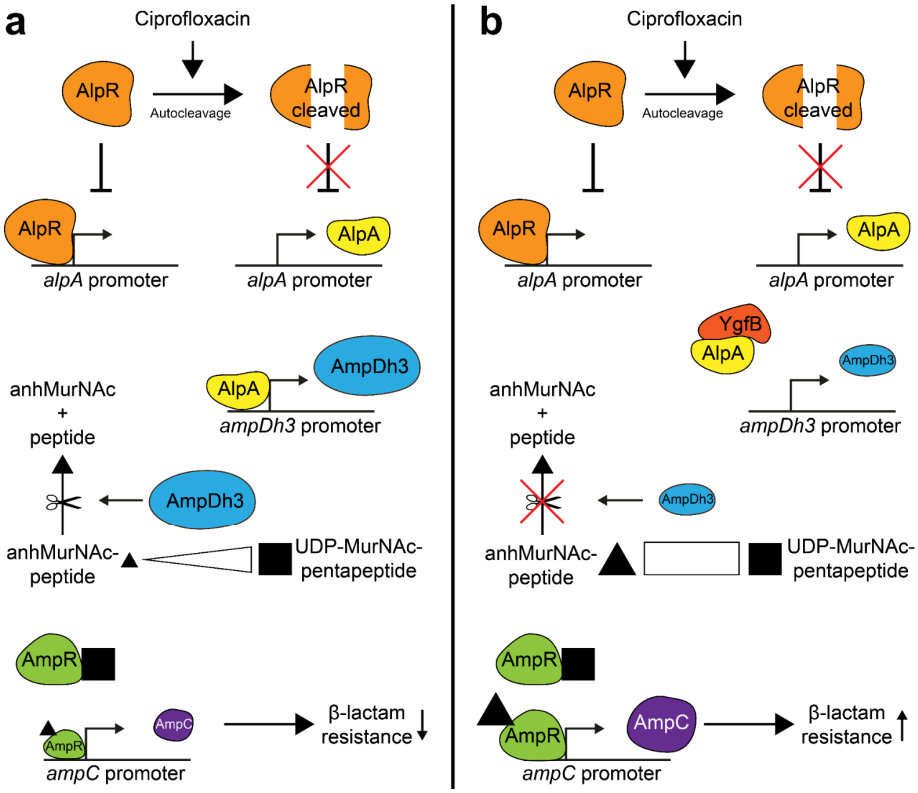

Figure 31: Working model of the role of YgfB. a) In the absence of YgfB, AlpA is able to bind to the promoter of *ampDh3* and induce expression of *ampDh3* by antitermination. Ciprofloxacin induces the autocleavage of AlpR which leads to derepression of the *alpA* promoter, thereby inducing production of AlpA and downstream, of AmpDh3. Increased levels of AmpDh3 lead to degradation of anhMurNAc-peptides by cleaving off the peptide chain, changing the balance between the anhMurNAc-peptides and UDP-MurNAc-pentapeptides towards UDP-MurNAc-pentapeptides. As anhMurNAc-peptides activate *ampC* expression by binding to AmpR and UDP-MurNAc-pentapeptides repress *ampC* expression by binding to AmpR, increased levels of AmpDh3 change the ratio of *ampC* activation and repression towards repression, resulting in reduced *ampC* levels and reduced β-lactam levels. **b)** YgfB interacts directly with AlpA, preventing it from binding to the *ampDh3* promoter. This results in reduced antitermination by AlpA and therefore reduced levels of AmpDh3. anhMurNAc-peptides accumulate and change the balance in favor of *ampC* activation. AmpC levels increase and the resistance to β-lactam antibiotics is increased. The figure was adapted and modified from Eggers et al. (2023) under CC BY 4.0 (https://creativecommons.org/licenses/by/4.0/).

Overall, the model of AlpA-mediated regulation of *ampDh3* by YgfB and the downstream effects on AmpC and resistance seem relatively watertight. The effect of ciprofloxacin on *ampC*

expression downstream is, however, only made by inference and by the observed effect on resistance to β-lactam antibiotics. In the transcriptomic experiment, no downregulation of *ampC* upon exposure to ciprofloxacin could be observed neither in the wildtype nor *ygfB* deletion background. These results challenge the proposed effect of ciprofloxacin in the working model. The finding of an *ampDh3/alpA*-dependent effect on crosstalk between ciprofloxacin and β-lactam antibiotics in a *ygfB* deletion background could potentially be explained by auxiliary effects of an overactive AlpA leading to increased cell death. It would therefore be imperative to show the relationship between ciprofloxacin and *ampC* expression by another method such as RT-qPCR to finally establish if there is an actual link between ciprofloxacin and *ampC* expression. The shown data links cell wall recycling with the programmed cell death and DNA damage via the AlpA-AmpDh3 regulation. As the Alp-pathway and AmpDh3 have been implicated in virulence (McFarland et al., 2015; Moya et al., 2008), deletion of *ygfB* and the effect of ciprofloxacin might affect colonization of the host somehow.

We propose that AmpDh3 is active in the cytoplasm, acting as a secondary amidase next to AmpD. AmpDh3 was described to locate to the cytoplasm and to preferentially degrade cell wall-bound muropeptides based on data generated using synthetic substrates (Lee et al., 2013; Zhang et al., 2013). However, data by our group and others have shown that AmpDh3 is likely localized in the cytoplasm (Colautti et al., 2023; Eggers et al., 2023). The effect of *ygfB* deletion on resistance of ID72 and ID143 was much more pronounced than in ID40 (3.1.4). The common difference between ID72 and ID143 in comparison to ID40 is that both strains carry potentially inactivating mutations in the *ampD* gene while *ampD* of ID40 is intact. Although ID72 and ID143 carry other mutations associated with *ampC* overexpression, *ampC* might be stably overexpressed at least in part due to the *ampD* mutation in both strains. If AmpDh3 levels are increased upon deletion of *ygfB*, the effect on reduction of resistance might be larger in ID72 and ID143 because AmpDh3 would be the sole amidase degrading anhMurNAc-peptides present in the cytosol, while in ID40 AmpDh3 acts secondary to AmpD in the cytosol and only takes on additional degradation roles, leading to smaller effects upon changes in abundance, underlining a role for AmpDh3 as a secondary amidase.

As it was described that the carbapenems meropenem and imipenem are stable to hydrolysis by AmpC, one might wonder how deletion of *ygfB* reduces the resistance towards these antibiotics. Earlier data has shown that resistance to imipenem is caused by a combination of loss of OprD, the porin responsible for the entry of carbapenems into the periplasm, and presence of AmpC

(Livermore, 1992). Mutational loss of *oprD* only conferred resistance if AmpC was present, highlighting the importance of the β-lactamase in imipenem resistance (Livermore, 1992) and that an interplay between the porin and AmpC is mandatory for resistance to imipenem.

An indirect positive regulation of the porin *oprD,* by AmpR negatively regulating *mexT,* was described by Balasubramanian et al. (2012). This putative regulation was independent of *ampC*-inducing conditions by exposure to penicillin G, suggesting muropeptide-independent regulation of *mexT* by AmpR. Using penicillin G as an AmpR activator is questionable due to the intrinsic resistance of *P. aeruginosa*, which is likely mediated by impermeability of the outer membrane (Suginaka et al., 1974, 1975). However, at the very high concentration of penicillin G used by Balasubramanian et al. (2012) (100 µg/ml), some drug might be able to cross the outer membrane and act as an inducer. As this potential crossregulation is independent of muropeptides, this data is likely irrelevant in the interplay between AmpC and OprD.

Another cause for an increased resistance spectrum of ID40 might be the AmpC T105A variant (PDC-3) found in ID40 (Sonnabend et al., 2020). This variant was described to lead to an extended spectrum of AmpC, increasing the catalytic efficiency for imipenem, piperacillin, and cefepime 10-fold, 6.25-fold and 15-fold respectively (Rodríguez-Martínez et al., 2009).

Zamorano et al. (2010), however, were not able to link AmpC polymorphisms to increased resistance to imipenem, cefepime, or meropenem, as they were able to demonstrate that these polymorphisms are also present in susceptible strains such as PA14 and the resistance of these strains to either of the antibiotics was not affected by the polymorphism. It might be possible that the effect of *ygfB* on the carbapenems can simply be explained by AmpC being able to hydrolyze carbapenems at very high enzyme concentrations, which are present in derepressed strains such as ID40. However, Zamorano et al. (2010) also found that deleting *dacB* or *ampD* to cause stable overexpression of *ampC* in susceptible strains with either wildtype or extended spectrum AmpC did not affect the resistance to imipenem or meropenem, while cefepime was affected. This suggests no effect of *ampC* overexpression or AmpC variants on carbapenem resistance.

Together, there is likely a large strain-by-strain variation in factors mediating resistance. The resistance to imipenem and reduced susceptibility to meropenem of ID40 is likely caused by a combination of *ampC* overexpression and reduced *oprD* expression (unpublished data of our group), but changing the A105 in AmpC of ID40 back to threonine to match the PAO1 AmpC and studying the effect of *ampC* deletion in ID40 might nevertheless give further insights into the role of the PDC-3 AmpC variant in ID40 and how resistance to carbapenems is affected by AmpC in ID40.

Another open question is, if and how *ygfB* is regulated in *P. aeruginosa*. So far, even identification of a promoter of *ygfB* in ID40 was unsuccessful. Additionally, expression levels of *ygfB* do not differ between the resistant strains ID40, ID72 and the susceptible strains PA14 and PAO1 (unpublished data of our group). Identifying a promoter of *ygfB* and finding potential regulators could provide further information on how *ygfB* affects resistance in *P. aeruginosa*. Even if a promoter was identified, it might also be possible that *ygfB* is simply constitutively expressed and not regulated. In this case, it might solely function as a repressor of overactive cellular responses and the effect of YgfB on β-lactam resistance might be merely a byproduct of this repression.

All in all, these results highlight the complicated and highly regulated pathways of resistance in *P. aeruginosa* and provide a new player in β-lactam resistance and potentially cross-resistance to fluoroquinolones. Unraveling these pathways and how they change by mutations in MDR clinical isolates is key to better understanding resistance of *P. aeruginosa* and to the development of new therapeutics to combat the gigantic threat of multi drug resistance in the post-antibiotic age.

4.2. The further cellular role of YgfB in *P. aeruginosa* and *E. coli*

As homologs of YgfB are found in many γ-proteobacteria while AlpA is found in no other species and AmpDh3 is found rather rarely, we sought to identify additional roles of YgfB in *P. aeruginosa* and *E. coli*. In addition, *E. coli* does not carry an *ampR* gene and *ampC* is not inducible in this species (Honoré et al., 1986). This suggested that there are other functions of YgfB in γ-proteobacteria that are unrelated to *ampC* expression and β-lactam resistance.
We hypothesized that *ygfB* might play a role in modulating the response to DNA damage and ciprofloxacin and that the limited transcriptomic response we initially observed in ID40 upon deletion of *ygfB* might be explained by the main regulation of *ygfB* taking place only under DNA damage-induced conditions. To answer these questions, we used transcriptomic analysis comparing *ygfB* deletion strains in *P. aeruginosa* ID40 and *E. coli* BW25113 with the respective wildtypes in the presence of non-induced or ciprofloxacin-induced DNA damage.

4.2.1. The transcriptomic response to *ygfB* and the *ygfB* modulated ciprofloxacin response

Repetition of the transcriptomic analysis of the ID40Δ*ygfB* and the ID40 wildtype resulted in different differentially expressed genes than before (3.3.1.1). As before, *ampDh3* was strongly upregulated upon deletion of *ygfB*, while *ampC* was non-significantly downregulated. In addition, the other genes identified previously were also regulated in the same direction as in the previous experiment but non-significantly. Novel significant differentially expressed genes comprised the genes *cefD_2*, *yjjL, mntH2,* and TUEID40_01950. Interestingly, these genes were also differentially expressed in the transcriptome done by Peña et al. (2021) as a response to ectopic overexpression of *alpA*. This suggests that *ygfB* might be a potential factor preventing overactivity of AlpA that could lead to toxic effects.

Analysis of the ciprofloxacin response of ID40 reflected the response of PAO1 to ciprofloxacin found before (Cirz et al., 2006), with most genes being part of the SOS-response or part of the DNA damage response (3.3.1.1). Interestingly, all genes that were upregulated by deletion of *ygfB* were also upregulated upon exposure to ciprofloxacin. Analysis of the *ygfB*-modulated response to ciprofloxacin yielded no differentially expressed genes except *ygfB*. Nevertheless, the expression of all *ygfB* regulated genes was slightly, non-significantly increased in a *ygfB* deletion background exposed to ciprofloxacin compared to the wildtype exposed to ciprofloxacin.

All *ygfB*-repressed genes therefore followed the trend that was also observed for AmpDh3 on the protein level (Figure 11, page 97). Together with the fact that *ygfB* repressed genes are also affected by AlpA overexpression (Peña et al., 2021), this provides further evidence that *ygfB* likely represses the activity of AlpA.

Surprisingly, *ampC* was not differentially expressed upon exposure to ciprofloxacin, neither in the wildtype nor *ygfB* deletion background, which questions the validity of the working model presented in 4.1.3.

Potentially, the concentration of ciprofloxacin used for induction of DNA damage was too low. In their experiment, Cirz et al. (2006) exposed PAO1 to 8x the MIC of ciprofloxacin for 2 hours, while the concentration used in our experiments (32 µg/ml) corresponded to 4x the MIC of ID40 towards ciprofloxacin. As described in 1.2.2, the effect of ciprofloxacin-induced DNA damage is supposedly dose-dependent, with lower concentrations leading to a slow death by inhibition of gyrase function and higher concentrations leading to gyrase poisoning and a fragmented genome (Bush et al., 2020; Carret et al., 1991; Drlica et al., 2008). Torres-Barceló et al.

(2015), however, also observed activation of the SOS-response at subinhibitory concentrations, suggesting that DNA damage is induced even at lower concentrations of ciprofloxacin. As the observed differentially expressed genes in the ciprofloxacin exposed condition vs. the unexposed condition matched previously described genes, the dose of ciprofloxacin was likely appropriate and there is simply no *ygfB*-modulated response to ciprofloxacin in ID40.

In *E. coli*, no effect of *ygfB* could be observed (3.3.1.2). While in the used BW25113Δ*ygfB* strain the flagella regulon was upregulated due to an insertion element in the *flhDC* gene (Parker et al., 2019), no other genes were differentially expressed upon deletion of *ygfB*. Similarly, to previous studies, the ciprofloxacin response included genes of the SOS-response and DNA repair (Bie et al., 2023; Sun et al., 2020). As in ID40, no *ygfB* modulated ciprofloxacin response could be observed in BW25113. The sole differentially expressed gene *pepP* lies downstream of *ygfB* in the same operon and we therefore figured that the differential expression was likely caused by the mutagenesis process itself.

In all the transcriptomic experiments, barely any downregulated genes were found and many genes that were less abundant or more abundant were non-significant. This might suggest that there could have potentially been a technical problem during the sequencing that affected the resolution of the sequencing. Due to this, it might be possible that some potential candidates were missed. Additionally, the BW25113Δ*ygfB* strain could have been a problem due to the upregulated flagella regulon masking the readout. Even though the data analysis was repeated with the flagella genes excluded, repetition of the RNAseq experiment itself using the in-frame deletion strain that was generated for the following experiments could provide additional clues on a potential effect of *ygfB* in *E. coli.*

4.2.2. The interactome of YgfB in *P. aeruginosa* and *E. coli*

As the main function of *ygfB* in *P. aeruginosa* and *E. coli* is likely not a transcriptional regulation and because the interaction of YgfB and AlpA had been shown to be likely causal for the repression of *ampDh3*, we hypothesized that YgfB exerts its function by interacting with other proteins and regulating cellular processes in this way. Pulldown assays using recombinant GST-tagged YgfB derived either from *P. aeruginosa* ID40 or *E. coli* BW25113 as a bait and cell lysates of *ygfB* deletion mutants of either strain as prey were done, and the interacting protein fraction analyzed by mass-spectrometry (3.3.2). In total, 118 potential interaction partners of YgfB in ID40 and 41 interaction partners in BW25113 could be identified.

4. Discussion

In *P. aeruginosa*, these were mostly proteins that play a role in DNA repair. Surprisingly, AlpA that was identified previously as an interaction partner, was not among the potential interactors of YgfB. A protein-fragment complementation assay (PCA) using a split-luciferase in which one part of the luciferase (SmBiT) was fused to YgfB and the other one (LgBiT) to a potential interacting protein was used as a follow-up screen to validate interactions partners. Three interactors could be validated in an initial screen, namely UvrB, RpsE and WaaC (Figure 26).
In *E. coli*, the interactome of YgfB mostly pertained to proteins involved in the biogenesis of LPS. The statistical analysis of the *E. coli* pulldown LFQ data had to be modified in comparison to that of ID40, as contaminants that might have been present due to the purification process of the bait protein in *E. coli* BL21 could not simply be excluded based on species. It might therefore be possible that potential interacting proteins have been lost during the analysis, explaining why only 41 potential interactors were found in BW25113 while 118 were found in ID40.
To further gain insights into the generalized role of YgfB in *P. aeruginosa* and *E. coli*, the interactomes of YgfB in both species were then compared to identify proteins that interacted with YgfB in both species. These were in total ten proteins (EttA, HemL, HflD, IbpA, Lon, AsrA (an alternative Lon protease in *P. aeruginosa*), LpxB, RpoC, UbiB, and WaaC). All these common interacting proteins were tested by PCA in *P. aeruginosa* (Figure 29). Of these ten, the proteins HflD, UbiB, and HemL were identified as new interactors, with WaaC having been identified previously.
Therefore, in total, six interacting proteins of YgfB in *P. aeruginosa* could be identified in the pulldown-MS approach: UvrB, RpsE, WaaC, HflD, UbiB, and HemL. UvrB and RpsE were found only in ID40, while the others were part of the interactome of both ID40 and BW25113. No inference whether this is a direct or indirect interaction could be made from this screen, however.

UvrB is part of the nucleotide excision repair (NER) that is mainly important for repairing interstrand cross links and bulky DNA adducts resulting from UV-irradiation, but can also repair other DNA-lesions (Verhoeven et al., 2002; reviewed in Wozniak & Simmons, 2022). The NER is carried out by four proteins, UvrA, UvrB and UvrC, and UvrD. $UvrA_2$ dimers recognize DNA-lesions and binds an $UvrB_2$ dimer, forming a tight complex with the damaged DNA (Case et al., 2019; Pakotiprapha et al., 2012). $UvrA_2$ leaves the complex and UvrC is recruited to the $UvrB_2$-DNA-complex. UvrC makes two incisions upstream and downstream of the DNA-lesion, allowing UvrD to remove the lesion, with the gap finally being filled by DNA polymerase (Kraithong et al., 2021; Lin & Sancar, 1990, 1992).

YgfB of *Haemophilus influenzae* was also described to form a dimer (Galkin et al., 2004). An interaction of a potential YgfB dimer with UvrB might affect the interaction of $UvrB_2$ and $UvrA_2$ or $UvrB_2$ and UvrC, regulating the NER in this way somehow. Interestingly, UvrA also appeared in the interactome of *P. aeruginosa* YgfB, although this protein was not tested in the PCA. Therefore, it might be possible that YgfB binds to either of the proteins during the initial formation of the DNA damage recognizing tetramer. Therefore, testing UvrA in a PCA to test for a potential interaction might provide further clues on the impact of YgfB on NER. In addition, testing for a direct protein-protein interaction using pulldown assays with recombinant proteins might give clues on which protein of the $UvrA_2B_2$ tetramer interacts with YgfB.

NER was described to be involved in higher mutation rates in *B. subtilis* (Million-Weaver et al., 2015). We hypothesized that an interaction of YgfB with UvrA or UvrB might affect the mutation rate of ID40 and therefore measured the frequency of mutation to streptomycin. Deletion of *ygfB* did not affect the mutation frequency of ID40. There is a difference between the mutation frequency and mutation rate, however, as mutation frequency represents the number of mutants in a culture at a particular time point, while mutation rate reflects the likelihood of a particular cell acquiring a mutation in its lifetime (Pope et al., 2008). Measurement of the mutation rate offers the benefit of being more robust to jack-pot mutations (Luria & Delbrück, 1943) and giving more insight into biological processes (Rosche & Foster, 2000), but requires a much higher effort and special assay design in comparison to the relatively simple measurement of the mutation frequency. Therefore, to initially test if clues for an altered mutation rate was present in ID40 upon deletion of *ygfB,* mutation frequency measurement was done (Figure 27a). As this did not seem to be the case, no follow-up studies were done.

Next to an effect on mutation rate, UvrB was also implicated in persister formation in *E. coli* as the cells rely on NER to repair accumulated oxidative DNA damage (Wilmaerts, Govers, et al., 2022). No change in persister formation upon deletion of *ygfB* was observed in ID40 (Figure 27b) or BW25113, however (data not shown). The actual role of the interaction of YgfB with the NER is therefore so far elusive.

RpsE or small ribosomal subunit S5 is a ribosomal protein that is part of the 30S subunit of the ribosome. Together with S3 and S4, S5 forms the entry pore for the mRNA into the ribosome (Schluenzen et al., 2000; Takyar et al., 2005; Wilson & Nierhaus, 2005). Mutations in the subunits S4 and S5 were associated with reduced translational fidelity and accuracy, suggesting a role in the same (Agarwal et al., 2015; Kirthi et al., 2006; Takyar et al., 2005). As YgfB also potentially interacts with other ribosomal proteins of the 30S and 50S subunit in both ID40 and BW25113, it might be possible that YgfB just binds somewhere to the ribosome and not directly

to the S5 subunit. Further studies into the role of YgfB in the ribosome and if it regulates some processes thereof are warranted before any interpretation can be made.

WaaC, also called RfaC in *E. coli,* is a glycosyltransferase important for the synthesis of the LPS inner core. WaaC catalyzes the addition of the first heptose moiety to Kdo_2-Lpid A (Lipid A that is functionalized by addition of two 3-deoxy-d-manno-octo-2-ulosonic acid moieties) (Chen & Coleman, 1993; de Kievit & Lam, 1997; Gronow et al., 2000; Kadrmas & Raetz, 1998), and therefore plays an integral role in the initial synthesis step of inner core biogenesis. Deletion of *waaC/rfaC* leads to truncated LPS and emergence of the deep-rough phenotype in *E. coli* (Brabetz et al., 1997). Such deep-rough mutants exhibit increased susceptibility to sodium dodecyl sulfate (SDS), bile salts and hydrophobic antibiotics in *E. coli* (Møller et al., 2003). In *P. aeruginosa*, deletion of *waaC* was not successful (de Kievit & Lam, 1997), however, strains with deep rough phenotypes do exist in *P. aeruginosa* and they were described to exhibit increased susceptibility to polymyxin (Yokota & Fujii, 2007). ID40Δ*ygfB* interestingly shows a slightly increased susceptibility to colistin, an antibiotic of the polymyxin group, in comparison to the wildtype (Sonnabend et al., 2020). The effect of an interaction of YgfB with WaaC/RfaC might be the underlying reason for this effect, but this requires further investigation in membrane hydrophobicity, permeability, and resistance to polymyxins. Next to WaaC/RfaC, also many other proteins that play a role in LPS were identified as interactors in ID40 and BW25113, providing clues that this cellular function might be of interest for further studies.

Another biosynthetic enzyme is the *hemL*-encoded glutamate-1-semialdehyde 2,1-aminomutase (GSA-AM). GSA-AM plays an important role in the early synthesis of porphyrin and heme. In particular, GSA-AM forms a complex with the glutamyl-tRNA reductase (GluTR) to synthesize 5-aminolevulinic acid, a precursor of tetrapyrrole, from the glutamyl-tRNA (Luer et al., 2005). The biosynthesis of heme is highly regulated by protein-protein interactions (Zamarreño Beas et al., 2022), but clues for a potential involvement of YgfB are so far lacking.

Not much is known about the function of UbiB in bacteria, except that it is a probable protein kinase and that in *E. coli* it has been described to be part of the first monooxygenation of octaprenylphenol as part of the biosynthesis of ubiquinone (Poon et al., 2000). The UbiB superfamily comprises an ancient kinase family that is present in bacteria, archaea, and eukaryotes (Leonard et al., 1998). However, experimental kinase activity of UbiB superfamily proteins and the role in ubiquinone biosynthesis have been rather elusive. Stefely et al. (2015) have shown that in mitochondria, the UbiB protein ADCK3 adopts a protein kinase-like (PKL) fold, but that certain parts of the structure lead to autoinhibition of kinase activity. Therefore, the exact role of UbiB in ubiquinone synthesis remains unclear. Interestingly, YgfB lies in an operon with the

genes *ubiI* and *ubiH*, both of which have also been associated with ubiquinone biosynthesis (Hajj Chehade et al., 2013; Young et al., 1973). An involvement of YgfB in ubiquinone biosynthesis might therefore be at least imaginable.
In *E. coli*, HflD was described to take part in degradation of the lambda CII protein, a transcriptional factor for lysogenization of the phage lambda, and therefore negatively regulating lysogenization of the phage (Kihara et al., 2001). As the Alp operon was described to be phage derived (Peña et al., 2021), this might be a link to YgfB.
The protein set that interacts with YgfB in *P. aeruginosa* so far is rather diverse. Three are involved in metabolic pathways (WaaC, UbiB, HemL), two in transcriptional regulation (AlpA, HflD), one in DNA repair (UvrB) and one in translation (RpsE).
The LgBiT-fusions of HemL, UbiB and HflD showed lower relative luciferase activity compared to UvrB, RpsE and WaaC and therefore the actual status as an interacting protein has a higher uncertainty.

Together, the interactome provides some hints on the cellular role of YgfB in *P. aeruginosa* and in *E. coli.* However, further work is needed to understand the implications of these potential interactors. For one, the proteins that tested positive in the PCA should be tested by pulldown assays using either recombinant proteins or cell-lysates as bait to further investigate their interaction with YgfB. With this, it might be possible to differentiate between directly interacting proteins and proteins that interact as part of larger complexes.

No clear impact on cellular function as a response to YgfB interaction can be made out. The proteins that were confirmed as potential interacting proteins are very heterogeneous and no direct link to a function can be deduced from an interaction at this point. It can be hypothesized that the primary function of YgfB might consist of interacting with other proteins and thereby influencing so far unknown cellular processes, with currently unknown consequences. Furthermore, regulation of transcriptional processes by interaction as it was observed for *P. aeruginosa* does not seem to be present in *E. coli*, and therefore seems to be an exception to *P. aeruginosa* rather than the rule.

5. References

Acebrón, I., Mahasenan, K. V., De Benedetti, S., Lee, M., Artola-Recolons, C., Hesek, D., Wang, H., Hermoso, J. A., & Mobashery, S. (2017). Catalytic Cycle of the N-Acetylglucosaminidase NagZ from *Pseudomonas aeruginosa*. *J Am Chem Soc*, *139*(20), 6795-6798. https://doi.org/10.1021/jacs.7b01626

Adewoye, L., Sutherland, A., Srikumar, R., & Poole, K. (2002). The *mexR* repressor of the *mexAB-oprM* multidrug efflux operon in *Pseudomonas aeruginosa*: characterization of mutations compromising activity. *Journal of bacteriology*, *184*(15), 4308-4312. https://doi.org/10.1128/jb.184.15.4308-4312.2002

Aedo, S., & Tse-Dinh, Y. C. (2013). SbcCD-mediated processing of covalent gyrase-DNA complex in *Escherichia coli*. *Antimicrobial agents and chemotherapy*, *57*(10), 5116-5119. https://doi.org/10.1128/aac.00130-13

Aeschlimann, J. R. (2003). The Role of Multidrug Efflux Pumps in the Antibiotic Resistance of *Pseudomonas aeruginosa* and Other Gram-Negative Bacteria. *Pharmacotherapy: The Journal of Human Pharmacology and Drug Therapy*, *23*(7), 916-924. https://doi.org/https://doi.org/10.1592/phco.23.7.916.32722

Agarwal, D., Kamath, D., Gregory, S. T., & O'Connor, M. (2015). Modulation of decoding fidelity by ribosomal proteins S4 and S5. *Journal of bacteriology*, *197*(6), 1017-1025. https://doi.org/10.1128/jb.02485-14

Aires, J. R., Köhler, T., Nikaido, H., & Plésiat, P. (1999). Involvement of an active efflux system in the natural resistance of *Pseudomonas aeruginosa* to aminoglycosides. *Antimicrobial agents and chemotherapy*, *43*(11), 2624-2628. https://doi.org/10.1128/aac.43.11.2624

Aldred, K. J., Kerns, R. J., & Osheroff, N. (2014). Mechanism of quinolone action and resistance. *Biochemistry*, *53*(10), 1565-1574. https://doi.org/10.1021/bi5000564

Aly, A., Laszlo, Z. I., Rajkumar, S., Demir, T., Hindley, N., Lamont, D. J., Lehmann, J., Seidel, M., Sommer, D., Franz-Wachtel, M., Barletta, F., Heumos, S., Czemmel, S., Kabashi, E., Ludolph, A., Boeckers, T. M., Henstridge, C. M., & Catanese, A. (2023). Integrative proteomics highlight presynaptic alterations and c-Jun misactivation as convergent pathomechanisms in ALS. *Acta Neuropathol*, *146*(3), 451-475. https://doi.org/10.1007/s00401-023-02611-y

Ambler, R. P. (1980). The structure of beta-lactamases. *Philosophical transactions of the Royal Society of London. Series B, Biological sciences*, *289*(1036), 321-331. https://doi.org/10.1098/rstb.1980.0049

Antimicrobial Resistance Collaborators. (2022). Global burden of bacterial antimicrobial resistance in 2019: a systematic analysis. *Lancet*, *399*(10325), 629-655. https://doi.org/10.1016/S0140-6736(21)02724-0

Anwar, A. I., Lu, L., Plaisance, C. J., Daniel, C. P., Flanagan, C. J., Wenger, D. M., McGregor, D., Varrassi, G., Kaye, A. M., Ahmadzadeh, S., Cornett, E. M., Shekoohi, S., & Kaye, A. D. (2024). Fluoroquinolones: Neurological Complications and Side Effects in Clinical Practice. *Cureus*, *16*(2), e54565. https://doi.org/10.7759/cureus.54565

Baba, T., Ara, T., Hasegawa, M., Takai, Y., Okumura, Y., Baba, M., Datsenko, K. A., Tomita, M., Wanner, B. L., & Mori, H. (2006). Construction of *Escherichia coli* K-12 in-frame, single-gene knockout mutants: the Keio collection. *Mol Syst Biol*, *2*, 2006 0008. https://doi.org/10.1038/msb4100050

Babic, A., Guerout, A. M., & Mazel, D. (2008). Construction of an improved RP4 (RK2)-based conjugative system. *Res Microbiol*, *159*(7-8), 545-549. https://doi.org/10.1016/j.resmic.2008.06.004

5. References

Bacik, J. P., Whitworth, G. E., Stubbs, K. A., Yadav, A. K., Martin, D. R., Bailey-Elkin, B. A., Vocadlo, D. J., & Mark, B. L. (2011). Molecular basis of 1,6-anhydro bond cleavage and phosphoryl transfer by *Pseudomonas aeruginosa* 1,6-anhydro-N-acetylmuramic acid kinase. *The Journal of biological chemistry*, *286*(14), 12283-12291. https://doi.org/10.1074/jbc.M110.198317

Badet, B., Vermoote, P., Haumont, P. Y., Lederer, F., & LeGoffic, F. (1987). Glucosamine synthetase from *Escherichia coli*: purification, properties, and glutamine-utilizing site location. *Biochemistry*, *26*(7), 1940-1948. https://doi.org/10.1021/bi00381a023

Bagge, N., Ciofu, O., Hentzer, M., Campbell, J. I., Givskov, M., & Høiby, N. (2002). Constitutive high expression of chromosomal β-lactamase in *Pseudomonas aeruginosa* caused by a new insertion sequence (IS 1669) located in *ampD*. *Antimicrobial agents and chemotherapy*, *46*(11), 3406-3411.

Balasubramanian, D., Schneper, L., Merighi, M., Smith, R., Narasimhan, G., Lory, S., & Mathee, K. (2012). The Regulatory Repertoire of *Pseudomonas aeruginosa* AmpC ß-Lactamase Regulator AmpR Includes Virulence Genes. *PloS one*, *7*(3), e34067. https://doi.org/10.1371/journal.pone.0034067

Barreteau, H., Kovac, A., Boniface, A., Sova, M., Gobec, S., & Blanot, D. (2008). Cytoplasmic steps of peptidoglycan biosynthesis. *FEMS microbiology reviews*, *32*(2), 168-207. https://doi.org/10.1111/j.1574-6976.2008.00104.x

Barrick, J., Deatherage, D., & Sowa, S. (2023). *FLP Recombination in E. coli*. Retrieved 23.01.2024 from https://barricklab.org/twiki/bin/view/Lab/ProcedureFLPFRTRecombination

Bassetti, M., Vena, A., Croxatto, A., Righi, E., & Guery, B. (2018). How to manage *Pseudomonas aeruginosa* infections. *Drugs in context*, *7*, 212527. https://doi.org/10.7573/dic.212527

Battesti, A., & Bouveret, E. (2006). Acyl carrier protein/SpoT interaction, the switch linking SpoT-dependent stress response to fatty acid metabolism. *Molecular microbiology*, *62*(4), 1048-1063. https://doi.org/10.1111/j.1365-2958.2006.05442.x

Bayer HealthCare Pharmaceuticals Inc. (2021). *CIPRO® (ciprofloxacin hydrochloride) tablet, for oral use, FULL PRESCRIBING INFORMATION*. FDA.gov Retrieved 26.02.2024 from https://www.accessdata.fda.gov/drugsatfda_docs/label/2021/019537s092lbl.pdf

Bayer HealthCare Pharmaceuticals Inc. (2022). *CIPRO®IV (ciprofloxacin) injection, for intravenous use, FULL PRESCRIBING INFORMATION*. FDA.gov Retrieved 26.02.2024 from https://www.accessdata.fda.gov/drugsatfda_docs/label/2022/019847s063lbl.pdf

Bayer Vital GmbH. (2023). *Ciprobay® 400 mg, 400 mg/200 ml, Infusionslösung, Fachinformation*. fachinfo.de Retrieved 26.02.2024 from https://www.fachinfo.de/suche/fi/011730/Ciprobay%C2%AE%20400%20mg

Becker, B., & Cooper, M. A. (2013). Aminoglycoside antibiotics in the 21st century. *ACS chemical biology*, *8*(1), 105-115.

Berenbaum, M. C. (1978). A method for testing for synergy with any number of agents. *The Journal of infectious diseases*, *137*(2), 122-130. https://doi.org/10.1093/infdis/137.2.122

Bergström, S., Olsson, O., & Normark, S. (1982). Common evolutionary origin of chromosomal beta-lactamase genes in enterobacteria. *Journal of bacteriology*, *150*(2), 528-534. https://doi.org/10.1128/jb.150.2.528-534.1982

Bie, L., Zhang, M., Wang, J., Fang, M., Li, L., Xu, H., & Wang, M. (2023). Comparative Analysis of Transcriptomic Response of *Escherichia coli* K-12 MG1655 to Nine Representative Classes of Antibiotics. *Microbiology spectrum*, *11*(2), e0031723. https://doi.org/10.1128/spectrum.00317-23

5. References

Bjarnsholt, T., Tolker-Nielsen, T., Høiby, N., & Givskov, M. (2010). Interference of *Pseudomonas aeruginosa* signalling and biofilm formation for infection control. *Expert Rev Mol Med*, *12*, e11. https://doi.org/10.1017/s1462399410001420

Blázquez, J. (2003). Hypermutation as a factor contributing to the acquisition of antimicrobial resistance. *Clin Infect Dis*, *37*(9), 1201-1209. https://doi.org/10.1086/378810

Blázquez, J., Gómez-Gómez, J. M., Oliver, A., Juan, C., Kapur, V., & Martín, S. (2006). PBP3 inhibition elicits adaptive responses in *Pseudomonas aeruginosa*. *Molecular microbiology*, *62*(1), 84-99. https://doi.org/10.1111/j.1365-2958.2006.05366.x

Blighe, K., Rana, S., Lewis, M. (2024). *EnhancedVolcano: Publication-ready volcano plots with enhanced colouring and labeling*. In (Version R package version 1.14.0) https://github.com/kevinblighe/EnhancedVolcano

Borchert, N., Dieterich, C., Krug, K., Schutz, W., Jung, S., Nordheim, A., Sommer, R. J., & Macek, B. (2010). Proteogenomics of *Pristionchus pacificus* reveals distinct proteome structure of nematode models. *Genome Res*, *20*(6), 837-846. https://doi.org/10.1101/gr.103119.109

Borisova, M., Gisin, J., & Mayer, C. (2014). Blocking peptidoglycan recycling in *Pseudomonas aeruginos*a attenuates intrinsic resistance to fosfomycin. *Microbial drug resistance*, *20*(3), 231-237. https://doi.org/10.1089/mdr.2014.0036

Borisova, M., Gisin, J., & Mayer, C. (2017). The N-Acetylmuramic Acid 6-Phosphate Phosphatase MupP Completes the *Pseudomonas* Peptidoglycan Recycling Pathway Leading to Intrinsic Fosfomycin Resistance. *mBio*, *8*(2), 1-12. https://doi.org/10.1128/mBio.00092-17

Bou, G., & Martínez-Beltrán, J. (2000). Cloning, nucleotide sequencing, and analysis of the gene encoding an AmpC beta-lactamase in *Acinetobacter baumannii*. *Antimicrobial agents and chemotherapy*, *44*(2), 428-432. https://doi.org/10.1128/aac.44.2.428-432.2000

Bouhss, A., Crouvoisier, M., Blanot, D., & Mengin-Lecreulx, D. (2004). Purification and characterization of the bacterial MraY translocase catalyzing the first membrane step of peptidoglycan biosynthesis. *The Journal of biological chemistry*, *279*(29), 29974-29980. https://doi.org/10.1074/jbc.M314165200

Brabetz, W., Muller-Loennies, S., Holst, O., & Brade, H. (1997). Deletion of the heptosyltransferase genes *rfaC* and *rfaF* in *Escherichia coli* K-12 results in an Re-type lipopolysaccharide with a high degree of 2-aminoethanol phosphate substitution. *Eur J Biochem*, *247*(2), 716-724. https://doi.org/10.1111/j.1432-1033.1997.00716.x

Bucior, I., Pielage, J. F., & Engel, J. N. (2012). *Pseudomonas aeruginosa* Pili and Flagella Mediate Distinct Binding and Signaling Events at the Apical and Basolateral Surface of Airway Epithelium. *PLoS Pathog*, *8*(4), e1002616. https://doi.org/10.1371/journal.ppat.1002616

Bundesamt für Arzneimittel und Medizinprodukte. (2019). *Fluorchinolone: Schwere und langanhaltende Nebenwirkungen im Bereich Muskeln, Gelenke und Nervensystem*. Retrieved 27.04.2024 from https://www.bfarm.de/SharedDocs/Risikoinformationen/Pharmakovigilanz/DE/RV_STP/a-f/fluorchinolone-bewegungsapparat.html

Bush, K., & Jacoby, G. A. (2010). Updated functional classification of beta-lactamases. *Antimicrobial agents and chemotherapy*, *54*(3), 969-976. https://doi.org/10.1128/aac.01009-09

Bush, K., Jacoby, G. A., & Medeiros, A. A. (1995). A functional classification scheme for beta-lactamases and its correlation with molecular structure. *Antimicrobial agents and chemotherapy*, *39*(6), 1211-1233. https://doi.org/10.1128/aac.39.6.1211

5. References

Bush, N. G., Diez-Santos, I., Abbott, L. R., & Maxwell, A. (2020). Quinolones: Mechanism, Lethality and Their Contributions to Antibiotic Resistance. *Molecules*, *25*(23). https://doi.org/10.3390/molecules25235662

Cabot, G., Ocampo-Sosa, A. A., Dominguez, M. A., Gago, J. F., Juan, C., Tubau, F., Rodriguez, C., Moya, B., Peña, C., Martinez-Martinez, L., Oliver, A., & Spanish Network for Research in Infectious, D. (2012). Genetic markers of widespread extensively drug-resistant *Pseudomonas aeruginosa* high-risk clones. *Antimicrobial agents and chemotherapy*, *56*(12), 6349-6357. https://doi.org/10.1128/AAC.01388-12

Cai, Z., Yang, F., Shao, X., Yue, Z., Li, Z., Song, Y., Pan, X., Jin, Y., Cheng, Z., Ha, U. H., Feng, J., Yang, L., Deng, X., Wu, W., & Bai, F. (2022). ECF Sigma Factor HxuI Is Critical for In Vivo Fitness of *Pseudomonas aeruginosa* during Infection. *Microbiology spectrum*, *10*(1), e0162021. https://doi.org/10.1128/spectrum.01620-21

Camacho, C., Coulouris, G., Avagyan, V., Ma, N., Papadopoulos, J., Bealer, K., & Madden, T. L. (2009). BLAST+: architecture and applications. *BMC Bioinformatics*, *10*, 421. https://doi.org/10.1186/1471-2105-10-421

Cao, L., Srikumar, R., & Poole, K. (2004). MexAB-OprM hyperexpression in NalC-type multidrug-resistant *Pseudomonas aeruginosa*: identification and characterization of the *nalC* gene encoding a repressor of PA3720-PA3719. *Molecular microbiology*, *53*(5), 1423-1436. https://doi.org/10.1111/j.1365-2958.2004.04210.x

Carret, G., Flandrois, J. P., & Lobry, J. R. (1991). Biphasic kinetics of bacterial killing by quinolones. *The Journal of antimicrobial chemotherapy*, *27*(3), 319-327. https://doi.org/10.1093/jac/27.3.319

Case, B. C., Hartley, S., Osuga, M., Jeruzalmi, D., & Hingorani, M. M. (2019). The ATPase mechanism of UvrA2 reveals the distinct roles of proximal and distal ATPase sites in nucleotide excision repair. *Nucleic acids research*, *47*(8), 4136-4152. https://doi.org/10.1093/nar/gkz180

Cashel, M., & Gallant, J. (1969). Two compounds implicated in the function of the RC gene of *Escherichia coli*. *Nature*, *221*(5183), 838-841. https://doi.org/10.1038/221838a0

Chen, C. R., Malik, M., Snyder, M., & Drlica, K. (1996). DNA gyrase and topoisomerase IV on the bacterial chromosome: quinolone-induced DNA cleavage. *J Mol Biol*, *258*(4), 627-637. https://doi.org/10.1006/jmbi.1996.0274

Chen, L., & Coleman, W. G., Jr. (1993). Cloning and characterization of the *Escherichia coli* K-12 rfa-2 (rfaC) gene, a gene required for lipopolysaccharide inner core synthesis. *Journal of bacteriology*, *175*(9), 2534-2540. https://doi.org/10.1128/jb.175.9.2534-2540.1993

Chen, S. (2023). Ultrafast one-pass FASTQ data preprocessing, quality control, and deduplication using fastp. *iMeta*, *2*(2), e107. https://doi.org/https://doi.org/10.1002/imt2.107

Chen, S., Zhou, Y., Chen, Y., & Gu, J. (2018). fastp: an ultra-fast all-in-one FASTQ preprocessor. *Bioinformatics*, *34*(17), i884-i890. https://doi.org/10.1093/bioinformatics/bty560

Chen, W., Zhang, Y. M., & Davies, C. (2017). Penicillin-Binding Protein 3 Is Essential for Growth of *Pseudomonas aeruginosa*. *Antimicrobial agents and chemotherapy*, *61*(1). https://doi.org/10.1128/aac.01651-16

Cherepanov, P. P., & Wackernagel, W. (1995). Gene disruption in *Escherichia coli*: TcR and KmR cassettes with the option of Flp-catalyzed excision of the antibiotic-resistance determinant. *Gene*, *158*(1), 9-14. https://doi.org/10.1016/0378-1119(95)00193-a

Choi, K. H., Kumar, A., & Schweizer, H. P. (2006). A 10-min method for preparation of highly electrocompetent *Pseudomonas aeruginosa* cells: application for DNA fragment

transfer between chromosomes and plasmid transformation. *J Microbiol Methods*, *64*(3), 391-397. https://doi.org/10.1016/j.mimet.2005.06.001

Choi, K. H., Mima, T., Casart, Y., Rholl, D., Kumar, A., Beacham, I. R., & Schweizer, H. P. (2008). Genetic tools for select-agent-compliant manipulation of *Burkholderia pseudomallei*. *Applied and environmental microbiology*, *74*(4), 1064-1075. https://doi.org/10.1128/AEM.02430-07

Choi, K. H., & Schweizer, H. P. (2006). mini-Tn7 insertion in bacteria with single attTn7 sites: example *Pseudomonas aeruginosa*. *Nature protocols*, *1*(1), 153-161. https://doi.org/10.1038/nprot.2006.24

Ciofu, O., Riis, B., Pressler, T., Poulsen, H. E., & Høiby, N. (2005). Occurrence of hypermutable *Pseudomonas aeruginosa* in cystic fibrosis patients is associated with the oxidative stress caused by chronic lung inflammation. *Antimicrobial agents and chemotherapy*, *49*(6), 2276-2282. https://doi.org/10.1128/aac.49.6.2276-2282.2005

Cirz, R. T., O'Neill, B. M., Hammond, J. A., Head, S. R., & Romesberg, F. E. (2006). Defining the *Pseudomonas aeruginosa* SOS response and its role in the global response to the antibiotic ciprofloxacin. *Journal of bacteriology*, *188*(20), 7101-7110. https://doi.org/10.1128/JB.00807-06

Clinical and Laboratory Standards Institute, Wayne, PA. (2018). *CLSI. Performance Standards for Antimicrobial Susceptibility Testing. 28th Edition. CLSI Guideline M100.*

Colautti, J., Bullen, N. P., & Whitney, J. C. (2023). Lack of evidence that *Pseudomonas aeruginosa* AmpDh3-PA0808 constitute a type VI secretion system effector-immunity pair. *Molecular microbiology*, *119*(2), 262-274. https://doi.org/10.1111/mmi.15021

Collins, J. A., & Osheroff, N. (2024). Gyrase and Topoisomerase IV: Recycling Old Targets for New Antibacterials to Combat Fluoroquinolone Resistance. *ACS Infectious Diseases*, *10*(4), 1097-1115. https://doi.org/10.1021/acsinfecdis.4c00128

Courcelle, J., Khodursky, A., Peter, B., Brown, P. O., & Hanawalt, P. C. (2001). Comparative gene expression profiles following UV exposure in wild-type and SOS-deficient *Escherichia coli*. *Genetics*, *158*(1), 41-64. https://doi.org/10.1093/genetics/158.1.41

Cox, J., & Mann, M. (2008). MaxQuant enables high peptide identification rates, individualized p.p.b.-range mass accuracies and proteome-wide protein quantification. *Nat Biotechnol*, *26*(12), 1367-1372. https://doi.org/10.1038/nbt.1511

Cox, J., Neuhauser, N., Michalski, A., Scheltema, R. A., Olsen, J. V., & Mann, M. (2011). Andromeda: a peptide search engine integrated into the MaxQuant environment. *J Proteome Res*, *10*(4), 1794-1805. https://doi.org/10.1021/pr101065j

Cushnie, T. P. T., O'Driscoll, N. H., & Lamb, A. J. (2016). Morphological and ultrastructural changes in bacterial cells as an indicator of antibacterial mechanism of action. *Cellular and Molecular Life Sciences*, *73*(23), 4471-4492. https://doi.org/10.1007/s00018-016-2302-2

Datsenko, K. A., & Wanner, B. L. (2000). One-step inactivation of chromosomal genes in *Escherichia coli* K-12 using PCR products. *Proceedings of the National Academy of Sciences of the United States of America*, *97*(12), 6640-6645. https://doi.org/10.1073/pnas.120163297

Davis, P. B. (2006). Cystic fibrosis since 1938. *American journal of respiratory and critical care medicine*, *173*(5), 475-482.

de Jonge, B. L., Karlowsky, J. A., Kazmierczak, K. M., Biedenbach, D. J., Sahm, D. F., & Nichols, W. W. (2016). In Vitro Susceptibility to Ceftazidime-Avibactam of Carbapenem-Nonsusceptible Enterobacteriaceae Isolates Collected during the INFORM Global Surveillance Study (2012 to 2014). *Antimicrobial agents and chemotherapy*, *60*(5), 3163-3169. https://doi.org/10.1128/aac.03042-15

5. References

de Kievit, T. R., & Lam, J. S. (1997). Isolation and characterization of two genes, *waaC* (*rfaC*) and *waaF* (*rfaF*), involved in *Pseudomonas aeruginosa* serotype O5 inner-core biosynthesis. *Journal of bacteriology*, *179*(11), 3451-3457. https://doi.org/10.1128/jb.179.11.3451-3457.1997

Demarre, G., Guerout, A. M., Matsumoto-Mashimo, C., Rowe-Magnus, D. A., Marliere, P., & Mazel, D. (2005). A new family of mobilizable suicide plasmids based on broad host range R388 plasmid (IncW) and RP4 plasmid (IncPalpha) conjugative machineries and their cognate *Escherichia coli* host strains. *Res Microbiol*, *156*(2), 245-255. https://doi.org/10.1016/j.resmic.2004.09.007

Deruelle, V., Bouillot, S., Job, V., Taillebourg, E., Fauvarque, M.-O., Attrée, I., & Huber, P. (2021). The bacterial toxin ExoU requires a host trafficking chaperone for transportation and to induce necrosis. *Nature communications*, *12*(1), 4024. https://doi.org/10.1038/s41467-021-24337-9

Dhar, S., Kumari, H., Balasubramanian, D., & Mathee, K. (2018). Cell-wall recycling and synthesis in *Escherichia coli* and *Pseudomonas aeruginosa* - their role in the development of resistance. *J Med Microbiol*, *67*(1), 1-21. https://doi.org/10.1099/jmm.0.000636

Dietsche, T., Tesfazgi Mebrhatu, M., Brunner, M. J., Abrusci, P., Yan, J., Franz-Wachtel, M., Scharfe, C., Zilkenat, S., Grin, I., Galan, J. E., Kohlbacher, O., Lea, S., Macek, B., Marlovits, T. C., Robinson, C. V., & Wagner, S. (2016). Structural and Functional Characterization of the Bacterial Type III Secretion Export Apparatus. *PLoS Pathog*, *12*(12), e1006071. https://doi.org/10.1371/journal.ppat.1006071

Dik, D. A., Fisher, J. F., & Mobashery, S. (2018). Cell-Wall Recycling of the Gram-Negative Bacteria and the Nexus to Antibiotic Resistance. *Chemical Reviews*, *118*(12), 5952-5984. https://doi.org/10.1021/acs.chemrev.8b00277

Drlica, K., Malik, M., Kerns, R. J., & Zhao, X. (2008). Quinolone-mediated bacterial death. *Antimicrobial agents and chemotherapy*, *52*(2), 385-392. https://doi.org/10.1128/aac.01617-06

Drlica, K., & Zhao, X. (1997). DNA gyrase, topoisomerase IV, and the 4-quinolones. *Microbiol Mol Biol Rev*, *61*(3), 377-392. https://doi.org/10.1128/mmbr.61.3.377-392.1997

Dubendorff, J. W., & Studier, F. W. (1991). Controlling basal expression in an inducible T7 expression system by blocking the target T7 promoter with *lac* repressor. *J Mol Biol*, *219*(1), 45-59. https://doi.org/10.1016/0022-2836(91)90856-2

Dwyer, D. J., Collins, J. J., & Walker, G. C. (2015). Unraveling the physiological complexities of antibiotic lethality. *Annu Rev Pharmacol Toxicol*, *55*, 313-332. https://doi.org/10.1146/annurev-pharmtox-010814-124712

Dwyer, D. J., Kohanski, M. A., Hayete, B., & Collins, J. J. (2007). Gyrase inhibitors induce an oxidative damage cellular death pathway in *Escherichia coli*. *Mol Syst Biol*, *3*, 91. https://doi.org/10.1038/msb4100135

Egan, A. J. F., Errington, J., & Vollmer, W. (2020). Regulation of peptidoglycan synthesis and remodelling. *Nature Reviews Microbiology*, *18*(8), 446-460. https://doi.org/10.1038/s41579-020-0366-3

Eggers, O., Renschler, F. A., Michalek, L. A., Wackler, N., Walter, E., Smollich, F., Klein, K., Sonnabend, M. S., Egle, V., Angelov, A., Engesser, C., Borisova, M., Mayer, C., Schutz, M., & Bohn, E. (2023). YgfB increases beta-lactam resistance in *Pseudomonas aeruginosa* by counteracting AlpA-mediated *ampDh3* expression. *Commun Biol*, *6*(1), 254. https://doi.org/10.1038/s42003-023-04609-4

El-Gamal, M. I., Brahim, I., Hisham, N., Aladdin, R., Mohammed, H., & Bahaaeldin, A. (2017). Recent updates of carbapenem antibiotics. *European Journal of Medicinal Chemistry*, *131*, 185-195. https://doi.org/https://doi.org/10.1016/j.ejmech.2017.03.022

5. References

Elias, J. E., & Gygi, S. P. (2010). Target-decoy search strategy for mass spectrometry-based proteomics. *Methods in molecular biology*, *604*, 55-71. https://doi.org/10.1007/978-1-60761-444-9_5

European Antimicrobial Resistance Collaborators. (2022). The burden of bacterial antimicrobial resistance in the WHO European region in 2019: a cross-country systematic analysis. *Lancet Public Health*, *7*(11), e897-e913. https://doi.org/10.1016/s2468-2667(22)00225-0

European Medicines Agency (EMA). (19/12/2023). *Fetcroja*. Retrieved 18.04.2024 from https://www.ema.europa.eu/en/medicines/human/EPAR/fetcroja

Ewels, P., Magnusson, M., Lundin, S., & Käller, M. (2016). MultiQC: summarize analysis results for multiple tools and samples in a single report. *Bioinformatics*, *32*(19), 3047-3048. https://doi.org/10.1093/bioinformatics/btw354

Feltman, H., Schulert, G., Khan, S., Jain, M., Peterson, L., & Hauser, A. R. (2001). Prevalence of type III secretion genes in clinical and environmental isolates of *Pseudomonas aeruginosa*. *Microbiology*, *147*(10), 2659-2669.

Feng, X., Zhang, Z., Li, X., Song, Y., Kang, J., Yin, D., Gao, Y., Shi, N., & Duan, J. (2019). Mutations in *gyrB* play an important role in ciprofloxacin-resistant *Pseudomonas aeruginosa*. *Infection and Drug Resistance*, *12*(null), 261-272. https://doi.org/10.2147/IDR.S182272

Fernández-Billón, M., Llambías-Cabot, A. E., Jordana-Lluch, E., Oliver, A., & Macià, M. D. (2023). Mechanisms of antibiotic resistance in *Pseudomonas aeruginosa* biofilms. *Biofilm*, *5*, 100129. https://doi.org/https://doi.org/10.1016/j.bioflm.2023.100129

Fitzgerald, D. M., Bonocora, R. P., & Wade, J. T. (2014). Comprehensive mapping of the *Escherichia coli* flagellar regulatory network. *PLoS genetics*, *10*(10), e1004649. https://doi.org/10.1371/journal.pgen.1004649

Fleming, A. (1922). On a Remarkable Bacteriolytic Element Found in Tissues and Secretions. *Proceedings of the Royal Society of London. Series B, Containing Papers of a Biological Character*, *93*(653), 306-317. http://www.jstor.org/stable/80959

Forrest, A., Nix, D. E., Ballow, C. H., Goss, T. F., Birmingham, M. C., & Schentag, J. J. (1993). Pharmacodynamics of intravenous ciprofloxacin in seriously ill patients. *Antimicrobial agents and chemotherapy*, *37*(5), 1073-1081. https://doi.org/10.1128/AAC.37.5.1073

Forterre, P., Gribaldo, S., Gadelle, D., & Serre, M.-C. (2007). Origin and evolution of DNA topoisomerases. *Biochimie*, *89*(4), 427-446. https://doi.org/https://doi.org/10.1016/j.biochi.2006.12.009

Foti, J. J., Devadoss, B., Winkler, J. A., Collins, J. J., & Walker, G. C. (2012). Oxidation of the guanine nucleotide pool underlies cell death by bactericidal antibiotics. *Science*, *336*(6079), 315-319. https://doi.org/10.1126/science.1219192

Fumeaux, C., & Bernhardt, T. G. (2017). Identification of MupP as a New Peptidoglycan Recycling Factor and Antibiotic Resistance Determinant in *Pseudomonas aeruginosa*. *mBio*, *8*(2), 1-13. https://doi.org/10.1128/mBio.00102-17

Galkin, A., Sarikaya, E., Lehmann, C., Howard, A., & Herzberg, O. (2004). X-ray structure of HI0817 from *Haemophilus influenzae*: protein of unknown function with a novel fold. *Proteins*, *57*(4), 874-877. https://doi.org/10.1002/prot.20260

Galleni, M., Amicosante, G., & Frère, J. M. (1988). A survey of the kinetic parameters of class C beta-lactamases. Cephalosporins and other beta-lactam compounds. *Biochem J*, *255*(1), 123-129. https://doi.org/10.1042/bj2550123

Galleni, M., & Frère, J. M. (1988). A survey of the kinetic parameters of class C beta-lactamases. Penicillins. *Biochem J*, *255*(1), 119-122. https://doi.org/10.1042/bj2550119

Gates, M. L., Sanders, C. C., Goering, R. V., & Sanders, W. E., Jr. (1986). Evidence for multiple forms of type I chromosomal beta-lactamase in *Pseudomonas aeruginosa*.

5. References

Antimicrobial agents and chemotherapy, *30*(3), 453-457. https://doi.org/10.1128/aac.30.3.453

GBD 2019 Antimicrobial Resistance Collaborators. (2022). Global mortality associated with 33 bacterial pathogens in 2019: a systematic analysis for the Global Burden of Disease Study 2019. *Lancet*, *400*(10369), 2221-2248. https://doi.org/10.1016/s0140-6736(22)02185-7

Gellatly, S. L., & Hancock, R. E. W. (2013). *Pseudomonas aeruginosa* : new insights into pathogenesis and host defenses. *Pathogens and disease*, *67*(3), 159-173. https://doi.org/10.1111/2049-632X.12033

Gellert, M., Mizuuchi, K., O'Dea, M. H., & Nash, H. A. (1976). DNA gyrase: an enzyme that introduces superhelical turns into DNA. *Proceedings of the National Academy of Sciences*, *73*(11), 3872-3876. https://doi.org/doi:10.1073/pnas.73.11.3872

Gérard-Vincent, M., Robert, V., Ball, G., Bleves, S., Michel, G. P., Lazdunski, A., & Filloux, A. (2002). Identification of XcpP domains that confer functionality and specificity to the *Pseudomonas aeruginosa* type II secretion apparatus. *Molecular microbiology*, *44*(6), 1651-1665. https://doi.org/10.1046/j.1365-2958.2002.02991.x

Germino, J., & Bastia, D. (1982). Primary structure of the replication initiation protein of plasmid R6K. *Proceedings of the National Academy of Sciences of the United States of America*, *79*(18), 5475-5479. https://doi.org/10.1073/pnas.79.18.5475

Gibson, D. G., Young, L., Chuang, R. Y., Venter, J. C., Hutchison, C. A., 3rd, & Smith, H. O. (2009). Enzymatic assembly of DNA molecules up to several hundred kilobases. *Nat Methods*, *6*(5), 343-345. https://doi.org/10.1038/nmeth.1318

Gisin, J., Schneider, A., Nagele, B., Borisova, M., & Mayer, C. (2013). A cell wall recycling shortcut that bypasses peptidoglycan *de novo* biosynthesis. *Nature chemical biology*, *9*(8), 491-493. https://doi.org/10.1038/nchembio.1289

Glauner, B., Höltje, J. V., & Schwarz, U. (1988). The composition of the murein of *Escherichia coli*. *The Journal of biological chemistry*, *263*(21), 10088-10095.

Goedhart, J., & Luijsterburg, M. S. (2020). VolcaNoseR is a web app for creating, exploring, labeling and sharing volcano plots. *Scientific reports*, *10*(1), 20560. https://doi.org/10.1038/s41598-020-76603-3

Goodall, E. C. A., Robinson, A., Johnston, I. G., Jabbari, S., Turner, K. A., Cunningham, A. F., Lund, P. A., Cole, J. A., & Henderson, I. R. (2018). The Essential Genome of *Escherichia coli* K-12. *mBio*, *9*(1). https://doi.org/10.1128/mBio.02096-17

Gronow, S., Brabetz, W., & Brade, H. (2000). Comparative functional characterization in vitro of heptosyltransferase I (*WaaC*) and II (*WaaF*) from *Escherichia coli*. *Eur J Biochem*, *267*(22), 6602-6611. https://doi.org/10.1046/j.1432-1327.2000.01754.x

Hajj Chehade, M., Loiseau, L., Lombard, M., Pecqueur, L., Ismail, A., Smadja, M., Golinelli-Pimpaneau, B., Mellot-Draznieks, C., Hamelin, O., Aussel, L., Kieffer-Jaquinod, S., Labessan, N., Barras, F., Fontecave, M., & Pierrel, F. (2013). *ubiI*, a new gene in *Escherichia coli* coenzyme Q biosynthesis, is involved in aerobic C5-hydroxylation. *The Journal of biological chemistry*, *288*(27), 20085-20092. https://doi.org/10.1074/jbc.M113.480368

Hammond, J. B., & Kruger, N. J. (1988). The bradford method for protein quantitation. *Methods in molecular biology*, *3*, 25-32. https://doi.org/10.1385/0-89603-126-8:25

Handfield, J., Gagnon, L., Dargis, M., & Huletsky, A. (1997). Sequence of the *ponA* gene and characterization of the penicillin-binding protein 1A of *Pseudomonas aeruginosa* PAO1. *Gene*, *199*(1-2), 49-56. https://doi.org/10.1016/s0378-1119(97)00345-4

Hanson, N. D., & Sanders, C. C. (1999). Regulation of inducible AmpC beta-lactamase expression among Enterobacteriaceae. *Current pharmaceutical design*, *5*(11), 881-894. https://www.ncbi.nlm.nih.gov/pubmed/10539994

5. References

Haseltine, W. A., & Block, R. (1973). Synthesis of guanosine tetra- and pentaphosphate requires the presence of a codon-specific, uncharged transfer ribonucleic acid in the acceptor site of ribosomes. *Proceedings of the National Academy of Sciences of the United States of America*, *70*(5), 1564-1568. https://doi.org/10.1073/pnas.70.5.1564

Hauser, A. R. (2009). The type III secretion system of *Pseudomonas aeruginosa*: infection by injection. *Nature Reviews Microbiology*, *7*(9), 654-665. https://doi.org/10.1038/nrmicro2199

Heeb, S., Blumer, C., & Haas, D. (2002). Regulatory RNA as mediator in GacA/RsmA-dependent global control of exoproduct formation in *Pseudomonas fluorescens* CHA0. *Journal of bacteriology*, *184*(4), 1046-1056. https://doi.org/10.1128/jb.184.4.1046-1056.2002

Heeb, S., Itoh, Y., Nishijyo, T., Schnider, U., Keel, C., Wade, J., Walsh, U., O'Gara, F., & Haas, D. (2000). Small, stable shuttle vectors based on the minimal pVS1 replicon for use in gram-negative, plant-associated bacteria. *Molecular plant-microbe interactions : MPMI*, *13*(2), 232-237. https://doi.org/10.1094/MPMI.2000.13.2.232

Heidrich, C., Templin, M. F., Ursinus, A., Merdanovic, M., Berger, J., Schwarz, H., de Pedro, M. A., & Höltje, J. V. (2001). Involvement of N-acetylmuramyl-L-alanine amidases in cell separation and antibiotic-induced autolysis of *Escherichia coli*. *Molecular microbiology*, *41*(1), 167-178. https://doi.org/10.1046/j.1365-2958.2001.02499.x

Heidrich, C., Ursinus, A., Berger, J., Schwarz, H., & Holtje, J. V. (2002). Effects of multiple deletions of murein hydrolases on viability, septum cleavage, and sensitivity to large toxic molecules in *Escherichia coli*. *Journal of bacteriology*, *184*(22), 6093-6099. https://doi.org/10.1128/jb.184.22.6093-6099.2002

Heilmann, H. D. (1972). On the peptidoglycan of the cell walls of *Pseudomonas aeruginosa*. *European Journal of Biochemistry*, *31*(3), 456-463.

Henderson-Begg, S. K., Livermore, D. M., & Hall, L. M. (2006). Effect of subinhibitory concentrations of antibiotics on mutation frequency in *Streptococcus pneumoniae*. *The Journal of antimicrobial chemotherapy*, *57*(5), 849-854. https://doi.org/10.1093/jac/dkl064

Henrichfreise, B., Wiegand, I., Pfister, W., & Wiedemann, B. (2007). Resistance mechanisms of multiresistant *Pseudomonas aeruginosa* strains from Germany and correlation with hypermutation. *Antimicrobial agents and chemotherapy*, *51*(11), 4062-4070.

Hervé, M., Boniface, A., Gobec, S., Blanot, D., & Mengin-Lecreulx, D. (2007). Biochemical characterization and physiological properties of *Escherichia coli* UDP-N-acetylmuramate:L-alanyl-gamma-D-glutamyl-meso-diaminopimelate ligase. *Journal of bacteriology*, *189*(11), 3987-3995. https://doi.org/10.1128/jb.00087-07

Higgins, P. G., Fluit, A. C., Milatovic, D., Verhoef, J., & Schmitz, F. J. (2003). Mutations in GyrA, ParC, MexR and NfxB in clinical isolates of *Pseudomonas aeruginosa*. *Int J Antimicrob Agents*, *21*(5), 409-413. https://doi.org/https://doi.org/10.1016/S0924-8579(03)00009-8

Hirsch, E. B., Ledesma, K. R., Chang, K. T., Schwartz, M. S., Motyl, M. R., & Tam, V. H. (2012). In vitro activity of MK-7655, a novel β-lactamase inhibitor, in combination with imipenem against carbapenem-resistant Gram-negative bacteria. *Antimicrobial agents and chemotherapy*, *56*(7), 3753-3757. https://doi.org/10.1128/aac.05927-11

Hmelo, L. R., Borlee, B. R., Almblad, H., Love, M. E., Randall, T. E., Tseng, B. S., Lin, C., Irie, Y., Storek, K. M., Yang, J. J., Siehnel, R. J., Howell, P. L., Singh, P. K., Tolker-Nielsen, T., Parsek, M. R., Schweizer, H. P., & Harrison, J. J. (2015). Precision-engineering the *Pseudomonas aeruginosa* genome with two-step allelic exchange. *Nature protocols*, *10*(11), 1820-1841. https://doi.org/10.1038/nprot.2015.115

5. References

Hoang, T. T., Kutchma, A. J., Becher, A., & Schweizer, H. P. (2000). Integration-proficient plasmids for *Pseudomonas aeruginosa:* site-specific integration and use for engineering of reporter and expression strains. *Plasmid*, *43*(1), 59-72. https://doi.org/10.1006/plas.1999.1441

Höltje, J. V. (1998). Growth of the stress-bearing and shape-maintaining murein sacculus of *Escherichia coli*. *Microbiol Mol Biol Rev*, *62*(1), 181-203. https://doi.org/10.1128/mmbr.62.1.181-203.1998

Höltje, J. V., Mirelman, D., Sharon, N., & Schwarz, U. (1975). Novel type of murein transglycosylase in *Escherichia coli*. *Journal of bacteriology*, *124*(3), 1067-1076. https://doi.org/10.1128/jb.124.3.1067-1076.1975

Hong, Y., Li, Q., Gao, Q., Xie, J., Huang, H., Drlica, K., & Zhao, X. (2020). Reactive oxygen species play a dominant role in all pathways of rapid quinolone-mediated killing. *The Journal of antimicrobial chemotherapy*, *75*(3), 576-585. https://doi.org/10.1093/jac/dkz485

Hong, Y., Zeng, J., Wang, X., Drlica, K., & Zhao, X. (2019). Post-stress bacterial cell death mediated by reactive oxygen species. *Proceedings of the National Academy of Sciences of the United States of America*, *116*(20), 10064-10071. https://doi.org/10.1073/pnas.1901730116

Honoré, N., Nicolas, M. H., & Cole, S. T. (1986). Inducible cephalosporinase production in clinical isolates of Enterobacter cloacae is controlled by a regulatory gene that has been deleted from *Escherichia coli*. *EMBO J*, *5*(13), 3709-3714. https://doi.org/10.1002/j.1460-2075.1986.tb04704.x

Horna, G., & Ruiz, J. (2021). Type 3 secretion system of *Pseudomonas aeruginosa*. *Microbiological Research*, *246*, 126719. https://doi.org/https://doi.org/10.1016/j.micres.2021.126719

Huang, S. N., Michaels, S. A., Mitchell, B. B., Majdalani, N., Vanden Broeck, A., Canela, A., Tse-Dinh, Y. C., Lamour, V., & Pommier, Y. (2021). Exonuclease VII repairs quinolone-induced damage by resolving DNA gyrase cleavage complexes. *Sci Adv*, *7*(10). https://doi.org/10.1126/sciadv.abe0384

Iglewski, B. H., Liu, P. V., & Kabat, D. (1977). Mechanism of action of *Pseudomonas aeruginosa* exotoxin Aiadenosine diphosphate-ribosylation of mammalian elongation factor 2 in vitro and in vivo. *Infection and immunity*, *15*, 138 - 144.

Ishino, F., Mitsui, K., Tamaki, S., & Matsuhashi, M. (1980). Dual enzyme activities of cell wall peptidoglycan synthesis, peptidoglycan transglycosylase and penicillin-sensitive transpeptidase, in purified preparations of *Escherichia coli* penicillin-binding protein 1A. *Biochemical and biophysical research communications*, *97*(1), 287-293. https://doi.org/10.1016/s0006-291x(80)80166-5

Islam, S., Jalal, S., & Wretlind, B. (2004). Expression of the MexXY efflux pump in amikacin-resistant isolates of *Pseudomonas aeruginosa*. *Clinical microbiology and infection : the official publication of the European Society of Clinical Microbiology and Infectious Diseases*, *10*(10), 877-883. https://doi.org/10.1111/j.1469-0691.2004.00991.x

Ito, A., Nishikawa, T., Matsumoto, S., Yoshizawa, H., Sato, T., Nakamura, R., Tsuji, M., & Yamano, Y. (2016). Siderophore Cephalosporin Cefiderocol Utilizes Ferric Iron Transporter Systems for Antibacterial Activity against *Pseudomonas aeruginosa*. *Antimicrobial agents and chemotherapy*, *60*(12), 7396-7401. https://doi.org/10.1128/aac.01405-16

Ito, A., Sato, T., Ota, M., Takemura, M., Nishikawa, T., Toba, S., Kohira, N., Miyagawa, S., Ishibashi, N., Matsumoto, S., Nakamura, R., Tsuji, M., & Yamano, Y. (2018). In Vitro Antibacterial Properties of Cefiderocol, a Novel Siderophore Cephalosporin, against

Gram-Negative Bacteria. *Antimicrobial agents and chemotherapy*, *62*(1). https://doi.org/10.1128/aac.01454-17

Jacobs, C., Frere, J. M., & Normark, S. (1997). Cytosolic intermediates for cell wall biosynthesis and degradation control inducible beta-lactam resistance in gram-negative bacteria. *Cell*, *88*(6), 823-832. https://doi.org/10.1016/s0092-8674(00)81928-5

Jacobs, C., Huang, L. J., Bartowsky, E., Normark, S., & Park, J. T. (1994). Bacterial cell wall recycling provides cytosolic muropeptides as effectors for beta-lactamase induction. *EMBO J*, *13*(19), 4684-4694. https://doi.org/10.1002/j.1460-2075.1994.tb06792.x

Jacobs, C., Joris, B., Jamin, M., Klarsov, K., Van Beeumen, J., Mengin-Lecreulx, D., van Heijenoort, J., Park, J. T., Normark, S., & Frere, J. M. (1995). AmpD, essential for both beta-lactamase regulation and cell wall recycling, is a novel cytosolic N-acetylmuramyl-L-alanine amidase. *Molecular microbiology*, *15*(3), 553-559. https://doi.org/10.1111/j.1365-2958.1995.tb02268.x. http://www.ncbi.nlm.nih.gov/pubmed/7783625. https://onlinelibrary.wiley.com/doi/pdfdirect/10.1111/j.1365-2958.1995.tb02268.x?download=true.

Jacoby, G. A. (2009). AmpC beta-lactamases. *Clin Microbiol Rev*, *22*(1), 161-182, Table of Contents. https://doi.org/10.1128/CMR.00036-08

Jaurin, B., Grundström, T., Edlund, T., & Normark, S. (1981). The *E. coli* beta-lactamase attenuator mediates growth rate-dependent regulation. *Nature*, *290*(5803), 221-225. https://doi.org/10.1038/290221a0

Jia, J., Wang, Y., Zhou, L., & Jin, S. (2006). Expression of *Pseudomonas aeruginosa* toxin ExoS effectively induces apoptosis in host cells. *Infection and immunity*, *74*(12), 6557-6570.

Johnson, S. J., Ernst, E. J., & Moores, K. G. (2011). Is double coverage of gram-negative organisms necessary? *Am J Health Syst Pharm*, *68*(2), 119-124. https://doi.org/10.2146/ajhp090360

Juan, C., Moya, B., Perez, J. L., & Oliver, A. (2006). Stepwise upregulation of the *Pseudomonas aeruginos*a chromosomal cephalosporinase conferring high-level beta-lactam resistance involves three AmpD homologues. *Antimicrobial agents and chemotherapy*, *50*(5), 1780-1787. https://doi.org/10.1128/AAC.50.5.1780-1787.2006

Kadrmas, J. L., & Raetz, C. R. (1998). Enzymatic synthesis of lipopolysaccharide in *Escherichia coli*. Purification and properties of heptosyltransferase i. *The Journal of biological chemistry*, *273*(5), 2799-2807. https://doi.org/10.1074/jbc.273.5.2799

Kahan, F. M., Kropp, H., Sundelof, J. G., & Birnbaum, J. (1983). Thienamycin: development of imipenen-cilastatin. *The Journal of antimicrobial chemotherapy*, *12 Suppl D*, 1-35. https://doi.org/10.1093/jac/12.suppl_d.1

Kalil, A. C., Metersky, M. L., Klompas, M., Muscedere, J., Sweeney, D. A., Palmer, L. B., Napolitano, L. M., O'Grady, N. P., Bartlett, J. G., Carratala, J., El Solh, A. A., Ewig, S., Fey, P. D., File, T. M., Jr., Restrepo, M. I., Roberts, J. A., Waterer, G. W., Cruse, P., Knight, S. L., & Brozek, J. L. (2016). Management of Adults With Hospital-acquired and Ventilator-associated Pneumonia: 2016 Clinical Practice Guidelines by the Infectious Diseases Society of America and the American Thoracic Society. *Clin Infect Dis*, *63*(5), e61-e111. https://doi.org/10.1093/cid/ciw353

Kamarthapu, V., Epshtein, V., Benjamin, B., Proshkin, S., Mironov, A., Cashel, M., & Nudler, E. (2016). ppGpp couples transcription to DNA repair in *E. coli*. *Science*, *352*(6288), 993-996. https://doi.org/doi:10.1126/science.aad6945

Kaminski, A., Gupta, K. H., Goldufsky, J. W., Lee, H. W., Gupta, V., & Shafikhani, S. H. (2018). *Pseudomonas aeruginosa* ExoS Induces Intrinsic Apoptosis in Target Host

Cells in a Manner That is Dependent on its GAP Domain Activity. *Scientific reports*, *8*(1), 14047. https://doi.org/10.1038/s41598-018-32491-2

Kanehisa, M. (2019). Toward understanding the origin and evolution of cellular organisms. *Protein Sci*, *28*(11), 1947-1951. https://doi.org/10.1002/pro.3715

Kanehisa, M., Furumichi, M., Sato, Y., Kawashima, M., & Ishiguro-Watanabe, M. (2023). KEGG for taxonomy-based analysis of pathways and genomes. *Nucleic acids research*, *51*(D1), D587-D592. https://doi.org/10.1093/nar/gkac963

Kanehisa, M., & Goto, S. (2000). KEGG: kyoto encyclopedia of genes and genomes. *Nucleic acids research*, *28*(1), 27-30. https://doi.org/10.1093/nar/28.1.27

Kaneko, K., Okamoto, R., Nakano, R., Kawakami, S., & Inoue, M. (2005). Gene mutations responsible for overexpression of AmpC beta-lactamase in some clinical isolates of *Enterobacter cloacae*. *J Clin Microbiol*, *43*(6), 2955-2958. https://doi.org/10.1128/jcm.43.6.2955-2958.2005

Kang, D., Kirienko, D. R., Webster, P., Fisher, A. L., & Kirienko, N. V. (2018). Pyoverdine, a siderophore from *Pseudomonas aeruginosa*, translocates into C. elegans, removes iron, and activates a distinct host response. *Virulence*, *9*(1), 804-817. https://doi.org/10.1080/21505594.2018.1449508

Kato, J.-i., Nishimura, Y., Imamura, R., Niki, H., Hiraga, S., & Suzuki, H. (1990). New topoisomerase essential for chromosome segregation in *E. coli*. *Cell*, *63*(2), 393-404. https://doi.org/https://doi.org/10.1016/0092-8674(90)90172-B

Kato, T., & Shinoura, Y. (1977). Isolation and characterization of mutants of *Escherichia coli* deficient in induction of mutations by ultraviolet light. *Mol Gen Genet*, *156*(2), 121-131. https://doi.org/10.1007/BF00283484

Kerem, B., Rommens, J. M., Buchanan, J. A., Markiewicz, D., Cox, T. K., Chakravarti, A., Buchwald, M., & Tsui, L. C. (1989). Identification of the cystic fibrosis gene: genetic analysis. *Science*, *245*(4922), 1073-1080. https://doi.org/10.1126/science.2570460

Keren, I., Wu, Y., Inocencio, J., Mulcahy, L. R., & Lewis, K. (2013). Killing by bactericidal antibiotics does not depend on reactive oxygen species. *Science*, *339*(6124), 1213-1216. https://doi.org/10.1126/science.1232688

Khodursky, A. B., Zechiedrich, E. L., & Cozzarelli, N. R. (1995). Topoisomerase IV is a target of quinolones in *Escherichia coli*. *Proceedings of the National Academy of Sciences of the United States of America*, *92*(25), 11801-11805. https://doi.org/10.1073/pnas.92.25.11801

Kihara, A., Akiyama, Y., & Ito, K. (2001). Revisiting the lysogenization control of bacteriophage lambda. Identification and characterization of a new host component, HflD. *The Journal of biological chemistry*, *276*(17), 13695-13700. https://doi.org/10.1074/jbc.M011699200

King, J. D., Kocíncová, D., Westman, E. L., & Lam, J. S. (2009). Lipopolysaccharide biosynthesis in *Pseudomonas aeruginosa*. *Innate immunity*, *15*(5), 261-312.

Kirthi, N., Roy-Chaudhuri, B., Kelley, T., & Culver, G. M. (2006). A novel single amino acid change in small subunit ribosomal protein S5 has profound effects on translational fidelity. *Rna*, *12*(12), 2080-2091. https://doi.org/10.1261/rna.302006

Klein, K., Sonnabend, M. S., Frank, L., Leibiger, K., Franz-Wachtel, M., Macek, B., Trunk, T., Leo, J. C., Autenrieth, I. B., Schutz, M., & Bohn, E. (2019). Deprivation of the Periplasmic Chaperone SurA Reduces Virulence and Restores Antibiotic Susceptibility of Multidrug-Resistant *Pseudomonas aeruginosa*. *Front Microbiol*, *10*, 100. https://doi.org/10.3389/fmicb.2019.00100

Köhler, T., Epp, S. F., Curty, L. K., & Pechère, J. C. (1999). Characterization of MexT, the regulator of the MexE-MexF-OprN multidrug efflux system of *Pseudomonas*

aeruginosa. *Journal of bacteriology*, *181*(20), 6300-6305. https://doi.org/10.1128/jb.181.20.6300-6305.1999

Köhler, T., Michea-Hamzehpour, M., Epp, S. F., & Pechere, J. C. (1999). Carbapenem activities against *Pseudomonas aeruginosa*: respective contributions of OprD and efflux systems. *Antimicrobial agents and chemotherapy*, *43*(2), 424-427. https://doi.org/10.1128/aac.43.2.424

Köhler, T., Michéa-Hamzehpour, M., Henze, U., Gotoh, N., Curty, L. K., & Pechère, J. C. (1997). Characterization of MexE-MexF-OprN, a positively regulated multidrug efflux system of *Pseudomonas aeruginosa*. *Molecular microbiology*, *23*(2), 345-354. https://doi.org/10.1046/j.1365-2958.1997.2281594.x

Kong, K.-F., Jayawardena, S. R., Indulkar, S., Del Puerto, A., Koh, C. L., Høiby, N., & Mathee, K. (2005). *Pseudomonas aeruginosa* AmpR Is a Global Transcriptional Factor That Regulates Expression of AmpC and PoxB β-Lactamases, Proteases, Quorum Sensing, and Other Virulence Factors. *Antimicrobial agents and chemotherapy*, *49*, 4567 - 4575.

Kong, K. F., Aguila, A., Schneper, L., & Mathee, K. (2010). *Pseudomonas aeruginosa* beta-lactamase induction requires two permeases, AmpG and AmpP. *BMC microbiology*, *10*, 328. https://doi.org/10.1186/1471-2180-10-328

Korza, H. J., & Bochtler, M. (2005). *Pseudomonas aeruginosa* LD-carboxypeptidase, a serine peptidase with a Ser-His-Glu triad and a nucleophilic elbow. *The Journal of biological chemistry*, *280*(49), 40802-40812. https://doi.org/10.1074/jbc.M506328200

Kraithong, T., Hartley, S., Jeruzalmi, D., & Pakotiprapha, D. (2021). A Peek Inside the Machines of Bacterial Nucleotide Excision Repair. *Int J Mol Sci*, *22*(2). https://doi.org/10.3390/ijms22020952

Kuga, A., Okamoto, R., & Inoue, M. (2000). ampR gene mutations that greatly increase class C beta-lactamase activity in *Enterobacter cloacae*. *Antimicrobial agents and chemotherapy*, *44*(3), 561-567. https://doi.org/10.1128/aac.44.3.561-567.2000

Lam, J. S., Taylor, V. L., Islam, S. T., Hao, Y., & Kocíncová, D. (2011). Genetic and Functional Diversity of *Pseudomonas aeruginosa* Lipopolysaccharide. *Front Microbiol*, *2*. https://doi.org/10.3389/fmicb.2011.00118

Lau, G. W., Hassett, D. J., Ran, H., & Kong, F. (2004). The role of pyocyanin in *Pseudomonas aeruginosa* infection. *Trends Mol Med*, *10*(12), 599-606. https://doi.org/10.1016/j.molmed.2004.10.002

Lee, M., Artola-Recolons, C., Carrasco-López, C., Martínez-Caballero, S., Hesek, D., Spink, E., Lastochkin, E., Zhang, W., Hellman, L. M., Boggess, B., Hermoso, J. A., & Mobashery, S. (2013). Cell-Wall Remodeling by the Zinc-Protease AmpDh3 from *Pseudomonas aeruginosa*. *J Am Chem Soc*, *135*(34), 12604-12607. https://doi.org/10.1021/ja407445x

Lee, M., Dhar, S., De Benedetti, S., Hesek, D., Boggess, B., Blazquez, B., Mathee, K., & Mobashery, S. (2016). Muropeptides in *Pseudomonas aeruginosa* and their Role as Elicitors of beta-Lactam-Antibiotic Resistance. *Angew Chem Int Ed Engl*, *55*(24), 6882-6886. https://doi.org/10.1002/anie.201601693

Lee, M., Hesek, D., Blázquez, B., Lastochkin, E., Boggess, B., Fisher, J. F., & Mobashery, S. (2015). Catalytic Spectrum of the Penicillin-Binding Protein 4 of *Pseudomonas aeruginosa*, a Nexus for the Induction of β-Lactam Antibiotic Resistance. *J Am Chem Soc*, *137*(1), 190-200. https://doi.org/10.1021/ja5111706

Legaree, B. A., Daniels, K., Weadge, J. T., Cockburn, D., & Clarke, A. J. (2007). Function of penicillin-binding protein 2 in viability and morphology of *Pseudomonas aeruginosa*. *The Journal of antimicrobial chemotherapy*, *59*(3), 411-424. https://doi.org/10.1093/jac/dkl536

5. References

Leonard, C. J., Aravind, L., & Koonin, E. V. (1998). Novel families of putative protein kinases in bacteria and archaea: evolution of the "eukaryotic" protein kinase superfamily. *Genome Res*, *8*(10), 1038-1047. https://doi.org/10.1101/gr.8.10.1038

Lewis, K. (2010). Persister Cells. *Annu Rev Microbiol*, *64*(Volume 64, 2010), 357-372. https://doi.org/https://doi.org/10.1146/annurev.micro.112408.134306

Li, X. Z., Barré, N., & Poole, K. (2000). Influence of the MexA-MexB-oprM multidrug efflux system on expression of the MexC-MexD-oprJ and MexE-MexF-oprN multidrug efflux systems in *Pseudomonas aeruginosa*. *The Journal of antimicrobial chemotherapy*, *46*(6), 885-893. https://doi.org/10.1093/jac/46.6.885

Li, X. Z., Nikaido, H., & Poole, K. (1995). Role of *mexA-mexB-oprM* in antibiotic efflux in *Pseudomonas aeruginosa*. *Antimicrobial agents and chemotherapy*, *39*(9), 1948-1953. https://doi.org/10.1128/aac.39.9.1948

Liao, X., & Hancock, R. E. (1997). Identification of a penicillin-binding protein 3 homolog, PBP3x, in *Pseudomonas aeruginosa*: gene cloning and growth phase-dependent expression. *Journal of bacteriology*, *179*(5), 1490-1496. https://doi.org/10.1128/jb.179.5.1490-1496.1997

Lima, L. M., da Silva, B. N. M., Barbosa, G., & Barreiro, E. J. (2020). β-lactam antibiotics: An overview from a medicinal chemistry perspective. *European Journal of Medicinal Chemistry*, *208*, 112829.

Lin, J. J., & Sancar, A. (1990). Reconstitution of nucleotide excision nuclease with UvrA and UvrB proteins from *Escherichia coli* and UvrC protein from Bacillus subtilis. *The Journal of biological chemistry*, *265*(34), 21337-21341.

Lin, J. J., & Sancar, A. (1992). Active site of (A)BC excinuclease. I. Evidence for 5' incision by UvrC through a catalytic site involving Asp399, Asp438, Asp466, and His538 residues. *The Journal of biological chemistry*, *267*(25), 17688-17692.

Lipman, J., Scribante, J., Gous, A. G., Hon, H., & Tshukutsoane, S. (1998). Pharmacokinetic profiles of high-dose intravenous ciprofloxacin in severe sepsis. The Baragwanath Ciprofloxacin Study Group. *Antimicrobial agents and chemotherapy*, *42*(9), 2235-2239. https://doi.org/10.1128/AAC.42.9.2235

Lister, P. D., Wolter, D. J., & Hanson, N. D. (2009). Antibacterial-resistant *Pseudomonas aeruginosa*: clinical impact and complex regulation of chromosomally encoded resistance mechanisms. *Clin Microbiol Rev*, *22*(4), 582-610. https://doi.org/10.1128/CMR.00040-09

Liu, Y., & Imlay, J. A. (2013). Cell death from antibiotics without the involvement of reactive oxygen species. *Science*, *339*(6124), 1210-1213. https://doi.org/10.1126/science.1232751

Livermore, D. M. (1992). Interplay of impermeability and chromosomal beta-lactamase activity in imipenem-resistant *Pseudomonas aeruginosa*. *Antimicrobial agents and chemotherapy*, *36*(9), 2046-2048. https://doi.org/10.1128/aac.36.9.2046

Livermore, D. M., & Yang, Y. J. (1987). Beta-lactamase lability and inducer power of newer beta-lactam antibiotics in relation to their activity against beta-lactamase-inducibility mutants of *Pseudomonas aeruginosa*. *The Journal of infectious diseases*, *155*(4), 775-782. https://doi.org/10.1093/infdis/155.4.775

López, E., & Blázquez, J. (2009). Effect of subinhibitory concentrations of antibiotics on intrachromosomal homologous recombination in *Escherichia coli*. *Antimicrobial agents and chemotherapy*, *53*(8), 3411-3415. https://doi.org/10.1128/aac.00358-09

López, E., Elez, M., Matic, I., & Blázquez, J. (2007). Antibiotic-mediated recombination: ciprofloxacin stimulates SOS-independent recombination of divergent sequences in *Escherichia coli*. *Molecular microbiology*, *64*(1), 83-93. https://doi.org/10.1111/j.1365-2958.2007.05642.x

5. References

Luer, C., Schauer, S., Mobius, K., Schulze, J., Schubert, W. D., Heinz, D. W., Jahn, D., & Moser, J. (2005). Complex formation between glutamyl-tRNA reductase and glutamate-1-semialdehyde 2,1-aminomutase in *Escherichia coli* during the initial reactions of porphyrin biosynthesis. *The Journal of biological chemistry*, *280*(19), 18568-18572. https://doi.org/10.1074/jbc.M500440200

Lupoli, T. J., Tsukamoto, H., Doud, E. H., Wang, T.-S. A., Walker, S., & Kahne, D. (2011). Transpeptidase-Mediated Incorporation of d-Amino Acids into Bacterial Peptidoglycan. *J Am Chem Soc*, *133*(28), 10748-10751. https://doi.org/10.1021/ja2040656

Luria, S. E., & Delbrück, M. (1943). Mutations of Bacteria from Virus Sensitivity to Virus Resistance. *Genetics*, *28*(6), 491-511. https://doi.org/10.1093/genetics/28.6.491

Macdougall, C. (2011). Beyond Susceptible and Resistant, Part I: Treatment of Infections Due to Gram-Negative Organisms With Inducible β-Lactamases. *J Pediatr Pharmacol Ther*, *16*(1), 23-30.

Maciá, M. D., Blanquer, D., Togores, B., Sauleda, J., Pérez, J. L., & Oliver, A. (2005). Hypermutation is a key factor in development of multiple-antimicrobial resistance in *Pseudomonas aeruginosa* strains causing chronic lung infections. *Antimicrobial agents and chemotherapy*, *49*(8), 3382-3386. https://doi.org/10.1128/aac.49.8.3382-3386.2005

Malik, M., Zhao, X., & Drlica, K. (2006). Lethal fragmentation of bacterial chromosomes mediated by DNA gyrase and quinolones. *Molecular microbiology*, *61*(3), 810-825. https://doi.org/10.1111/j.1365-2958.2006.05275.x

Mandsberg, L. F., Ciofu, O., Kirkby, N., Christiansen, L. E., Poulsen, H. E., & Hoiby, N. (2009). Antibiotic resistance in *Pseudomonas aeruginosa* strains with increased mutation frequency due to inactivation of the DNA oxidative repair system. *Antimicrobial agents and chemotherapy*, *53*(6), 2483-2491. https://doi.org/10.1128/AAC.00428-08

Maseda, H., Saito, K., Nakajima, A., & Nakae, T. (2000). Variation of the mexT gene, a regulator of the MexEF-oprN efflux pump expression in wild-type strains of *Pseudomonas aeruginosa*. *FEMS microbiology letters*, *192*(1), 107-112. https://doi.org/10.1111/j.1574-6968.2000.tb09367.x

Maseda, H., Sawada, I., Saito, K., Uchiyama, H., Nakae, T., & Nomura, N. (2004). Enhancement of the mexAB-oprM efflux pump expression by a quorum-sensing autoinducer and its cancellation by a regulator, MexT, of the *mexEF-oprN* efflux pump operon in *Pseudomonas aeruginosa*. *Antimicrobial agents and chemotherapy*, *48*(4), 1320-1328. https://doi.org/10.1128/aac.48.4.1320-1328.2004

McFarland, K. A., Dolben, E. L., LeRoux, M., Kambara, T. K., Ramsey, K. M., Kirkpatrick, R. L., Mougous, J. D., Hogan, D. A., & Dove, S. L. (2015). A self-lysis pathway that enhances the virulence of a pathogenic bacterium. *Proceedings of the National Academy of Sciences of the United States of America*, *112*(27), 8433-8438. https://doi.org/10.1073/pnas.1506299112

Meini, S., Tascini, C., Cei, M., Sozio, E., & Rossolini, G. M. (2019). AmpC β-lactamase-producing Enterobacterales: what a clinician should know. *Infection*, *47*(3), 363-375. https://doi.org/10.1007/s15010-019-01291-9

Meisner, J., & Goldberg, J. B. (2016). The *Escherichia coli* rhaSR-PrhaBAD Inducible Promoter System Allows Tightly Controlled Gene Expression over a Wide Range in *Pseudomonas aeruginosa*. *Applied and environmental microbiology*, *82*(22), 6715-6727. https://doi.org/10.1128/AEM.02041-16

Mengin-Lecreulx, D., Texier, L., Rousseau, M., & van Heijenoort, J. (1991). The *murG* gene of *Escherichia coli* codes for the UDP-N-acetylglucosamine: N-acetylmuramyl-(pentapeptide) pyrophosphoryl-undecaprenol N-acetylglucosamine transferase

involved in the membrane steps of peptidoglycan synthesis. *Journal of bacteriology*, *173*(15), 4625-4636. https://doi.org/10.1128/jb.173.15.4625-4636.1991

Mengin-Lecreulx, D., & van Heijenoort, J. (1996). Characterization of the essential gene *glmM* encoding phosphoglucosamine mutase in *Escherichia coli*. *The Journal of biological chemistry*, *271*(1), 32-39. https://doi.org/10.1074/jbc.271.1.32

Mengin-Lecreulx, D., van Heijenoort, J., & Park, J. T. (1996). Identification of the *mpl* gene encoding UDP-N-acetylmuramate: L-alanyl-gamma-D-glutamyl-meso-diaminopimelate ligase in *Escherichia coli* and its role in recycling of cell wall peptidoglycan. *Journal of bacteriology*, *178*(18), 5347-5352. https://doi.org/10.1128/jb.178.18.5347-5352.1996

Million-Weaver, S., Samadpour, A. N., Moreno-Habel, D. A., Nugent, P., Brittnacher, M. J., Weiss, E., Hayden, H. S., Miller, S. I., Liachko, I., & Merrikh, H. (2015). An underlying mechanism for the increased mutagenesis of lagging-strand genes in Bacillus subtilis. *Proceedings of the National Academy of Sciences of the United States of America*, *112*(10), E1096-1105. https://doi.org/10.1073/pnas.1416651112

Mizuuchi, K., O'Dea, M. H., & Gellert, M. (1978). DNA gyrase: subunit structure and ATPase activity of the purified enzyme. *Proceedings of the National Academy of Sciences*, *75*(12), 5960-5963. https://doi.org/doi:10.1073/pnas.75.12.5960

Møller, A. K., Leatham, M. P., Conway, T., Nuijten, P. J., de Haan, L. A., Krogfelt, K. A., & Cohen, P. S. (2003). An *Escherichia coli* MG1655 lipopolysaccharide deep-rough core mutant grows and survives in mouse cecal mucus but fails to colonize the mouse large intestine. *Infection and immunity*, *71*(4), 2142-2152. https://doi.org/10.1128/iai.71.4.2142-2152.2003

Montanari, S., Oliver, A., Salerno, P., Mena, A., Bertoni, G., Tümmler, B., Cariani, L., Conese, M., Döring, G., & Bragonzi, A. (2007). Biological cost of hypermutation in *Pseudomonas aeruginosa* strains from patients with cystic fibrosis. *Microbiology (Reading)*, *153*(Pt 5), 1445-1454. https://doi.org/10.1099/mic.0.2006/003400-0

Moya, B., Dötsch, A., Juan, C., Blazquez, J., Zamorano, L., Haussler, S., & Oliver, A. (2009). Beta-lactam resistance response triggered by inactivation of a nonessential penicillin-binding protein. *PLoS Pathog*, *5*(3), e1000353. https://doi.org/10.1371/journal.ppat.1000353

Moya, B., Juan, C., Alberti, S., Perez, J. L., & Oliver, A. (2008). Benefit of having multiple *ampD* genes for acquiring beta-lactam resistance without losing fitness and virulence in *Pseudomonas aeruginosa*. *Antimicrobial agents and chemotherapy*, *52*(10), 3694-3700. https://doi.org/10.1128/AAC.00172-08

Mulcahy, L. R., Burns, J. L., Lory, S., & Lewis, K. (2010). Emergence of *Pseudomonas aeruginosa* strains producing high levels of persister cells in patients with cystic fibrosis. *Journal of bacteriology*, *192*(23), 6191-6199.

Murata, T., Minami, S., Yasuda, K., Iyobe, S., Inoue, M., & Mitsuhashi, S. (1981). Purification and properties of cephalosporinase from *Pseudomonas aeruginosa*. *J Antibiot (Tokyo)*, *34*(9), 1164-1170. https://doi.org/10.7164/antibiotics.34.1164

Obranic, S., Babic, F., & Maravic-Vlahovicek, G. (2013). Improvement of pBBR1MCS plasmids, a very useful series of broad-host-range cloning vectors. *Plasmid*, *70*(2), 263-267. https://doi.org/10.1016/j.plasmid.2013.04.001

Ochs, M. M., McCusker, M. P., Bains, M., & Hancock, R. E. (1999). Negative regulation of the *Pseudomonas aeruginosa* outer membrane porin OprD selective for imipenem and basic amino acids. *Antimicrobial agents and chemotherapy*, *43*(5), 1085-1090. https://doi.org/10.1128/aac.43.5.1085

Oliver, A., Baquero, F., & Blázquez, J. (2002). The mismatch repair system (*mutS, mutL* and *uvrD* genes) in *Pseudomonas aeruginosa*: molecular characterization of naturally

occurring mutants. *Molecular microbiology*, *43*(6), 1641-1650. https://doi.org/10.1046/j.1365-2958.2002.02855.x

Oliver, A., Canton, R., Campo, P., Baquero, F., & Blazquez, J. (2000). High frequency of hypermutable *Pseudomonas aeruginosa* in cystic fibrosis lung infection. *Science*, *288*(5469), 1251-1254. https://doi.org/10.1126/science.288.5469.1251

Olson, R. D., Assaf, R., Brettin, T., Conrad, N., Cucinell, C., Davis, J. J., Dempsey, D. M., Dickerman, A., Dietrich, E. M., Kenyon, R. W., Kuscuoglu, M., Lefkowitz, E. J., Lu, J., Machi, D., Macken, C., Mao, C., Niewiadomska, A., Nguyen, M., Olsen, G. J., . . . Stevens, R. L. (2023). Introducing the Bacterial and Viral Bioinformatics Resource Center (BV-BRC): a resource combining PATRIC, IRD and ViPR. *Nucleic acids research*, *51*(D1), D678-d689. https://doi.org/10.1093/nar/gkac1003

Otero-Asman, J. R., García-García, A. I., Civantos, C., Quesada, J. M., & Llamas, M. A. (2019). *Pseudomonas aeruginosa* possesses three distinct systems for sensing and using the host molecule haem. *Environ Microbiol*, *21*(12), 4629-4647. https://doi.org/10.1111/1462-2920.14773

Pakotiprapha, D., Samuels, M., Shen, K., Hu, J. H., & Jeruzalmi, D. (2012). Structure and mechanism of the UvrA-UvrB DNA damage sensor. *Nat Struct Mol Biol*, *19*(3), 291-298. https://doi.org/10.1038/nsmb.2240

Park, J. T., & Uehara, T. (2008). How bacteria consume their own exoskeletons (turnover and recycling of cell wall peptidoglycan). *Microbiol Mol Biol Rev*, *72*(2), 211-227, table of contents. https://doi.org/10.1128/MMBR.00027-07

Parker, D. J., Demetci, P., & Li, G. W. (2019). Rapid Accumulation of Motility-Activating Mutations in Resting Liquid Culture of *Escherichia coli*. *Journal of bacteriology*, *201*(19). https://doi.org/10.1128/JB.00259-19

Parks, T. D., Leuther, K. K., Howard, E. D., Johnston, S. A., & Dougherty, W. G. (1994). Release of proteins and peptides from fusion proteins using a recombinant plant virus proteinase. *Analytical biochemistry*, *216*(2), 413-417. https://doi.org/10.1006/abio.1994.1060

Patel, H., Ewels, P., Peltzer, A., Botvinnik, O., Sturm, G., Moreno, D., Vemuri, P., Silviamorins, Garcia, M. U., Pantano, L., Binzer-Panchal, M., Bot, N.-C., Zepper, M., Kelly, G., Syme, R., Hanssen, F., Yates, J. A. F., Cheshire, C., Rfenouil, . . . Talbot, A. (2023). *nf-core/rnaseq: nf-core/rnaseq v3.11.2 - Resurrected Radium Rhino*. In (Version 3.11.2) Zenodo. https://doi.org/10.5281/zenodo.7862091.

Patel, V., & Matange, N. (2021). Adaptation and compensation in a bacterial gene regulatory network evolving under antibiotic selection. *eLife*, *10*. https://doi.org/10.7554/eLife.70931

Paul, M., Benuri-Silbiger, I., Soares-Weiser, K., & Leibovici, L. (2004). β lactam monotherapy versus β lactam-aminoglycoside combination therapy for sepsis in immunocompetent patients: systematic review and meta-analysis of randomised trials. *BMJ*, *328*(7441), 668. https://doi.org/10.1136/bmj.38028.520995.63

Paul, M., Carrara, E., Retamar, P., Tängdén, T., Bitterman, R., Bonomo, R. A., de Waele, J., Daikos, G. L., Akova, M., Harbarth, S., Pulcini, C., Garnacho-Montero, J., Seme, K., Tumbarello, M., Lindemann, P. C., Gandra, S., Yu, Y., Bassetti, M., Mouton, J. W., . . . Rodríguez-Baño, J. (2022). European Society of Clinical Microbiology and Infectious Diseases (ESCMID) guidelines for the treatment of infections caused by multidrug-resistant Gram-negative bacilli (endorsed by European society of intensive care medicine). *Clinical Microbiology and Infection*, *28*(4), 521-547. https://doi.org/https://doi.org/10.1016/j.cmi.2021.11.025

Paulsson, M., Granrot, A., Ahl, J., Tham, J., Resman, F., Riesbeck, K., & Månsson, F. (2017). Antimicrobial combination treatment including ciprofloxacin decreased the mortality

rate of *Pseudomonas aeruginosa* bacteraemia: a retrospective cohort study. *European Journal of Clinical Microbiology & Infectious Diseases*, *36*(7), 1187-1196. https://doi.org/10.1007/s10096-017-2907-x

Pederson, K. J., Vallis, A. J., Aktories, K., Frank, D. W., & Barbieri, J. T. (1999). The amino-terminal domain of *Pseudomonas aeruginosa* ExoS disrupts actin filaments via small-molecular-weight GTP-binding proteins. *Molecular microbiology*, *32*(2), 393-401.

Peña, J. M., Prezioso, S. M., McFarland, K. A., Kambara, T. K., Ramsey, K. M., Deighan, P., & Dove, S. L. (2021). Control of a programmed cell death pathway in *Pseudomonas aeruginosa* by an antiterminator. *Nature communications*, *12*(1), 1702. https://doi.org/10.1038/s41467-021-21941-7

Perley-Robertson, G. E., Yadav, A. K., Winogrodzki, J. L., Stubbs, K. A., Mark, B. L., & Vocadlo, D. J. (2016). A Fluorescent Transport Assay Enables Studying AmpG Permeases Involved in Peptidoglycan Recycling and Antibiotic Resistance. *ACS chemical biology*, *11*(9), 2626-2635. https://doi.org/10.1021/acschembio.6b00552

Peter J. Mogayzel, J., Naureckas, E. T., Robinson, K. A., Brady, C., Guill, M., Lahiri, T., Lubsch, L., Matsui, J., Oermann, C. M., Ratjen, F., Rosenfeld, M., Simon, R. H., Hazle, L., Sabadosa, K., & Marshall, B. C. (2014). Cystic Fibrosis Foundation Pulmonary Guideline. Pharmacologic Approaches to Prevention and Eradication of Initial *Pseudomonas aeruginosa* Infection. *Annals of the American Thoracic Society*, *11*(10), 1640-1650. https://doi.org/10.1513/AnnalsATS.201404-166OC

Pfaffl, M. W. (2001). A new mathematical model for relative quantification in real-time RT-PCR. *Nucleic acids research*, *29*(9), e45. https://doi.org/10.1093/nar/29.9.e45

Pier, G. B. (2007). *Pseudomonas aeruginosa* lipopolysaccharide: A major virulence factor, initiator of inflammation and target for effective immunity. *International Journal of Medical Microbiology*, *297*(5), 277-295. https://doi.org/https://doi.org/10.1016/j.ijmm.2007.03.012

Platt, R., Drescher, C., Park, S. K., & Phillips, G. J. (2000). Genetic system for reversible integration of DNA constructs and *lacZ* gene fusions into the *Escherichia coli* chromosome. *Plasmid*, *43*(1), 12-23. https://doi.org/10.1006/plas.1999.1433

Plotly Technologies Inc. (2015). *Collaborative data science*. Plotly Technologies Inc. https://plot.ly

Poole, K., Krebes, K., McNally, C., & Neshat, S. (1993). Multiple antibiotic resistance in *Pseudomonas aeruginosa*: evidence for involvement of an efflux operon. *Journal of bacteriology*, *175*(22), 7363-7372. https://doi.org/10.1128/jb.175.22.7363-7372.1993

Poole, K., & Srikumar, R. (2001). Multidrug efflux in *Pseudomonas aeruginosa*: components, mechanisms and clinical significance. *Current topics in medicinal chemistry*, *1*(1), 59-71. https://doi.org/10.2174/1568026013395605

Poon, W. W., Davis, D. E., Ha, H. T., Jonassen, T., Rather, P. N., & Clarke, C. F. (2000). Identification of *Escherichia coli ubiB*, a gene required for the first monooxygenase step in ubiquinone biosynthesis. *Journal of bacteriology*, *182*(18), 5139-5146. https://doi.org/10.1128/JB.182.18.5139-5146.2000

Pope, C. F., O'Sullivan, D. M., McHugh, T. D., & Gillespie, S. H. (2008). A practical guide to measuring mutation rates in antibiotic resistance. *Antimicrobial agents and chemotherapy*, *52*(4), 1209-1214. https://doi.org/10.1128/aac.01152-07

R Core Team. (2023). R: A Language and Environment for Statistical Computing. *R Foundation for Statistical Computing, Vienna, Austria.* https://www.R-project.org

Rappsilber, J., Mann, M., & Ishihama, Y. (2007). Protocol for micro-purification, enrichment, pre-fractionation and storage of peptides for proteomics using StageTips. *Nature protocols*, *2*(8), 1896-1906. https://doi.org/10.1038/nprot.2007.261

5. References

Ray-Soni, A., Bellecourt, M. J., & Landick, R. (2016). Mechanisms of bacterial transcription termination: all good things must end. *Annual review of biochemistry*, *85*, 319-347.

Rees, V. E., Deveson Lucas, D. S., López-Causapé, C., Huang, Y., Kotsimbos, T., Bulitta, J. B., Rees, M. C., Barugahare, A., Peleg, A. Y., & Nation, R. L. (2019). Characterization of hypermutator *Pseudomonas aeruginosa* isolates from patients with cystic fibrosis in Australia. *Antimicrobial agents and chemotherapy*, *63*(4), 10.1128/aac. 02538-02518.

Reynolds, D., & Kollef, M. (2021). The Epidemiology and Pathogenesis and Treatment of *Pseudomonas aeruginosa* Infections: An Update. *Drugs*, *81*(18), 2117-2131. https://doi.org/10.1007/s40265-021-01635-6

Rice, L. B. (2008). Federal funding for the study of antimicrobial resistance in nosocomial pathogens: no ESKAPE. *The Journal of infectious diseases*, *197*(8), 1079-1081. https://doi.org/10.1086/533452

Ried, J. L., & Collmer, A. (1987). An *nptI-sacB-sacR* cartridge for constructing directed, unmarked mutations in gram-negative bacteria by marker exchange-eviction mutagenesis. *Gene*, *57*(2-3), 239-246. https://doi.org/10.1016/0378-1119(87)90127-2

Rietsch, A., Vallet-Gely, I., Dove, S. L., & Mekalanos, J. J. (2005). ExsE, a secreted regulator of type III secretion genes in *Pseudomonas aeruginosa*. *Proceedings of the National Academy of Sciences of the United States of America*, *102*(22), 8006-8011. https://doi.org/10.1073/pnas.0503005102

Robert Koch Institut. *Antibiotika Resistenz Surveillance (ARS)*. Retrieved 18.04.2024 from https://ars.rki.de

Rodríguez-Martínez, J. M., Poirel, L., & Nordmann, P. (2009). Extended-spectrum cephalosporinases in *Pseudomonas aeruginosa*. *Antimicrobial agents and chemotherapy*, *53*(5), 1766-1771. https://doi.org/10.1128/aac.01410-08

Ropy, A., Cabot, G., Sánchez-Diener, I., Aguilera, C., Moya, B., Ayala, J. A., & Oliver, A. (2015). Role of *Pseudomonas aeruginosa* low-molecular-mass penicillin-binding proteins in AmpC expression, β-lactam resistance, and peptidoglycan structure. *Antimicrobial agents and chemotherapy*, *59*(7), 3925-3934. https://doi.org/10.1128/aac.05150-14

Rosche, W. A., & Foster, P. L. (2000). Determining mutation rates in bacterial populations. *Methods*, *20*(1), 4-17. https://doi.org/10.1006/meth.1999.0901

Saito, K., Akama, H., Yoshihara, E., & Nakae, T. (2003). Mutations affecting DNA-binding activity of the MexR repressor of *mexR-mexA-mexB-oprM* operon expression. *Journal of bacteriology*, *185*(20), 6195-6198. https://doi.org/10.1128/jb.185.20.6195-6198.2003

Sanders, C. C., Bradford, P. A., Ehrhardt, A. F., Bush, K., Young, K. D., Henderson, T. A., & Sanders Jr, W. E. (1997). Penicillin-binding proteins and induction of AmpC beta-lactamase. *Antimicrobial agents and chemotherapy*, *41*(9), 2013-2015.

Sanders, C. C., & Sanders, W. E., Jr. (1986). Type I beta-lactamases of gram-negative bacteria: interactions with beta-lactam antibiotics. *The Journal of infectious diseases*, *154*(5), 792-800. https://doi.org/10.1093/infdis/154.5.792

Sato, H., Frank, D. W., Hillard, C. J., Feix, J. B., Pankhaniya, R. R., Moriyama, K., Finck-Barbançon, V., Buchaklian, A., Lei, M., & Long, R. M. (2003). The mechanism of action of the *Pseudomonas aeruginosa*-encoded type III cytotoxin, ExoU. *EMBO J*, *22*(12), 2959–2969. https://doi.org/10.1093/emboj/cdg290

Sauvage, E., Kerff, F., Terrak, M., Ayala, J. A., & Charlier, P. (2008). The penicillin-binding proteins: structure and role in peptidoglycan biosynthesis. *FEMS microbiology reviews*, *32*(2), 234-258. https://doi.org/10.1111/j.1574-6976.2008.00105.x

5. References

Scheurwater, E., Reid, C. W., & Clarke, A. J. (2008). Lytic transglycosylases: Bacterial space-making autolysins. *The international journal of biochemistry & cell biology*, *40*(4), 586-591. https://doi.org/https://doi.org/10.1016/j.biocel.2007.03.018

Scheurwater, E. M., Pfeffer, J. M., & Clarke, A. J. (2007). Production and purification of the bacterial autolysin N-acetylmuramoyl-L-alanine amidase B from *Pseudomonas aeruginosa*. *Protein Expr Purif*, *56*(1), 128-137. https://doi.org/10.1016/j.pep.2007.06.009

Schlender, J. F., Teutonico, D., Coboeken, K., Schnizler, K., Eissing, T., Willmann, S., Jaehde, U., & Stass, H. (2018). A Physiologically-Based Pharmacokinetic Model to Describe Ciprofloxacin Pharmacokinetics Over the Entire Span of Life. *Clinical pharmacokinetics*, *57*(12), 1613-1634. https://doi.org/10.1007/s40262-018-0661-6

Schluenzen, F., Tocilj, A., Zarivach, R., Harms, J., Gluehmann, M., Janell, D., Bashan, A., Bartels, H., Agmon, I., Franceschi, F., & Yonath, A. (2000). Structure of Functionally Activated Small Ribosomal Subunit at 3.3 Å Resolution. *Cell*, *102*(5), 615-623. https://doi.org/https://doi.org/10.1016/S0092-8674(00)00084-2

Schmidtke, A. J., & Hanson, N. D. (2006). Model system to evaluate the effect of *ampD* mutations on AmpC-mediated beta-lactam resistance. *Antimicrobial agents and chemotherapy*, *50*(6), 2030-2037. https://doi.org/10.1128/aac.01458-05

Schmidtke, A. J., & Hanson, N. D. (2008). Role of ampD homologs in overproduction of AmpC in clinical isolates of *Pseudomonas aeruginosa*. *Antimicrobial agents and chemotherapy*, *52*(11), 3922-3927. https://doi.org/10.1128/AAC.00341-08

Schneider, C. A., Rasband, W. S., & Eliceiri, K. W. (2012). NIH Image to ImageJ: 25 years of image analysis. *Nat Methods*, *9*(7), 671-675. https://doi.org/10.1038/nmeth.2089

Shafferman, A., Kolter, R., Stalker, D., & Helinski, D. R. (1982). Plasmid R6K DNA replication. III. Regulatory properties of the pi initiation protein. *J Mol Biol*, *161*(1), 57-76. https://doi.org/10.1016/0022-2836(82)90278-9

Shah, A., Lettieri, J., Kaiser, L., Echols, R., & Heller, A. H. (1994). Comparative pharmacokinetics and safety of ciprofloxacin 400 mg i.v. thrice daily versus 750 mg po twice daily. *The Journal of antimicrobial chemotherapy*, *33*(4), 795-801. https://doi.org/10.1093/jac/33.4.795

Shah, A., Lettieri, J., Nix, D., Wilton, J., & Heller, A. H. (1995). Pharmacokinetics of high-dose intravenous ciprofloxacin in young and elderly and in male and female subjects. *Antimicrobial agents and chemotherapy*, *39*(4), 1003-1006. https://doi.org/10.1128/AAC.39.4.1003

Shea, M. E., & Hiasa, H. (2003). The RuvAB branch migration complex can displace topoisomerase IV.quinolone.DNA ternary complexes. *The Journal of biological chemistry*, *278*(48), 48485-48490. https://doi.org/10.1074/jbc.M304217200

Sidorova, N. Y., Hung, S., & Rau, D. C. (2010). Stabilizing labile DNA-protein complexes in polyacrylamide gels. *Electrophoresis*, *31*(4), 648-653. https://doi.org/10.1002/elps.200900573

Simmons, L. A., Foti, J. J., Cohen, S. E., & Walker, G. C. (2008). The SOS Regulatory Network. *EcoSal Plus*, *3*(1). https://doi.org/10.1128/ecosalplus.5.4.3

Simon, R., Priefer, U., & Puhler, A. (1983). A Broad Host Range Mobilization System for Invivo Genetic-Engineering - Transposon Mutagenesis in Gram-Negative Bacteria. *Bio-Technology*, *1*(9), 784-791. https://doi.org/Doi 10.1038/Nbt1183-784

Snyder, D. S., & McIntosh, T. J. (2000). The Lipopolysaccharide Barrier: Correlation of Antibiotic Susceptibility with Antibiotic Permeability and Fluorescent Probe Binding Kinetics. *Biochemistry*, *39*(38), 11777-11787. https://doi.org/10.1021/bi000810n

Sobel, M. L., Hocquet, D., Cao, L., Plesiat, P., & Poole, K. (2005). Mutations in PA3574 (*nalD*) lead to increased MexAB-OprM expression and multidrug resistance in laboratory and

clinical isolates of *Pseudomonas aeruginosa*. *Antimicrobial agents and chemotherapy*, *49*(5), 1782-1786. https://doi.org/10.1128/aac.49.5.1782-1786.2005

Sonnabend, M. S., Klein, K., Beier, S., Angelov, A., Kluj, R., Mayer, C., Gross, C., Hofmeister, K., Beuttner, A., Willmann, M., Peter, S., Oberhettinger, P., Schmidt, A., Autenrieth, I. B., Schütz, M., & Bohn, E. (2020). Identification of Drug Resistance Determinants in a Clinical Isolate of *Pseudomonas aeruginosa* by High-Density Transposon Mutagenesis. *Antimicrobial agents and chemotherapy*, *64*(3). https://doi.org/10.1128/aac.01771-19

Sopirala, M. M., Mangino, J. E., Gebreyes, W. A., Biller, B., Bannerman, T., Balada-Llasat, J. M., & Pancholi, P. (2010). Synergy testing by Etest, microdilution checkerboard, and time-kill methods for pan-drug-resistant *Acinetobacter baumannii*. *Antimicrobial agents and chemotherapy*, *54*(11), 4678-4683. https://doi.org/10.1128/AAC.00497-10

Stael, S., Miller, L. P., Fernández-Fernández, Á. D., & Van Breusegem, F. (2022). Detection of Damage-Activated Metacaspase Activity by Western Blot in Plants. In M. Klemenčič, S. Stael, & P. F. Huesgen (Eds.), *Plant Proteases and Plant Cell Death: Methods and Protocols* (pp. 127-137). Springer US. https://doi.org/10.1007/978-1-0716-2079-3_11

Stalker, D. M., Kolter, R., & Helinski, D. R. (1982). Plasmid R6K DNA replication. I. Complete nucleotide sequence of an autonomously replicating segment. *J Mol Biol*, *161*(1), 33-43. https://doi.org/10.1016/0022-2836(82)90276-5

Stefely, J. A., Reidenbach, A. G., Ulbrich, A., Oruganty, K., Floyd, B. J., Jochem, A., Saunders, J. M., Johnson, I. E., Minogue, C. E., Wrobel, R. L., Barber, G. E., Lee, D., Li, S., Kannan, N., Coon, J. J., Bingman, C. A., & Pagliarini, D. J. (2015). Mitochondrial ADCK3 employs an atypical protein kinase-like fold to enable coenzyme Q biosynthesis. *Mol Cell*, *57*(1), 83-94. https://doi.org/10.1016/j.molcel.2014.11.002

Steinmetz, M., Le Coq, D., Djemia, H. B., & Gay, P. (1983). [Genetic analysis of *sacB*, the structural gene of a secreted enzyme, levansucrase of *Bacillus subtilis* Marburg]. *Mol Gen Genet*, *191*(1), 138-144. https://doi.org/10.1007/BF00330901 (Analyse genetique de sacB, gene de structure d'une enzyme secretee, la levane-saccharase de *Bacillus subtilis* Marburg.)

Stothard, P. (2000). The sequence manipulation suite: JavaScript programs for analyzing and formatting protein and DNA sequences. *Biotechniques*, *28*(6), 1102, 1104. https://doi.org/10.2144/00286ir01

Stubbs, K. A., Scaffidi, A., Debowski, A. W., Mark, B. L., Stick, R. V., & Vocadlo, D. J. (2008). Synthesis and use of mechanism-based protein-profiling probes for retaining beta-D-glucosaminidases facilitate identification of *Pseudomonas aeruginosa* NagZ. *J Am Chem Soc*, *130*(1), 327-335. https://doi.org/10.1021/ja0763605

Sugawara, E., Nagano, K., & Nikaido, H. (2012). Alternative folding pathways of the major porin OprF of Pseudomonas aeruginosa. *The FEBS journal*, *279*(6), 910-918. https://doi.org/https://doi.org/10.1111/j.1742-4658.2012.08481.x

Suginaka, H., Ichikawa, A., & Kotani, S. (1974). Penicillin-resistant mechanisms in *Pseudomonas aeruginosa*: effects of penicillin G and carbenicillin on transpeptidase and C -alanine carboxypeptidase activities. *Antimicrobial agents and chemotherapy*, *6*(6), 672-675. https://doi.org/10.1128/aac.6.6.672

Suginaka, H., Ichikawa, A., & Kotani, S. (1975). Penicillin-resistant mechanisms in *Pseudomonas aeruginosa*: binding of penicillin to *Pseudomonas aeruginosa* KM 338. *Antimicrobial agents and chemotherapy*, *7*(5), 629-635. https://doi.org/10.1128/aac.7.5.629

Sun, R., Zhang, C., Zhao, X., Han, X., Zhao, Q., Jiang, P., Liu, X., Zhang, W., Zhang, F., & Fu, Y. (2020). Genome-wide screening and characterization of genes involved in response to high dose of ciprofloxacin in *Escherichia coli*. In: Research Square.

5. References

Suzuki, H., van Heijenoort, Y., Tamura, T., Mizoguchi, J., Hirota, Y., & van Heijenoort, J. (1980). In vitro peptidoglycan polymerization catalysed by penicillin binding protein 1b of *Escherichia coli* K-12. *FEBS letters*, *110*(2), 245-249. https://doi.org/10.1016/0014-5793(80)80083-4

Szklarczyk, D., Kirsch, R., Koutrouli, M., Nastou, K., Mehryary, F., Hachilif, R., Gable, A. L., Fang, T., Doncheva, N. T., Pyysalo, S., Bork, P., Jensen, L. J., & von Mering, C. (2023). The STRING database in 2023: protein-protein association networks and functional enrichment analyses for any sequenced genome of interest. *Nucleic acids research*, *51*(D1), D638-d646. https://doi.org/10.1093/nar/gkac1000

Tacconelli, E., Carrara, E., Savoldi, A., Harbarth, S., Mendelson, M., Monnet, D. L., Pulcini, C., Kahlmeter, G., Kluytmans, J., Carmeli, Y., Ouellette, M., Outterson, K., Patel, J., Cavaleri, M., Cox, E. M., Houchens, C. R., Grayson, M. L., Hansen, P., Singh, N., . . . Group, W. H. O. P. P. L. W. (2018). Discovery, research, and development of new antibiotics: the WHO priority list of antibiotic-resistant bacteria and tuberculosis. *Lancet Infect Dis*, *18*(3), 318-327. https://doi.org/10.1016/S1473-3099(17)30753-3

Takyar, S., Hickerson, R. P., & Noller, H. F. (2005). mRNA Helicase Activity of the Ribosome. *Cell*, *120*(1), 49-58. https://doi.org/https://doi.org/10.1016/j.cell.2004.11.042

Tam, V. H., Schilling, A. N., LaRocco, M. T., Gentry, L. O., Lolans, K., Quinn, J. P., & Garey, K. W. (2007). Prevalence of AmpC over-expression in bloodstream isolates of *Pseudomonas aeruginosa*. *Clinical microbiology and infection : the official publication of the European Society of Clinical Microbiology and Infectious Diseases*, *13*(4), 413-418. https://doi.org/10.1111/j.1469-0691.2006.01674.x

Tamayo, M., Santiso, R., Gosalvez, J., Bou, G., & Fernández, J. L. (2009). Rapid assessment of the effect of ciprofloxacin on chromosomal DNA from *Escherichia coli* using an in situ DNA fragmentation assay. *BMC microbiology*, *9*, 69. https://doi.org/10.1186/1471-2180-9-69

Tamma, P. D., Aitken, S. L., Bonomo, R. A., Mathers, A. J., van Duin, D., & Clancy, C. J. (2021). Infectious Diseases Society of America Guidance on the Treatment of Extended-Spectrum β-lactamase Producing Enterobacterales (ESBL-E), Carbapenem-Resistant Enterobacterales (CRE), and *Pseudomonas aeruginosa* with Difficult-to-Treat Resistance (DTR-*P. aeruginosa*). *Clin Infect Dis*, *72*(7), e169-e183. https://doi.org/10.1093/cid/ciaa1478

Tamma, P. D., Cosgrove, S. E., & Maragakis, L. L. (2012). Combination therapy for treatment of infections with gram-negative bacteria. *Clin Microbiol Rev*, *25*(3), 450-470. https://doi.org/10.1128/cmr.05041-11

Tamma, P. D., Doi, Y., Bonomo, R. A., Johnson, J. K., & Simner, P. J. (2019). A Primer on AmpC β-Lactamases: Necessary Knowledge for an Increasingly Multidrug-resistant World. *Clin Infect Dis*, *69*(8), 1446-1455. https://doi.org/10.1093/cid/ciz173

Templin, M. F., Ursinus, A., & Holtje, J. V. (1999). A defect in cell wall recycling triggers autolysis during the stationary growth phase of *Escherichia coli*. *EMBO J*, *18*(15), 4108-4117. https://doi.org/10.1093/emboj/18.15.4108

Terrak, M., Ghosh, T. K., van Heijenoort, J., Van Beeumen, J., Lampilas, M., Aszodi, J., Ayala, J. A., Ghuysen, J. M., & Nguyen-Distèche, M. (1999). The catalytic, glycosyl transferase and acyl transferase modules of the cell wall peptidoglycan-polymerizing penicillin-binding protein 1b of *Escherichia coli*. *Molecular microbiology*, *34*(2), 350-364. https://doi.org/10.1046/j.1365-2958.1999.01612.x

The European Committee on Antimicrobial Susceptibility Testing. (2024). *Breakpoint tables for interpretation of MICs and zone diameters, version 14.0*. Retrieved 26.02.2024 from https://www.eucast.org/clinical_breakpoints

5. References

The UniProt Consortium. (2023). UniProt: the Universal Protein Knowledgebase in 2023. *Nucleic acids research*, *51*(D1), D523-D531. https://doi.org/10.1093/nar/gkac1052

Thi, M. T. T., Wibowo, D., & Rehm, B. H. (2020). *Pseudomonas aeruginosa* biofilms. *International journal of molecular sciences*, *21*(22), 8671.

Thi, T. D., López, E., Rodríguez-Rojas, A., Rodríguez-Beltrán, J., Couce, A., Guelfo, J. R., Castañeda-García, A., & Blázquez, J. (2011). Effect of *recA* inactivation on mutagenesis of *Escherichia coli* exposed to sublethal concentrations of antimicrobials. *The Journal of antimicrobial chemotherapy*, *66*(3), 531-538. https://doi.org/10.1093/jac/dkq496

Tipper, D. (1979). Mode of action of β-lactam antibiotics. *Reviews of Infectious Diseases*, *1*(1), 39-53.

Tomioka, S., Nikaido, T., Miyakawa, T., & Matsuhashi, M. (1983). Mutation of the N-acetylmuramyl-L-alanine amidase gene of *Escherichia coli* K-12. *Journal of bacteriology*, *156*(1), 463-465. https://doi.org/10.1128/jb.156.1.463-465.1983

Tooke, C. L., Hinchliffe, P., Bragginton, E. C., Colenso, C. K., Hirvonen, V. H. A., Takebayashi, Y., & Spencer, J. (2019). β-Lactamases and β-Lactamase Inhibitors in the 21st Century. *J Mol Biol*, *431*(18), 3472-3500. https://doi.org/https://doi.org/10.1016/j.jmb.2019.04.002

Torrens, G., Hernandez, S. B., Ayala, J. A., Moya, B., Juan, C., Cava, F., & Oliver, A. (2019). Regulation of AmpC-Driven beta-Lactam Resistance in *Pseudomonas aeruginosa*: Different Pathways, Different Signaling. *mSystems*, *4*(6). https://doi.org/10.1128/mSystems.00524-19

Torres-Barceló, C., Kojadinovic, M., Moxon, R., & MacLean, R. C. (2015). The SOS response increases bacterial fitness, but not evolvability, under a sublethal dose of antibiotic. *Proc Biol Sci*, *282*(1816), 20150885. https://doi.org/10.1098/rspb.2015.0885

Trebosc, V., Gartenmann, S., Royet, K., Manfredi, P., Totzl, M., Schellhorn, B., Pieren, M., Tigges, M., Lociuro, S., Sennhenn, P. C., Gitzinger, M., Bumann, D., & Kemmer, C. (2016). A Novel Genome-Editing Platform for Drug-Resistant Acinetobacter baumannii Reveals an AdeR-Unrelated Tigecycline Resistance Mechanism. *Antimicrobial agents and chemotherapy*, *60*(12), 7263-7271. https://doi.org/10.1128/AAC.01275-16

Turnidge, J. D. (1998). The Pharmacodynamics of β-Lactams. *Clinical Infectious Diseases*, *27*(1), 10-22. https://doi.org/10.1086/514622

Tyanova, S., Temu, T., & Cox, J. (2016). The MaxQuant computational platform for mass spectrometry-based shotgun proteomics. *Nature protocols*, *11*(12), 2301-2319. https://doi.org/10.1038/nprot.2016.136

Tyanova, S., Temu, T., Sinitcyn, P., Carlson, A., Hein, M. Y., Geiger, T., Mann, M., & Cox, J. (2016). The Perseus computational platform for comprehensive analysis of (prote)omics data. *Nat Methods*, *13*(9), 731-740. https://doi.org/10.1038/nmeth.3901

Valencia, E. Y., Esposito, F., Spira, B., Blázquez, J., & Galhardo, R. S. (2017). Ciprofloxacin-Mediated Mutagenesis Is Suppressed by Subinhibitory Concentrations of Amikacin in *Pseudomonas aeruginosa*. *Antimicrobial agents and chemotherapy*, *61*(3). https://doi.org/10.1128/aac.02107-16

Vardakas, K. Z., Tansarli, G. S., Bliziotis, I. A., & Falagas, M. E. (2013). β-Lactam plus aminoglycoside or fluoroquinolone combination versus β-lactam monotherapy for *Pseudomonas aeruginosa* infections: a meta-analysis. *Int J Antimicrob Agents*, *41*(4), 301-310. https://doi.org/10.1016/j.ijantimicag.2012.12.006

Verhoeven, E. E., Wyman, C., Moolenaar, G. F., & Goosen, N. (2002). The presence of two UvrB subunits in the UvrAB complex ensures damage detection in both DNA strands. *EMBO J*, *21*(15), 4196-4205. https://doi.org/10.1093/emboj/cdf396

5. References

Vestergaard, M., Paulander, W., Marvig, R. L., Clasen, J., Jochumsen, N., Molin, S., Jelsbak, L., Ingmer, H., & Folkesson, A. (2016). Antibiotic combination therapy can select for broad-spectrum multidrug resistance in *Pseudomonas aeruginosa*. *Int J Antimicrob Agents*, *47*(1), 48-55. https://doi.org/10.1016/j.ijantimicag.2015.09.014

Vinella, D., Albrecht, C., Cashel, M., & D'Ari, R. (2005). Iron limitation induces SpoT-dependent accumulation of ppGpp in *Escherichia coli*. *Molecular microbiology*, *56*(4), 958-970. https://doi.org/10.1111/j.1365-2958.2005.04601.x

Vogne, C., Aires, J. R., Bailly, C., Hocquet, D., & Plésiat, P. (2004). Role of the multidrug efflux system MexXY in the emergence of moderate resistance to aminoglycosides among *Pseudomonas aeruginosa* isolates from patients with cystic fibrosis. *Antimicrobial agents and chemotherapy*, *48*(5), 1676-1680. https://doi.org/10.1128/aac.48.5.1676-1680.2004

Vollmer, W., Blanot, D., & De Pedro, M. A. (2008). Peptidoglycan structure and architecture. *FEMS microbiology reviews*, *32*(2), 149-167. https://doi.org/10.1111/j.1574-6976.2007.00094.x

Voulhoux, R., Taupiac, M. P., Czjzek, M., Beaumelle, B., & Filloux, A. (2000). Influence of deletions within domain II of exotoxin A on its extracellular secretion from *Pseudomonas aeruginosa*. *Journal of bacteriology*, *182*(14), 4051-4058. https://doi.org/10.1128/jb.182.14.4051-4058.2000

Walsh, T. J., Peter, J., McGough, D. A., Fothergill, A. W., Rinaldi, M. G., & Pizzo, P. A. (1995). Activities of amphotericin B and antifungal azoles alone and in combination against Pseudallescheria boydii. *Antimicrobial agents and chemotherapy*, *39*(6), 1361-1364. https://doi.org/10.1128/AAC.39.6.1361

Wang, T., Hu, Z., Du, X., Shi, Y., Dang, J., Lee, M., Hesek, D., Mobashery, S., Wu, M., & Liang, H. (2020). A type VI secretion system delivers a cell wall amidase to target bacterial competitors. *Molecular microbiology, 114*(2), 308-321. https://doi.org/10.1111/mmi.14513

Wassermann, T., Meinike Jørgensen, K., Ivanyshyn, K., Bjarnsholt, T., Khademi, S. H., Jelsbak, L., Høiby, N., & Ciofu, O. (2016). The phenotypic evolution of *Pseudomonas aeruginosa* populations changes in the presence of subinhibitory concentrations of ciprofloxacin. *Microbiology*, *162*(5), 865-875.

Waxman, D. J., & Strominger, J. L. (1983). Penicillin-binding proteins and the mechanism of action of beta-lactam antibiotics. *Annual review of biochemistry*, *52*(1), 825-869.

Weirich, J., Brautigam, C., Muhlenkamp, M., Franz-Wachtel, M., Macek, B., Meuskens, I., Skurnik, M., Leskinen, K., Bohn, E., Autenrieth, I., & Schutz, M. (2017). Identifying components required for OMP biogenesis as novel targets for antiinfective drugs. *Virulence*, *8*(7), 1170-1188. https://doi.org/10.1080/21505594.2016.1278333

Wen, A., Zhao, M., Jin, S., Lu, Y. Q., & Feng, Y. (2022). Structural basis of AlpA-dependent transcription antitermination. *Nucleic acids research*, *50*(14), 8321-8330. https://doi.org/10.1093/nar/gkac608

Westfall, L. W., Carty, N. L., Layland, N., Kuan, P., Colmer-Hamood, J. A., & Hamood, A. N. (2006). *mvaT* mutation modifies the expression of the *Pseudomonas aeruginosa* multidrug efflux operon *mexEF-oprN*. *FEMS microbiology letters*, *255*(2), 247-254. https://doi.org/10.1111/j.1574-6968.2005.00075.x

White, R. L., Burgess, D. S., Manduru, M., & Bosso, J. A. (1996). Comparison of three different in vitro methods of detecting synergy: time-kill, checkerboard, and E test. *Antimicrobial agents and chemotherapy*, *40*(8), 1914-1918. https://doi.org/10.1128/AAC.40.8.1914

Wickham, H. (2016). *ggplot2: Elegant Graphics for Data Analysis*. Springer-Verlag New York. ISBN 978-3-319-24277-4, https://ggplot2.tidyverse.org.

5. References

Wilkins, M. R., Gasteiger, E., Bairoch, A., Sanchez, J. C., Williams, K. L., Appel, R. D., & Hochstrasser, D. F. (1999). Protein identification and analysis tools in the ExPASy server. *Methods in molecular biology*, *112*, 531-552. https://doi.org/10.1385/1-59259-584-7:531

Willmann, M., Goettig, S., Bezdan, D., Macek, B., Velic, A., Marschal, M., Vogel, W., Flesch, I., Markert, U., Schmidt, A., Kübler, P., Haug, M., Javed, M., Jentzsch, B., Oberhettinger, P., Schütz, M., Bohn, E., Sonnabend, M., Klein, K., . . . Peter, S. (2018). Multi-omics approach identifies novel pathogen-derived prognostic biomarkers in patients with *Pseudomonas aeruginosa* bloodstream infection. *biorxiv*, 1-35. https://doi.org/10.1101/309898

Wilmaerts, D., Focant, C., Matthay, P., & Michiels, J. (2022). Transcription-coupled DNA repair underlies variation in persister awakening and the emergence of resistance. *Cell Rep*, *38*(9), 110427. https://doi.org/10.1016/j.celrep.2022.110427

Wilmaerts, D., Govers, S. K., & Michiels, J. (2022). Assessing persister awakening dynamics following antibiotic treatment in *E. coli*. *STAR Protoc*, *3*(3), 101476. https://doi.org/10.1016/j.xpro.2022.101476

Wilmaerts, D., Windels, E. M., Verstraeten, N., & Michiels, J. (2019). General Mechanisms Leading to Persister Formation and Awakening. *Trends in Genetics*, *35*(6), 401-411. https://doi.org/https://doi.org/10.1016/j.tig.2019.03.007

Wilson, D. N., & Nierhaus, K. H. (2005). Ribosomal Proteins in the Spotlight. *Critical Reviews in Biochemistry and Molecular Biology*, *40*(5), 243-267. https://doi.org/10.1080/10409230500256523

Wong, D., & van Duin, D. (2017). Novel Beta-Lactamase Inhibitors: Unlocking Their Potential in Therapy. *Drugs*, *77*(6), 615-628. https://doi.org/10.1007/s40265-017-0725-1

Wood, T. K., Knabel, S. J., & Kwan, B. W. (2013). Bacterial persister cell formation and dormancy. *Applied and environmental microbiology*, *79*(23), 7116-7121. https://doi.org/10.1128/aem.02636-13

World Health Organization. (2024). *WHO Bacterial Priority Pathogens List, 2024: bacterial pathogens of public health importance to guide research, development and strategies to prevent and control antimicrobial resistance.* Geneva https://www.who.int/publications/i/item/9789240093461

Wozniak, K. J., & Simmons, L. A. (2022). Bacterial DNA excision repair pathways. *Nature Reviews Microbiology*, *20*(8), 465-477.

Yakhnina, A. A., McManus, H. R., & Bernhardt, T. G. (2015). The cell wall amidase AmiB is essential for *Pseudomonas aeruginosa* cell division, drug resistance and viability. *Molecular microbiology*, *97*(5), 957-973. https://doi.org/10.1111/mmi.13077

Yang, F., Zhou, Y., Chen, P., Cai, Z., Yue, Z., Jin, Y., Cheng, Z., Wu, W., Yang, L., Ha, U. H., & Bai, F. (2022). High-Level Expression of Cell-Surface Signaling System Hxu Enhances *Pseudomonas aeruginosa* Bloodstream Infection. *Infection and immunity*, *90*(10), e0032922. https://doi.org/10.1128/iai.00329-22

Yates, S. P., & Merrill, A. R. (2004). Elucidation of eukaryotic elongation factor-2 contact sites within the catalytic domain of *Pseudomonas aeruginosa* exotoxin A. *Biochem J*, *379*(Pt 3), 563-572. https://doi.org/10.1042/bj20031731

Yem, D. W., & Wu, H. C. (1976). Purification and properties of beta-N-acetylglucosaminidase from *Escherichia coli*. *Journal of bacteriology*, *125*(1), 324-331. https://doi.org/10.1128/jb.125.1.324-331.1976

Yokota, S.-i., & Fujii, N. (2007). Contributions of the lipopolysaccharide outer core oligosaccharide region on the cell surface properties of *Pseudomonas aeruginosa*. *Comparative Immunology, Microbiology and Infectious Diseases*, *30*(2), 97-109. https://doi.org/https://doi.org/10.1016/j.cimid.2006.11.002

5. References

Yoshimura, F., & Nikaido, H. (1982). Permeability of *Pseudomonas aeruginosa* outer membrane to hydrophilic solutes. *Journal of bacteriology*, *152*(2), 636-642 http://www.ncbi.nlm.nih.gov/pubmed/6813310. https://journals.asm.org/doi/pdf/10.1128/jb.152.2.636-642.1982?download=true

Young, I. G., Stroobant, P., Macdonald, C. G., & Gibson, F. (1973). Pathway for ubiquinone biosynthesis in *Escherichia coli* K-12: gene-enzyme relationships and intermediates. *Journal of bacteriology*, *114*(1), 42-52. https://doi.org/10.1128/jb.114.1.42-52.1973

Zamarreño Beas, J., Videira, M. A. M., & Saraiva, L. M. (2022). Regulation of bacterial haem biosynthesis. *Coordination Chemistry Reviews*, *452*, 214286. https://doi.org/https://doi.org/10.1016/j.ccr.2021.214286

Zamorano, L., Moyá, B., Juan, C., & Oliver, A. (2010). Differential β-lactam resistance response driven by *ampD* or *dacB* (PBP4) inactivation in genetically diverse *Pseudomonas aeruginosa* strains. *Journal of Antimicrobial Chemotherapy*, *65*(7), 1540-1542. https://doi.org/10.1093/jac/dkq142

Zhanel, G. G., Lawrence, C. K., Adam, H., Schweizer, F., Zelenitsky, S., Zhanel, M., Lagacé-Wiens, P. R. S., Walkty, A., Denisuik, A., Golden, A., Gin, A. S., Hoban, D. J., Lynch, J. P., 3rd, & Karlowsky, J. A. (2018). Imipenem-Relebactam and Meropenem-Vaborbactam: Two Novel Carbapenem-β-Lactamase Inhibitor Combinations. *Drugs*, *78*(1), 65-98. https://doi.org/10.1007/s40265-017-0851-9

Zhang, W., Lee, M., Hesek, D., Lastochkin, E., Boggess, B., & Mobashery, S. (2013). Reactions of the three AmpD enzymes of *Pseudomonas aeruginosa*. *J Am Chem Soc*, *135*(13), 4950-4953. https://doi.org/10.1021/ja400970n

6. Figures

7. Tables

7. Tables

7. Tables

8. Equations

8. Equations

9. Appendix

9.1. Protein purification

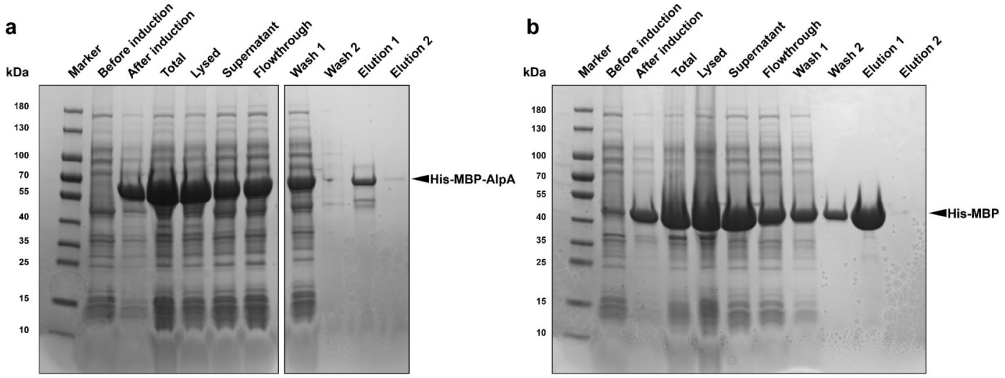

Figure 32: SDS-PAGE gels stained with Coomassie monitoring the purification of His-MBP-AlpA and His-MBP. a) Purification of His-MBP-AlpA (64.57 kDa) expressed in one liter of LB medium using the strain *E. coli* BL21(DE3) pETM41_*alpA* after induction with 1 mM IPTG overnight at 20°C. **b)** Purification of His-MBP (44.52 kDa) expressed in one liter of LB medium using the strain *E. coli* BL21(DE3) pETM41 and 1 mM IPTG for induction. **a + b)** Purification was done by Ni^{2+}-NTA affinity chromatography using 50 mM Tris pH 7.5, 150 mM NaCl and 25 mM imidazole as a buffer, followed by a dialysis against 50 mM Tris pH 7.5, 150 mM NaCl and 20% (V/V) glycerol. Samples of the indicated, purified fractions were taken, loaded on an SDS-PAGE gel, and subsequently stained with Coomassie. His-MBP-AlpA: Elution 1 and 2 pooled, final concentration of 24.4 µM in 15 ml. Yield: 23.63 mg of protein per 1 liter of culture. His-MBP: Elution 1 kept, final concentration of 297.4 µM in 10 ml. Yield 132.4 mg of protein per liter of expression culture.

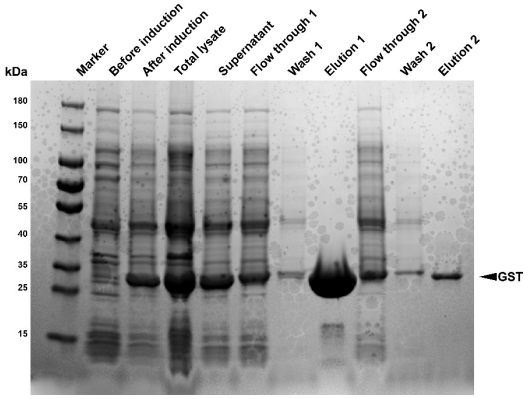

Figure 33: SDS-PAGE gels stained with Coomassie monitoring the purification of GST. Purification of GST (25.50 kDa) expressed in one liter of LB medium using the strain *E. coli* BL21(DE3) pGEX4T3 after induction with 1 mM IPTG overnight at 25°C. Purification was done using a GSTrap HP 1ml column as described in the method section with 50 mM Tris, 150 mM NaCl, 1 mM DTT, pH 7.5 as a lysis buffer, and eluted using 50 mM Tris, 150 mM NaCl, 10 mM reduced glutathione, pH 8 as a buffer. The eluate fractions were dialyzed against 10 liter of PBS pH 7.4 containing 0.5 mM DTT with a ZelluTrans dialysis tube. Samples of the indicated purified fractions were taken, loaded on an SDS-PAGE gel, and subsequently stained with Coomassie. Elution 1 and 2 were pooled. Final concentration: 152.1 µM GST in 9 ml. Yield of 34.9 mg protein per liter of expression culture. Protein was frozen in dialysis buffer.

9. Appendix

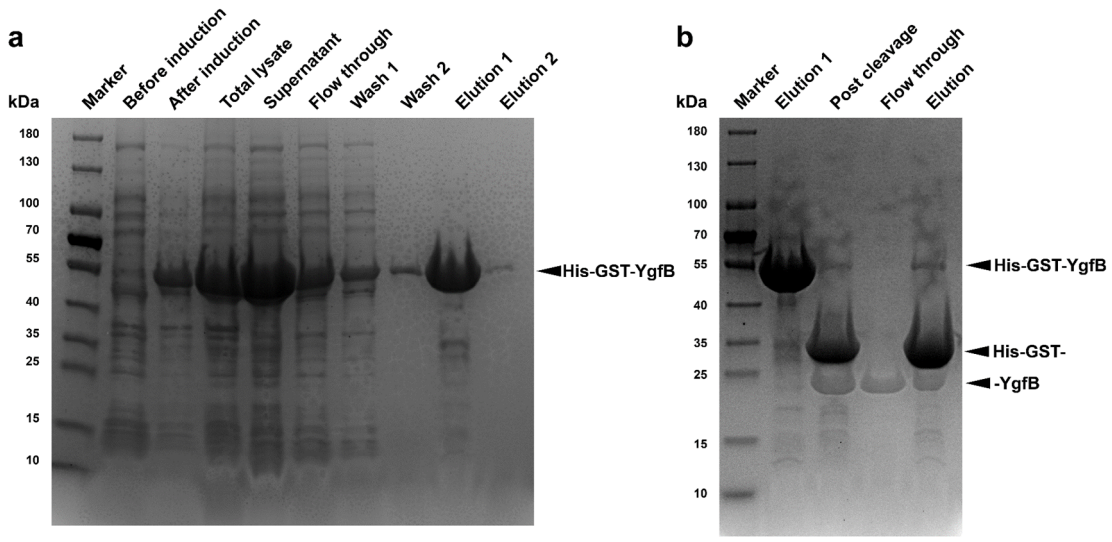

Figure 34: SDS-PAGE analysis of YgfB purification fractions. a) Purification of His-GST-YgfB (48.53 kDa) expressed in one liter of LB medium using the strain *E. coli* BL21(DE3) pETM30_*ygfB* after induction with 1 mM IPTG overnight at 25°C. Purification was done by Ni^{2+}-NTA affinity chromatography. **b)** Results of TEV cleavage of His-GST-YgfB, yielding His-GST- (28.86 kDa) and -YgfB (19.69 kDa). Elution 1 stems from the purification shown in **(a)** and served as an input to the TEV cleavage. Post cleavage indicates the whole reaction after overnight digest. The flow through contains all proteins in the digestion mix that have not bound to the Ni^{2+}-NTA beads, containing -YgfB. Elution reflects an elution of the reverse Ni^{2+}-NTA chromatography and contains all 6xHis-tagged components of the reaction that have bound to the Ni^{2+}-NTA beads. Yield: 22 ml of YgfB at a concentration of 123.3 µM. 53.4 mg of protein per 1 liter of expression culture

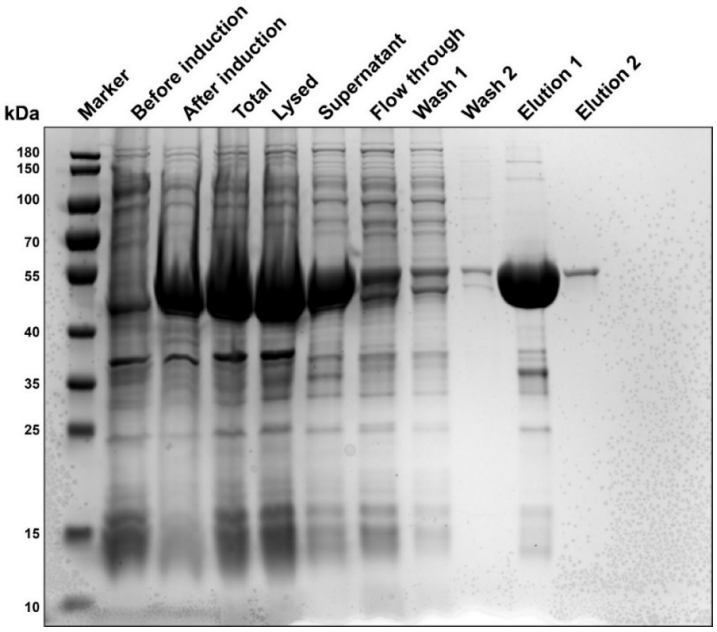

Figure 35: SDS-PAGE of purification fractions by Ni^{2+}-NTA chromatography for His-GST-EcYgfB. Purification of His-GST-EcYgfB (50.30 kDa) expressed in one liter of LB medium using the strain *E. coli* BL21(DE3) pETM30_Ec_*ygfB* after induction with 1 mM IPTG overnight at 25°C. Purification was done by Ni^{2+}-NTA affinity chromatography using 50 mM Tris pH 7.5, 150 mM NaCl and 25 mM imidazole and 1 mM DTT as a buffer. Elution 1 was dialyzed against 50 mM Tris pH 7.5, 150 mM NaCl and 10% (m/V) glycerol and 1 mM DTT. Samples of the indicated purified fractions were taken, loaded on an SDS-PAGE gel, and subsequently stained with Coomassie. Elution 1 was taken for further purification by SEC.

9. Appendix

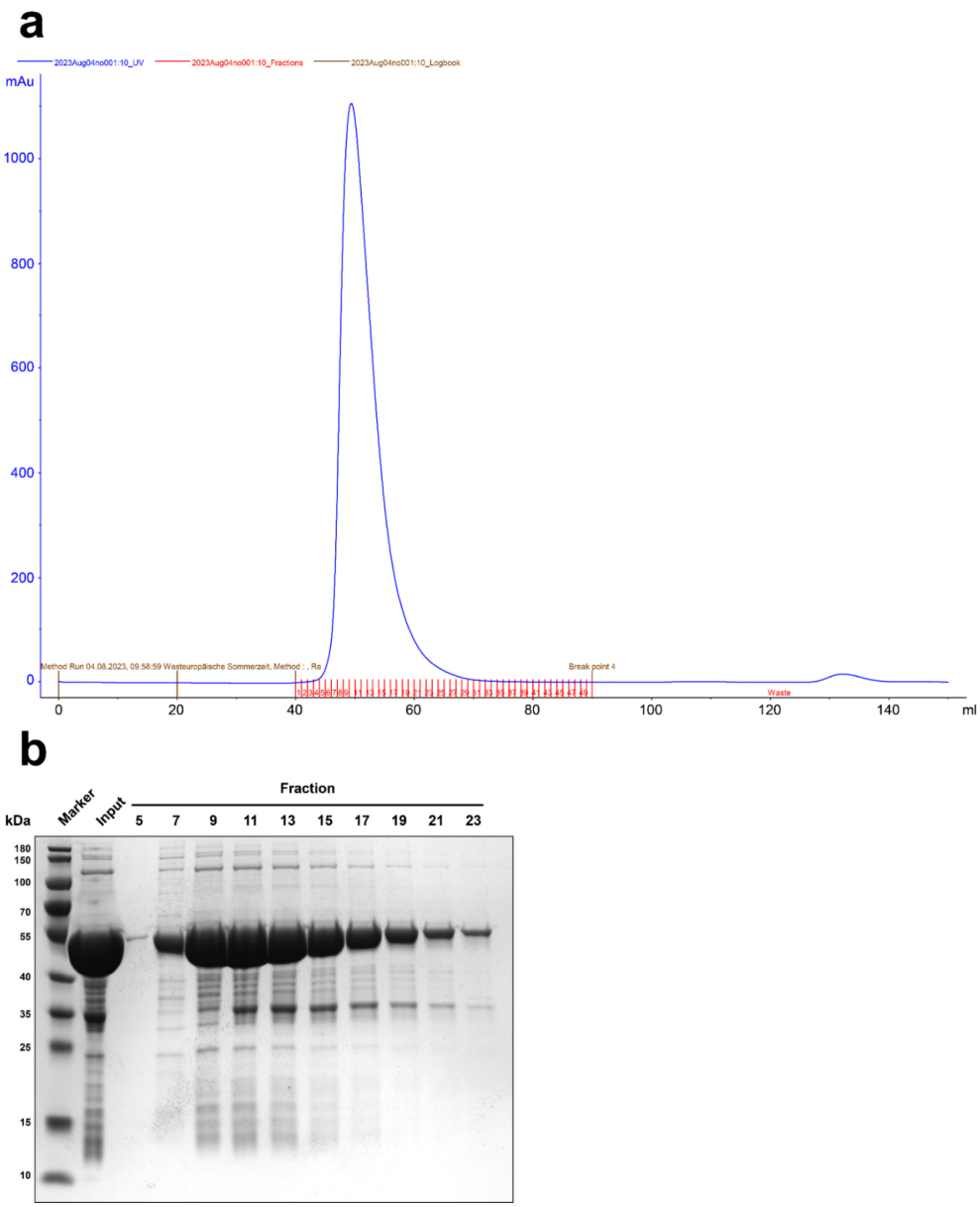

Figure 36: Size-exclusion chromatography of His-GST-EcYgfB. Elution fraction 1 of the Ni^{2+}-NTA affinity chromatography containing His-GST-EcYgfB (50.03 kDa) was upconcentrated using a 30 kDa Amicon Ultra Centrifugal Filter. The upconcentrated protein solution was loaded on a HiLoad 16/600 Superdex 75 pg size exclusion column with 50 mM Tris pH 7.5, 150 mM NaCl, 10% glycerol (m/V) and 1 mM DTT as a running buffer. **a)** Chromatogram of the SEC purification. Fractions of 1 ml were collected at the indicated steps of the chromatogram, and loaded on an SDS-PAGE gel **(b)**,which was then stained with Coomassie. Fractions 8-20 were pooled for storage of the protein.

9. Appendix

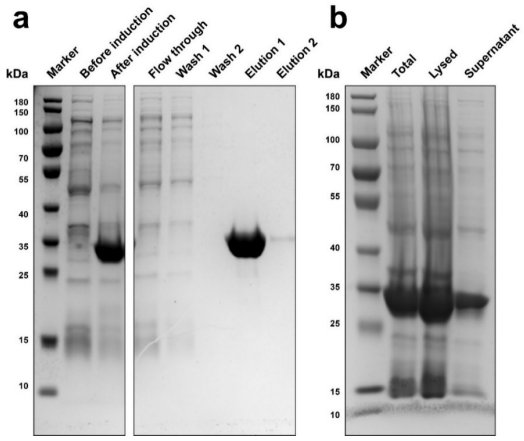

Figure 37: Purification of His-GST. Purification of His-GST (29.09 kDa) expressed in one liter of LB medium using the strain *E. coli* BL21(DE3) pETM30_stop after induction with 1 mM IPTG overnight at 25°C. Purification was done by Ni^{2+}-NTA affinity chromatography using 50 mM Tris pH 7.5, 150 mM NaCl and 25 mM imidazole and 1 mM DTT as a buffer. Elution 1 was dialyzed against 50 mM Tris pH 7.5, 150 mM NaCl and 10% (m/V) glycerol and 1 mM DTT. Samples of the indicated purified fractions were taken, loaded on an SDS-PAGE gel, and subsequently stained with Coomassie. **a)** Gel showing samples before induction, after induction as well as purification. All samples were run on the same gel but the image has been trimmed for better visualization. **b)** Second gel showing total cells, lysate after sonication as well as supernatant after centrifugation.

9. Appendix

9.2. RNAseq

9.2.1. Differentially expressed genes ID40Δ*ygfB* vs. ID40

Table 34: Significantly differentially expressed genes in transcriptome of *P. aeruginosa* ID40Δ*ygfB* vs. ID40. Data analysis as described in the methods. $n = 3$. Genes with an adjusted p value of ≤0.01 and a $\log_2$ fold change of ≥2 or ≤-2 were considered differentially expressed.

Gene ID	Gene names	Product	PAO1 ortholog	$\log_2$ fold change	Adjusted p value
TUEID40_01949	*cefD_2*	Isopenicillin N epimerase	PA0813	3.22	5.27E-04
TUEID40_01950	TUEID40_01950	hypothetical protein	PA0812	4.46	1.73E-16
TUEID40_01951	*yjjL*	L-galactonate transporter	PA0811	3.71	9.51E-09
TUEID40_01953	*mntH2*	Divalent metal cation transporter MntH	PA0809	3.95	5.12E-12
TUEID40_01955	*ampDh3*	N-acetylmuramoyl-L-alanine amidase AmiD precursor	PA0807	5.63	9.98E-43
TUEID40_03245	*ygfB*	hypothetical protein	PA5225	-5.03	2.61E-11

9.2.2. Differentially expressed genes in ID40 +CIP vs. ID40

Table 35: Significantly differentially expressed genes in transcriptome of *P. aeruginosa* ID40 +CIP vs. ID40. Data analysis as described in the methods. $n = 3$. Genes with an adjusted p value of ≤0.01 and a $\log_2$ fold change of ≥2 or ≤-2 were considered differentially expressed.

Gene ID (ID40)	Gene name	ID40 product	Ortholog ID (PAO1 or phage)	Ortholog organism (If not PAO1)	$\log_2$ fold change	Adjusted p value
TUEID40_00161	TUEID40_00161	Mu-like prophage I protein	A0A2D1GNS3_9CAUD	Pseudomonas phage VW-6B	6.08	1.19E-59
TUEID40_00162	TUEID40_00162	Mu-like prophage major head subunit gpT	Q6TM67_BPD31	Pseudomonas phage D3112 (Bacteriophage D3112)	6.53	3.86E-91
TUEID40_00205	TUEID40_00205	hypothetical protein	PA2288	PAO1	3.58	3.84E-12
TUEID40_00206	TUEID40_00206	hypothetical protein	PA2287	PAO1	3.94	2.93E-21
TUEID40_00207	TUEID40_00207	M48 family peptidase	PA2286	PAO1	4.07	1.35E-25
TUEID40_00600	TUEID40_00600	hypothetical protein	PA1942	PAO1	3.39	1.88E-08
TUEID40_01195	*aruI*	putative 2-ketoarginine decar-boxylase AruI	PA1417	PAO1	3.50	1.02E-14
TUEID40_01197	TUEID40_01197	putative FAD-linked oxidore-ductase	PA1416	PAO1	3.19	2.21E-07

9. Appendix

Gene ID (ID40)	Gene name	ID40 product	Ortholog ID (PAO1 or phage)	Ortholog organism (If not PAO1)	log_2 fold change	Adjusted *p* value
TUEID40_01319	TUEID40_01319	Acyl-CoA dehydrogenase, short-chain specific	PA1284	PAO1	3.76	6.15E-13
TUEID40_01320	TUEID40_01320	transcriptional regulator BetI	PA1283	PAO1	3.63	5.10E-07
TUEID40_01321	*smvA*	Methyl viologen resistance protein SmvA	PA1282	PAO1	5.04	5.26E-35
TUEID40_01457	*nrdA*	Ribonucleoside-diphosphate reductase 1 subunit alpha	PA1156	PAO1	4.03	2.24E-17
TUEID40_01458	*nrdB*	Ribonucleoside-diphosphate reductase subunit beta	PA1155	PAO1	3.86	1.69E-25
TUEID40_01460	TUEID40_01460	hypothetical protein	PA1153	PAO1	3.77	2.52E-18
TUEID40_01461	*pys2*	Pyocin-S2	PA1150	PAO1	6.50	3.86E-197
TUEID40_01836	TUEID40_01836	hypothetical protein	PA0912	PAO1	5.88	1.29E-44
TUEID40_01837	*alpE*	hypothetical protein	PA0911	PAO1	5.67	1.55E-51
TUEID40_01838	*alpD*	hypothetical protein	PA0910	PAO1	6.72	2.38E-61
TUEID40_01839	*alpC*	hypothetical protein	PA0909	PAO1	5.76	1.33E-28
TUEID40_01840	*alpB*	hypothetical protein	PA0908	PAO1	5.77	2.76E-30
TUEID40_01841	*alpA*	hypothetical protein	PA0907	PAO1	3.64	2.67E-09
TUEID40_01948	TUEID40_01948	Endoribonuclease L-PSP	PA0814	PAO1	4.35	4.79E-08
TUEID40_01949	*cefD_2*	Isopenicillin N epimerase	PA0813	PAO1	3.50	2.50E-08
TUEID40_01950	TUEID40_01950	hypothetical protein	PA0812	PAO1	5.02	1.03E-27
TUEID40_01951	*yjjL*	L-galactonate transporter	PA0811	PAO1	4.36	1.64E-19
TUEID40_01952	*hdl IVa*	(S)-2-haloacid dehalogenase 4A	PA0810	PAO1	2.94	1.02E-03
TUEID40_01953	*mntH2*	Divalent metal cation transporter MntH	PA0809	PAO1	4.21	1.43E-17
TUEID40_01955	*ampDh3*	N-acetylmuramoyl-L-alanine amidase AmiD precursor	PA0807	PAO1	6.86	6.28E-80
TUEID40_02147	TUEID40_02147	ABM domain-containing protein	PA0709	PAO1	3.77	5.08E-07
TUEID40_02186	*sulA2*	SOS cell division inhibitor	PA0671	PAO1	3.34	5.05E-03
TUEID40_02187	*imuB*	impB/mucB/samB family protein	PA0670	PAO1	3.27	1.06E-06
TUEID40_02545	TUEID40_02545	hypothetical protein	PA4623	PAO1	3.17	8.07E-03
TUEID40_02708	*recN*	DNA repair protein RecN	PA4763	PAO1	3.17	1.92E-06
TUEID40_02834	TUEID40_02834	hypothetical protein	PA4881	PAO1	4.20	9.00E-12
TUEID40_03605	gyrB	DNA gyrase subunit B	PA0004	PAO1	-2.64	1.37E-03

9. Appendix

Gene ID (ID40)	Gene name	ID40 product	Ortholog ID (PAO1 or phage)	Ortholog organism (If not PAO1)	log_2 fold change	Adjusted *p* value
TUEID40_03608	TUEID40_03608	hypothetical protein	PA0007	PAO1	-2.74	1.39E-03
TUEID40_03662	TUEID40_03662	hypothetical protein	PA0050	PAO1	-3.08	2.32E-03
TUEID40_04247	*prtN*	Pyocin activator protein PrtN	PA0610	PAO1	4.43	4.19E-55
TUEID40_04249	TUEID40_04249	hypothetical protein	No ortholog	PAO1	5.64	1.14E-45
TUEID40_04250	*ptrB*	hypothetical protein	PA0612	PAO1	5.98	2.67E-154
TUEID40_04251	TUEID40_04251	hypothetical protein	PA0613	PAO1	5.52	6.96E-97
TUEID40_04252	TUEID40_04252	hypothetical protein	PA0614	PAO1	6.99	9.88E-125
TUEID40_04253	TUEID40_04253	Chitinase class I	PA0629	PAO1	6.84	1.52E-121
TUEID40_04254	TUEID40_04254	hypothetical protein	PA0630	PAO1	6.85	9.56E-132
TUEID40_04255	TUEID40_04255	hypothetical protein	PA0631	PAO1	6.74	6.33E-176
TUEID40_04256	TUEID40_04256	hypothetical protein	PA0633	PAO1	7.54	3.50E-178
TUEID40_04257	TUEID40_04257	hypothetical protein	PA0634	PAO1	7.50	1.33E-294
TUEID40_04258	TUEID40_04258	hypothetical protein	PA0635	PAO1	7.58	2.84E-234
TUEID40_04259	TUEID40_04259	Lambda phage tail tape-measure protein (Tape_meas_lam_C)	PA0636	PAO1	6.82	1.92E-138
TUEID40_04260	TUEID40_04260	Phage minor tail protein	PA0637	PAO1	6.77	1.92E-138
TUEID40_04261	TUEID40_04261	Phage minor tail protein L	PA0638	PAO1	6.58	1.62E-191
TUEID40_04262	TUEID40_04262	NlpC/P60 family protein	PA0639	PAO1	6.64	3.45E-179
TUEID40_04263	TUEID40_04263	Bacteriophage lambda tail assembly protein I	PA0640	PAO1	6.11	9.87E-125
TUEID40_04264	TUEID40_04264	hypothetical protein	PA0641	PAO1	6.22	2.44E-142
TUEID40_04265	TUEID40_04265	hypothetical protein	No ortholog		6.00	1.70E-56
TUEID40_04266	TUEID40_04266	hypothetical protein	PA0643	PAO1	5.50	4.81E-66
TUEID40_04267	TUEID40_04267	hypothetical protein	PA0644	PAO1	5.06	1.43E-36
TUEID40_04268	TUEID40_04268	hypothetical protein	PA0645	PAO1	5.29	1.54E-54
TUEID40_04269	TUEID40_04269	hypothetical protein	PA0646	PAO1	4.98	4.42E-51
TUEID40_04270	TUEID40_04270	hypothetical protein	PA0647	PAO1	5.09	1.13E-49
TUEID40_04271	TUEID40_04271	hypothetical protein	PA0648	PAO1	4.94	2.36E-40
TUEID40_04678	TUEID40_04678	hypothetical protein	A0A481UZH5_9CAUD	Pseudomonas phage vB_Pae_CF118b	3.89	1.13E-13
TUEID40_04679	TUEID40_04679	hypothetical protein	Q6TM48_BPD31	Pseudomonas phage D3112 (Bacteriophage D3112)	3.69	1.10E-16

9. Appendix

Gene ID (ID40)	Gene name	ID40 product	Ortholog ID (PAO1 or phage)	Ortholog organism (If not PAO1)	log_2 fold change	Adjusted *p* value
TUEID40_04680	TUEID40_04680	hypothetical protein	Q6TM49_BPD31	Pseudomonas phage D3112 (Bacteriophage D3112)	4.44	3.62E-33
TUEID40_04681	TUEID40_04681	hypothetical protein	Q6TM50_BPD31	Pseudomonas phage D3112 (Bacteriophage D3112)	4.65	1.47E-21
TUEID40_04682	TUEID40_04682	hypothetical protein	Q6TM51_BPD31	Pseudomonas phage D3112 (Bacteriophage D3112)	5.00	9.87E-25
TUEID40_04683	TUEID40_04683	hypothetical protein	A0A5A4MZC4_9CAUD	Pseudomonas phage Ps60	4.82	1.33E-43
TUEID40_04684	TUEID40_04684	hypothetical protein	A0A075CEZ1_9CAUD	Pseudomonas phage MP48	4.98	4.88E-44
TUEID40_04685	TUEID40_04685	hypothetical protein	A0A076FWZ1_9CAUD	Pseudomonas phage PaMx73	5.35	8.99E-53
TUEID40_04686	TUEID40_04686	hypothetical protein	A0A076FR13_9CAUD	Pseudomonas phage PaMx73	5.19	1.92E-56
TUEID40_04687	TUEID40_04687	Prophage tail length tape measure protein	A0A0U5KRL2_9VIRU	Bacteriophage sp	5.74	3.59E-58
TUEID40_04688	TUEID40_04688	hypothetical protein	A0A076FST1_9CAUD	Pseudomonas phage PaMx73	6.09	2.54E-50
TUEID40_04689	TUEID40_04689	hypothetical protein	Q6TM60_BPD31	Pseudomonas phage D3112 (Bacteriophage D3112)	6.09	4.57E-64
TUEID40_04690	TUEID40_04690	hypothetical protein	A0A0A7DJQ8_9CAUD	Pseudomonas phage H70	6.10	2.19E-116
TUEID40_04691	TUEID40_04691	hypothetical protein	Q6TM62_BPD31	Pseudomonas phage D3112 (Bacteriophage D3112)	6.02	9.46E-55
TUEID40_04692	TUEID40_04692	hypothetical protein	Q6TM63_BPD31	Pseudomonas phage D3112 (Bacteriophage D3112)	5.88	2.01E-70
TUEID40_04693	TUEID40_04693	hypothetical protein	A0A481V096_9CAUD	Pseudomonas phage vB_Pae_CF177b	6.04	6.71E-49
TUEID40_04694	TUEID40_04694	hypothetical protein	A0A076FRF0_9CAUD	Pseudomonas phage PaMx73	5.87	1.13E-65
TUEID40_04695	TUEID40_04695	hypothetical protein	A0A0U5DWN1_9VIRU	Bacteriophage sp	6.20	4.84E-103

9. Appendix

Gene ID (ID40)	Gene name	ID40 product	Ortholog ID (PAO1 or phage)	Ortholog organism (If not PAO1)	log_2 fold change	Adjusted *p* value
TUEID40_04696	TUEID40_04696	Mu-like prophage major head subunit gpT	A0A7T8C3C6_9CAUD	Pseudomonas phage AIIMS-Pa-B1	6.13	3.55E-99
TUEID40_04697	TUEID40_04697	hypothetical protein	Q6TM68_BPD31	Pseudomonas phage D3112 (Bacteriophage D3112)	6.17	3.61E-42
TUEID40_04698	TUEID40_04698	Mu-like prophage I protein	A0A0U5KMY7_9VIRU	Bacteriophage sp	5.87	7.77E-51
TUEID40_04702	TUEID40_04702	Phage virion morphogenesis family protein	Q6TM73_BPD31	Pseudomonas phage D3112 (Bacteriophage D3112)	4.95	1.07E-37
TUEID40_04703	TUEID40_04703	Phage Mu protein F like protein	A0A0U5G7H2_9VIRU	Bacteriophage sp	5.31	1.18E-52
TUEID40_04704	TUEID40_04704	hypothetical protein	A0A0A7DJC8_9CAUD	Pseudomonas phage H70	5.51	1.62E-70
TUEID40_04705	TUEID40_04705	hypothetical protein	A0A0A7DJQ1_9CAUD	Pseudomonas phage H70	5.80	9.19E-74
TUEID40_04706	TUEID40_04706	hypothetical protein	L7P7N6_9CAUD	Pseudomonas phage JBD24	2.92	4.47E-04
TUEID40_04707	TUEID40_04707	hypothetical protein	L7P832_9CAUD	Pseudomonas phage JBD24	4.50	7.87E-22
TUEID40_04708	TUEID40_04708	hypothetical protein	H6V8N3_9CAUD	Pseudomonas phage JBD26	5.75	1.41E-54
TUEID40_04709	TUEID40_04709	hypothetical protein	Q6TM79_BPD31	Pseudomonas phage D3112 (Bacteriophage D3112)	6.23	5.26E-61
TUEID40_04710	TUEID40_04710	hypothetical protein	A0A125RNH0_9CAUD	Pseudomonas phage JBD93	6.19	3.21E-62
TUEID40_04711	TUEID40_04711	hypothetical protein	L7P831_9CAUD	Pseudomonas phage JBD24	6.30	9.63E-60
TUEID40_04712	TUEID40_04712	hypothetical protein	L7P7J8_9CAUD	Pseudomonas phage JBD24	6.56	1.44E-84
TUEID40_04713	TUEID40_04713	hypothetical protein	A0SMN0_9CAUD	Casadabanvirus DMS3	6.60	2.78E-56
TUEID40_04714	TUEID40_04714	hypothetical protein	L7P7T5_9CAUD	Pseudomonas phage JBD24	6.54	3.67E-34
TUEID40_04715	TUEID40_04715	Mor transcription activator family protein	Q6TM83_BPD31	Pseudomonas phage D3112 (Bacteriophage D3112)	3.63	1.41E-15
TUEID40_04716	TUEID40_04716	hypothetical protein	A0A0S2SYM3_9CAUD	Pseudomonas phage YMC11/11/R1836	5.16	1.40E-67

9. Appendix

Gene ID (ID40)	Gene name	ID40 product	Ortholog ID (PAO1 or phage)	Ortholog organism (If not PAO1)	log_2 fold change	Adjusted *p* value
TUEID40_04717	TUEID40_04717	hypothetical protein	L7P7Y1_9CAUD	Pseudomonas phage JBD88a	5.33	1.81E-33
TUEID40_04718	TUEID40_04718	hypothetical protein	Q6TM86_BPD31	Pseudomonas phage D3112 (Bacteriophage D3112)	6.25	4.29E-114
TUEID40_04719	TUEID40_04719	hypothetical protein	Q6TM87_BPD31	Pseudomonas phage D3112 (Bacteriophage D3112)	6.56	2.06E-90
TUEID40_04720	TUEID40_04720	hypothetical protein	A0A125RNA3_9CAUD	Pseudomonas phage JBD69	6.48	9.74E-191
TUEID40_04721	TUEID40_04721	hypothetical protein	Q6TM88_BPD31	Pseudomonas phage D3112 (Bacteriophage D3112)	6.53	1.19E-170
TUEID40_04722	TUEID40_04722	hypothetical protein	L7P7W6_9CAUD	Pseudomonas phage JBD24	6.36	2.84E-272
TUEID40_04723	TUEID40_04723	Bacteriophage Mu Gam like protein	A0A125RN99_9CAUD	Pseudomonas phage JBD69	6.42	8.57E-154
TUEID40_04724	TUEID40_04724	hypothetical protein	A0A125RN98_9CAUD	Pseudomonas phage JBD69	6.56	2.50E-99
TUEID40_04725	TUEID40_04725	hypothetical protein	A0A0A1IWY8_9CAUD	Pseudomonas phage vB_PaeS_PAO1_Ab30	6.21	8.37E-251
TUEID40_04726	TUEID40_04726	hypothetical protein	A0A076FX19_9CAUD	Pseudomonas phage PaMx73	6.54	6.01E-57
TUEID40_04727	TUEID40_04727	hypothetical protein	B7SDS0_9CAUD	Pseudomonas phage MP29	6.68	6.95E-206
TUEID40_04728	TUEID40_04728	hypothetical protein	L7P7S2_9CAUD	Pseudomonas phage JBD88a	6.71	7.44E-231
TUEID40_04729	TUEID40_04729	Mu DNA-binding domain protein	B7SDR8_9CAUD	Pseudomonas phage MP29	6.36	2.73E-121
TUEID40_04730	TUEID40_04730	hypothetical protein	A0A125RN92_9CAUD	Pseudomonas phage JBD69	5.32	2.67E-51
TUEID40_04731	TUEID40_04731	hypothetical protein	A0A125RN90_9CAUD	Pseudomonas phage JBD69	5.11	1.02E-55
TUEID40_04732	TUEID40_04732	DNA-binding transcriptional regulator Nlp	A0A125RN89_9CAUD	Pseudomonas phage JBD69	2.96	5.48E-09

9. Appendix

Gene ID (ID40)	Gene name	ID40 product	Ortholog ID (PAO1 or phage)	Ortholog organism (If not PAO1)	log_2 fold change	Adjusted *p* value
TUEID40_04751	*eddA*	Alkaline phosphatase D precursor	PA3910	PAO1	4.40	1.81E-21
TUEID40_04800	*pys2_2*	Pyocin-S2	PA3866	PAO1	6.11	1.50E-147
TUEID40_05070	*recA*	recombinase A	PA3617	PAO1	2.84	1.78E-05
TUEID40_05264	TUEID40_05264	hypothetical protein	PA3414	PAO1	3.51	1.94E-15
TUEID40_05265	*yebG*	DNA damage-inducible protein YebG	PA3413	PAO1	3.41	1.67E-09
TUEID40_05687	*sulA*	Cell division inhibitor SulA	PA3008	PAO1	2.75	1.53E-04
TUEID40_05688	*lexA*	LexA repressor	PA3007	PAO1	3.25	2.36E-08
TUEID40_06142	TUEID40_06142	Phage integrase family protein	A0A5Q2F3N6_9CAUD	Pseudomonas phage AUS531phi	4.09	7.97E-30
TUEID40_06143	TUEID40_06143	hypothetical protein	A0A5Q2F449_9CAUD	Pseudomonas phage AUS531phi	5.17	2.07E-25
TUEID40_06144	TUEID40_06144	hypothetical protein	A0A2K8HL62_9CAUD	Pseudomonas phage vB_PaeP_E220	4.24	2.94E-40
TUEID40_06145	TUEID40_06145	hypothetical protein	A0A5Q2FAH0_9CAUD	Pseudomonas phage AUS531phi	5.02	3.22E-58
TUEID40_06146	TUEID40_06146	hypothetical protein	H2BD41_9CAUD	Pseudomonas phage phi297	4.52	1.06E-35
TUEID40_06147	TUEID40_06147	hypothetical protein	A0A2K8I958_9CAUD	Pseudomonas phage vB_PaeP_E220	5.05	2.95E-35
TUEID40_06148	TUEID40_06148	hypothetical protein	No ortholog		2.97	3.44E-03
TUEID40_06153	TUEID40_06153	hypothetical protein	A0A140IES9_9CAUD	Pseudomonas phage YMC11/07/P54_PAE_BP	2.77	8.97E-07
TUEID40_06154	TUEID40_06154	hypothetical protein	H2BD48_9CAUD	Pseudomonas phage phi297	3.40	1.31E-20
TUEID40_06155	*recT*	recombination and repair protein RecT	A0A0P0AJB0_PSEAI	Pseudomonas aeruginosa	5.75	3.72E-144
TUEID40_06156	TUEID40_06156	YqaJ-like viral recombinase domain protein	A0A481UYA2_9CAUD	Pseudomonas phage vB_Pae_BR153a	5.47	1.72E-77
TUEID40_06157	TUEID40_06157	hypothetical protein	No ortholog		3.75	1.66E-19
TUEID40_06158	TUEID40_06158	hypothetical protein	A0A5Q2F8M0_9CAUD	Pseudomonas phage AUS531phi	3.09	4.79E-05
TUEID40_06159	TUEID40_06159	hypothetical protein	No ortholog		3.31	2.17E-12

9. Appendix

Gene ID (ID40)	Gene name	ID40 product	Ortholog ID (PAO1 or phage)	Ortholog organism (If not PAO1)	log_2 fold change	Adjusted *p* value
TUEID40_06160	TUEID40_06160	hypothetical protein	Q9MC67_BPD3	Pseudomonas phage D3 (Bacteriophage D3)	4.65	5.63E-35
TUEID40_06161	TUEID40_06161	hypothetical protein	A0A2K8I9C2_9CAUD	Pseudomonas phage vB_PaeP_E220	5.18	5.86E-60
TUEID40_06162	TUEID40_06162	hypothetical protein	A0A481V406_9CAUD	Pseudomonas phage vB_Pae_BR150a	5.46	8.86E-31
TUEID40_06163	TUEID40_06163	hypothetical protein	A0A127KNE3_9CAUD	Pseudomonas phage YMC11/07/P54_PAE_BP	5.88	2.48E-77
TUEID40_06164	TUEID40_06164	hypothetical protein	A0A9X4SUP9_PSEAI	Pseudomonas aeruginosa	5.28	1.55E-35
TUEID40_06165	TUEID40_06165	hypothetical protein	A0A481V3J9_9CAUD	Pseudomonas phage vB_Pae_CF126a	5.58	8.13E-45
TUEID40_06166	TUEID40_06166	hypothetical protein	No ortholog		6.04	3.77E-54
TUEID40_06170	TUEID40_06170	hypothetical protein	A0AA36VMC8_9CAUD	Pseudomonas phage vB_PaeS-D14H	4.94	1.36E-41
TUEID40_06171	TUEID40_06171	hypothetical protein	H2BD69_9CAUD	Pseudomonas phage phi297	5.21	3.10E-42
TUEID40_06172	*dnaB*	Replicative DNA helicase	PA4931	PAO1	5.40	5.28E-71
TUEID40_06173	TUEID40_06173	Endodeoxyribonuclease RusA	A0A127KND5_9CAUD	Pseudomonas phage YMC11/07/P54_PAE_BP	5.10	6.51E-27
TUEID40_06174	TUEID40_06174	hypothetical protein	A0A5Q2FAE6_9CAUD	Pseudomonas phage AUS531phi	4.12	6.38E-23
TUEID40_06181	TUEID40_06181	Terminase-like family protein	A0A5Q2F495_9CAUD	Pseudomonas phage AUS531phi	3.44	2.93E-09
TUEID40_06182	TUEID40_06182	hypothetical protein	A0A5Q2F2W3_9CAUD	Pseudomonas phage AUS531phi	3.07	5.06E-04
TUEID40_06184	TUEID40_06184	hypothetical protein	A0A5Q2F417_9CAUD	Pseudomonas phage AUS531phi	3.99	1.15E-17
TUEID40_06185	TUEID40_06185	hypothetical protein	A0AA36VLD8_9CAUD	Pseudomonas phage vB_PaeS-D14H	4.16	6.65E-19
TUEID40_06186	TUEID40_06186	hypothetical protein	A0A5Q2FAD9_9CAUD	Pseudomonas phage AUS531phi	3.54	4.79E-07
TUEID40_06187	TUEID40_06187	hypothetical protein	A0A5Q2F981_9CAUD	Pseudomonas phage AUS531phi	3.31	1.10E-04

9. Appendix

Gene ID (ID40)	Gene name	ID40 product	Ortholog ID (PAO1 or phage)	Ortholog organism (If not PAO1)	log_2 fold change	Adjusted *p* value
TUEID40_06188	TUEID40_06188	hypothetical protein	A0A5Q2F7A0_9CAUD	Pseudomonas phage AUS531phi	3.40	3.02E-04
TUEID40_06189	TUEID40_06189	hypothetical protein	A0A5Q2F8J3_9CAUD	Pseudomonas phage AUS531phi	3.71	9.44E-09
TUEID40_06191	TUEID40_06191	Phage tail protein	A0A5Q2F486_9CAUD	Pseudomonas phage AUS531phi	2.89	1.20E-03
TUEID40_06200	TUEID40_06200	Arc-like DNA binding domain protein	A0A8E7KYR6_9CAUD	Pseudomonas phage Me-dea1	6.52	2.66E-114
TUEID40_06201	TUEID40_06201	hypothetical protein	No ortholog		5.88	3.28E-154
TUEID40_06202	TUEID40_06202	hypothetical protein	A0A8E7FQ38_9CAUD	Pseudomonas phage Me-dea1	6.19	4.18E-136
TUEID40_06203	TUEID40_06203	hypothetical protein	No ortholog		5.59	1.52E-105
TUEID40_06215	TUEID40_06215	hypothetical protein	No ortholog		3.73	7.24E-07

9.2.3. Differentially expressed genes in ID40Δ*ygfB* +CIP vs. ID40 +CIP

Table 36: Significantly differentially expressed genes in transcriptome of *P. aeruginosa* ID40Δ*ygfB* +CIP vs. ID40 +CIP. Data analysis as described in the methods. $n = 3$. Genes with an adjusted *p* value of ≤0.01 and a log_2 fold change of ≥2 or ≤-2 were considered differentially expressed.

Gene ID	Gene names	Product	PAO1 ortholog	log_2 fold change	Adjusted *p* value
TUEID40_03245	*ygfB*	hypothetical protein	PA5225	-5.80	3.13E-18

9.2.4. Differentially expressed genes in BW25113Δ*ygfB* vs. BW25113

Table 37: Significantly differentially expressed genes in transcriptome of *E. coli* BW25113Δ*ygfB* vs. BW25113. Data analysis as described in the methods. $n = 3$. Genes with an adjusted *p* value of ≤0.01 and a log_2 fold change of ≥2 or ≤-2 were considered differentially expressed.

BW25113 ID	Gene name	K12 UniProt Entry Name	Protein names	log_2 fold change	Adjusted *p* value
BW25113_1071	*flgM*	FLGM_ECOLI	Negative regulator of flagellin synthesis (Anti-sigma-28 factor)	3.17	2.66E-04
BW25113_1073	*flgB*	FLGB_ECOLI	Flagellar basal body rod protein FlgB (Putative proximal rod protein)	5.24	2.68E-05
BW25113_1074	*flgC*	FLGC_ECOLI	Flagellar basal-body rod protein FlgC (Putative proximal rod protein)	5.64	1.98E-05
BW25113_1075	*flgD*	FLGD_ECOLI	Basal-body rod modification protein FlgD	4.89	4.18E-07
BW25113_1076	*flgE*	FLGE_ECOLI	Flagellar hook protein FlgE	4.10	3.29E-05

9. Appendix

BW25113 ID	Gene name	K12 UniProt Entry Name	Protein names	log_2 fold change	Adjusted *p* value
BW25113_1077	*flgF*	FLGF_ECOLI	Flagellar basal-body rod protein FlgF (Putative proximal rod protein)	3.74	1.85E-03
BW25113_1078	*flgG*	FLGG_ECOLI	Flagellar basal-body rod protein FlgG (Distal rod protein)	4.47	2.44E-04
BW25113_1080	*flgI*	FLGI_ECOLI	Flagellar P-ring protein (Basal body P-ring protein)	4.03	6.05E-03
BW25113_1082	*flgK*	FLGK_ECOLI	Flagellar hook-associated protein 1 (HAP1)	5.03	3.16E-34
BW25113_1083	*flgL*	FLGL_ECOLI	Flagellar hook-associated protein 3 (HAP3) (Hook-filament junction protein)	3.87	3.81E-14
BW25113_1194	*ycgR*	YCGR_ECOLI	Flagellar brake protein YcgR (Cyclic di-GMP binding protein YcgR)	3.99	3.82E-07
BW25113_1421	*trg*	MCP3_ECOLI	Methyl-accepting chemotaxis protein III (MCP-III) (Ribose and galactose chemoreceptor protein)	3.09	1.95E-03
BW25113_1881	*cheZ*	CHEZ_ECOLI	Protein phosphatase CheZ (EC 3.1.3.-) (Chemotaxis protein CheZ)	3.93	2.49E-13
BW25113_1882	*cheY*	CHEY_ECOLI	Chemotaxis protein CheY	3.67	2.69E-08
BW25113_1883	*cheB*	CHEB_ECOLI	Protein-glutamate methylesterase/protein-glutamine glutaminase (EC 3.1.1.61) (EC 3.5.1.44) (Chemotaxis response regulator protein-glutamate methylesterase/glutamine de-amidase) (Methyl-accepting chemotaxis proteins-specific methylesterase/deamidase) (MCP-specific methylesterase/deamidase)	4.28	8.97E-10
BW25113_1884	*cheR*	CHER_ECOLI	Chemotaxis protein methyltransferase (EC 2.1.1.80)	5.22	1.97E-10
BW25113_1885	*tap*	MCP4_ECOLI	Methyl-accepting chemotaxis protein IV (MCP-IV) (Dipeptide chemoreceptor protein)	6.26	2.09E-37
BW25113_1886	*tar*	MCP2_ECOLI	Methyl-accepting chemotaxis protein II (MCP-II) (Aspartate chemoreceptor protein)	7.33	2.09E-37
BW25113_1887	*cheW*	CHEW_ECOLI	Chemotaxis protein CheW	4.79	2.05E-17
BW25113_1888	*cheA*	CHEA_ECOLI	Chemotaxis protein CheA (EC 2.7.13.3)	6.17	5.34E-37
BW25113_1889	*motB*	MOTB_ECOLI	Motility protein B (Chemotaxis protein MotB)	5.26	7.17E-25
BW25113_1890	*motA*	MOTA_ECOLI	Motility protein A (Chemotaxis protein MotA)	7.07	8.74E-29
BW25113_1922	*fliA*	FLIA_ECOLI	RNA polymerase sigma factor FliA (RNA polymerase sigma factor for flagellar operon) (Sigma F) (Sigma-27) (Sigma-28)	6.13	5.37E-23
BW25113_1923	*fliC*	FLIC_ECOLI	Flagellin	4.30	1.00E-29
BW25113_1924	*fliD*	FLID_ECOLI	Flagellar hook-associated protein 2 (HAP2) (Filament cap protein) (Flagellar cap protein)	4.55	4.95E-11
BW25113_1938	*fliF*	FLIF_ECOLI	Flagellar M-ring protein	4.23	1.06E-03
BW25113_2908	*pepP*	AMPP_ECOLI	Xaa-Pro aminopeptidase (EC 3.4.11.9) (Aminoacylproline aminopeptidase) (Aminopepti-dase P II) (APP-II) (X-Pro aminopeptidase)	-2.35	5.06E-03
BW25113_2909	*ygfB*	YGFB_ECOLI	UPF0149 protein YgfB	-9.46	6.57E-32

Table 38: Significantly differentially expressed genes in transcriptome of *E. coli* BW25113Δ*ygfB* vs. BW25113 with flagella genes upregulated by *flhDC* mutation excluded. Data analysis as described in the methods. $n = 3$. Genes with an adjusted p value of ≤ 0.01 and a log_2 fold change of ≥ 2 or ≤ -2 were considered differentially expressed.

BW25113 ID	Gene name	K12 UniProt Entry Name	Protein names	log_2 fold change	Adjusted *p* value
BW25113_2909	*ygfB*	YGFB_ECOLI	UPF0149 protein YgfB	-9.45	4.06E-31

9. Appendix

9.2.5. Differentially expressed genes in BW25113 +CIP vs. BW25113

Table 39: Significantly differentially expressed genes in transcriptome of *E. coli* BW25113 +CIP vs. BW25113. Data analysis as described in the methods. $n = 3$. Genes with an adjusted p value of ≤0.01 and a $\log_2$ fold change of ≥2 or ≤-2 were considered differentially expressed.

BW25113 ID	Gene name	K12 UniProt Entry Name	K12 Protein names	$\log_2$ fold change	Adjusted p value
BW25113_0060	*polB*	DPO2_ECOLI	DNA polymerase II (Pol II)	3.454	6.82E-14
BW25113_0231	*dinB*	DPO4_ECOLI	DNA polymerase IV (Pol IV) (Translesion synthesis polymerase IV) (TSL polymerase IV)	4.263	8.18E-62
BW25113_0621	*dcuC*	DCUC_ECOLI	Anaerobic C4-dicarboxylate transporter DcuC	3.935	8.61E-12
BW25113_0946	*zapC*	ZAPC_ECOLI	Cell division protein ZapC (FtsZ-associated protein C) (Z-ring-associated protein C)	-4.199	4.32E-05
BW25113_0958	*sulA*	SULA_ECOLI	Cell division inhibitor SulA	5.173	9.11E-124
BW25113_1061	*dinI*	DINI_ECOLI	DNA damage-inducible protein I	5.553	1.45E-89
BW25113_1140	*intE*	INTE_ECOLI	Prophage integrase IntE (Int(Lambda)) (Prophage e14 integrase) (Prophage lambda integrase)	5.333	5.76E-28
BW25113_1141	*xisE*	VXIS_ECOLI	Prophage excisionase-like protein (Excisionase-like protein from lambdoid prophage 14)	7.484	1.13E-44
BW25113_1143	*ymfI*	YMFI_ECOLI	Uncharacterized protein YmfI	6.076	4.97E-190
BW25113_1144	*ymfJ*	YMFJ_ECOLI	Uncharacterized protein YmfJ	9.362	1.20E-208
BW25113_1146	*croE*	CROE_ECOLI	Prophage transcriptional regulatory protein (Putative lambdoid prophage e14 transcriptional regulatory protein)	7.700	9.18E-49
BW25113_1147	*ymfL*	YMFL_ECOLI	Uncharacterized protein YmfL	8.403	2.03E-136
BW25113_1148	*ymfM*	YMFM_ECOLI	Uncharacterized protein YmfM	8.863	2.54E-51
BW25113_1150	*ymfR*	YMFR_ECOLI	Uncharacterized protein YmfR	7.967	3.10E-16
BW25113_1151	*beeE*	BEEE_ECOLI	Protein BeeE	8.058	6.04E-42
BW25113_1152	*jayE*	JAYE_ECOLI	Putative protein JayE (Putative protein JayE from lambdoid prophage e14 region)	8.195	1.46E-37
BW25113_1153	*ymfQ*	YMFQ_ECOLI	Uncharacterized protein YmfQ (Uncharacterized protein YmfQ in lambdoid prophage e14 region)	7.677	2.83E-18
BW25113_1154	*stfP*	STFP_ECOLI	Uncharacterized protein StfP (Uncharacterized protein StfP from lambdoid prophage e14 region)	7.641	5.33E-06
BW25113_1155	*tfaP*	YMFS_ECOLI	Uncharacterized protein YmfS	5.977	3.13E-08
BW25113_1156	*tfaE*	TFAE_ECOLI	Prophage tail fiber assembly protein homolog TfaE (Tail fiber assembly protein homolog from lambdoid prophage e14)	5.674	5.50E-12

9. Appendix

BW25113 ID	Gene name	K12 UniProt Entry Name	K12 Protein names	log_2 fold change	Adjusted *p* value
BW25113_1157	*stfE*	STFE_ECOLI	Putative uncharacterized protein StfE (Side tail fiber protein homolog from lambdoid prophage e14)	8.277	2.10E-05
BW25113_1166	*ariR*	ARIR_ECOLI	Probable two-component-system connector protein AriR	5.393	3.99E-12
BW25113_1183	*umuD*	UMUD_ECOLI	Protein UmuD (DNA polymerase V) (Pol V)	4.926	1.82E-10
BW25113_1184	*umuC*	UMUC_ECOLI	Protein UmuC (DNA polymerase V) (Pol V)	3.675	2.75E-08
BW25113_1285	*gmr*	PDER_ECOLI	Cyclic di-GMP phosphodiesterase PdeR	-3.358	1.45E-06
BW25113_1497	*ydeM*	YDEM_ECOLI	Anaerobic sulfatase-maturating enzyme homolog YdeM (AnSME homolog)	3.909	1.91E-03
BW25113_1498	*ydeN*	YDEN_ECOLI	Uncharacterized sulfatase YdeN	3.158	1.80E-04
BW25113_1511	*lsrK*	LSRK_ECOLI	Autoinducer-2 kinase (AI-2 kinase)	-2.914	6.06E-03
BW25113_1513	*lsrA*	LSRA_ECOLI	Autoinducer 2 import ATP-binding protein LsrA (AI-2 import ATP-binding protein LsrA)	-3.381	5.78E-05
BW25113_1514	*lsrC*	LSRC_ECOLI	Autoinducer 2 import system permease protein LsrC (AI-2 import system permease protein LsrC)	-3.201	2.16E-03
BW25113_1521	*uxaB*	UXAB_ECOLI	Altronate oxidoreductase (Tagaturonate dehydrogenase) (Tagaturonate reductase)	3.341	1.46E-03
BW25113_1847	*yebF*	YEBF_ECOLI	Protein YebF	3.516	4.68E-29
BW25113_1848	*yebG*	YEBG_ECOLI	Uncharacterized protein YebG	5.462	7.24E-125
BW25113_2008	*yeeA*	YEEA_ECOLI	Inner membrane protein YeeA	3.595	1.33E-41
BW25113_2009	*sbmC*	SBMC_ECOLI	DNA gyrase inhibitor	3.848	9.39E-38
BW25113_2234	*nrdA*	RIR1_ECOLI	Ribonucleoside-diphosphate reductase 1 subunit alpha (Protein B1) (Ribonucleoside-diphosphate reductase 1 R1 subunit) (Ribonucleotide reductase 1)	3.957	4.28E-12
BW25113_2235	*nrdB*	RIR2_ECOLI	Ribonucleoside-diphosphate reductase 1 subunit beta (EC 1.17.4.1) (Protein B2) (Protein R2) (Ribonucleotide reductase 1)	2.919	2.34E-06
BW25113_2236	*yfaE*	YFAE_ECOLI	Uncharacterized ferredoxin-like protein YfaE	3.397	1.03E-05
BW25113_2255	*arnA*	ARNA_ECOLI	Bifunctional polymyxin resistance protein ArnA (Polymyxin resistance protein PmrI)	-3.184	1.89E-06
BW25113_2567	*rnc*	RNC_ECOLI	Ribonuclease 3 (Ribonuclease III) (RNase III)	-2.861	7.74E-03
BW25113_2616	*recN*	RECN_ECOLI	DNA repair protein RecN (Recombination protein N)	6.395	6.35E-303
BW25113_2698	*recX*	RECX_ECOLI	Regulatory protein RecX (Protein OraA)	5.137	2.15E-40
BW25113_2699	*recA*	RECA_ECOLI	Protein RecA (Recombinase A)	5.585	2.31E-203
BW25113_2882	*xanQ*	XANQ_ECOLI	Xanthine permease XanQ	-3.956	8.14E-07
BW25113_2883	*guaD*	GUAD_ECOLI	Guanine deaminase (Guanase) (Guanine aminase) (Guanine aminohydrolase)	-3.775	4.32E-05

9. Appendix

BW25113 ID	Gene name	K12 UniProt Entry Name	K12 Protein names	log_2 fold change	Adjusted *p* value
BW25113_3091	*uxaA*	UXAA_ECOLI	Altronate dehydratase (D-altronate hydro-lyase)	3.820	8.48E-11
BW25113_3092	*uxaC*	UXAC_ECOLI	Uronate isomerase (Glucuronate isomerase) (Uronic isomerase)	4.072	7.14E-18
BW25113_3645	*dinD*	DIND_ECOLI	DNA damage-inducible protein D	6.343	4.68E-149
BW25113_3707	*tnaC*	LPTN_ECOLI	Tryptophanase operon leader peptide (TnaC)	3.724	8.14E-07
BW25113_3708	*tnaA*	TNAA_ECOLI	Tryptophanase (L-tryptophan indole-lyase) (TNase)	3.102	1.78E-03
BW25113_3832	*rmuC*	RMUC_ECOLI	DNA recombination protein RmuC	2.963	2.07E-06
BW25113_4043	*lexA*	LEXA_ECOLI	LexA repressor	3.634	7.09E-49
BW25113_4044	*dinF*	DINF_ECOLI	DNA damage-inducible protein F	2.779	1.99E-07
BW25113_4464	*ygfQ*	GHXQ_ECOLI	Guanine/hypoxanthine permease GhxQ	-3.596	9.46E-07
BW25113_4519	*icdC*	IDH_ECOLI	Isocitrate dehydrogenase [NADP] (IDH)	6.756	6.79E-18
BW25113_4613	*dinQ*	DINQ_ECOLI	Uncharacterized protein DinQ	2.558	6.43E-03
BW25113_4618	*tisB*	TISB_ECOLI	Small toxic protein TisB (LexA-regulated protein TisB)	8.462	9.36E-224
BW25113_4692	*ymfN*	YMFN_ECOLI	Protein YmfN	8.995	4.23E-36
BW25113_4693	*ymfN*	YMFN_ECOLI	Protein YmfN	8.613	6.78E-113

9.2.6. Differentially expressed genes of BW25113Δ*ygfB* +CIP vs. BW25113 +CIP

Table 40: Significantly differentially expressed genes in transcriptome of *E. coli* BW25113Δ*ygfB* +CIP vs. BW25113 +CIP. Data analysis as described in the methods. $n = 3$. Genes with an adjusted *p* value of ≤0.01 and a log_2 fold change of ≥2 or ≤-2 were considered differentially expressed.

BW25113 ID	Gene name	K12 UniProt Entry Name	Protein names	log_2 fold change	Adjusted *p* value
BW25113_1885	*tap*	MCP4_ECOLI	Methyl-accepting chemotaxis protein IV (MCP-IV) (Dipeptide chemoreceptor protein)	4.98	1.54E-06
BW25113_1886	*tar*	MCP2_ECOLI	Methyl-accepting chemotaxis protein II (MCP-II) (Aspartate chemoreceptor protein)	6.38	3.42E-07
BW25113_1887	*cheW*	CHEW_ECOLI	Chemotaxis protein CheW	4.47	1.67E-08
BW25113_1888	*cheA*	CHEA_ECOLI	Chemotaxis protein CheA (EC 2.7.13.3)	5.78	2.31E-20
BW25113_1889	*motB*	MOTB_ECOLI	Motility protein B (Chemotaxis protein MotB)	4.52	3.78E-10
BW25113_1890	*motA*	MOTA_ECOLI	Motility protein A (Chemotaxis protein MotA)	5.87	1.43E-11
BW25113_1922	*fliA*	FLIA_ECOLI	RNA polymerase sigma factor FliA (RNA polymerase sigma factor for flagellar operon) (Sigma F) (Sigma-27) (Sigma-28)	4.27	8.91E-03
BW25113_1923	*fliC*	FLIC_ECOLI	Flagellin	2.96	5.46E-04
BW25113_2908	*pepP*	AMPP_ECOLI	Xaa-Pro aminopeptidase (EC 3.4.11.9) (Aminoacylproline aminopeptidase) (Aminopeptidase P II) (APP-II) (X-Pro aminopeptidase)	-2.61	3.78E-10
BW25113_2909	*ygfB*	YGFB_ECOLI	UPF0149 protein YgfB	-11.69	1.12E-17

9. Appendix

Table 41: Significantly differentially expressed genes in transcriptome of *E. coli* BW25113Δ*ygfB* +CIP vs. BW25113 +CIP with flagella genes upregulated by *flhDC* mutation excluded. Data analysis as described in the methods. $n = 3$. Genes with an adjusted p value of ≤0.01 and a $\log_2$ fold change of ≥2 or ≤-2 were considered differentially expressed.

BW25113 ID	Gene name	K12 UniProt Entry Name	Protein names	$\log_2$ fold change	Adjusted p value
BW25113_2908	*pepP*	AMPP_ECOLI	Xaa-Pro aminopeptidase (EC 3.4.11.9) (Aminoacylproline aminopeptidase) (Aminopeptidase P II) (APP-II) (X-Pro aminopeptidase)	-2.60	1.42E-09
BW25113_2909	*ygfB*	YGFB_ECOLI	UPF0149 protein YgfB	-11.68	2.37E-17

9.3. Interactomic analysis

9.3.1. Interactome of YgfB in ID40

Table 42: Interactome of YgfB in *P. aeruginosa* ID40. $\log_2$ fold change calculated by two-sided two-sample t test with an FDR of 1%. q value (multiplicity adjusted p value) is shown as calculated in two-sided t test. $-\log_{10} p$ value is shown as volcano plots show this data. All proteins that had a q value of ≤0.01 were classified as interactors

Gene names	Majority protein IDs	Protein names	$\log_2$ fold change GST-YgfB vs. GST	q value	$-\log_{10} p$ value
aer	Q9I3F6	Methyl-accepting chemotaxis protein Aer (Aerotaxis receptor Aer)	1.77	3.24E-03	2.41
amn	Q9HX46	AMP nucleosidase (EC 3,2,2,4)	2.39	1.64E-03	2.43
chpA	Q9I696	histidine kinase (EC 2,7,13,3)	4.55	0	3.47
clpA	Q9I0L8	ATP-binding protease component ClpA	2.54	0	2.11
clpV1	Q9I742	AAA+ ATPase ClpV1	3.49	0	3.36
cobW	Q9HZQ2	Zinc chaperone CobW (EC 3,6,5,-)	2.96	0	1.84
dctD	Q9HU19	C4-dicarboxylate transport transcriptional regulatory protein DctD	1.82	5.31E-03	1.65
deaD	Q9I003	ATP-dependent RNA helicase DeaD (EC 3,6,4,13) (Cold-shock DEAD box protein A)	3.96	0	2.33
dnaA	Q9I7C5	Chromosomal replication initiator protein DnaA	2.04	5.27E-03	1.16
dnaB	Q9HUN3	Replicative DNA helicase (EC 3,6,4,12)	2.59	0	2.91
dnaE	Q9HXZ1	DNA polymerase III subunit alpha (EC 2,7,7,7)	3.98	0	1.69
dnaX	Q9I3I1	DNA polymerase III subunit gamma/tau (EC 2,7,7,7)	3.69	0	3.00
ettA	Q9HVJ1	Energy-dependent translational throttle protein EttA (EC 3,6,1,-) (Translational regulatory factor EttA)	2.28	2.88E-03	2.23
ffh	Q9HXP8	Signal recognition particle protein (EC 3,6,5,4) (Fifty-four homolog)	2.38	0	2.83

9. Appendix

Gene names	Majority protein IDs	Protein names	log_2 fold change GST-YgfB vs. GST	*q* value	$-log_{10}$ *p* value
fruI	Q9HY55	phosphoenolpyruvate--protein phosphotransferase (EC 2,7,3,9)	3.31	0	2.72
ftsA	P47203	Cell division protein FtsA	2.86	0	2.57
glpK1	Q9HY41	Glycerol kinase 1 (EC 2,7,1,30) (ATP:glycerol 3-phosphotransferase 1) (Glycerokinase 1) (GK 1)	3.06	0	2.29
gor	P23189	Glutathione reductase (GR) (GRase) (EC 1,8,1,7)	2.10	2.57E-03	2.17
gyrB	Q9I7C2	DNA gyrase subunit B (EC 5,6,2,2)	3.91	0	2.70
hemL	P48247	Glutamate-1-semialdehyde 2,1-aminomutase (GSA) (EC 5,4,3,8) (Glutamate-1-semialdehyde aminotransferase) (GSA-AT)	2.85	0	1.63
hflD	Q9I0L1	High frequency lysogenization protein HflD homolog	4.99	0	3.61
hisC2	Q9HZ68	Histidinol-phosphate aminotransferase 2 (EC 2,6,1,9) (Imidazole acetol-phosphate transaminase 2)	3.55	0	2.36
hom	P29365	Homoserine dehydrogenase (HDH) (EC 1,1,1,3)	3.38	0	2.14
ibpA	Q9HZ98	Heat-shock protein IbpA	4.42	0	3.34
lepA	Q9I5G8	Elongation factor 4 (EF-4) (EC 3,6,5,n1) (Ribosomal back-translocase LepA)	4.81	0	2.99
lon (PA1803)	Q9I2T9	Lon protease (EC 3,4,21,53) (ATP-dependent protease La)	1.84	9.14E-03	1.36
lon; asrA (PA0779)	Q9I5F9	Lon protease (EC 3,4,21,53) (ATP-dependent protease La)	1.88	7.20E-03	1.35
lptB	Q9HVV6	Lipopolysaccharide export system ATP-binding protein LptB	3.41	0	2.10
lptD	Q9I5U2	LPS-assembly protein LptD	1.95	2.43E-03	2.21
lpxB	Q9HXY8	Lipid-A-disaccharide synthase (EC 2,4,1,182)	2.72	0	2.75
lrp	Q9HTP6	Leucine-responsive regulatory protein	3.48	0	2.89
mexT	Q9I0Z0	Transcriptional regulator MexT	2.00	3.36E-03	1.60
mfd	Q9HZK3	Transcription-repair-coupling factor (TRCF) (EC 3,6,4,-)	2.19	3.86E-03	1.05
miaB	Q51470	tRNA-2-methylthio-N(6)-dimethylallyladenosine synthase (EC 2,8,4,3) ((Dimethylallyl)adenosine tRNA methylthiotransferase MiaB) (tRNA-i(6)A37 methylthiotransferase)	3.14	0	4.08
mreB	Q9HVU0	Cell shape-determining protein MreB	4.32	0	2.51
murG	Q9HW01	UDP-N-acetylglucosamine--N-acetylmuramyl-(pentapeptide) pyrophosphoryl-undecaprenol N-acetylglucosamine transferase (EC 2,4,1,227) (Undecaprenyl-PP-MurNAc-pentapeptide-UDPGlcNAc GlcNAc transferase)	3.30	0	2.50
mutL	Q9HUL8	DNA mismatch repair protein MutL	4.93	0	2.56
nirQ	Q51481	Denitrification regulatory protein NirQ	4.84	0	2.73
PA0399	Q9I6A1	Cystathionine beta-synthase	2.16	3.40E-03	1.33
PA0429	Q9I688	Nucleotide-diphospho-sugar transferase	2.05	2.48E-03	2.09
PA0495	Q9I623	Carboxyltransferase domain-containing protein	1.84	9.00E-03	1.37

9. Appendix

Gene names	Majority protein IDs	Protein names	$\log_2$ fold change GST-YgfB vs. GST	*q* value	$-\log_{10}$ *p* value
PA0853	Q9I588	Probable oxidoreductase	3.97	0	3.78
PA1339	Q9I405	Amino acid ABC transporter ATP binding protein	1.77	5.36E-03	1.83
PA1458	G3XCT6	Chemotaxis protein CheA (EC 2,7,13,3)	2.27	3.93E-03	1.05
PA1807	Q9I2T7	Probable ATP-binding component of ABC transporter	2.38	2.99E-03	2.37
PA1964	Q9I2E0	Probable ATP-binding component of ABC transporter	3.60	0	2.27
PA2462	Q9I120	Filamentous haemagglutinin FhaB/tRNA nuclease CdiA-like TPS domain-containing protein	2.30	0	2.95
PA2537	Q9I0U7	Probable acyltransferase	2.23	2.91E-03	2.79
PA2567	Q9I0R8	Cyclic di-GMP phosphodiesterase PA2567 (c-di-GMP PDE) (EC 3,1,4,52)	2.72	0	1.88
PA2707	Q9I0D5	AAA+ ATPase domain-containing protein	3.92	0	3.37
PA2725	Q9I0B7	Probable chaperone	2.68	0	2.84
PA2812	Q9I031	Probable ATP-binding component of ABC transporter	2.48	2.78E-03	1.66
PA3024	Q9HZI2	Probable carbohydrate kinase	1.91	2.34E-03	2.20
PA3026	Q9HZI0	FAD-binding PCMH-type domain-containing protein	9.61	0	5.21
PA3271	Q9HYX0	histidine kinase (EC 2,7,13,3)	1.95	3.46E-03	1.88
PA3285	Q9HYV8	Probable sigma-70 factor, ECF subfamily	5.02	0	4.61
PA3297	Q9HYU6	Probable ATP-dependent helicase	3.14	0	1.94
PA3349	Q9HYP7	Probable chemotaxis protein	4.70	0	1.55
PA3481	Q9HYC8	Iron-sulfur cluster carrier protein	2.73	2.59E-03	1.15
PA3728	Q9HXR4	AAA family ATPase	1.81	3.97E-03	1.99
PA3822	Q9HXI0	Sec translocon accessory complex subunit YajC	1.85	4.00E-03	1.87
PA3849	Q9HXF7	Nucleoid-associated protein PA3849	2.58	0	2.48
PA4465	Q9HVV3	Nucleotide-binding protein PA4465	2.29	2.51E-03	1.56
PA4604	Q9HVI5	CobW C-terminal domain-containing protein	1.86	6.23E-03	1.39
PA4686	Q9HVA9	Chromosome partitioning protein ParA	4.58	0	3.45
PA4722	Q9HV76	Aminotransferase (EC 2,6,1,-)	2.45	0	2.51
PA4843	Q9HUW7	Probable two-component response regulator	3.77	0	3.12
PA4928	Q9HUN6	UPF0313 protein PA4928	5.58	0	3.99
PA4974	Q9HUJ1	Probable outer membrane protein	1.76	3.83E-03	1.97
PA5027	Q9HUE2	UspA domain-containing protein	2.02	3.19E-03	1.46
PA5028	Q9HUE1	AAA domain-containing protein	2.00	5.40E-03	1.26
PA5196	Q9HTZ3	Putative ATP-dependent zinc protease domain-containing protein	2.82	0	3.03
PA5225	Q9HTW5	UPF0149 protein PA5225	7.13	0	3.93
PA5252	Q9HTU2	Probable ATP-binding component of ABC transporter	2.90	0	2.22
PA5376	Q9HTI8	Probable ATP-binding component of ABC transporter	3.29	0	2.02

9. Appendix

Gene names	Majority protein IDs	Protein names	log_2 fold change GST-YgfB vs. GST	*q* value	$-log_{10}$ *p* value
PA5438	Q9HTC8	Probable transcriptional regulator	3.15	0	2.88
parE	Q9HUJ8	DNA topoisomerase 4 subunit B (EC 5,6,2,2) (Topoisomerase IV subunit B)	3.65	0	4.00
phhC	P43336	Aromatic-amino-acid aminotransferase (EC 2,6,1,57)	3.09	0	1.90
pilB	P22608	Type IV pilus assembly ATPase PilB	2.21	2.54E-03	1.77
pilY1	Q9HVM8	Type IV pilus biogenesis factor PilY1 (Pilus-associated adhesin PilY1)	2.75	0	2.46
plsB	Q9HXW7	Glycerol-3-phosphate acyltransferase (GPAT) (EC 2,3,1,15)	3.46	0	2.01
ppk	P0DP44	Polyphosphate kinase (EC 2,7,4,1) (ATP-polyphosphate phosphotransferase) (Polyphosphoric acid kinase)	4.35	0	2.16
ppx	Q9ZN70	Exopolyphosphatase (ExopolyPase) (EC 3,6,1,11) (Polyphosphate:ADP phosphotransferase) (PolyP:ADP phosphotransferase) (EC 2,7,4,1)	1.95	2.46E-03	2.21
pqsC	Q9I4X1	2-heptyl-4(1H)-quinolone synthase subunit PqsC (EC 2,3,1,230)	2.83	0	2.28
pqsD	P20582	Anthraniloyl-CoA anthraniloyltransferase (EC 2,3,1,262) (2-heptyl-4(1H)-quinolone synthase PqsD) (PqsD)	2.04	3.21E-03	1.43
pslB	Q9I1N7	mannose-1-phosphate guanylyltransferase (EC 2,7,7,13)	6.29	0	2.75
pslH	Q9I1N1	PslH	3.93	0	3.60
ptxS	G3XD97	HTH-type transcriptional regulator PtxS	2.59	0	2.23
pyrH	O82852	Uridylate kinase (UK) (EC 2,7,4,22) (Uridine monophosphate kinase) (UMP kinase) (UMPK)	2.53	3.27E-03	0.93
radA	P96963	DNA repair protein RadA (EC 3,6,4,-) (Branch migration protein RadA)	4.73	0	2.85
rapA	Q9HYT6	RNA polymerase-associated protein RapA (EC 3,6,4,-) (ATP-dependent helicase HepA)	4.54	0	2.76
rdgC	Q9HYX7	Recombination-associated protein RdgC	2.77	0	2.46
recA	P08280	Protein RecA (Recombinase A)	2.46	0	2.78
recG	Q9HTL3	ATP-dependent DNA helicase RecG (EC 3,6,4,12)	2.27	2.62E-03	1.88
relA	Q9I524	GTP pyrophosphokinase	4.56	0	5.08
rhlB	Q9HXE5	ATP-dependent RNA helicase RhlB (EC 3,6,4,13)	2.80	2.68E-03	1.20
rho	Q9HTV1	Transcription termination factor Rho (EC 3,6,4,-) (ATP-dependent helicase Rho)	1.75	3.33E-03	2.64
ribH	Q9HWX5	6,7-dimethyl-8-ribityllumazine synthase (DMRL synthase) (LS) (Lumazine synthase) (EC 2,5,1,78)	1.92	3.43E-03	1.92
rne	Q9HZM8	Ribonuclease E (RNase E) (EC 3,1,26,12)	1.98	2.41E-03	1.97
rph	P50597	Ribonuclease PH (RNase PH) (EC 2,7,7,56) (tRNA nucleotidyltransferase)	3.14	0	2.67
rplS	Q9HXQ2	Large ribosomal subunit protein bL19 (50S ribosomal protein L19)	1.81	2.36E-03	2.74
rpoC	Q9HWC9	DNA-directed RNA polymerase subunit beta' (RNAP subunit beta') (EC 2,7,7,6) (RNA polymerase subunit beta') (Transcriptase subunit beta')	3.58	0	2.74
rpoN	P49988	RNA polymerase sigma-54 factor	2.29	2.29E-03	1.25
rpsB	O82850	Small ribosomal subunit protein uS2 (30S ribosomal protein S2)	2.00	2.84E-03	3.97

9. Appendix

Gene names	Majority protein IDs	Protein names	log_2 fold change GST-YgfB vs. GST	*q* value	$-log_{10}$ *p* value
rpsE	Q9HWF2	Small ribosomal subunit protein uS5 (30S ribosomal protein S5)	4.32	0	5.38
selB	Q9HV02	Selenocysteine-specific elongation factor	2.40	2.81E-03	1.85
speE1	Q9X6R0	Polyamine aminopropyltransferase 1 (Putrescine aminopropyltransferase 1) (PAPT 1) (Spermidine synthase 1) (SPDS 1) (SPDSY 1) (EC 2,5,1,16)	3.61	0	1.59
spuB	Q9I6J3	Probable glutamine synthetase	4.23	0	2.78
srkA	Q9I632	Stress response kinase A (EC 2,7,11,1) (Serine/threonine-protein kinase SrkA)	3.39	0	2.50
trkA	Q9I7B0	Trk system potassium uptake protein TrkA	3.26	0	2.48
ttcA	Q9I4E6	tRNA-cytidine(32) 2-sulfurtransferase (EC 2,8,1,-) (Two-thiocytidine biosynthesis protein A) (tRNA 2-thiocytidine biosynthesis protein TtcA)	2.26	2.74E-03	2.05
ubiB	Q9HUB8	Probable protein kinase UbiB (EC 2,7,-,-) (Ubiquinone biosynthesis protein UbiB)	2.86	0	2.17
uup	Q9HZI7	ATP-binding protein Uup (EC 3,6,1,-)	4.91	0	2.80
uvrA	Q9HWG0	UvrABC system protein A (UvrA protein) (Excinuclease ABC subunit A)	2.51	2.71E-03	1.53
uvrB	P72174	UvrABC system protein B (Protein UvrB) (Excinuclease ABC subunit B)	3.53	0	2.33
waaC	Q9HUF5	Heptosyltransferase I	8.95	0	4.73
waaG	Q9HUF6	UDP-glucose:(Heptosyl) LPS alpha 1,3-glucosyltransferase WaaG	9.78	0	3.76
xpt	Q9HTQ6	Xanthine phosphoribosyltransferase (XPRTase) (EC 2,4,2,22)	3.44	0	3.25

9.3.2. Interactome of YgfB in BW25113

Table 43: Interactome of YgfB in *E. coli* BW25113. log_2 fold change calculated by two-sided two-sample *t* test with an FDR of 1%. *q* value (multiplicity adjusted *p* value) is shown as calculated in two-sided *t* test. $-log_{10}$ *p* value is shown as volcano plots show this data. All proteins that had a *q* value of ≤0.01 in the comparison of both "GST-YgfB + Lysate vs. GST + Lysate" and" GST-YgfB + Lysate vs. GST-YgfB + Mock" were classified as interactors

Gene names	Majority protein IDs	Protein names	log_2 fold change GST-YgfB + Lysate vs. GST + Lysate	*q* value	$-log_{10}$ *p* value
amiA	P36548	N-acetylmuramoyl-L-alanine amidase AmiA	2.45	1.46E-03	2.04
bipA	P0DTT0	Large ribosomal subunit assembly factor BipA	2.66	0	2.57
ettA	P0A9W3	Energy-dependent translational throttle protein EttA	2.15	2.39E-03	2.13
fadI	P76503	3-ketoacyl-CoA thiolase	6.81	0	4.50
fadJ	P77399	Fatty acid oxidation complex subunit alpha;Enoyl-CoA hydratase/3-hydroxybutyryl-CoA epimerase;3-hydroxyacyl-CoA dehydrogenase	6.64	0	3.06
gadE	P63204	Transcriptional regulator GadE	3.63	0	3.65
gadX	P37639	HTH-type transcriptional regulator GadX	4.62	0	3.40

9. Appendix

Gene names	Majority protein IDs	Protein names	log_2 fold change GST-YgfB + Lysate vs. GST + Lysate	*q* value	$-log_{10}$ *p* value
gatY	P0C8J6	D-tagatose-1,6-bisphosphate aldolase subunit GatY	4.47	0	4.47
glpC	P0A996	Anaerobic glycerol-3-phosphate dehydrogenase subunit C	6.63	0	3.97
glyQ	P00960	Glycine--tRNA ligase alpha subunit	3.30	0	1.57
hemG	P0ACB4	Protoporphyrinogen IX dehydrogenase [menaquinone]	4.90	0	2.61
hemL	P23893	Glutamate-1-semialdehyde 2,1-aminomutase	1.87	3.31E-03	2.94
hflD	P25746	High frequency lysogenization protein HflD	5.34	0	4.04
hsdS	P05719	Type-1 restriction enzyme EcoKI specificity protein	4.10	0	3.63
htrL	P25666	Protein HtrL	5.26	0	4.84
ibpA	P0C054	Small heat shock protein IbpA	3.49	0	4.97
lon	P0A9M0	Lon protease	10.94	0	4.03
lpxB	P10441	Lipid-A-disaccharide synthase	6.02	0	6.81
minD	P0AEZ3	Septum site-determining protein MinD	2.87	0	1.94
narG	P09152	Respiratory nitrate reductase 1 alpha chain	2.19	2.42E-03	2.09
pflB	P09373	Formate acetyltransferase 1	3.16	0	2.73
pssA	P23830	CDP-diacylglycerol--serine O-phosphatidyltransferase	11.32	0	5.34
rfaB	P27127	Lipopolysaccharide 1,6-galactosyltransferase	4.81	0	2.80
rfaC	P24173	Lipopolysaccharide heptosyltransferase 1	2.99	0	2.80
rfaY	P27240	Lipopolysaccharide core heptose(II) kinase RfaY	4.61	0	2.97
rplF	P0AG55	50S ribosomal protein L6	2.29	3.37E-03	1.52
rplK	P0A7J7	50S ribosomal protein L11	3.05	1.41E-03	1.14
rplX	P60624	50S ribosomal protein L24	2.06	3.34E-03	2.01
rpoB	P0A8V2	DNA-directed RNA polymerase subunit beta	2.18	2.37E-03	2.01
rpoC	P0A8T7	DNA-directed RNA polymerase subunit beta	10.31	0	4.83
rsxC	P77611	Electron transport complex subunit RsxC	8.21	0	6.71
secA	P10408	Protein translocase subunit SecA	3.21	0	2.88
ubiB	P0A6A0	Probable protein kinase UbiB	2.35	1.55E-03	2.85
usg	P08390	USG-1 protein	3.26	0	2.76
waaU	P27242	Lipopolysaccharide 1,2-N-acetylglucosaminetransferase	5.93	0	3.69
wbbK	P37751	Putative glycosyltransferase WbbK	2.85	0	2.36
wecF	P56258	TDP-N-acetylfucosamine:lipid II N-acetylfucosaminyltransferase	5.06	0	3.27
ybjX	P75829	Uncharacterized protein YbjX	7.48	0	5.15
yeeX	P0A8M6	UPF0265 protein YeeX	7.87	0	4.22
yheO	P64624	Uncharacterized protein YheO	6.56	0	3.41
yijO	P32677	Uncharacterized HTH-type transcriptional regulator YijO	6.26	0	6.88

10. Danksagung

Diese Arbeit wurde gefördert durch die Deutsche Forschungsgemeinschaft (DFG) - Projektnummer 451686679.

Ich möchte auf diesem Wege all den Leuten danken, die mich während dieser Promotion begleitet haben, sei es durch Betreuung, guten Rat, Mitarbeit im Labor oder durch mentale Unterstützung. Ohne Euch wäre diese Zeit eine andere gewesen und ich bin Euch allen zu tiefstem Dank verpflichtet.

Zunächst möchte ich mich bei Dir, Erwin, für die enge und freundschaftliche Betreuung, die Möglichkeit bei Dir zu promovieren und das gute persönliche Verhältnis bedanken. Deine kreative und sympathische Art sowie Deine wissenschaftliche Expertise haben meine Promotionszeit sehr bereichert. Ich danke Moni und Fabi für all die guten Einfälle, Ideen, Diskussionen und die Betreuung. Vielen Dank auch für die vielen schönen Erinnerungen und die freundschaftliche Beziehung.
Des Weiteren danke ich meinem Zweitbetreuer Harald Groß und Christoph Mayer als Drittem im Bunde meines Thesis Advisory Committees für die produktiven TAC-Meetings, Rückmeldungen und Tipps nicht nur im wissenschaftlichen Sinne, sondern auch für meine persönliche Entwicklung. Zudem danke ich Bertolt Gust für den Vorsitz in der Prüfungskommission meiner mündlichen Prüfung. Auch möchte ich Libera Lo Presti für das Korrekturlesen dieser Arbeit sowie unseres Papers und für die großartigen Vorschläge, Anregungen und Kommentare danken.
Vielen Dank an alle derzeitigen und ehemaligen Mitglieder der AG Bohn/Schütz mit denen ich über die Jahre hinweg zusammenarbeiten durfte. Ganz besonders möchte ich Vale für die gegenseitige Unterstützung, die Freundschaft, die Partys, und die generell einfach gute Zeit zusammen danken. Ganz vielen Dank auch an meinen ehemaligen Masterstudenten Fabi: Du hast viel zum Erfolg dieser Promotion beigetragen und ich bin froh, dass uns so eine gute Freundschaft verbindet. Des Weiteren danke ich Andi, Tanja, Anja, Ann-Sophie, Julia, Katharina, Nora, Laura, Lydia, Elias und all den anderen die ich hier nicht aufzählen kann.
Vielen Dank auch an die ganzen anderen Mitarbeitenden vom Institut für Medizinische Mikrobiologie. Vielen Dank an Christina für die Insidertips und jahrelange Erfahrung, danke auch an Johannes, Annika, Sandra, Udo und Stefan.

Auch möchte ich meinen Freunden danken. Vielen Dank an Daniel für unsere jahrelang bestehende Freundschaft. Auch wenn wir uns zur Promotion schlussendlich doch trennen mussten, haben wir schon so viel zusammen erlebt und sind so einen weiten Weg zusammen gegangen, wer weiß wo wir am Ende dann noch enden. Vielen Dank auch an meine Jungs Luci, Niclas und Martin. Ich freue mich schon auf viele weitere Trips in diverse Städte.
Ganz besonders möchte ich meiner Familie danken, insbesondere meinen Eltern für alles, was Ihr mir ermöglicht habt und dafür, dass Ihr immer für mich da seid. Des Weiteren danke ich meiner Schwester Marie für Deine lebensfrohe Art und dass ich durch Dich immer neue Dinge Lernen kann.
Zu guter Letzt gebührt ganz besonders viel Dank meiner liebsten Julia. Danke für Deine bedingungslose Unterstützung, Deine liebevolle Art und Dein offenes Ohr. Ohne Dich wäre die Zeit meiner Promotion deutlich härter geworden und ich bin unglaublich dankbar Dich an meiner Seite zu haben.
Vielen Dank auch an alle Personen, die ich namentlich nicht nennen konnte. Auch Euch danke ich von Herzen für die Unterstützung in den letzten Jahren!

11. Eidesstattliche Erklärung

Ich erkläre hiermit, dass ich die zur Promotion eingereichte Arbeit mit dem Titel:

„Insights into the Role of YgfB in β-Lactam Resistance and Beyond“

selbständig verfasst, nur die angegebenen Quellen und Hilfsmittel benutzt und wörtlich oder inhaltlich übernommene Stellen als solche gekennzeichnet habe. Ich erkläre, dass die Richtlinien zur Sicherung guter wissenschaftlicher Praxis der Universität Tübingen (Beschluss des Senats vom 25.5.2000) beachtet wurden. Ich versichere an Eides statt, dass diese Angaben wahr sind und dass ich nichts verschwiegen habe. Mir ist bekannt, dass die falsche Abgabe einer Versicherung an Eides statt mit Freiheitsstrafe bis zu drei Jahren oder mit Geldstrafe bestraft wird.

Tübingen, den 24.06.2024